Chemical communication in the root microbiome

Ke Yu

Chemical communication in the root microbiome
PhD thesis
Ke Yu, February 2019
Utrecht University

Cover: Xiaoyu Sun|Ins: sxy_sun0202
Layout: Ridderprint BV | www.ridderprint.nl
Printing: Ridderprint BV | www.ridderprint.nl

Chemical communication in the root microbiome

Chemische communicatie in het microbioom van de plantenwortel

(met een samenvatting in het Nederlands)

Proefschrift

ter verkrijging van de graad van doctor aan de Universiteit Utrecht op gezag van de rector magnificus, prof.dr. H.R.B.M. Kummeling, ingevolge het besluit van het college voor promoties in het openbaar te verdedigen op woensdag 6 februari 2019 des middags te 4.15 uur

door

Ke Yu

geboren op 2 december 1987
te Zhengzhou, China

Promotor:	Prof. dr. ir. C.M.J. Pieterse
Copromotoren:	Dr. P.A.H.M. Bakker
	Dr. R.L. Berendsen

This thesis was partly accomplished with financial support from China Scholarship Council (No.201306300051).

CONTENT

CHAPTER 1

General introduction

1. BENEFICIAL ROOT-MICROBIOME INTERACTIONS

Growing in soil, plant roots interact with a wide variety of microbes. Microbial communities hosted by plant roots constitute the root microbiome and include pathogenic, commensal, as well as beneficial microbes (Mendes et al., 2011; Bulgarelli et al., 2012; Lundberg et al., 2012; Philippot et al., 2013; Turner et al., 2013a). The complex interactions between the roots and their associated microbiomes are important determinants of plant health (Berendsen et al., 2012; Turner et al., 2013a; Panke-Buisse et al., 2015; Schlaeppi and Bulgarelli, 2015; Raaijmakers and Mazzola, 2016; Mauchline and Malone, 2017). Associations formed between roots and beneficial microbes can promote plant growth by assisting in the nutrient uptake, enhancing stress tolerance, or by inhibiting pathogens and eliciting systemic resistance against pathogens and insects (Berendsen et al., 2012; Bulgarelli et al., 2013; Pieterse et al., 2014). Well-studied examples include the rhizobial bacteria living in symbiosis with legumes and mycorrhizal fungi associated with most terrestrial plants, but there are many other free-living plant growth-promoting rhizobacteria (PGPR) and fungi (PGPF) described that benefit a wide range of plant species, including the model plant *Arabidopsis thaliana* (hereafter *Arabidopsis*; Zamioudis and Pieterse, 2012; Bulgarelli et al., 2013). Like pathogens, beneficial microbes are confronted with the plant immune system and it is becoming more and more evident that beneficial microbes similarly need to evade or suppress root immune responses. In addition to immune suppression, however, selected beneficial microbes can also boost plant immunity by eliciting systemic resistance against potential attacks by pathogens and insects, a phenomenon known as induced systemic resistance (ISR).

2. INITIATION OF IMMUNE SIGNALING IN ROOTS

2.1 Plant immune signaling

Plants have evolved a sophisticated immune system to detect and respond to potential invaders (Jones and Dangl, 2006). Beneficial microbes are confronted with the root immune system when they are in intimate contact with plant cells. In plants, cell surface-localized pattern recognition receptors (PRRs) can detect surrounding microbes by recognizing microbe-associated molecular patterns (MAMPs), which are generally conserved molecules shared by a wide range of microbes (Boller and Felix, 2009). In the past two decades, numerous MAMPs, such as flagellin, elongation factor Tu (EF-Tu), cold-shock protein (CSP), lipopolysaccharide (LPS), chitin, elicitin, and Nep1-like protein have been characterized in various plant pathosystems together with their cognate PRRs (Boutrot and Zipfel, 2017). Despite recognizing specific MAMPs, diverse PRRs have been shown to activate convergent cellular immune signaling pathways. Upon MAMP recognition, PRRs recruit regulatory receptor kinases to form PRR complexes that activate a multi-layered immune signaling cascade through receptor-like cytoplasmic kinases (Macho and Zipfel, 2014). The activated immune signaling events, known as MAMP-triggered immunity (MTI), function in the elimination of potential pathogenic infections (Macho and Zipfel, 2014; Couto and Zipfel, 2016). Ion (H^+ and Ca^{2+}) fluxes and transient bursts of reactive oxygen species (ROS) are two typical cellular responses happening within minutes after immune signaling activation (Boller and Felix, 2009; Yu et al., 2017). Immune signaling is transduced through activation of Ca^{2+}-dependent protein kinase and mitogen-activated protein kinase (MAPK) cascades, which triggers downstream transcriptional regulation of defense-related genes, *inter alia* leading to callose deposition, antimicrobial compounds accumulation and defense hormone

regulation (Boller and Felix, 2009; Couto and Zipfel, 2016; Yu et al., 2017). Plant hormones act as central modulators of many components in the immune signaling network. Two major defense hormones, salicylic acid (SA) and jasmonic acid (JA), form a complicated regulatory network to fine-tune plant immune homeostasis. Other hormones such as auxin, ethylene, abscisic acid, cytokinins, brassinosteroids and gibberellin, also interact with the SA/JA signaling pathway, together orchestrating the immune signaling network (Pieterse et al., 2009; Pieterse et al., 2012).

2.2 Transient immune activation in roots

Our knowledge of plant immune signaling mainly comes from studies on interactions between microbes and aboveground plant parts. However, plant roots are also capable of mounting strong immune responses upon PRR-mediated MAMP recognition, including callose deposition, camalexin biosynthesis and defense-related gene activation (Millet et al., 2010; Beck et al., 2014; Wyrsch et al., 2015; Stringlis et al., 2018a). Like pathogens, beneficial microbes possess immunogenic MAMPs (Millet et al., 2010; Jacobs et al., 2011; Lopez-Gomez et al., 2012; Pel and Pieterse, 2013; Stringlis et al., 2018a). During their initial contact with roots, beneficial microbes are recognized by plant PRRs, activating immune signaling. Root immune activation by beneficial microbes was observed in many root-microbe associations. For example, *Bradyrhizobium japonicum* strongly induces defense gene expression at the early stage of infection in soybean root hair cells (Libault et al., 2010), and an arbuscular mycorrhizal fungus *Glomus versiforme* induces a substantial set of defense and stress-related genes during the initial contact with *Medicago truncatula* (Liu et al., 2003). Similarly, the cellular components of two PGPRs, *Pseudomonas simiae* WCS417 (hereafter WCS417) and *Pseudomonas capeferrum* WCS358 (hereafter WCS358), can trigger immune responses in *Arabidopsis* roots and tobacco cell suspension, such as ROS production, MAMP-responsive gene expression and callose deposition (Van Loon et al., 2008; Millet et al., 2010; Stringlis et al., 2018a). Moreover, *Piriformospora indica* has significantly reduced colonization on the roots of a MAMP-hyper-responsive *Arabidopsis* mutant *pub22/23/24*, indicating that this PGPF can be recognized by plant PRRs (Jacobs et al., 2011). All these studies show that root immune responses induced by beneficial microbes are mostly restricted to the early stages of the beneficial associations, suggesting an active interference of root immunity by beneficial microbes.

3. MICROBIAL EVASION AND SUPPRESSION OF PRR SIGNALING IN ROOTS

To promote infection, successful plant pathogens utilize virulence factors that interfere with immune signaling events, including immune recognition, PRR complex formation, activation of immune signaling, signal transduction, defense gene regulation and hormonal modulation (Couto and Zipfel, 2016). Such virulence factors have been well-documented for many plant pathosystems (Xin and He, 2013; Lo Presti et al., 2015; Macho and Zipfel, 2015; Couto and Zipfel, 2016). Despite the fact that more and more beneficial plant-microbe associations have been reported, little is known about how beneficial microbes modulate plant immune signaling (Zamioudis and Pieterse, 2012). So far, some immune modulating factors deployed by beneficial microbes have been characterized, which include bacterial or fungal effector proteins, fungal effector-type small secreted proteins (SSPs) and other conserved microbial molecules. In the following sections, we will present an overview of microbial factors targeting distinct plant immune signaling events.

3.1 Evasion of apoplastic recognition

Since MAMPs are conserved molecules shared by many members throughout the microbial kingdoms, it is likely that all plant-colonizing microbes, either pathogens or mutualists, have evolved strategies to evade host immune recognition under the selection pressure posed by plant PRRs during the co-evolution process. The strategies include evolving divergent MAMPs or releasing apoplastic effector proteins to mask the presence of immunogenic MAMPs, thus evading plant PRR-mediated immune recognition (Zamioudis and Pieterse, 2012; Pel and Pieterse, 2013).

3.1.1 Evolving divergent MAMPs. Flagellin monomers are the building blocks of bacterial flagella, an essential organelle responsible for bacterial motility (Rossez et al., 2015). The *Arabidopsis* PRR FLS2 can recognize flagellin by binding the immunogenic flg22 epitope, a highly-conserved sequence of 22 amino acids at the N-terminus of the protein (Felix et al., 1999; Gomez-Gomez and Boller, 2000; Sun et al., 2013). Driven by co-evolution, variation of flagellin sequences enables pathogenic bacteria to evade immune recognition in both mammals and plants (Rossez et al., 2015). Interestingly, flagellin sequences of *Sinorhizobium meliloti* also exhibit an exceptional divergence in this region, resulting in a complete abolishment of immune activation in *Arabidopsis* (Felix et al., 1999). Also in *Lotus japonicus*, purified flagellin from *Mesorhizobium loti* failed to activate immune responses, whereas the commonly-used flg22 epitope of *Pseudomonas aeruginosa* induces typical immune responses such as ethylene production, MAPK activation and defense-related gene expression, which indicates that the FLS2 receptor homolog in *L. japonicus* is fully functional (Lopez-Gomez et al., 2012). Similar observations were made in the beneficial association formed by an endophytic PGPR *Burkholderia phytofirmans* and grapevine. The grapevine FLS2 receptor differentially recognizes flg22 epitopes derived from beneficial *B. phytofirmans*, initiating significantly reduced immune responses compared to the immune responses induced by the flg22 epitopes derived from the pathogenic bacteria *P. aeruginosa* and *Xanthomonas campestris* (Trda et al., 2014). It is known that *Arabidopsis* can recognize the bacterial MAMPs flagellin and EF-Tu through the cognate PRRs FLS2 and EFR, whereas this plant species is unresponsive to CSP for which it misses the cognate PRR CORE (Gomez-Gomez and Boller, 2000; Zipfel et al., 2006; Wang et al., 2016). This possibly explains why metagenomes of healthy *Arabidopsis* root microbiota possess a 4-10 fold higher percentage of genes encoding the non-immunogenic epitope of CSP than of genes encoding the immunogenic epitopes of flagellin and EF-Tu (Hacquard et al., 2017). These results together suggest that plants actively select the members of its microbiome through the function of PRRs, while many soil-borne microbes have evolved to evade PRR-mediated immune recognition in order to form an association with their host plants.

3.1.2 Hiding excessive MAMPs. Both pathogenic and beneficial microbes have been found to conceal the presence of certain immunogenic MAMPs. AprA is an extracellular alkaline protease that is secreted by the pathogenic bacteria *P. aeruginosa* and *Pseudomonas syringae.* AprA degrades flagellin monomers, thereby preventing immune recognition of flagellin in both mammals and plants (Bardoel et al., 2011; Pel et al., 2014). AprA homologs are present in a wide range of bacterial species, among which many are plant-beneficial, including nitrogen-fixing rhizobia and plant growth-promoting pseudomonads (Pel et al., 2014). Chitin is a major component of fungal cell walls, which triggers immune responses upon recognition by its cognate PRRs in various hosts (Shimizu et al., 2010; Cao et al., 2014). However, the fungal pathogen *Cladosporium fulvum* secretes two lectin-type chitin-binding effectors, Avr4 and Ecp6, that strengthen fungal cell walls against hydrolysis by plant-derived

chitinases and prevent immune recognition of chitin by the plant PRR CERK1, respectively (Van den Burg et al., 2006; De Jonge et al., 2010). Ecp6-like proteins were also found in many other fungal species, including the biological control agent *Chaetomium globosum* (Bolton et al., 2008). Although the role of AprA and Ecp6 homologs in prevention of immune recognition of beneficial microbes still requires confirmation, similar mechanisms were revealed in *P. indica* during colonization of both barley and *Arabidopsis* roots. β-glucan, a fungal cell wall component, can trigger immune responses upon recognition by an uncharacterized PRR complex (Wawra et al., 2016). The PGPF *P. indica* secretes a SSP called fungal-specific β-glucan-binding lectin (FGB1), which potentially increases fungal cell wall integrity and interferes with host immune recognition through its high affinity with β-glucan (Wawra et al., 2016). This suggests that, like pathogens, beneficial microbes also evolved ways to obscure their most excessively present MAMPs to prevent recognition by their host plants and avoid activation of the plant immune system.

3.2 Suppression of cytoplasmic signaling

Pathogens deliver effector proteins into plant cells through a type III secretion system (T3SS) for gram-negative bacteria or through intracellular infection structures for fungi and oomycetes, therewith dampening various components of plant immune signaling initiated upon MAMP recognition (Dodds and Rathjen, 2010; Win et al., 2012; Couto and Zipfel, 2016). Like plant pathogens, beneficial microbes also utilize a diverse range of effector proteins to suppress plant immune activation. The T3SS was revealed in the genomes of many plant beneficial rhizobacteria including rhizobia and pseudomonads (Deakin and Broughton, 2009; Loper et al., 2012; Berendsen et al., 2015; Miwa and Okazaki, 2017). Likewise, genomes of many beneficial fungi, such as *Laccaria bicolor* and *P. indica*, possess a substantial set of highly expressed genes encoding effector-type SSPs during root colonization (Martin et al., 2008; Zuccaro et al., 2011). Moreover, metagenomes of the root microbiomes of cucumber, wheat, citrus and barley display a significant enrichment of T3SS genes at a community level that are possibly involved in suppression of root immune responses (Ofek-Lalzar et al., 2014; Bulgarelli et al., 2015; Zhang et al., 2017). This suggests that beneficial members in the root microbiome actively interfere with plant immune signaling.

3.2.1 Eliminating ROS burst. Rhizobial T3SS effectors are designated nodulation outer proteins (Nops) and mostly function in the regulation of nodulation or determination of host specificity (Miwa and Okazaki, 2017). Nonetheless, several Nop effectors have shown a direct role in suppressing PRR-mediated immune signaling. ROS is rapidly generated within minutes upon PRR-mediated MAMP recognition, functioning as an important signaling molecule in plant immunity (Torres et al., 2006; Kimura et al., 2017). NopM, an effector secreted by *Sinorhizobium* sp. strain NGR234 (hereafter NGR234), is an E3 ubiquitin ligase that is essential for normal nodulation in *Lablab purpureus* (Xin et al., 2012). Interestingly, in *Nicotiana benthamiana*, NopM was found to suppress flg22-induced ROS bursts (Xin et al., 2012). Orthologs of pathogen T3SS effector genes *ropAA*, *ropB*, and *ropM*, were characterized in the genome of a biological control strain *Pseudomonas fluorescens* Q8r1-96 and were also found to be expressed in the rhizosphere (Mavrodi et al., 2011). Infiltration of each effector suppressed flg22-induced ROS production in *Nicotiana tabacum*, although deletion of the effector genes did not affect bacterial rhizosphere competence (Mavrodi et al., 2011). Another example is the fungal effector PIIN_08944 secreted by *P. indica*, which promotes fungal colonization of the roots of *Arabidopsis* and barley (Akum et al., 2015). Overexpression of *PIIN_08944* significantly reduced the flg22/chitin-induced ROS burst in barley, however, not in *Arabidopsis* (Akum et al., 2015). These examples suggest

that effectors delivered by beneficial microbes can efficiently perturb plant immunity by eliminating the transient ROS burst.

3.2.2 Targeting MAPK cascades. MAPK cascades, controlling numerous downstream immune signaling events, are targets of many evolved pathogen effectors (Meng and Zhang, 2013), and seem to be targeted by beneficial microbes as well. For example, *in planta* expression of the effector NopL from the rhizobial strain NGR234 suppresses the expression of pathogenesis-related defense proteins in *N. tabacum* and *L. japonicus*, and cell death induced by overexpression of *SIPK* (a MAPK gene; Bartsev et al., 2004; Zhang et al., 2011; Ge et al., 2016). By mimicking a MAPK phosphorylation substrate, NopL is multiply phosphorylated by SIPK in the nucleus, thus potentially inhibiting phosphorylation of other natural MAPK substrates that is required in regulating the expression of defense-related genes, which ultimately results in an interruption of immune signaling (Zhang et al., 2011; Ge et al., 2016). It has been shown that MPK4 regulates the expression of genes encoding WRKY, MYB and bHLH transcription factors in soybean, preventing SA accumulation and defense-related gene expression (Liu et al., 2011). In soybean inoculated with *Sinorhizobium fredii* HH103, MPK4 is significantly induced at the early stage of infection in a T3SS-dependent manner, indicating that this rhizobial strain suppresses early root immune responses by MAPK-targeting T3SS effectors (Jimenez-Guerrero et al., 2015). By interfering with MAPK cascades, beneficial microbes can thus block immune signaling transduction and activation of downstream immune responses.

3.2.3 Modulation of hormonal signaling. Since plants use hormones to fine-tune immune homeostasis during plant-microbe interactions (Pieterse et al., 2009; Pieterse et al., 2012), many pathogens evolved effectors that hijack hormonal signaling pathways (Kazan and Lyons, 2014). Also beneficial microbes have been found to target JA, auxin and ethylene signaling pathways to suppress root immune responses and promote their association with the host plant (Jacobs et al., 2011; Kloppholz et al., 2011; Lakshmanan et al., 2012; Plett et al., 2014; Stringlis et al., 2018a). For example, the arbuscular mycorrhizal fungus *Rhizophagus irregularis* secrets the effector SP7, which directly interacts with the JA/ethylene inducible-ERF19 transcription factor and prevents the expression of EFR19-activated defense-related genes in *M. truncatula* roots (Kloppholz et al., 2011). The ectomycorrhizal fungus *L. bicolor* secrets the MiSSP7 effector to promote the establishment of a mutualistic association with *Populus* (Plett et al., 2014). MiSSP7 prevents JA-induced degradation of JAZ6, a protein functioning as a negative regulator of JA-induced genes, thus suppressing JA-mediated transcriptional activation of immune responses such as cell wall modifications (Plett et al., 2014). The PGPF *P. indica* broadly suppresses flg22-induced root immune responses in *Arabidopsis* (Jacobs et al., 2011). However, the immunosuppressive phenotype is compromised in JA-signaling deficient mutants *jar1-1* and *jin1-1* (Jacobs et al., 2011). Moreover, PIIN_08944 effector of *P. indica* has been shown to suppress the expression of flg22-induced SA marker gene *CBP60g* in *Arabidopsis*, which encodes a transcription factor that is required for the production of SA by regulating the key biosynthetic enzyme Isochorismate Synthase 1 (Zhang et al., 2010; Wang et al., 2011; Akum et al., 2015). Similarly, the PGPR *Bacillus subtilis* FB17 (hereafter FB17), can suppress early flg22-induced root immune responses in *Arabidopsis* by releasing an unidentified low-molecular weight component, and this immune suppression phenotype also requires functional JA signaling components JAR1, JIN1 and MYC2 (Lakshmanan et al., 2012). Collectively, these findings provide evidence that beneficial microbes suppress root immune responses through various immune suppressors such as effector proteins, targeting multiple signaling components that are initiated upon MAMP recognition.

3.3 Interplay with symbiosis signaling

Plant immunity and symbiosis share similar signaling events, from recognition of immunogenic or symbiotic signals to activation of downstream signaling pathways, whereas the interactions of the two signaling pathways are largely unknown (Zipfel and Oldroyd, 2017). In addition to MAMPs, symbiotic microbes also produce different types of symbiosis-related molecules, which can be recognized by host symbiotic receptors and initiate symbiosis signaling (Zipfel and Oldroyd, 2017). Many of these symbiotic molecules are very similar to MAMPs. For example, rhizobial Nod factors and fungal Myc factors can be perceived by cognate receptors in host plants and initiate rhizobial or arbuscular mycorrhizal symbiotic process (Zipfel and Oldroyd, 2017). Interestingly, both Nod factors and Myc factors are lipochitin oligosaccharides that are structurally similar to the well-studied MAMPs chitin and peptidoglycans (Liang et al., 2014). Rhizobial LPS is required for the establishment of successful symbiosis in legume plants (Gibson et al., 2008), whereas LPS derived from pathogens typically triggers immune responses upon recognition by their cognate PRR LORE in *Arabidopsis* (Ranf et al., 2015). For long, it was unclear how plants discriminate between the symbiotic and immunogenic signals when both types of molecules are present. However, it was recently shown that legume roots can separately recognize the fungal MAMP chitin (immunogenic signal) and Nod factors (symbiotic signal) through two sets of distinct LysM PRRs (Bozsoki et al., 2017). Interestingly, many symbiotic molecules derived from beneficial microbes seem to suppress MAMP-triggered root immune responses. Nod factors of *B. japonicum* can strongly suppress immune responses induced by various MAMPs in both soybean and *Arabidopsis*, likely as a result of significantly reduced protein levels of cognate PRRs on the cell membrane (Liang et al., 2013). Surprisingly, Nod factors can still suppress immune responses in soybean mutants lacking Nod factor receptors, but not in an *Arabidopsis* mutant lacking the LysM PRR LYK3 (Liang et al., 2013). Similarly, LPS of *S. meliloti* suppresses not only early immune responses such as ROS burst, but also late defense-related transcriptional reprogramming in *M. truncatula*, despite inducing a strong ROS burst in the non-host *N. tabacum* (Scheidle et al., 2005; Tellstrom et al., 2007). A recent study has shown that EPR3-mediated recognition of compatible exopolysaccharides (EPS) in *L. japonicus* is crucial in controlling successful entry by *M. loti* (Kawaharada et al., 2015). In addition to its role in symbiosis, EPS derived from *S. meliloti* can block flg22-induced calcium influx through chelation with calcium ions, thus suppressing downstream immune responses (Aslam et al., 2008). The abovementioned findings suggest a role of symbiotic molecules in suppressing immune responses, but more studies are required to understand the complicated immunity-symbiosis interplay.

3.4 Interplay with nutritional deficiency

A mechanistic link between plant immunity and nutritional deficiency has been proposed (Bakker et al., 2018). The endophytic fungus *Colletotrichum tofieldiae* has an intriguing life-style when colonizing *Arabidopsis* roots (Hiruma et al., 2016). It can promote phosphate uptake and growth of *Arabidopsis* growing under phosphate-deficient conditions and can even become pathogenic on the *Arabidopsis cyp79B2*/*cyp79B3* double mutant, which is defective in producing defense compounds camalexin and indole glucosinolates (Hiruma et al., 2016). This indicates that plant defense responses are repressed under phosphate-deficient but not under phosphate-sufficient growth conditions, suggesting that a trade-off between immune responses and phosphate stress responses drives the beneficial association of *C. tofieldiae* with *Arabidopsis* (Hacquard et al., 2016; Hiruma et al., 2016). Moreover, it was recently discovered that a synthetic microbiome can enhance the phosphate stress

response of *Arabidopsis* through the master transcriptional regulator PHR1 (Castrillo et al., 2017). Strikingly, in addition to regulating the phosphate stress responses, PHR1 was also found to negatively regulate flg22-induced immune responses in *Arabidopsis* (Castrillo et al., 2017). Evidence for the interplay between plant immunity and nutritional deficiency was additionally observed in *Arabidopsis* colonized by the PGPR WCS417 (Zamioudis et al., 2015). WCS417 induces the expression of the root-specific transcription factor *MYB72,* which is required for the onset of ISR (Van der Ent et al., 2008; Segarra et al., 2009). MYB72 also plays an important role in the adaptive response to iron limitation (Sivitz et al., 2012; Palmer et al., 2013). These findings suggest that plants can coordinate their response to nutritional stress and immunogenic elicitation, and beneficial microbes may modulate this balance for their own benefit.

4. MODULATION OF PLANT IMMUNITY BY NON-INVASIVE BENEFICIAL MICROBES

The interactions between plant root and associated microbes occur in either the rhizosphere or the endophytic root compartment (Berendsen et al., 2012; Turner et al., 2013a). Although it is difficult to discretely separate these two compartments, here, we define the rhizosphere as the root surface or rhizoplane plus the soil surrounding the root that is influenced by the root and thus is different from the unplanted bulk soil. Consequently, the endophytic root compartment is composed by those root parts interior to the epidermis. Most of the abovementioned examples describe immune modulation strategies utilized by beneficial microbes that are invading host roots. Rhizobial cells differentiate intercellularly in legume nodules and also hyphae of mycorrhizal fungi penetrate host roots to form their symbiotic structures (Desbrosses and Stougaard, 2011; Schmitz and Harrison, 2014; Garcia et al., 2015). In nature, plants also form diverse beneficial associations with microbes that colonize the rhizosphere and that promote plant growth or help the plant cope with adverse (a)biotic conditions (Berendsen et al., 2012). It can be debated to what extent the plant immune system responds to symbionts living on the outside of the root. It was shown that the root PRR gene *FLS2* displays a tissue- and cell type-specific higher expression level at bacterial infection sites and at the inner cellular layers of *Arabidopsis* roots (Beck et al., 2014). Moreover, immune responses of the root pericycle were found to be stronger upon MAMP perception than those of other tissues (Wyrsch et al., 2015). These studies suggest that plants desensitize their root immune system at the outer cell layers of the root to prevent over-responsiveness to the microbiologically complex soil environment. A non-invasive lifestyle of certain beneficial microbes may thus prevent strong activation of plant immune responses. Indeed, beneficial rhizosphere inhabitants such as WCS417 and FB17 can actively suppress root immune responses (Millet et al., 2010; Lakshmanan et al., 2012; Stringlis et al., 2018a). In *Arabidopsis* roots, both heat-killed WCS417 cells and the WCS417 flg22 peptide can activate immune responses (Millet et al., 2010; Stringlis et al., 2018a). Interestingly, expression of more than 50% of the root immune-responsive genes triggered by flg22 was repressed by live WCS417 cells (Stringlis et al., 2018a). The PGPR FB17 also suppresses flg22-induced immune responses in *Arabidopsis* roots in a JA-dependent manner (Lakshmanan et al., 2012). The molecular mechanism of immune suppression mediated by WCS417 and FB17 remains to be investigated, but nonetheless, the ability to suppress immunity does suggest this is a useful trait in the rhizosphere.

The role of the plant immune system in the assembly of root-associated microbiome has been well studied in the past decade. Lebeis and colleagues found that *Arabidopsis* mutants in which SA-dependent defense signaling was disrupted have distinct root microbiomes (Lebeis et al., 2015), indicating that the immune system gates access

and determines which microbes can colonize the roots. Moreover, they found that SA-dependent signaling primarily modulates the composition of the endophytic root microbiome, while the rhizosphere microbiome was less affected (Lebeis et al., 2015). Also an assessment of wheat microbiomes after exogenous JA application demonstrated that JA signaling affects microbiome assembly in a compartment-specific manner, and that the endophytic root microbiome is mostly affected (Liu et al., 2017). However, JA signaling did affect the composition of *Arabidopsis* rhizosphere microbiomes, which could be associated to differences in root exudate profiles of JA signaling mutants compared to wild-type plants (Carvalhais et al., 2015). Moreover, aboveground activation of the immune system by both microbial pathogens and insects has been demonstrated to result in alterations in rhizosphere microbiomes of several plant species (Dudenhöffer et al., 2016; Kong et al., 2016; Berendsen et al., 2018; Yuan et al., 2018). Again the microbiome alteration could be related to differential root exudation in response to activation of the immune system (Yuan et al., 2018). Together these findings suggest that although the gate keeping functions of the plant immune system might differ for different root compartments, the influence of the immune system does extend into the rhizosphere.

5. INDUCED SYSTEMIC RESISTANCE BY BENEFICIAL MICROBES

Besides suppressing root immune responses, specific beneficial microbes can also strengthen plant defenses. Once specific beneficial microbes colonize the plant roots, not only the sites of microbial colonization, but also more distant tissues are primed to confer faster and stronger defense responses against a wide range of pathogenic microbes and herbivorous insects (Pieterse et al., 2014). This phenomenon, known as ISR, has been demonstrated in numerous plant species (Pieterse et al., 2014). Beneficial microbes that are capable of eliciting ISR in plants include PGPR, PGPF and arbuscular mycorrhizal fungi, but ISR depends on the right combination of microbial and plant genotype (Pieterse et al., 2014; Berendsen et al., 2015). The signaling events that confer broad-spectrum ISR have been extensively investigated and different components have been revealed using the model PGPR strain WCS417 and plant *Arabidopsis* (Pieterse et al., 1996; Van Wees et al., 1997; Pieterse et al., 1998; Pozo et al., 2008; Van der Ent et al., 2008; Zamioudis et al., 2014).

WCS417 was first isolated from the wheat rhizosphere (Lamers et al., 1988) and it was discovered to elicit ISR in carnation and radish (Van Peer et al., 1991; Leeman et al., 1996). Since then, WCS417 was shown to be capable of eliciting ISR in multiple plant species including *Arabidopsis* (Pieterse et al., 1996; Bakker et al., 2007; Berendsen et al., 2015). The initiation of ISR signaling requires mutual recognition of reciprocal signals derived from both parties involved. Several microbial molecules can elicit ISR, such as flagella, lipopolysaccharides, siderophores, volatiles and antibiotic metabolites (Bakker et al., 2007; Pieterse et al., 2014). By using *Arabidopsis* mutants that are defective in different hormone signaling pathways, it was demonstrated that JA and ethylene are dominant regulators of ISR signaling elicited by WCS417 (Pieterse et al., 1996; Van Wees et al., 1997; Pieterse et al., 1998), whereas some rhizobacterial strains such as *Pseudomonas fluorescens* SS101 induce a phenotypically similar systemic resistance in host plants in a SA-dependent manner (Van de Mortel et al., 2012; Pieterse et al., 2014). Surprisingly, colonization of WCS417 did not alter the level of JA/ethylene biosynthesis or the expression of JA/ethylene-responsive genes in systemic tissues (Van Wees et al., 1999; Pieterse et al., 2000). Transcriptional profiling revealed that WCS417-elicited ISR in *Arabidopsis* foliar tissues relies on the primed or potentiated expression of defense-related genes upon attack rather than constitutive defense activation (Verhagen et al., 2004), thus avoiding direct activation of costly defenses. The transcription factor MYC2, which orchestrates dynamic JA responses (Kazan and

Manners, 2013), is the key regulator of potentiated expression of JA-responsive genes (Pozo et al., 2008). Interestingly, despite the fact that WCS417-elicited ISR is SA-independent, the master transcriptional regulator of the SA signaling pathway, NPR1, is indispensable for the signaling initiation (Pieterse et al., 1998). However, the exact molecular function of NPR1 in WCS417-ISR is as yet unknown.

6. MYB72: KEY COMPONENT OF ISR SIGNALING

Following colonization by WCS417, transcriptional changes in the roots are more pronounced than in the shoots (Verhagen et al., 2004). The root-specific transcription factor MYB72, and the MYB72-dependent β-glucosidase BGLU42 have been identified as key components in the onset of ISR signaling triggered by different microbes (Van der Ent et al., 2008; Segarra et al., 2009; Zamioudis et al., 2014). Colonization by WCS417 significantly induces the expression of MYB72 and BGLU42 in *Arabidopsis* roots (Zamioudis et al., 2014; Zamioudis et al., 2015) and both *myb72* and *bglu42* mutants are unable to mount effective ISR (Van der Ent et al., 2008; Segarra et al., 2009; Zamioudis et al., 2014). Although overexpression of *MYB72* fails to initiate ISR signaling, overexpression of *BGLU42* does lead to constitutive disease resistance (Van der Ent et al., 2008; Zamioudis et al., 2014). Hence, it is likely that MYB72-regulated activity of BGLU42 in plant roots is important for the onset of ISR. Interestingly, *MYB72* and *BGLU42* are also activated in *Arabidopsis* roots in response to iron deficiency (Colangelo and Guerinot, 2004; Buckhout et al., 2009; Palmer et al., 2013). In fact, a significant proportion of the WCS417-induced genes are also activated in plant roots under conditions of iron deficiency (Zamioudis et al., 2015). In iron-starved plants, MYB72 was shown to act together with its paralog MYB10 in the survival of plants growing in alkaline soil where iron availability is limited (Palmer et al., 2013). Under iron deficient conditions, MYB72 was shown to regulate the production of iron-mobilizing phenolic compounds such as coumarins and BGLU42 was shown to be important for their subsequent release into the rhizosphere (Zamioudis et al., 2014). These coumarins are synthesized via FERULOYL-COA 6'-HYDROXYLASE1 (F6'H1) in the phenylpropanoid pathway and secreted by the iron deficiency-regulated ABC transporter PDR9 into the rhizosphere, where they aid in mobilization and uptake of iron from the soil environment (Rodríguez-Celma et al., 2013; Fourcroy et al., 2014; Schmid et al., 2014; Schmidt et al., 2014; Tsai and Schmidt, 2017b; Rajniak et al., 2018; Tsai et al., 2018). The overlap between the root responses that are initiated by WCS417 and conditions of iron starvation, suggests that the onset of rhizobacteria-ISR shares components of the iron deficiency response (Zamioudis et al., 2015; Verbon et al., 2017). The expression of *MYB72* and other iron uptake-related genes was not affected by the colonization of an ISR non-eliciting rhizobacterial strain *Pseudomonas defensor* WCS374, further strengthening the mechanistic link between ISR and iron deficiency responses (Berendsen et al., 2015; Zamioudis et al., 2015). One scenario is that MYB72-dependent phenolic metabolites are participating in ISR signaling, functioning in either long-distance signal transmission or in direct antimicrobial defense responses. Alternatively, free living ISR-eliciting microbes such as WCS417 may sense and respond to these phenolic metabolites in root exudates, thus reprograming their transcriptome to produce microbial signals or to modify their behavior. This chemical dialogue between microbes and their hosts can enable their establishment on the root and initiate their mutualistic functioning. A well-known example for such semiochemical communication between roots and beneficial microbes is presented by symbiotic rhizobia, which can sense legume-derived flavonoids and produce nodulation factors that activate symbiosis signaling (Oldroyd, 2013; Zipfel and Oldroyd, 2017).

7. THESIS OUTLINE

Plants can form beneficial associations with selected members of their root microbiome. The establishment of beneficial associations requires a constant molecular dialogue between beneficial microbes and their hosts. The plant immune system can sense MAMPs of beneficial microbes and initiate immune responses that also affect microbiota in the rhizosphere. Thus, active immune modulation by beneficial microbes could be essential for the establishment of mutually beneficial plant-microbe associations in the rhizosphere. Root exudates also play a major role in shaping root microbiome. Well-adapted free-living rhizobacteria are likely recruited by root exudates and then rapidly alter their transcriptional profile to express features required for root colonization. In this thesis, we explored the interaction of *Arabidopsis* roots with selected root microbiome members to obtain a deep understanding of the molecular mechanisms that play a role in the chemical communication between plant roots and beneficial members of the root microbiome.

Beneficial rhizobacteria have been shown to suppress MTI responses in *Arabidopsis* roots (Millet et al., 2010; Lakshmanan et al., 2012; Stringlis et al., 2018a). In chapter 2, we studied root immune modulation by the ISR-eliciting rhizobacterium WCS358. We found that *pqqF* and *cyoB* are required for the suppression of flg22-induced expression of $CYP71A12_{pro}$*:GUS*, a marker for root immune activation. PqqF and CyoB are involved in the oxidation of glucose to gluconic acid, which lowers environmental pH in which the bacterium resides. A low pH was subsequently found sufficient to suppress root immune responses. Moreover, the mutation *pqqF* reduced the rhizosphere colonization by WCS358.

Arabidopsis roots synthesize and secrete fluorescent phenolic compounds in a MYB72/BGLU42-dependent manner when growing under iron deficiency (Zamioudis et al., 2014). In chapter 3, we aimed to reveal the identities of these MYB72-dependent metabolites and understand their role in root microbiome assembly. We found that both MYB72 and BGLU42 participate in the biosynthetic route of coumarins, which are dominantly present in the root exudates under iron deficiency. Coumarins can have selective antimicrobial activity but the ISR-eliciting rhizobacteria WCS417 and WCS358 were highly insensitive. We found that coumarin-deficient *f6'h1* mutant plants assembled a distinct root microbiome, indicating that coumarins can shape the root microbiome assembly.

WCS417 was found to induce root transcriptomic changes that overlap with the responses induced by iron deficiency (Zamioudis et al., 2015), but to what extent the root metabolome in response to WCS417 and iron starvation also show similarities is unclear. In chapter 4, we investigated the metabolic changes of *Arabidopsis* roots upon colonization by WCS417. We found that WCS417 strongly affects the root metabolome, and that production of the coumarins scopolin, scopoletin and esculin was increased. Aliphatic glucosinolate biosynthesis and fatty acid metabolism, both associated with root immune responses, also appeared to be induced by WCS417 in *Arabidopsis* roots.

Coumarins are produced in response to iron deficiency and WCS417 colonization (Chapter 3 and 4). However, nothing is known about how WCS417 responds to these coumarins. In chapter 5, we aimed to reveal the transcriptional responses of WCS417 to coumarins in root exudates of *Arabidopsis*. We found that transport and metabolism of carbohydrates, amino acids, and nucleotides were induced, while cell motility, the bacterial mobilome, and energy production and conversion were repressed by coumarin containing root exudates. Moreover, these root exudates repressed the expression of cell-motility related genes, likely by repressing flagellar biosynthesis.

In chapter 6, the results and the remaining questions are discussed. Future directions for further investigations of beneficial plant-microbe interactions are proposed.

CHAPTER 2

Plant-beneficial *Pseudomonas capeferrum* WCS358 suppresses root immune responses by lowering environmental pH

Ke Yu[1], Ramon Tichelaar[1], Niharika Savant[1], Sanne van Kuijk[1], Ellen Lagendijk[2], Corné M.J. Pieterse[1], Peter A.H.M. Bakker[1], Roeland L. Berendsen[1]

[1]Plant-Microbe Interactions, Institute of Environmental Biology, Utrecht University, Padualaan 8, 3584 CH Utrecht, The Netherlands
[2]Koppert B.V., 2650 AD Berkel en Rodenrijs, The Netherlands

ABSTRACT

Pseudomonas capeferrum WCS358 (hereafter WCS358) is a plant-beneficial root-colonizing bacterium, which can promote plant growth and protect the plant against attack by pathogens. Beneficial members of the root microbiome possess microbe-associated molecular patterns (MAMPs) similar to those of plant pathogens. Consequently, they can be recognized by plants through cell surface-localized pattern recognition receptors (PRRs), which can lead to the initiation of host immune signaling. Suppression of root immune responses is essential for beneficial microbes to successfully colonize the plant. In this study, we found that a range of rhizobacteria, including WCS358, is able to quench *Arabidopsis thaliana* root immune responses that were triggered by the synthetic MAMP flg22. By screening a transposon-insertion mutant library of WCS358 for the capacity to suppress flg22-induced *CYP71A12*$_{pro}$*:GUS* expression, we identified two mutants that had lost their ability to suppress MAMP-triggered root immune responses. The transposon insertions in these mutants were mapped to the genes *pqqF* and *cyoB*, which are involved in the production of gluconic acid and its derivative 2-keto gluconic acid. Both mutants are impaired in the production of these acids and reduced their extracellular pH to a lesser extent than wild-type WCS358. Lowering the pH of the plant growth medium suppressed flg22-induced *CYP71A12*$_{pro}$*:GUS* expression, suggesting a role for rhizobacterial gluconic acid-mediated modulation of the extracellular pH in the evasion of root immunity. Rhizosphere population densities of the *pqqF* mutant were significantly reduced compared to wild-type WCS358, suggesting that modulation of the root immune system is important for bacterial rhizosphere colonization.

INTRODUCTION

The complex microbial community that interacts with plant roots harbors harmful, commensal but also plant-beneficial organisms. These plant-beneficial microbes in the root microbiome can affect plant health by providing nutrients, enhancing stress tolerance, or by suppressing plant pathogens (Berendsen et al., 2012; Bakker et al., 2018). Their intimate contact with the host implies that beneficial microbes must interact with the plant immune system. The plant immune system has evolved to efficiently detect potential invaders by recognizing microbe-associated molecular patterns (MAMPs) through pattern recognition receptors (PRRs) localized on the cell surface (Macho and Zipfel, 2014). MAMPs are conserved molecules, such as bacterial flagellin and fungal chitin (Pel and Pieterse, 2013; Yu et al., 2017). Upon recognition, PRRs recruit regulatory receptor kinases and activate immune signaling through receptor-like cytoplasmic kinases (Macho and Zipfel, 2014; Boutrot and Zipfel, 2017). Despite recognizing specific MAMPs, multiple PRRs may activate convergent downstream immune signaling (Macho and Zipfel, 2014; Boutrot and Zipfel, 2017). The activated immune responses, known as MAMP-triggered immunity (MTI), aim to eliminate potential pathogenic invasions. Plant pathogens have evolved multiple strategies to suppress or evade plant immune responses. For example, the model bacterial plant-pathogen, *Pseudomonas syringae* pv *tomato* DC3000 (*Pst*), delivers effector proteins through the type 3 secretion system (T3SS) and produces other virulence factors such as coronatine, to disrupt downstream immune signaling upon MAMP recognition (Xin and He, 2013). Moreover, *Pst* prevents PRR recognition through extracellular degradation of MAMPs (Pel et al., 2014).

Since beneficial microbes possess MAMPs similar to those of pathogens, they are initially detected by the plant immune system and root immune responses are subsequently mounted (Libault et al., 2010; Jacobs et al., 2011; Zamioudis and Pieterse, 2012; Stringlis et al., 2018a). Induction of root immune responses can affect the establishment of

associations between plant roots and endophytic beneficial microbes. Synthetic MAMPs have been widely used to investigate plant innate immune responses, such as flg22, a 22 amino acid peptide which represents the conserved domain in the N-terminal of flagellin protein derived from the opportunistic pathogen *Pseudomonas* aeruginosa PAO1 (Felix et al., 1999). For example, root immune responses triggered by the synthetic MAMP flg22 negatively affected rhizobial infection and nodule organogenesis in *Lotus japonicus* (Lopez-Gomez et al., 2012). In the *Arabidopsis thaliana* (hereafter *Arabidopsis*) mutant *pub22/23/24* that displays hyperactivated MTI upon chitin application, the beneficial fungus *Piriformospora indica* only achieved significantly less colonization (Jacobs et al., 2011). In successful beneficial associations, however, root immune responses seem to be restricted to the early stages of the interaction (Liu et al., 2003; Libault et al., 2010; Jacobs et al., 2011; Stringlis et al., 2018a). For root-invading beneficial microbes, such as rhizobia or arbuscular mycorrhiza, it is becoming increasingly clear that many of them actively suppress early root immune responses through evasion of apoplastic recognition or deactivation of cytoplasmic signaling (Kloppholz et al., 2011; Xin et al., 2012; Liang et al., 2013; Plett et al., 2014; Trda et al., 2014; Akum et al., 2015; Wawra et al., 2016). The importance of immune suppression for microbiome members that colonize the root surface and the rhizosphere, however, has not been studied in detail.

The plant hormones salicylic acid (SA) and jasmonic acid (JA), are central regulators of plant immune signaling (Pieterse et al., 2012). Both SA- and JA-dependent immune responses can affect root microbial communities, possibly through altering root exudate composition (Carvalhais et al., 2013; Carvalhais et al., 2015; Lebeis et al., 2015). In a recent study it was shown that downy mildew infection of *Arabidopsis* leaves results in the promotion of specific rhizosphere microbiota, that in turn promote plant growth and protect the plant against downy mildew infection (Berendsen et al., 2018). Together these findings indicate that the plant immune system indeed affects the composition of the root microbiome. Vice versa, it is known that specific rhizosphere colonizers can elicit a state of induced systemic resistance (ISR), which primes the plant immune system for accelerated defense against a range of microbial and insect attackers (Van der Ent et al., 2008; Kumar et al., 2012; Pieterse et al., 2014). The ISR-eliciting rhizobacteria *P. simiae* WCS417 (hereafter WCS417) and *Bacillus subtilis* FB17 were found to be able to suppress root immune responses (Millet et al., 2010; Lakshmanan et al., 2012). We hypothesize that suppression of root immune responses facilitates rhizosphere colonization by beneficial rhizobacteria.

In this study, we investigated the suppression of flg22-triggered root immune responses by rhizosphere inhabitants. To this end, we made use of the *Arabidopsis CYP71A12*$_{pro}$*:GUS* reporter line, which displays GUS activity in the root elongation zone in response to the synthetic MAMP flg22 (Millet et al., 2010). We found that the ability to suppress flg22-triggered root immune responses is widespread but not a ubiquitous trait among rhizosphere colonizers. To examine the mechanism of suppression of root immune responses, we screened a transposon-insertion mutant library of *Pseudomonas capeferrum* WCS358 (hereafter WCS358) for the loss of this ability. WCS358 is a plant-beneficial rhizobacterium that elicits ISR in *Arabidopsis* for which bacterial determinants involved in ISR elicitation have been investigated in detail (Meziane et al., 2005; Bakker et al., 2007). We discovered that WCS358 produces gluconic acid (GA) and 2-keto gluconic acid (2-KGA) to lower its environmental pH, and that this acidification suppresses root immune responses. A mutant of WCS358 impaired in GA and 2-KGA production reached significantly lower population densities in *Arabidopsis* rhizosphere than the wild-type strain, suggesting that suppression of root immune responses is required for effective rhizosphere colonization by this beneficial bacterium.

RESULTS

The ISR-eliciting rhizobacteria WCS417 and WCS358 both suppress root immune responses

To visualize MAMP-induced root immune responses, we employed three *Arabidopsis* transgenic lines carrying β-glucuronidase (GUS) reporters *CYP71A12$_{pro}$:GUS*, *MYB51$_{pro}$:GUS* and *WRKY11$_{pro}$:GUS.* All three reporter lines display high GUS activity in the root elongation zone when treated with the flg22 epitope (Figure 1A; Denoux et al., 2008; Millet et al., 2010). To test the effect of plant-beneficial rhizobacteria on flg22-induced root responses, we pre-inoculated roots of *Arabidopsis* seedlings with WCS417 and WCS358 bacteria 18 hours prior to treatment of the roots with flg22. We found that live bacterial cells of WCS417 and WCS358, which possess immune-eliciting flagellin, did not induce GUS expression in the

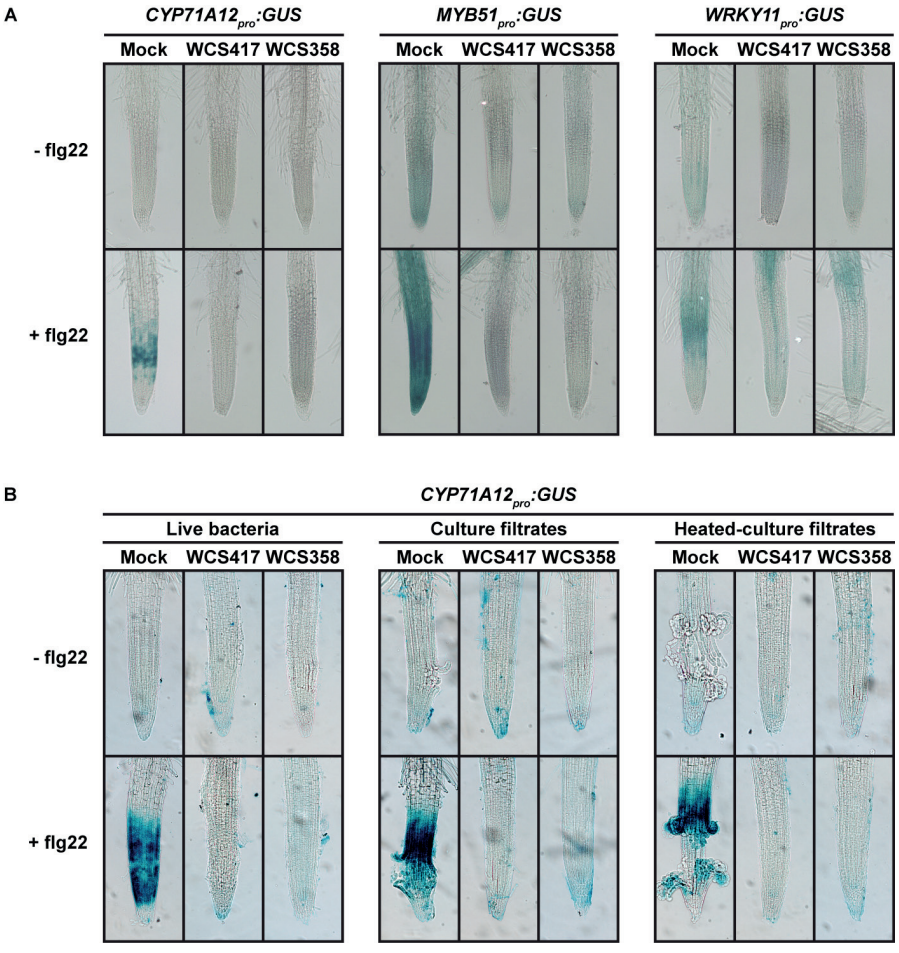

Figure 1. *Pseudomonas* strains WCS417 and WCS358 suppress flg22-induced immune responses in *Arabidopsis* roots. (A) Effects of WCS417 and WCS358 on flg22-induced *CYP71A12$_{pro}$:GUS*, *MYB51$_{pro}$:GUS* and *WRKY11$_{pro}$:GUS* expression in the root elongation zone of *Arabidopsis* seedlings. **(B)** Effects of live bacterial cells, culture filtrates, and heat-treated culture filtrates of WCS417 and WCS358 on flg22-induced *CYP71A12$_{pro}$:GUS* expression in the root elongation zone.

root elongation zone (Figure 1A). Moreover, both WCS417 and WCS358 suppressed flg22-induced *CYP71A12*$_{pro}$*:GUS* expression in the root elongation zone (Figure 1A), supporting previous findings (Millet et al., 2010). Filter-sterilized culture filtrates of WCS417 and WC358 similarly suppressed flg22-induced *CYP71A12*$_{pro}$*:GUS* expression (Figure 1B), indicating that the immune-suppressive compounds are secreted into the culture medium. Moreover, heat-treatment of the culture filtrates did not affect the ability to suppress flg22-induced *CYP71A12*$_{pro}$*:GUS* expression (Figure 1B), suggesting that the immune- suppressive compounds produced by WCS417 and WCS358 are not proteinaceous.

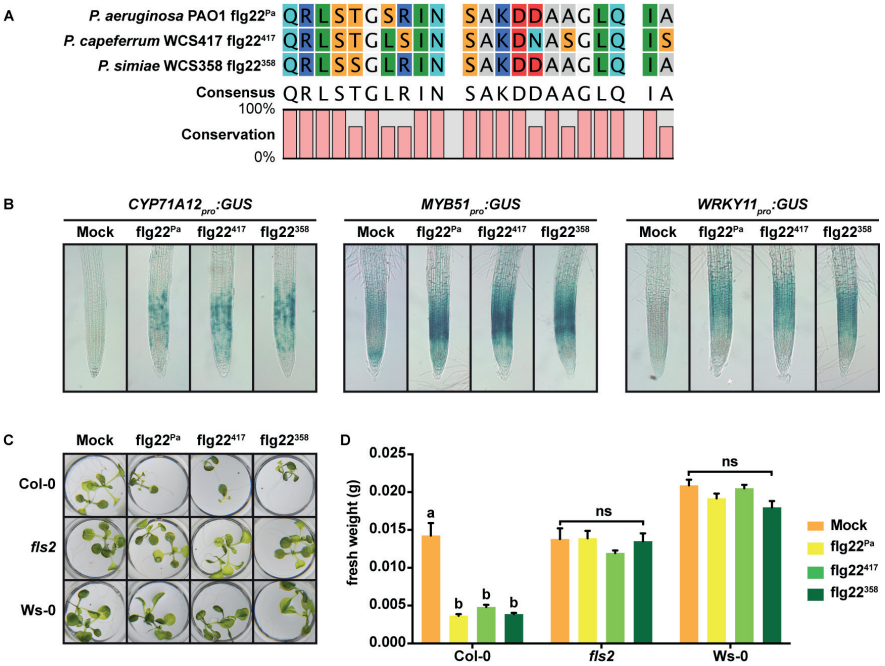

Figure 2. Flg22 epitopes derived from *Pseudomonas* strains WCS417 and WCS358 induce defense responses in *Arabidopsis thaliana*. (A) Sequence alignment of flg22 epitopes derived from *P. aeruginosa* PAO1 (flg22^{Pa}), *P. simiae* WCS417 (flg22^{417}) and *P. capeferrum* WCS358 (flg22^{358}). **(B)** Effects of flg22^{Pa}, flg22^{417} and flg22^{358} on *CYP71A12*$_{pro}$*:GUS*, *MYB51*$_{pro}$*:GUS* and *WRKY11*$_{pro}$*:GUS* expression in the root elongation zone of *Arabidopsis* seedlings. **(C)** Effects of flg22^{Pa}, flg22^{417} and flg22^{358} peptides on growth of Col-0, *fls2* and Ws-0 seedlings. **(D)** Fresh weight of *Arabidopsis* seedlings shown in **(C)**. The data shown are means of five replicates. Error bars represent SEM. Letters indicate significant differences (One-way ANOVA followed by Tukey's test; $P < 0.05$; ns, not significant).

Only a small subset of *Arabidopsis*-associated microbiota possess genes that encode the flg22 epitope (Hacquard et al., 2017) and examples of plant-beneficial bacteria that have evolved divergent flagellin molecules to evade immune recognition in their hosts have been described (Lopez-Gomez et al., 2012; Trda et al., 2014). The flg22 epitopes derived from WCS417 (flg22^{417}) and WCS358 (flg22^{358}) are distinct from each other as well as from the standard flg22 derived from *P. aeruginosa* PAO1 (flg22^{Pa}, Figure 2A). We therefore tested if these divergent flg22 epitopes could still activate root immune responses. After incubation with flg22^{Pa}, flg22^{417}, or flg22^{358}, all three reporter lines showed clear GUS expression in the root elongation zone (Figure 2B). Because activation of MAMP-triggered immune responses can severely inhibit plant growth through growth-defense tradeoffs (Vos et al., 2013; Huot et al., 2014), we tested whether flg22^{417} and flg22^{358} from the plant growth-

promoting rhizobacteria would act differently than flg22^{Pa} in this respect. However, flg22^{417} and flg22^{358} inhibited the growth of Col-0 seedlings to the same extent as flg22^{Pa}, while all flg22 peptides did not affect growth of *fls2* and Ws-0 seedlings that lack the flagellin receptor FLS2 (Figure 2C and 2D; Gomez-Gomez and Boller, 2000). Thus, both flg22^{Pa} and the flg22 epitopes derived from the beneficial rhizobacteria are recognized by *Arabidopsis* and induce root immune responses in a FLS2-dependent manner, which is in concordance with previous findings (Millet et al., 2010; Stringlis et al., 2018a). We therefore routinely only used flg22^{Pa} (hereafter referred to as flg22) in the following experiments.

Table 1. Screening of 28 rhizobacterial isolates of diverse taxonomy for their abilities to induce and suppress immune responses in *Arabidopsis* roots.

Isolate ID	Taxonomy	*CYP71A12$_{pro}$:GUS* expression	
		Bacteria only	Bacteria + flg22
P. simiae WCS417	*Pseudomonas*	-	-
WCS2014-257	*Actinomycetales*	-	+
WCS2014-89	*Agrobacterium*	-	-
WCS2014-170	*Arhtrobacter*	-	+
WCS2014-243	*Bosea*	-	+
WCS2014-69	*Brevundimonas*	-	-
WCS2014-409	*Burkholderia*	-	-
WCS2014-70	*Caulobacter*	-	-
WCS2014-238	*Chitinophaga*	-	-
WCS2014-255	*Comamonadaceae*	-	+
WCS2014-209	*Cupriavidus*	-	-
WCS2014-166	*Dyadobacter*	-	+
WCS2014-2	*Flavobacterium*	-	-
WCS2014-35	*Herbaspirillum*	-	+
WCS2014-110	*Masilia*	+	+
WCS2014-259	*Microbacterium*	+	+
WCS2014-80	*Mycoplana*	+	+
WCS2014-302	*Ochrobactrum*	-	+
WCS2014-273	*Oxalobacteraceae*	-	+
WCS2014-3	*Pedobacter*	-	-
WCS2014-226	*Phyllobacterium*	-	+
WCS2014-247	*Polaromonas*	-	+
WCS2014-9	*Pseudomonas*	-	-
WCS2014-8	*Rhizobium*	-	+
WCS2014-387	*Sphingobium*	-	+
WCS2014-113	*Stenotrophomonas*	+	+
WCS2014-272	*Terrabacter*	-	-
WCS2014-5	*Variovorax*	-	+
WCS2014-20	*Xanthomonas*	+	+

[1]A positive blue staining in the root elongation zone of *CYP71A12$_{pro}$:GUS Arabidopsis* seedlings inoculated with the bacterial isolates in presence or absence of flg22 was scored with "+". [2]*P. simiae* WCS417 was used as a positive control.

Diverse rhizobacteria suppress flg22-induced immune responses in *Arabidopsis* roots

To investigate whether the ability to suppress root immune responses is a general phenomenon among different members of the root microbiome, we screened 28 taxonomically-diverse bacterial strains isolated from the *Arabidopsis* rhizosphere (Berendsen et al., 2018) for their effects on *CYP71A12$_{pro}$:GUS* expression in the root elongation zone in the presence or absence of flg22. In the absence of flg22, the majority of rhizobacterial strains did not induce *CYP71A12$_{pro}$:GUS* expression, suggesting that these bacteria avoid MAMP-triggered immune responses in the roots (Table 1). However, five bacterial strains, belonging to the genera *Masilia*, *Microbacterium*, *Mycoplana*, *Stenotrophomonas* and *Xanthomonas* respectively, did induce *CYP71A12$_{pro}$:GUS* expression in the absence of flg22, indicating that they are able to trigger root immune responses. In the presence of flg22, 10 of the 28 bacterial strains tested, belonging respectively to the genera *Agrobacterium*, *Brevundimonas*, *Burkholderia*, *Caulobacter*, *Chitinophaga*, *Cupriavidus*, *Flavobacterium*, *Pedobacter*, *Pseudomonas*, and *Terrabacter,* suppressed flg22-induced *CYP71A12$_{pro}$:GUS* expression in the root elongation zone. Together, these results indicate that the rhizosphere microbiome contains members that are capable of activating MTI in plant roots, but also a large diversity of microbiota members that actively suppress it.

Root immune suppression mediated by WCS358 is independent of SA and JA signaling

To test whether root immune suppression mediated by WCS358 relies on the SA or JA signaling pathway, we used transgenic lines carrying the *CYP71A12$_{pro}$:GUS* reporter in the wild-type Col-0 background as well as in the SA or JA hormonal signaling-deficient mutant backgrounds of *sid2-2*, *npr1-1*, *jar1-1* and *jin1-7* (Millet et al., 2010). We pre-inoculated *Arabidopsis* seedlings with WCS358 to test the immune-suppressive effect on flg22-induced *CYP71A12$_{pro}$:GUS* expression in the roots of the different mutants. In the absence of WCS358, all mutant lines showed clear *CYP71A12$_{pro}$:GUS* expression in the root elongation zone in responses to flg22 treatment (Figure 3A), confirming previous findings (Millet et al., 2010). Like in the wild-type Col-0 background, colonization of the roots of the hormonal signaling-deficient mutants by WCS358 did not induce *CYP71A12$_{pro}$:GUS* expression in the root elongation zone, and suppressed *CYP71A12$_{pro}$:GUS* expression when elicited by flg22 (Figure 3). These results indicate that the suppression of root immune responses mediated by plant-beneficial rhizobacterium WCS358 is not regulated by these defense-related hormones.

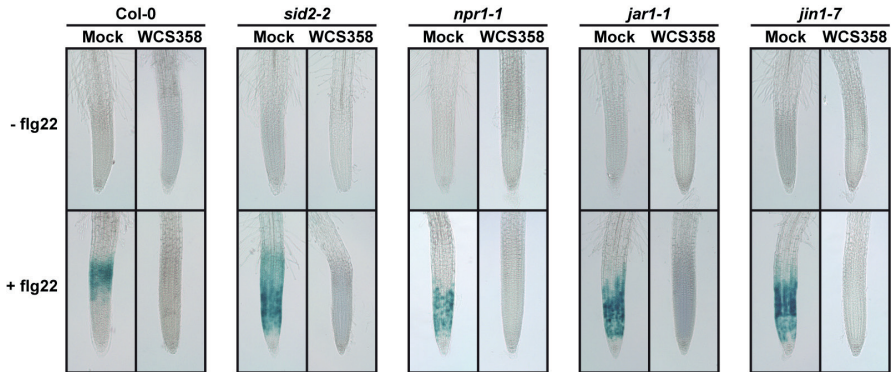

Figure 3. WCS358 suppresses flg22-induced immune responses in *Arabidopsis* roots in a SA/JA-independent manner. Effects of WCS358 on flg22-induced *CYP71A12$_{pro}$:GUS* expression in the root elongation zone of wild-type and the hormonal signaling-deficient mutants *sid2-2, npr1-1, jar1-1* and *jin1-7*.

Root immune suppression mediated by WCS358 requires PqqF and CyoB

To investigate the bacterial determinants of WCS358-mediated root immune suppression, we generated a mini-Tn5 transposon insertion mutant library of WCS358 and screened it for mutants that failed to suppress flg22-induced *CYP71A12*$_{pro}$*:GUS* expression in the root elongation zone. We screened more than 4000 mutants and found over 120 mutants that did not suppress *CYP71A12*$_{pro}$*:GUS* expression in the initial screen. When repeatedly tested only 32 of these mutant were found consistently unable to suppress flg22-induced *CYP71A12*$_{pro}$*:GUS* expression. Moreover, out of those 32, the growth of 30 mutants was severely impaired when cultivated in root exudates. Thus, only 2 mutants remained for further investigation. Arbitrary PCR mapped the Tn5 transposon insertion sites in the remaining 2 mutants to two genes: *pqqF* and *cyoB*. Like wild-type WCS358, neither mutant *pqqF*::Tn5 nor mutant *cyoB*::Tn5 induced *CYP71A12*$_{pro}$*:GUS* expression in the absence of flg22 (data not shown). But in contrast to WCS358, both mutants were unable to suppress flg22-induced *CYP71A12*$_{pro}$*:GUS* expression in the root elongation zone (Figure 4A). The growth of both mutants in root exudates was in the same order and even significantly increased compared to wild-type WCS358 (Figure 4B). PqqF is a putative protease belonging to M16 peptidases required for the pyrroloquinoline quinone (PQQ) biosynthesis (Wei et al., 2016). PQQ is a redox active molecule, functioning as a cofactor for many bacterial dehydrogenases involved in the utilization of carbon sources (Shen et al., 2012). CyoB is the subunit I of terminal ubiquinol cytochrome *bo*$_3$ oxidase (CYO) complex, a macromolecular protein embedded in the cytoplasmic membrane (Stenberg et al., 2007). CYO functions in the aerobic respiratory chain for energy generation and regulates the expression of genes involved in the utilization of carbon sources (Morales et al., 2006). The results suggest that both PqqF and CyoB are essential in the root immune suppression mediated by WCS358.

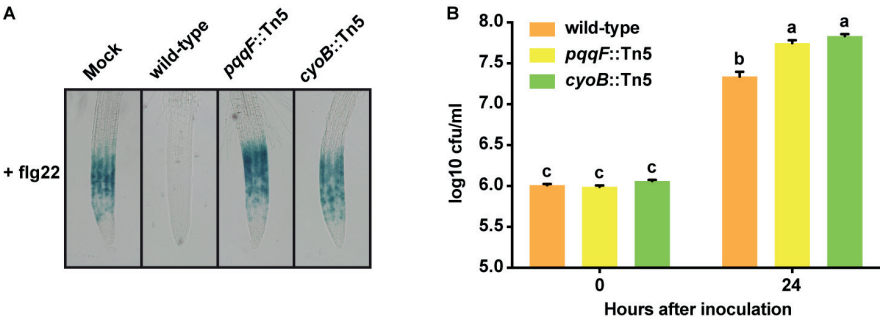

Figure 4. Screening of a transposon mutant library of WCS358 for loss of suppression of flg22-induced immune responses in *Arabidopsis* roots. (A) Effects of wild-type WCS358 and its derivatives *pqqF*::Tn5 and *cyoB*::Tn5 on flg22-induced *CYP71A12*$_{pro}$*:GUS* expression in the root elongation zone. **(B)** Growth of wild-type WCS358 and its derivatives *pqqF*::Tn5 and *cyoB*::Tn5 in root exudates of *Arabidopsis* seedlings. The data shown are means of eight replicates. Error bars represent SEM. Letters indicate significant difference (Two-way ANOVA followed by Tukey's test; $P < 0.05$).

Root immune suppression mediated by WCS358 relies on gluconic acid production

Since WCS358 can suppress root immune responses by releasing diffusible compounds (Figure 1B), we tested the effects of culture filtrates derived from WC358 and its derivatives *pqqF*::Tn5 and *cyoB*::Tn5 on flg22-induced *CYP71A12*$_{pro}$*:GUS* expression in the root elongation zone. We found that whereas culture filtrates from wild-type WCS358 suppressed flg22-induced *CYP71A12*$_{pro}$*:GUS* expression, culture filtrates from both the *pqqF*::Tn5 *and cyoB*::Tn5

mutants failed to suppress this response (Figure 5A), suggesting that the production of the immune-suppressive diffusible compounds is impaired in both mutants.

PQQ and CYO play important roles in bacterial glucose metabolism, resulting in production of D-gluconic acid (GA) and 2-keto-D-gluconic (2-KGA; Fender et al., 2012). We analyzed all bacterial filtrates, as well as that of model ISR-eliciting rhizobacterial strain *P. simiae* WCS417, by using ultra-performance liquid chromatography - mass spectrometry (UPLC-MS) to detect the production of GA and 2-KGA. We found that wild-type WCS358 produced both GA and 2-KGA (Figure 5B). Mutation of *pqqF* completely abolished the production of both GA and 2-KGA, whereas mutation of *cyoB* moderately reduced the

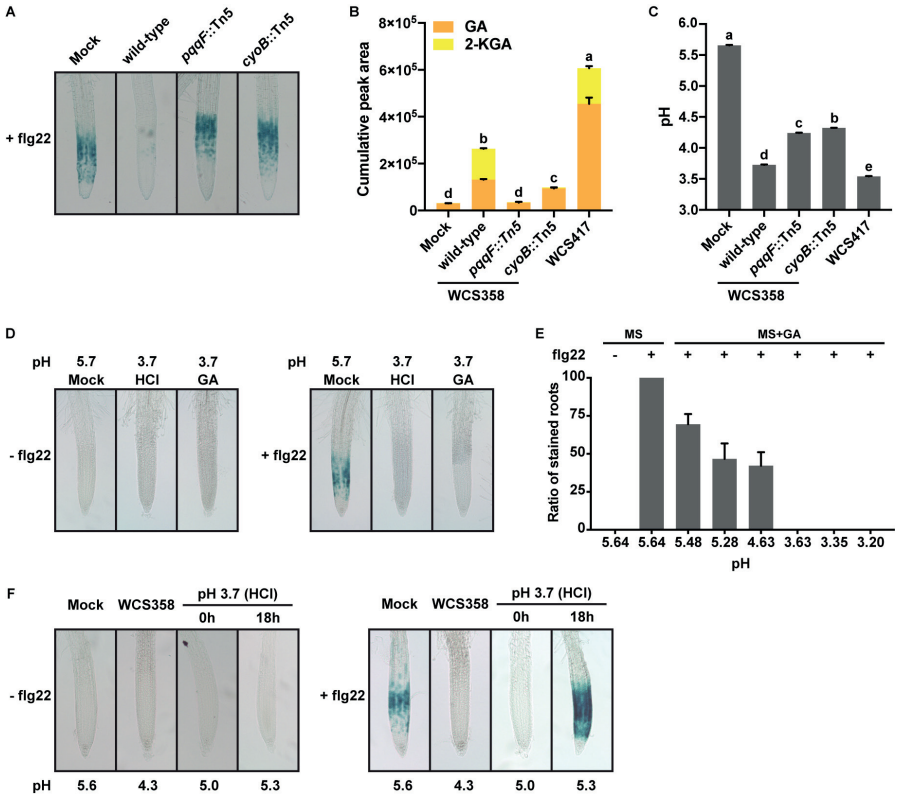

Figure 5. WCS358 suppresses flg22-induced immune responses in *Arabidopsis* roots by producing GA and 2-KGA. (A) Effects of sterile culture filtrates derived from wild-type WCS358 and its derivatives *pqqF*::Tn5 and *cyoB*::Tn5 on flg22-induced *CYP71A12*$_{pro}$*:GUS* expression in the root elongation zone. **(B)** HPLC-MS measurement of GA and 2-KGA shown as the cumulative peak area (GA + 2-KGA) of mass spectra detected in 2 channels on a UPLC-MS in negative ionization mode. **(C)** Acidity in the culture filtrates derived from wild-type WCS358, its derivatives *pqqF*::Tn5 and *cyoB*::Tn5 and WCS417. The data shown in **B** and **C** are means of three replicates. Error bars represent SEM. Letters indicate significant differences (One-way ANOVA followed by Tukey's test; $P < 0.05$). **(D)** Effects of low environmental pH on flg22-induced *CYP71A12*$_{pro}$*:GUS* expression in the root elongation zone. HCl and GA was used to adjust the pH of root exudates to 3.7. **(E)** Effects of a pH gradient on flg22-induced *CYP71A12*$_{pro}$*:GUS* expression in the root elongation zone. Ratio of root tips with *CYP71A12*$_{pro}$*:GUS* expression as a percentage of total root tips. The data shown are means of three replicates. Error bars represent SEM. **(F)** Effects of pre-incubation in low environmental pH on flg22-induced *CYP71A12*$_{pro}$*:GUS* expression in the root elongation zone. Under each picture the pH shown was measured at the time before GUS staining.

production of GA and abolished the production of 2-KGA (Figure 5B). Notably, WCS417 produced significantly higher amount of GA than wild-type WCS358 (Figure 5B). Production of these organic acids can substantially decrease extracellular pH (Fender et al., 2012). Indeed, the pH of culture filtrates from wild-type WCS358 was significantly lower (pH 3.7) than that of culture filtrates derived from *pqqF*::Tn5 or *cyoB*::Tn5 mutants (pH 4.2 and 4.3, respectively; Figure 5C), suggesting that WCS358 acidifies its extracellular environment through the production of GA and 2-KGA. The pH of culture filtrates derived from WCS417 is the lowest among all tested samples (pH 3.5), which is consistent with higher production of GA and 2-KGA by this strain (Figure 5B and 5C). The magnitude of flg22-induced immune responses in *Arabidopsis* changes dramatically when environmental pH varies (Lee et al., 2012). We therefore hypothesized that WCS358 may suppress root immune responses by acidifying its environment through the production of GA and 2-KGA and examined how the pH of the plant growth medium affects flg22-induced $CYP71A12_{pro}$*:GUS* expression in the root elongation zone. When the pH of the medium was adjusted to 3.7 by adding either HCl or GA, flg22-induced $CYP71A12_{pro}$*:GUS* expression was completely abolished (Figure 5D). However, at pH 4.6 or higher $CYP71A12_{pro}$*:GUS* expression was still induced by flg22 (Figure 5E). We noticed however that the timing of adjusting the pH is crucial. Only when the pH was modified immediately before addition of flg22 did we find the effects of pH on $CYP71A12_{pro}$*:GUS* expression described above (Figure 5F). When pH of the plant growth medium was modified to pH 3.7 at 18 h before application of flg22, we found that pH of growth medium was restored to 5.3 and resulted in expression of $CYP71A12_{pro}$*:GUS* in the root elongation zone (Figure 5F), suggesting that plants actively modify the environmental acidity.

Mutations in *pqqF* or *cyoB* do not affect plant growth promotion by WCS358

Colonization of *Arabidopsis* roots by WCS358 promotes plant growth and modulates root architecture *in vitro* (Zamioudis et al., 2013). We assessed whether *pqqF*::Tn5 *and cyoB*::Tn5 mutants, which failed to suppress flg22-induced root immune responses, could promote the growth and modulate the root architecture like the wild-type bacterium. We inoculated wild-type WCS358, *pqqF*::Tn5 or *cyoB*::Tn5 directly on the roots of *Arabidopsis* seedlings, and used shoot fresh weight and the numbers of lateral roots as indexes of growth promotion and root architecture modulation (Zamioudis et al., 2013). The wild-type WCS358, as well as

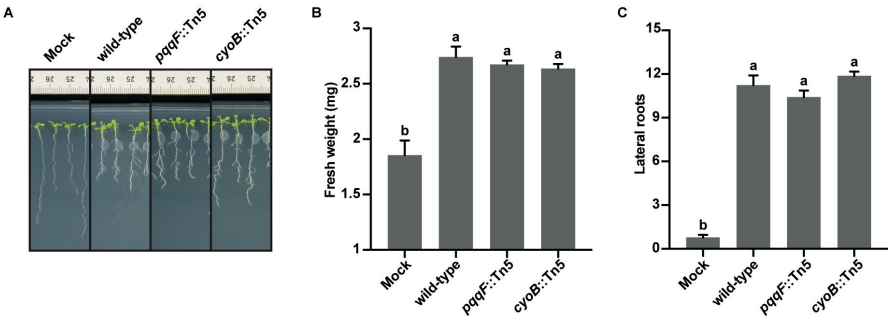

Figure 6. Mutations in *pqqF* or *cyoB* do not affect plant growth promotion by WCS358 *in vitro*. (A) Effects of wild-type WCS358 and its derivatives *pqqF*::Tn5 and *cyoB*::Tn5 on growth of *Arabidopsis* seedlings. **(B)** Plant fresh weight and **(C)** number of lateral roots of *Arabidopsis* seedlings shown in A. The data shown in B and C are means of three replicates. Error bars represent SEM. Letters indicate significant difference (One-way ANOVA followed by Tukey's test; $P < 0.05$).

both *pqqF*::Tn5 or *cyoB*::Tn5 mutants, promoted *Arabidopsis* growth to a similar extent at 6 days after inoculation (Figure 6A and 6B). Moreover, there was no significant difference in the numbers of lateral roots formed by *Arabidopsis* roots upon inoculation with wild-type WCS358 or its mutant derivatives (Figure 6A and 6C), indicating that mutations in *pqqF* or *cyoB* had no effect on the growth promotion and root architecture modulation ability of WCS358.

Mutation in *pqqF* impairs rhizosphere colonization by WCS358

Activation of the root immune system can affect rhizosphere microbiome assembly (Carvalhais et al., 2013; Carvalhais et al., 2015; Lebeis et al., 2015; Liu et al., 2017; Berendsen et al., 2018; Yuan et al., 2018). Consequently, we hypothesized that root immune suppression is required for successful colonization by rhizobacteria and expected the WCS358 derivatives *pqqF*::Tn5 *and cyoB*::Tn5 to have a diminished capability to colonize the *Arabidopsis* rhizosphere compared to wild-type WCS358. We transferred *Arabidopsis* seedlings to potting soil, which was pre-inoculated with wild-type WCS358, *pqqF*::Tn5 or *cyoB::*Tn5 with an initial population density of $10^{4.6\pm0.1}$ colony-forming units (CFU) g^{-1} of soil. Without a plant to support their growth, the population densities of all three strains declined over time to a similar extent (Figure 7A). In the *Arabidopsis* rhizosphere, population densities of wild-type WCS358 and the *cyoB*::Tn5 mutant significantly increased over a two-week period. However, the population density of *pqqF*::Tn5 did not increase over time (Figure 7B), suggesting that the mutation in *pqqF*, but not in *cyoB*, negatively affects rhizosphere colonization of WCS358.

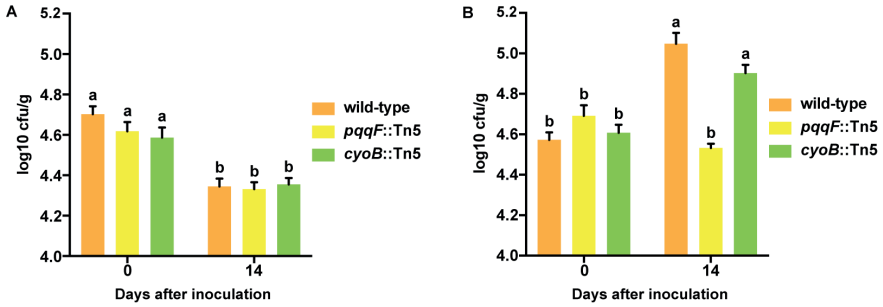

Figure 7. Mutation in *pqqF*, but not in *cyoB*, impairs rhizosphere colonization by WCS358. (A) Population densities of wild-type WCS358 and its derivatives *pqqF*::Tn5 and *cyoB*::Tn5 in unplanted bulk soil and **(B)** *Arabidopsis* rhizosphere. The y-axis shows the $\log_{10}$ of colony-forming units (CFU) g^{-1} of bulk soil in A and *Arabidopsis* rhizosphere in B. The data shown are means of eight replicates. Error bars represent SEM. Letters indicate significant difference (Two-way ANOVA followed by Tukey's test; $P < 0.05$).

DISCUSSION

The plant immune system can affect microbial communities in the endophytic compartment of roots as well as in the rhizosphere (Carvalhais et al., 2013; Carvalhais et al., 2015; Lebeis et al., 2015; Liu et al., 2017; Berendsen et al., 2018; Yuan et al., 2018). For some beneficial rhizosphere-colonizing bacteria it was shown that they can suppress root immune responses (Millet et al., 2010; Lakshmanan et al., 2012; Stringlis et al., 2018a) and such manipulation may affect their root colonizing abilities. However, whether suppression of root immune responses is required for successful rhizosphere colonization or how rhizosphere-colonizing bacteria suppress root immune responses is largely unknown. In this study, we observed

that the plant-beneficial rhizobacterium *P. capeferrum* WCS358, suppresses flg22-induced root immune responses. In this immune-suppressive activity, it behaves similarly to *P. simiae* WCS417 in that live cells, culture filtrates, and heat-treated culture filtrates similarly suppress the flg22-induced responses. To elucidate the microbial traits that govern suppression of root immune responses, we screened a random Tn5 transposon mutant library of WCS358. Two mutants were identified that had lost their ability to suppress root immune responses. The transposon insertions were mapped to two genes, *cyoB* and *pqqF,* that are both involved in the production of GA and 2-KGA and it was demonstrated that the mutants are indeed impaired in the production of these acids. Consequently, the mutants acidify their environment much less than wild-type WCS358 and it was postulated that a shift in pH can modulate the root immune response to flg22 treatment. Indeed, lowering the pH of the plant growth medium to the same level that was brought about by the wild-type bacterium was sufficient to suppress flg22-induced root immune responses. Together these results suggest that WCS358 suppresses root immune responses by increasing the acidity of the environment surrounding the roots. The observation that WCS417 also produces GA and 2-KGA and that it lowers pH of the plant growth medium suggest that, like WCS358, strain WCS417 similarly suppresses flg22-induced root immune responses by changing environmental pH.

Plant immune responses induced by flg22 have previously been found to be dependent on environmental pH, although the mechanism has not been clarified (Lee et al., 2012). We noticed that, when *Arabidopsis* seedlings were incubated in MS growth medium with an initial pH of 3.7, the plants elevated the pH of the growth medium to a pH of 5.3 and regained their responsiveness to flg22 after 18 hours. A notable cellular event following the FLS2-mediated immune recognition of flg22 is the rapid extracellular alkalization process (Navarro et al., 2004). It seems plausible that bacterial acidification of the root exterior interferes with the flg22-induced alkalization process, thus preventing or buffering the initiation of downstream immune signaling. Again, however, flg22-induced *CYP71A12*$_{pro}$*:GUS* expression is still observed in the cotyledons of *sid2-2* in the presence of WCS358 (data not shown), implying that this pH-dependent suppression only takes place in the root.

Many fungi modulate the pH of their environment by secreting organic acids, ammonia or regulatory peptides and modulation of environmental pH is often required by pathogenic fungi to conquer their hosts (Masachis et al., 2016; Vylkova, 2017). Notably, GA-mediated acidification was found to regulate the expression of virulence factors in the apple pathogen *Penicillium expansum*, thus enhancing its aggressiveness (Barad et al., 2016). Despite the fact that also rhizobacteria are commonly found to affect environmental pH (Fender et al., 2012; Cheng et al., 2015; Poitout et al., 2017), little is known about the function of this process in modulating host immune responses. Although several studies have shown that activation of root immune responses impaired the establishment of beneficial associations with endophytically living microbes (Jacobs et al., 2011; Lopez-Gomez et al., 2012), there is little evidence showing that root immune suppression is required for rhizosphere microbes to achieve successful colonization. In this study, we found that one mutant that failed to suppress flg22-induced root immune responses, *pqqF*::Tn5, had lost its ability to colonize *Arabidopsis* rhizosphere. However, the other mutant, *cyoB*::Tn5, was not significantly affected in rhizosphere competence, although it also failed to suppress flg22-induced root immune responses. It could be argued that this is because of the residual GA production by this mutant. It is likely that in the rhizosphere the microbial regulation of GA and 2-KGA production is different from that of bacteria growing *in vitro*. It is known that e.g. under conditions of phosphate stress or conditions when glucose is the sole source of carbon, *Pseudomomas putida* KT2440 produces more GA in a PQQ-dependent manner to assist

phosphate uptake (An and Moe, 2016). Specific rhizosphere conditions might therefore determine to what extent each mutant can still suppress root immune responses. We speculate that root immune responses activated by *pqqF*::Tn5 limited the initial attachment and early accumulation of the mutant on the root surface, whereas the suppressed root immune responses allowed the proliferation of the wild-type. Alternatively, *pqqF*::Tn5 could be impaired in its rhizosphere competence and be outcompeted by other microbes. However, the fact WCS358 and its derivatives survive equally well in unplanted soil, indicates that the plants are favoring wild-type WCS358 over *pqqF*::Tn5 in the rhizosphere. To demonstrate that it is the activation of root immune responses that affect the rhizosphere colonization by *pqqF*::Tn5, we are currently investigating the colonization by WCS358 and its derivatives on immune-deficient *Arabidopsis* mutants.

In addition to *Pseudomonas* spp., we found that representatives of several bacterial genera, isolated from the *Arabidopsis* rhizosphere, can suppress flg22-induced root immune responses. This indicates that the ability to quench root immune responses is shared among a taxonomically-diverse group of microbes, but it is not ubiquitous. However, we also observed that some rhizobacteria strongly elicit root immune responses, indicating that MAMPs derived from these bacteria trigger immune responses and these bacteria are not able to suppress them. It is not clear how those rhizobacteria are affected by the root immune responses triggered by themselves. Moreover, in a natural situation, roots are colonized by a plethora of different microbes simultaneously and it is intriguing to speculate how microbe-suppressed immune responses affect the non-suppressing organisms in close proximity of the suppressing organism. Plants can shape the composition and functions of their root microbiome via the immune system (Mendes et al., 2011; Carvalhais et al., 2013; Carvalhais et al., 2015; Lebeis et al., 2015; Castrillo et al., 2017; Berendsen et al., 2018; Yuan et al., 2018). For example, selected members of the root microbiome can protect plants against pathogen attack and enhance phosphate stress responses as well as iron deficiency responses (Mendes et al., 2011; Zamioudis et al., 2015; Castrillo et al., 2017; Verbon et al., 2017; Berendsen et al., 2018). Intriguingly, *Arabidopsis* plants were found to coordinate their investments in different microbiome functions and for instance to prioritize phosphate stress responses over immune responses through the activity of PHR1, a transcription factor positively regulating nutritional stress while negatively regulating immunity (Castrillo et al., 2017; Bakker et al., 2018). This interplay between immune responses and nutritional stress was also observed for plants growing in the presence of beneficial rhizobacteria (Zamioudis et al., 2015). Specific members of the root microbiome activate MYB72, a transcription factor involved in both the ISR signaling and iron deficiency responses (Van der Ent et al., 2008; Zamioudis et al., 2014; Zamioudis et al., 2015; Verbon et al., 2017). Since the rhizosphere is a MAMP-rich environment, the tight regulation of root immune responses is vital to avoid constitutive activation of immunity. Thus, the health of a plant may be the result of balanced regulation of the root immune responses by different members in the microbiome, as well as the controlled investment of energy based on nutrition and immune conditions.

MATERIALS AND METHODS

Plant materials

In this study, we used the *Arabidopsis thaliana* wild-type accessions Col-0 and Ws-0, and Col-0 mutant *fls2* (Gomez-Gomez and Boller, 2000). Additionally, we used GUS reporter lines *CYP71A12*$_{pro}$*:GUS, MYB51*$_{pro}$*:GUS* and *WRKY11*$_{pro}$*:GUS* in Col-0 background, and

CYP71A12$_{pro}$*:GUS* in the background of Col-0 mutants s*id2-2*, *npr1-1*, *jar1-1* and *jin1-7* (Millet et al., 2010). All *Arabidopsis* GUS reporter lines were kindly provided by Dr. Frederick M. Ausubel (Harvard Medical School, Boston, MA). For experiments performed in *vitro*, *Arabidopsis* seeds were surface sterilized for 4 hours with chlorine gas in a bell jar containing a beaker filled with 100 ml bleach and 3.2 ml 37% HCl. Surface-sterilized seeds were left in the flow cabinet for an additional 2 hours to clear the chlorine gas. For all experiments, *Arabidopsis* seeds were incubated at 4°C for a 2-day stratification before being moved to the plant growth chambers (Van Wees et al., 2013).

Mutant library generation

A mini-Tn5 transposon insertion mutant library for *P. capeferrum* WCS358 was generated through triparental mating using donor strain *Escherichia coli* CC118λ*pir* harboring pBAM1 and helper strain *E. coli* HB101 harboring pRK600 (Martinez-Garcia et al., 2011), both kindly provided by Dr. Víctor de Lorenzo (Centro Nacional de Biotecnología, Madrid, Spain). The donor and helper strains were inoculated in liquid Luria-Bertani medium (LB, 10 g l^{-1} of tryptone, 5 g l^{-1} of yeast extract and 5 g l^{-1} of NaCl) supplemented with 150 µg ml^{-1} of ampicillin or 30 µg ml^{-1} of chloramphenicol, respectively. The recipient strain WCS358 was inoculated in liquid King's medium B (KB; King et al., 1954) supplemented with 150 µg ml^{-1} of rifampicin. All three bacteria were incubated in a shaker at 180 rpm at 37°C (for donor and helper) or 28°C (for recipient) for 16 h. Bacterial cultures were pelleted by centrifuging at 3500 *g* for 5 min, gently washed and resuspended in 10 mM $MgSO_4$. This pellet-wash-resuspend step was repeated three times and then the bacterial suspension was adjusted to a final OD_{660} of 10. The donor, helper and recipient strains were mixed in a 1:1:1 ratio to a total volume of 3 ml. 750 µl of the mixture was vacuum filtered through a 0.2 µm Millipore filter (Merck KGaA, Darmstadt, Germany) and 4 of these filters were placed on a pre-warmed plate (30°C) filled with agar-solidified LB medium for 18 h at 30°C. The filters were then transferred to 4 ml 10 mM $MgSO_4$ and vortexed for 30 s to resuspend the bacteria. The bacterial suspension was dispensed to 50 µl aliquots and stored at -80°C. To select individual mutant colonies, each aliquot was diluted in 1 ml LB medium and then 50 µl of the dilution was plated on agar-solidified LB medium supplemented with 150 µg ml^{-1} of rifampicin, 50 µg ml^{-1} of kanamycin and 100 µg ml^{-1} of nalidixic acid. The plates were incubated at 28°C for 48 h and single colonies were selected.

Bacterial cultures and culture filtrates

P. simiae WCS417 and *P. capeferrum* WCS358 were inoculated in liquid KB supplemented with 150 µg ml^{-1} of rifampicin and incubated at 28°C for 16 h. Bacterial strains from a collection of rhizobacteria isolated from *Arabidopsis* roots (Berendsen et al., 2018) were inoculated in 1/10 strength liquid tryptic soy broth and incubated at 20°C for 48 h. Bacterial strains from the mutant library were inoculated on agar-solidified KB plates supplemented with 150 µg ml^{-1} of rifampicin, 50 µg ml^{-1} of kanamycin and 100 µg ml^{-1} of nalidixic acid and incubated at 28°C for 24 h and then the bacteria were scraped off the plates into 10 mM $MgSO_4$. Before usage, fresh bacterial cultures were pelleted by centrifuging at 3500 *g* for 5 min, gently washed and resuspended in 10 mM $MgSO_4$. This pellet-wash-resuspend step was repeated three times after which the bacterial suspension was adjusted to the desired density based on OD_{660}. Bacterial suspensions were directly used in experiments or the preparation of culture filtrates.

Root exudates were collected from 10-day-old Col-0 seedlings growing in 12-well microtiter plates placed in a plant growth chamber simulating long-day conditions (21°C,

16 h light/8 h dark, light intensity 100 µmol m^{-2} s^{-1}). Each well contained 10 to 12 seeds and was filled with 1 ml Murashige and Skoog medium (Murashige and Skoog, 1962) supplemented with 0.5 g l^{-1} of MES monohydrate and 5 g l^{-1} of sucrose (MS medium). The pH of MS medium was adjusted to 5.7 with KOH. The collected root exudates were filtered through 0.2 µm Millipore filters (Merck KGaA, Darmstadt, Germany). Bacterial culture filtrates were collected from 22-h old bacterial cultures growing in 12-well microtiter plates placed in a plant growth chamber simulating long-day conditions as described (Millet et al., 2010). Each well was filled with 1 ml root exudates and inoculated with bacteria at an initial density of OD_{660} = 0.002. The bacterial cultures were then filtered through 0.2 µm Millipore filters (Merck KGaA, Darmstadt, Germany). The heated-culture filtrates were prepared by heating the culture filtrates for 1 h at 100°C.

Visualization of root immune responses

All flg22 peptides (GenScript, Piscataway, NJ) were prepared in Milli-Q water (Milliport Corp., Bedford, MA) as 100 µM stock solutions. To visually assess GUS activity in the roots, seeds of *Arabidopsis* transgenic lines were sown in 12-well microtiter plates. Each well contained 10 to 12 seeds and was filled with 1 ml MS medium. Seeds were allowed to germinate and grow in a plant growth chamber simulating long-day conditions. 100 nM flg22 was added to the growth medium of 10-day-old *Arabidopsis* seedlings in 12-well microtiter plates. GUS histochemical staining assays were performed at 3 h (for *MYB51$_{pro}$:GUS* and *WRKY11$_{pro}$:GUS*) or 5 h (for *CYP71A12$_{pro}$:GUS*) after flg22 treatment as described (Millet et al., 2010). The assay to determine the growth-inhibiting effect of flg22 was performed as described with modifications (Navarro et al., 2008). Seeds of Col-0, *fls2* or Ws-0 were sown in 12-well microtiter plates. Each well contained 2 seeds and was filled with 1 ml MS medium. After 5 days, 100 nM flg22 epitopes derived from *P. aeruginosa* PAO1, *P. simiae* WCS417 or *P. capeferrum* WCS358 ($flg22^{Pa}$, $flg22^{417}$, or $flg22^{358}$) were added to the growth medium of 5-day-old *Arabidopsis* seedlings and the weight of the seedlings was weighed at 7 days after flg22 treatment.

Root immune suppression by live bacteria

To assess the immune suppression ability of live bacteria, rhizobacterial strains were pre-inoculated to the growth medium of 9-day-old *Arabidopsis* seedlings in 12-well microtiter plates to a final density of OD_{660} = 0.002 and 100 nM flg22 was added to the growth medium after 18 hours. GUS histochemical staining assays were performed at 3 h (for *MYB51$_{pro}$:GUS* and *WRKY11$_{pro}$:GUS*) or 5 h (for *CYP71A12$_{pro}$:GUS*) after flg22 treatment (Millet et al., 2010).

Root immune suppression by bacterial culture filtrates

To assess the immune suppression ability of bacterial culture filtrates, culture filtrates or heat-treated culture filtrates were used to replace the growth medium of 10-day-old *Arabidopsis* transgenic line *CYP71A12$_{pro}$:GUS* seedlings in 12-well microtiter plates and 100 nM flg22 was added to bacterial culture filtrates after 1.5 hours (Millet et al., 2010). GUS histochemical staining assays were performed at 5 h after flg22 treatment.

Mutant library screening

To screen the bacterial mutant library, seeds of *Arabidopsis* transgenic line *CYP71A12$_{pro}$:GUS* were sown in 96-well microtiter plates. Each well contained 1 seed and was filled with 200 µl MS medium. Seeds were allowed to germinate and grow in a plant growth chamber

simulating long-day conditions. Live bacteria were pre-inoculated to the growth medium of 9-day-old *Arabidopsis* seedlings to a final density of OD_{660} = 0.002 and 100 nM flg22 was added to the growth medium after 18 hours. GUS histochemical staining assays were performed at 5 h after flg22 treatment. To assess the growth of selected putative mutants in root exudates, bacterial suspension was inoculated in 96-well microtiter plates containing 200 µl root exudates per well, at an initial bacterial density at OD_{660} = 0.002. Bacterial densities were assessed at 0 and 24 h after inoculation, by plating serial dilutions on agar-solidified KB plates supplemented with antibiotics as described above. The plates were incubated at 28°C for 24 h and numbers of colony-forming units (CFU) were determined.

Mapping transposon insertions

Arbitrary PCR was used to determine the localization of transposon insertions using primers described previously (Martinez-Garcia et al., 2011). Bacterial mutants of interest were inoculated in liquid LB medium supplemented with 150 µg ml^{-1} of rifampicin, 50 µg ml^{-1} of kanamycin and 100 µg ml^{-1} of nalidixic acid and then incubated at 28°C for 24 hours. Genomic DNA of the mutants was isolated from bacterial cultures using GenElute™ Bacterial Genomic DNA Kits (Sigma-Aldrich, Inc., St. Louis, MO). Bacterial genomic DNA was diluted in Milli-Q water (Milliport Corp., Bedford, MA) to 10 ng $µl^{-1}$ and then 1 µl was used as the template in the first PCR reaction. The 50 µl PCR reaction mixture contained the following components: 1X DreamTaq Buffer (Thermo Fisher Scientific Inc., Waltham, MA), 0.2 mM dNTP Mix (Thermo Fisher Scientific Inc., Waltham, MA), 0.2 µM primer ARB6, 0.2 µM primer ME-O-extF, 1 µl template, 1.25 u DreamTaq DNA Polymerase (Thermo Fisher Scientific Inc., Waltham, MA), 0.6 µl DMSO and Milli-Q water (Milliport Corp., Bedford, MA). The PCR was performed on a C1000 Touch™ Thermal Cycler (Bio-Rad Laboratories, Inc., Hercules, CA) using the thermal cycling conditions as follows: 5 min at 95°C for initial denaturation; 6 cycles of 30 s at 95°C, 30 s at 30°C, 1.5 min at 72°C; 30 cycles of 30 s at 95°C, 30 s at 45°C, 1.5 min at 72°C; followed by an extra extension of 4 min at 72°C. Then, 2 µl PCR product from the first PCR was used as the template in the second PCR reaction. The 50 µl PCR reaction mixture contained the following components: 1X DreamTaq Buffer, 0.2 mM dNTP Mix, 0.2 µM primer ARB2, 0.2 µM primer ME-O-intF, 2 µl template, 1.25 u DreamTaq DNA Polymerase, 0.6 µl DMSO and Milli-Q water. The PCR was performed using the thermal cycling conditions as follows: 1 min at 95°C for initial denaturation; 30 cycles of 30 s at 95°C, 30 s at 52°C, 1.5 min at 72°C; followed by an extra extension of 4 min at 72°C. The product from the second PCR round was purified with Agencourt AMPure XP beads (Beckman Coulter, Inc, Indianapolis, IN) and sequenced using ME-O-intF primer (Macrogen, Inc., Seoul, South Korea). Sequencing results were analyzed in CLC Main Workbench (QIAGEN, Venlo, The Netherlands).

Detection of GA and 2-KGA

GA and 2-KGA concentrations in bacterial culture filtrates were determined using ultra-performance liquid chromatography - mass spectrometry (UPLC-MS). Compounds were separated on a Waters Acquity UPLC BEH Amide Column (130Å, 1.7 µm particle size, 2.1 mm X 50 mm) by an Acquity UPLC system (Waters, Milford, MA, USA). The mobile phase A was 90% water, 10% acetonitrile, 0.1% formic acid and the mobile phase B was 100% acetonitrile, 0.1% formic acid. All solutions were ULC/MS grade (Biosolve B.V., Valkenswaard, The Netherlands). The gradient was set from 10% to 90 % with a flow rate of 0.25 ml min^{-1}. The run time was 6 min and the inject volume was 1 µl. Mass spectrometric detection was performed in negative ionization mode m/z 50 – 1250 and SIR of 2 channels m/z 193 and m/z 195 on a Waters Acquity QDa detector (Waters, Milford, MA, USA). GA and 2-KGA was

quantified by peak area obtained from standards for D-Gluconic acid sodium salt (Sigma-Aldrich, Inc., St. Louis, MO) and 2-Keto-D-gluconic acid hemi-calcium salt hydrate (Sigma-Aldrich, Inc., St. Louis, MO).

Effect of pH on root immune responses

The pH-adjusted root exudates or MS medium were prepared using 10% HCl or 10% D-gluconic acid to adjust the pH of root exudates or MS medium to 3.7 or other desired pH. To assess the effect of pH on flg22-induced *CYP71A12*$_{pro}$*:GUS* expression, pH-adjusted root exudates or MS medium, both were used to replace the growth medium of 9-day-old *Arabidopsis* seedlings in 12-well microtiter plates and 100 nM flg22 was added to pH-adjusted root exudates after 18 hours. Alternatively, pH-adjusted root exudates or MS medium were used to replace the growth medium of 10-day-old *Arabidopsis* seedlings and 100 nM flg22 was added to pH-adjusted root exudates at the same time. GUS histochemical staining assays were performed at 5 h after flg22 treatment.

Growth promotion assay

To assess bacterial growth-promoting activity, seeds of Col-0 were sown on square Petri dishes. Each plate contained 30 seeds and was filled with 50 ml agar-solidified MS medium. *S*eeds were allowed to germinate and grow in a plant growth chamber simulating short-day conditions (21°C, 10 h light/14 h dark, light intensity 100 µmol m^{-2} s^{-1}) for 5 days. The seedlings were then transferred to new square Petri dishes. Each plate contained 15 seedlings and was filled with 50 ml agar-solidified modified Hoagland medium (5 mM KNO_3, 2 mM $MgSO_4$, 2 mM $Ca(NO_3)_2$, 2.5 mM KH_2PO_4, 70 µM H_3BO_3, 14 µM $MnCl_2$, 1 µM $ZnSO_4$, 0.5 µM $CuSO_4$, 10 µM NaCl, 0.2 µM Na_2MoO_4, 4.7 mM MES, 50 µM Fe(III)EDTA) supplemented with 14.7 g l^{-1} of sucrose. The pH of MS medium was adjusted to 5.5 with KOH. After 7 days, 10 µl bacterial suspension with an OD_{660} = 0.1 was inoculated directly below the hypocotyls of *Arabidopsis* seedlings as described (Zamioudis et al., 2015). Shoot fresh weight and numbers of lateral roots were recorded at 6 days after bacterial inoculation.

Rhizosphere colonization assay

To assess bacterial rhizosphere colonization, *Arabidopsis* seeds were sown on river sand saturated with modified half-strength Hoagland solution (Van Wees et al., 2013). The seeds were allowed to germinate and grow in a plant growth chamber simulating short-day conditions for 12 days. Bacterial suspensions were mixed into a potting soil-sand mixture at an initial bacterial density of approximately $4.5´10^4$ cfu g^{-1} soil as described (Pieterse et al., 1996). *Arabidopsis* seedlings were then transferred to 60-ml pots containing soil pre-inoculated with bacteria. Unplanted bulk soil samples as well as rhizosphere plus root samples were harvested at 0 and 14 days after transplanting. All samples were placed in 2-ml pre-weighed Eppendorf tubes containing 3 glass beads, weighed and suspended in 1 ml 10 mM $MgSO_4$ using TissueLyser II (QIAGEN, Venlo, The Netherlands) with a frequency of 30 beats per second. Bacterial densities were assessed by plating serial dilutions of the samples on agar-solidified KB supplemented with 150 µg ml^{-1} rifampicin, 50 µg ml^{-1} ampicillin, 13 µg ml^{-1} chloramphenicol and 100 µg ml^{-1} Delvocid (DSM, Heerlen, The Netherlands). The plates were incubated at 28°C for 24 h and numbers of CFU were determined.

GUS histochemical staining assay

The growth medium of *Arabidopsis* seedlings was replaced with an equal amount of freshly-prepared GUS substrate solution (50 mM sodium phosphate with a pH at 7, 10 mM EDTA, 0.5 mM $K_4[Fe(CN)_6]$, 0.5 mM $K_3[Fe(CN)_6]$, 0.5 mM X-Gluc, and 0.01% Silwet L-77) as described (Millet et al., 2010). Plates were incubated in the dark at room temperature for 16 h (Pel, 2013). The GUS substrate solution was subsequently replaced with 96% ethanol and ethanol was refreshed after 24 h. *Arabidopsis* seedlings were then cleared in a solution of chloral hydrate: glycerol: water (8: 1: 2, v/v/v) as described (Zamioudis et al., 2015) and pictures were taken using an Axioskop 2 stereo microscope (Zeiss, Jena, Germany) with a Lumenera Inifinity 1 camera (Lumenera Corporation, Ottawa, ON) and the software Image-Pro Insight 9.1 (Media Cybernetics, Inc, Rockville, MD).

Statistics

Analysis of variance in all experiments was performed using GraphPad Prism 7 (GraphPad Software, La Jolla, CA).

Author contributions

K.Y., C.M.J.P., P.A.H.M.B., and R.L.B. designed experiments; K.Y., R.T., N.S., S.V.K., and E.L. performed experiments; K.Y. analyzed data; and K.Y., C.M.J.P., P.A.H.M.B., and R.L.B. wrote the manuscript.

CHAPTER 3

MYB72-dependent coumarin exudation shapes root microbiome assembly to promote plant health

Ioannis A. Stringlis[1,6], Ke Yu[1,6], Kirstin Feussner[2,6], Ronnie de Jonge[1,3,4], Sietske Van Bentum[1], Marcel C. Van Verk[1], Roeland L. Berendsen[1], Peter A.H.M. Bakker[1], Ivo Feussner[2,5], and Corné M.J. Pieterse[1,7]

[1]Plant-Microbe Interactions, Institute of Environmental Biology, Utrecht University, Padualaan 8, 3584 CH Utrecht, The Netherlands
[2]Department of Plant Biochemistry, Albrecht-von-Haller-Institute for Plant Sciences, University of Goettingen, 37077 Goettingen, Germany
[3]Department of Plant Systems Biology, VIB, Technologiepark 927, 9052 Ghent, Belgium
[4]Department of Plant Biotechnology and Bioinformatics, Ghent University, Technologiepark 927, 9052 Ghent, Belgium
[5]Department of Plant Biochemistry, Goettingen Center for Molecular Biosciences (GZMB), University of Goettingen, 37077 Goettingen, Germany
[6]These authors contributed equally to this work
[7]Corresponding author

Published in PNAS (DOI: 10.1073/pnas.1722335115)

ABSTRACT

Plant roots nurture a tremendous diversity of microbes via exudation of photosynthetically fixed carbon sources. In turn, probiotic members of the root microbiome promote plant growth and protect the host plant against pathogens and pests. In the *Arabidopsis thaliana-Pseudomonas simiae* WCS417 model system, the root-specific transcription factor MYB72 and the MYB72-controlled β-glucosidase BGLU42 emerged as important regulators of beneficial rhizobacteria-induced systemic resistance (ISR) and iron uptake responses. MYB72 regulates the biosynthesis of iron-mobilizing fluorescent phenolic compounds after which BGLU42 activity is required for their excretion into the rhizosphere. Metabolite fingerprinting revealed the antimicrobial coumarin scopoletin as a dominant metabolite that is produced in the roots and excreted into the rhizosphere in a MYB72- and BGLU42-dependent manner. Shotgun-metagenome sequencing of root-associated microbiota of Col-0, *myb72,* and the scopoletin biosynthesis mutant *f6'h1* showed that scopoletin selectively impacts the assembly of the microbial community in the rhizosphere. We show that scopoletin selectively inhibits the soil-borne fungal pathogens *Fusarium oxysporum* and *Verticillium dahliae*, while the growth-promoting and ISR-inducing rhizobacteria *P. simiae* WCS417 and *Pseudomonas capeferrum* WCS358 are highly tolerant to the antimicrobial effect of scopoletin. Collectively, our results demonstrate a role for coumarins in microbiome assembly and point to a scenario in which plants and probiotic rhizobacteria join forces to trigger MYB72/BGLU42-dependent scopolin production and scopoletin excretion, resulting in improved niche establishment for the microbial partner and growth and immunity benefits for the host plant.

INTRODUCTION

Plant roots exude a significant proportion of their photosynthetically fixed carbon into the rhizosphere (Bais et al., 2006). As a result, the rhizosphere nurtures one of the richest microbial ecosystems on Earth. The microbial community that inhabits the root-soil interface contains up to 10^{11} microbial cells per gram of root and collectively represents the root microbiome (Mendes et al., 2011; Berendsen et al., 2012). Root exudates greatly influence the composition of the root microbiome, a phenomenon called the rhizosphere effect (Berendsen et al., 2012; Bulgarelli et al., 2013). Besides detrimental pathogens, the root microbiome also harbors beneficial members that promote plant growth or stimulate plant health (Berendsen et al., 2012; Hacquard et al., 2017). Such mutualistic microbes serve plants in acquiring water and nutrients, in fixing nitrogen, in suppressing soil-borne pathogens, or in stimulating plant immunity (Berendsen et al., 2012; Bulgarelli et al., 2013).

Selected plant growth-promoting rhizobacteria (PGPR) can trigger an induced systemic resistance (ISR) that is effective against a broad range of foliar pathogens and even insect herbivores (Pieterse et al., 2014). ISR is well-studied in the interaction between *Arabidopsis thaliana* (hereafter *Arabidopsis*) and the PGPR *Pseudomonas simiae* WCS417 (hereafter WCS417; Berendsen et al., 2015). WCS417-ISR in *Arabidopsis* functions independently of the defense hormone salicylic acid (SA), but instead requires a functional response to the plant hormones ethylene and jasmonic acid (JA; Pieterse et al., 1998; Pieterse et al., 2014). In the absence of a pathogen, WCS417-ISR-expressing leaves do not display abundant transcriptional changes (Verhagen et al., 2004). However, upon pathogen or insect attack, ISR-expressing leaves develop an accelerated, primed defense response that is associated with enhanced resistance (Verhagen et al., 2004; Pozo et al., 2008; Martinez-Medina et al., 2016). In contrast to foliar tissues, WCS417-colonized roots show abundant transcriptional changes (Verhagen et al., 2004; Pozo et al., 2008; Zamioudis et al., 2014;

Stringlis et al., 2018a). Amongst the WCS417-induced genes, the root-specific R2R3-type MYB transcription factor gene *MYB72* emerged as a central regulator of the onset of ISR (Verhagen et al., 2004; Van der Ent et al., 2008). *MYB72* is also induced in *Arabidopsis* roots in response to colonization by the ISR-inducing fungi *Trichoderma asperellum* T-34 and *Trichoderma harzianum* T-78 (Martinez-Medina et al., 2017). Knockout *myb72* mutants are unable to mount ISR upon colonization of the roots by WCS417 or *T. asperellum* T-34 (Van der Ent et al., 2008; Segarra et al., 2009), suggesting that MYB72 plays a central role in the regulation of ISR triggered by different root-associated beneficial microbes. Downstream of MYB72 action, the β-glucosidase BGLU42 was identified as an important player in the onset of ISR (Zamioudis et al., 2014). Constitutive overexpression of *BGLU42* resulted in enhanced systemic disease resistance against *Botrytis cinerea, Pseudomonas syringae,* and *Hyaloperonospora arabidopsidis*, while mutant *bglu42* was blocked in the ability to mount WCS417-ISR.

Besides being essential for the onset of ISR, MYB72 emerged as an integral part of the plant's adaptive strategy to iron deficiency. Together with its closest paralog MYB10, MYB72 is essential for plant survival in alkaline soils where iron availability is largely restricted (Palmer et al., 2013). Under iron-limiting conditions, *MYB72* is strongly induced in the roots of *Arabidopsis* as part of a set of coordinated responses that boost iron mobilization and uptake from the soil environment, collectively referred to as the Strategy I iron deficiency response (Colangelo and Guerinot, 2004; Kobayashi and Nishizawa, 2012). The core of this response consists of rhizosphere acidification by the activity of the H^+-ATPase AHA2 (Santi and Schmidt, 2009), which increases the concentration of soluble ferric iron (Fe^{3+}). Fe^{3+} is subsequently reduced to ferrous iron (Fe^{2+}) by FERRIC REDUCTION OXIDASE2 (FRO2), after which it is transported from the soil environment into root cells via IRON-REGULATED TRANSPORTER1 (IRT1; Eide et al., 1996; Robinson et al., 1999). The bHLH transcription factor FIT (FER-LIKE IRON DEFICIENCY TRANSCRIPTION FACTOR) is a central regulator of the iron uptake response (Colangelo and Guerinot, 2004) and also regulates the expression of *MYB72* (Zamioudis et al., 2015).

During iron deprivation, plant roots exude a whole suite of secondary metabolites into the rhizosphere, which aids in the mobilization and uptake of iron. These metabolites include phenolics, organic acids, flavins, and flavonoids (Rodríguez-Celma et al., 2013; Fourcroy et al., 2014; Schmid et al., 2014). In *Arabidopsis* roots, MYB72 is required for the biosynthesis of iron mobilizing fluorescent phenolic compounds, while β-glucosidase BGLU42 is important for their subsequent excretion into the rhizosphere (Zamioudis et al., 2014). These so-called coumarins are synthesized in the phenylpropanoid pathway via FERULOYL-COA 6-HYDROXYLASE1 (F6'H1) and excreted into the rhizosphere by the iron deficiency–regulated ABC transporter PLEIOTROPIC DRUG RESISTANCE9 (PDR9; Rodríguez-Celma et al., 2013; Fourcroy et al., 2014; Schmid et al., 2014; Fourcroy et al., 2016). *Arabidopsis* knockout mutants *myb72* and *bglu42* are impaired in the excretion of iron-mobilizing coumarins and in the ability to mount rhizobacteria-mediated ISR, suggesting a mechanistic link between the iron deficiency response and plant immunity (Zamioudis et al., 2014; Verbon et al., 2017).

Interplay between plant immunity and adaptive plant responses to nutrient deficiencies is also reported for the phosphate starvation response (Castrillo et al., 2017). Interestingly, phosphate-starved plants release metabolites into the rhizosphere that are also exuded during conditions of iron deficiency (Ziegler et al., 2016; Tsai and Schmidt, 2017a). Plants responding to changes in their biotic or abiotic environment show changes in root exudation (Dakora and Phillips, 2002; Carvalhais et al., 2013), which in turn affects the composition of the root microbiome (Bais et al., 2006). Likewise, mutations in defense and

phosphate starvation signaling pathways significantly impact the composition of the root-associated microbial community (Carvalhais et al., 2015; Lebeis et al., 2015; Castrillo et al., 2017). Collectively the picture is emerging that components of the plant immune system and the plant's adaptive response to nutrient starvation are interlinked in influencing the assembly of the root-associated microbiome and vice versa (Bakker et al., 2018). However, the molecular mechanisms and the ecological and evolutionary advantage of this apparent relationship are largely unknown.

Because MYB72 is an essential regulator of 1) the onset of ISR by beneficial members of the root microbiome and 2) the excretion of iron-mobilizing coumarins into the rhizosphere, we set out to investigate the identity of the MYB72-dependent metabolites that are excreted into the rhizosphere and their impact on the root-associated microbiome. We performed metabolite fingerprinting analysis of root extracts and exudates of wild-type Col-0 and mutant *myb72* and *bglu42* plants. We identified the coumarin scopoletin as a major metabolite that is produced and excreted into the rhizosphere in a MYB72-BGLU42-dependent manner. Scopoletin possesses antimicrobial activity (Gnonlonfin et al., 2012) and was previously linked to disease resistance in different plant species (Kim et al., 2000; El Oirdi et al., 2010; Sun et al., 2014). Metagenome analysis of microbiota associated with roots of Col-0 plants and roots of the scopoletin biosynthesis mutant *f6'h1* shows that this antimicrobial and iron-mobilizing coumarin impacts the assembly of the root-associated microbiome. We further show that scopoletin selectively inhibits growth of two soil-borne fungal pathogens *in vitro,* but has little or no effect on growth of two beneficial ISR-inducing rhizobacteria. Collectively, our results suggest that MYB72-BGLU42-mediated production and excretion of scopoletin favors the interaction between plant roots and probiotic members of the root microbiome.

RESULTS

Metabolite fingerprinting of root exudates

In *Arabidopsis* roots, MYB72 and BGLU42 are both required for the onset of rhizobacteria-mediated ISR. Moreover, MYB72 is required for the biosynthesis of iron mobilizing fluorescent phenolic compounds, while BGLU42 has a role in their subsequent excretion into the rhizosphere (Zamioudis et al., 2014). Under iron starvation conditions, Col-0 roots exuded high quantities of fluorescent phenolic compounds (Figure 1A) and activated the iron deficiency marker genes *FRO2, IRT1, MYB72,* and *F6'H1* (Figure 1B). Mutant *myb72* did not exude detectable levels of the fluorescent compounds, while in *bglu42* their exudation was significantly impaired, confirming previous findings (Zamioudis et al., 2014). To identify the metabolites that were synthesized and secreted from *Arabidopsis* roots in a MYB72- and BGLU42-dependent manner, we analyzed the metabolome of root exudates of wild-type Col-0 and mutant *myb72* and *bglu42* plants. Therefore, the three genotypes were grown under iron-sufficient and iron-deficient conditions and the root exudates were analyzed by metabolite fingerprinting using UPLC-ESI-TOF-MS (Dataset S1). Filtering the data resulted in a set of 722 metabolite features with a false discovery rate (FDR) below 0.001. Principal component analysis (PCA) of the profiles of these 722 metabolite features indicates that the exudates of the different genotypes grown under iron-sufficient conditions are similar (Figure 1C and S1). In contrast, the root exudates of iron-starved plants were clearly different from those of iron-sufficient plants. The root exudates of iron-starved *myb72* plants clearly separated from those of iron-starved Col-0 and *bglu42* plants, indicating that the metabolite profiles of *myb72* root exudates are markedly different from those of Col-0 and *bglu42.*

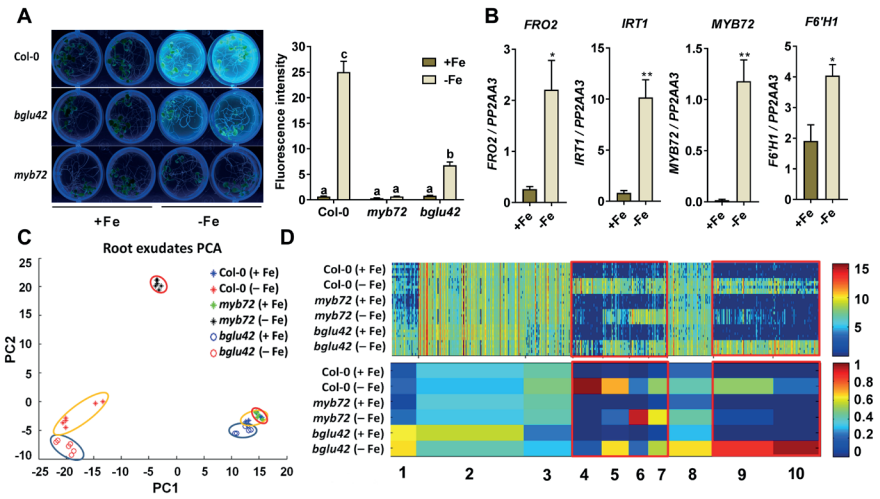

Figure 1. Metabolite fingerprinting of root exudates of Col-0, *myb72* and *bglu42* grown under iron sufficient and iron starvation conditions. (A) Accumulation and secretion of fluorescent phenolic compounds of 20-d-old Col-0, *myb72* and *bglu42* plants grown in Hoagland medium with (+Fe) or without (-Fe) iron. Visualization of fluorescence was achieved under UV light (365 nm). Fluorescence intensity was quantified in a 96-well microplate reader (excitation: 360nm; emission: 528 nm) after removal of the seedlings from the growth medium. Different letters indicate significant differences (Two-way ANOVA, Tukey's test, $P < 0.05$). **(B)** Gene expression profiles of the iron-deficiency marker genes *FRO2, IRT1, MYB72,* and *F6'H1* in roots of 20-d-old Col-0 plants grown in Hoagland medium with (+Fe) or without (-Fe) iron, quantified by qRT-PCR. Transcript levels were normalized to that of reference gene *PP2AA3* (At1g13320). Data are means of 3 biological replicates. Error bars represent SEM. Asterisks indicate significant differences between treatments (Student's *t*-test, $**P < 0.001$; $*P < 0.05$). **(C)** PCA plot of root exudates of 20-d-old Col-0 (encircled in yellow), *myb72* (encircled in red) and *bglu42* plants (encircled in blue) grown in Hoagland medium with (+Fe) or without (-Fe) iron. Data were obtained by metabolite fingerprinting (UPLC-ESI-TOF-MS analysis in positive and negative ionization mode) and the PCA represents the data subset after the filtering. **(D)** 1D-SOM clustering and prototype assignment of 722 high-quality metabolite features (FDR < 0.001) derived from positive as well as negative ionization mode of the metabolite fingerprinting analysis. The number of features assigned to one prototype determines its width. The raw intensity of individual features (top panel) and prototypes (bottom panel) mostly affected by iron deficiency are highlighted in the red box. Heatmaps correspond to the intensity of each individual feature (top panel) and the average intensity of each cluster/prototype (bottom panel). Color key reflects range of signal intensities. Three biological replicates per treatment were used for analysis.

To obtain a global overview of the metabolite features and their relative abundances in the root exudates, we clustered the profiles of the selected 722 metabolite features by one-dimensional self-organizing maps (1D-SOMs; Kaever et al., 2015). 1D-SOMs organized the intensity profiles in 10 clusters (prototypes; Figure 1D). Analogous to the PCA plot, the intensity profiles of the metabolite features of Col-0, *myb72* and *bglu42* grown under iron-sufficient conditions are highly similar. For all three genotypes, the iron starvation treatment changed the metabolome of root exudates, which resulted mainly in increased signal intensities, most strikingly visible in clusters 4-7 and 9-10. Clusters 1-3 and 8 represent features with a rather indifferent intensity profile or with only a weak accumulation in the *bglu42* mutant. Cluster 4 represents features that accumulated highly in exudates of Col-0 plants, while clusters 6 and 10 show features mainly enriched in *myb72* or *bgu42* exudates, respectively. The metabolite features of clusters 5 and 9 show lower intensities for iron-starved *myb72* than for iron-starved Col-0 and *blgu42.* Collectively, these results indicate

that MYB72 activity affects the composition of the root exudate metabolite profile under conditions in which the iron deficiency response is activated.

Exudation of MYB72- and BGLU42-dependent metabolites

To determine the identity of the MYB72- and BGLU42-dependent metabolites in the root exudates of iron-starved *Arabidopsis* plants, we generated a data subset of the metabolome data shown in Figure 1 containing only the metabolite fingerprinting analyses of the root exudates of iron-deprived Col-0, *myb72,* and *bglu42* plants. Filtering the data of this subset resulted in 311 metabolite features with a FDR below 0.001 (Dataset S2). The intensity profiles of these 311 features were clustered by means of 1D-SOMs, resulting in five prototypes (Figure 2A). Metabolite features in clusters 1, 2 and 5 showed clearly lower intensities in *myb72* than in Col-0, indicating that the abundance of the corresponding metabolites increased in Col-0 root exudates in a MYB72-dependent manner. The metabolite features of prototype 1 showed in addition a depletion in *bglu42,* suggesting that the corresponding MYB72-dependent metabolites are excreted in a BGLU42-dependent manner.

Amongst the metabolite features that showed depletion in the root exudates of iron-starved *myb72*, the majority matched to coumarins by data base search on basis of exact masses comparison. Coumarins play a role in iron mobilization and uptake from alkaline substrates (Rodríguez-Celma et al., 2013; Fourcroy et al., 2014; Schmid et al., 2014). The intensity profiles of the coumarins scopolin, scopoletin, esculin, esculetin and isofraxidin show a strong increase in root exudates of iron-starved Col-0 (with scopoletin being the most abundant one), while no increase is observed in root exudates of iron-starved *myb72* (Figure S2). Most of the features summarized in cluster 1 (Figure 2A) are related to scopoletin. The diversity of the scopoletin-related features is caused by the intense adduct formation of highly abundant scopoletin during electrospray ionization. The scopoletin non-related features in cluster 1 showed very low signal intensities and inconclusive data base matches. High-resolution MS/MS analysis confirmed the identity of the detected coumarins (Table S1). Of these excreted MYB72-dependent coumarins, only scopoletin levels were reduced in the root exudates of iron-starved *bglu42* plants.

Quantification of scopolin and its aglycone scopoletin by HPLC-DAD (Figure 2B) confirmed their patterns observed in the non-targeted metabolite fingerprinting approach (Figure S2). Scopoletin accumulated to over 3 µg ml^{-1} in root exudates of iron-starved Col-0 plants, while it was undetectable or strongly reduced in root exudates of the *myb72* and *bglu42,* respectively. Figure 2B shows that also the glycosylated form of scopoletin, scopolin, accumulated in a MYB72-dependent manner in the exudates of iron-starved roots, albeit only to about 10% of the concentration of scopoletin (compare scales of Y-axes). However, the *bglu42* mutation had no effect on the iron-starvation-induced levels of scopolin. Collectively, these results show that scopoletin is the major MYB72- and BGLU42-dependent metabolite that is secreted by roots of iron-starved *Arabidopsis* plants. Besides coumarins, also the coumarin precursor phenylalanine and the citric acid cycle components citrate, malate and succinate increased in abundance in root exudates of iron-starved Col-0 plants (Figure S2 and Table S1), confirming previous findings (Fourcroy et al., 2014). However, their excretion was not dependent on MYB72 and BGLU42.

Role of BGLU42 in excretion of scopoletin

BGLU42 encodes a β-glucosidase that belongs to glycoside hydrolase (GH) family 1 and it was previously shown that GH family 1 members BGLU21, BGLU22 and BGLU23 can hydrolyze scopolin, resulting in the production of scopoletin (Ahn et al., 2010). Glycosylation

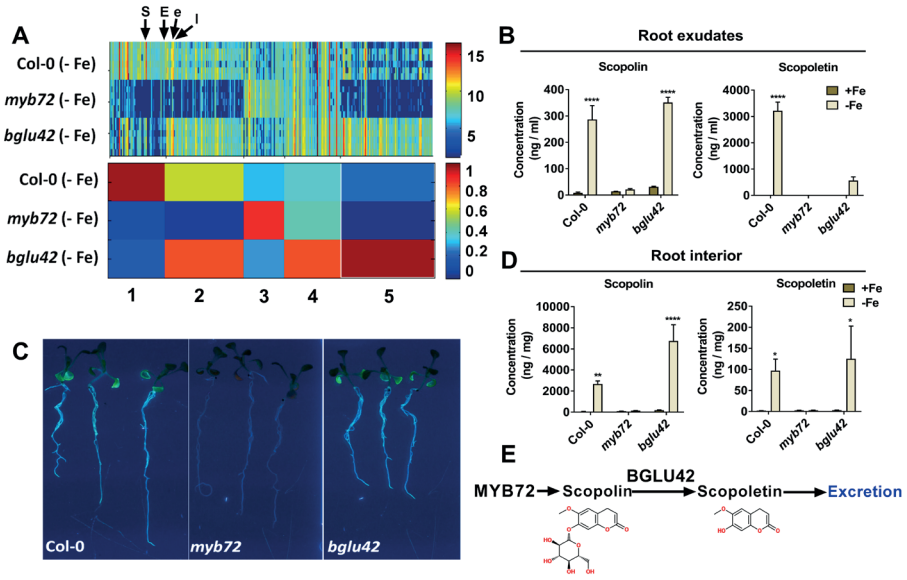

Figure 2. MYB72- and BGLU42-dependent metabolites in root exudates and roots of Col-0, *myb72,* and *bglu42* plants. (A) 1D-SOM clustering and prototype assignment of 311 high-quality metabolite features (FDR < 0.001) in root exudates of iron-starved Col-0, *myb72,* and *bglu42* plants. The number of features assigned to one prototype determines its width. Heatmaps correspond to the intensity of each individual feature (top panel) and the average intensity of each cluster/prototype (bottom panel). Color key reflects range of signal intensities. Arrows display the position of scopoletin (S), esculin **(E)**, esculetin (e) and isofraxidin (I). For details on selected metabolite features see Supplementary Figure S2 and Table S1. **(B)** HPLC-DAD quantification of scopolin and scopoletin in root exudates of Col-0, *myb72* and *bglu42* grown under iron-sufficient (+Fe) and iron-starved (-Fe) conditions. The data are means of 3 replicates of the pooled root exudates of 50-60 plants per replicate. Error bars represent SEM. Asterisks indicate significant differences between the iron conditions within a genotype (Two-way ANOVA, Sidak's test; ****P < 0.0001; **P < 0.01; *P < 0.05). **(C)** Photographs of iron-starved Col-0, *myb72,* and *bglu42* plants grown in 12-well plates with liquid Hoagland medium without iron. Visualization of fluorescent phenolic compounds was achieved under UV light (365 nm). **(D)** HPLC-DAD quantification of scopolin and scopoletin in the root of Col-0, *myb72* and *bglu42* grown under iron-sufficient and iron-starved conditions. The data are means of 3 replicates of the pooled root extracts of 130 plants per replicate. Error bars represent SEM. Asterisks indicate significant differences between the iron conditions within a genotype (Two-way ANOVA, Sidak's test; ****P < 0.0001; **P < 0.01; *P < 0.05). **(E)** Schematic representation of the role of MYB72 in the production of coumarin scopolin and the activity of BGLU42 in the deglycosylation of scopolin and the subsequent production of the aglycone scopoletin before its excretion into the rhizosphere. The presented molecules were created using the website https://www.emolecules.com.

and deglycosylation can change phenylpropanoid solubility, stability and toxic potential, and influence their compartmentalization and biological activity (Le Roy et al., 2016). While *myb72* plants are blocked in the ability to produce fluorescent phenolic compounds in their roots, iron-starved *bglu42* roots still accumulate significant amounts (Figure 2C). Hence, we hypothesized that if BGLU42 activity facilitates the excretion of scopoletin, then iron-starved *bglu42* mutant plants should still accumulate the glycosylated form scopolin within their roots. To test this, we analyzed the metabolite profiles of the polar and non-polar extractions of the roots of Col-0, *myb72* and *bglu42* plants grown under iron-sufficient and iron-starved conditions by UPLC-ESI-TOF-MS (Datasets S3 and S4). Similar to what was observed for the root exudates, the root metabolome showed different metabolite profiles in terms of

iron treatment and plant genotype (Figure S1, S3A and S3B). Metabolite features related to coumarins were abundantly present in the polar extracts of the root, with scopolin, scopoletin and esculin showing highly abundant signal intensities (Figure S3C, and Table S2). Scopolin, scopoletin and esculin were produced within the roots in a MYB72-dependent manner, while BGLU42 did not negatively impact their abundance in the roots (Figure 2D and S3C). Scopolin even increased to higher levels in the roots of iron-starved *bglu42* plants compared to Col-0, supporting the notion that BGLU42-mediated deglycosylation of scopolin is impaired in this mutant. As opposed to root exudates of iron-starved Col-0 plants, where scopoletin levels were about 10-fold higher than that of scopolin (Figure 2B), within the root of iron-starved Col-0 plants scopoletin levels were over 25-fold lower than those of scopolin (Figure 2D). Collectively, these results indicate that roots of iron-starved Col-0 plants produce scopolin and scopoletin in a MYB72-dependent manner and that BGLU42 activity is important for the deglycosylation of scopolin and the subsequent excretion of the aglycone scopoletin into the rhizosphere (Figure 2E).

In addition to the polar fraction, we also analyzed the non-polar fraction of the root extracts (Dataset S4 and Figure S3B). Metabolite fingerprinting yielded a rich source of metabolite features with either MYB72- or BGLU42-dependent patterns. However, because none of them was impaired in both the *myb72* and the *bglu42* mutant background, they are not further described in this study.

Effect of scopoletin on rhizosphere microbiome assembly

Previously, coumarin derivatives were shown to possess antimicrobial activity (Gnonlonfin et al., 2012). Because beneficial ISR-inducing members of the root microbiome induce *MYB72* and coumarin biosynthesis genes upon colonization of the roots (Zamioudis et al., 2014), we hypothesized that coumarins may play a role in shaping the microbial community in the rhizosphere. To investigate the effect of MYB72-dependent coumarins, in particular scopoletin, on the composition of the root-associated microbial community, we analysed the root-associated microbiomes of Col-0 and *myb72*, and the scopoletin biosynthesis mutant *f6'h1* (Kai et al., 2008; Schmid et al., 2014). *Arabidopsis* seedlings were grown *in vitro* under iron-sufficient or iron-starved conditions to verify their coumarin-exudation status at the start of the experiment. As expected, iron-starved Col-0 seedlings abundantly exuded fluorescent phenolic compounds, while *myb72* and *f6'h1* seedlings did not (Figure 3A). Subsequently, the plants were transplanted into natural Reijerscamp soil (Berendsen et al., 2018) that was limed to maintain iron limitation and differential coumarin excretion patterns. At the moment of transplanting, *MYB72, FRO2* and *IRT1* were strongly induced in the roots of iron-starved Col-0 seedlings (Figure 3B). Their induced expression levelled off over time but was still detectable at day 3 after transplanting. In this experimental setup, differences in iron availability of the Col-0 seedlings after transplanting to the natural Reijerscamp soil had no major effect on the expression of the root immunity marker gene *CYP71A12,* the glucosinolate biosynthesis genes *CYP79B2* and *CYP79F2,* and the pathogenesis-related protein gene *PR3* (Figure S4). Hence, potential differences in microbiome composition are not likely the result of differences in basal root defenses. Next, we analyzed the microbiota associated with roots of iron-starved Col-0, *myb72,* and *f6'h1* plants that were grown in limed soil for 3 d. As a control, we characterized the root microbiota of Col-0 plants that were pre-grown under iron-sufficient conditions. Day 3 after transplanting was chosen because enhanced expression levels of *MYB72, FRO2,* and *IRT1* were still detectable at that time point (Figure 3B), and phenolics excreted by the roots can reside in the soil for several days (Mimmo et al., 2014). To analyze the effect of MYB72 and F6'H1 activity on the composition of the root microbiome, genomic DNA of the root-associated microbiota

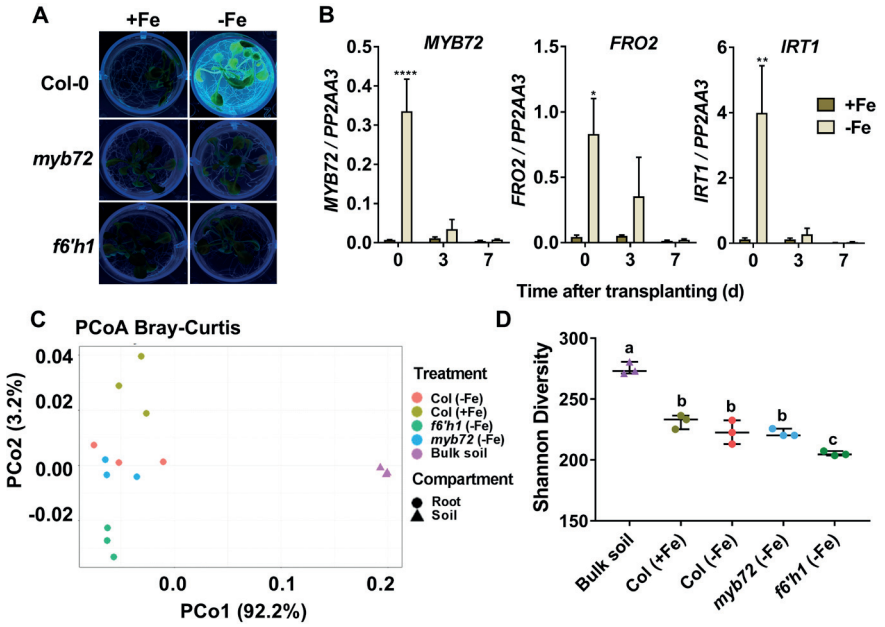

Figure 3. Metagenome analysis of bulk soil and root-associated microbiomes of Col-0, *myb72,* and *f6'h1* plants. (A) Excretion of fluorescent phenolic compounds by 26-d-old Col-0, *myb72* and *f6'h1* plants grown in Hoagland medium with (+Fe) or without (-Fe) iron. Visualization of fluorescence was achieved under UV light (365 nm). **(B)** Gene expression profiles of *MYB72* and the iron-deficiency marker genes *FRO2* and *IRT1* in roots of Col-0 plants pre-grown for 14 days in Hoagland medium with (+Fe) or without (-Fe) iron and transplanted on day 0 to limed Reijerscamp soil. Gene expression was quantified by qRT-PCR. Transcript levels were normalized to that of reference gene *PP2AA3* (At1g13320). Data are means of 3 biological replicates. Error bars represent SEM. Asterisks indicate significant differences between treatments (Two-way ANOVA, Sidak's test, ****$P < 0.0001$; **$P < 0.01$; *$P < 0.05$). **(C)** Principal coordinates analysis (PCoA) using Bray-Curtis metrics displays dissimilarity of microbial communities between soil (triangles) and root samples (circles) and between Col-0 pre-grown under iron-sufficient (+Fe) conditions, and Col-0, *myb72* and *f6'h1* pre-grown under iron-starved conditions (-Fe). **(D)** Shannon diversity (effective number of species) displaying the within-sample diversity of different treatments. Horizontal bars correspond to median and interquartile range of values. Different letters indicate significant differences (One-way ANOVA, Tukey's test; $P < 0.05$).

was subjected to shotgun metagenome sequencing. Per sample, Illumina NextSeq 500 sequencing yielded between 52.4 and 108.7 million (M) paired-end reads with a length of 150 bp (Table S3). For the analysis of the metagenomes we followed a classification-first approach using Kaiju, a program that estimates sequence similarity of metagenomic reads with reference prokaryotic and eukaryotic microbial protein databases (Menzel et al., 2016). For the root samples, Kaiju classified 28-32% of the reads at genus level to *Arabidopsis* and 21-24% of the reads to microbiota in the reference database (Table S3). For the bulk soil samples, a very small number of reads compared to the total sample reads were classified to *Arabidopsis* (sample "B1": 10995 / 0.03%; sample "B2": 3534 / 0.01%; sample "B3": 2802 / 0.01%), while 37% matched with microbiota in the reference database. For all samples, between 45 to 60% of the reads couldn't be classified at genus level.

Genus level classification using publicly available taxonomy databases as reference (Federhen, 2012) allowed us to track shifts in higher taxonomic ranking between the root-associated microbiota and those assembled in the unplanted soil (Figure S5A and S5B). Taxonomic classification at the genus level resulted in the assignment of reads to 4,046

genera belonging to the domains of Bacteria, Eukaryota and Archaea (Dataset S5). Bacteria were the most dominant domain in terms of relative abundance (RA), with Eukaryota being the second and Archaea representing only a small fraction of the microbial communities (Figure S5A). Bacteria displayed a significant decrease in the root samples of all genotypes compared to bulk soil. In contrast, Eukaryota showed a significant increase in the root samples, while RA of Archaea remained unaffected in both compartments (Figure S5A). At phylum level, we focused on phyla with a RA of over 0.5% (Figure S5B). Proteobacteria were the most abundant (around 50% RA) with Actinobacteria, Firmicutes and Bacteroidetes being overrepresented as well but with lower RA. The phyla Acidobacteria, Actinobacteria, Bacteroidetes and Firmicutes showed statistically significant changes in RA between soil and all root/rhizosphere samples. For the phyla Chlorophyta, Mucoromycota, Planctomycetes, and Proteobacteria only a subset of the genotype-treatment combinations showed significant changes in the RA in root/rhizosphere versus bulk soil samples, while the phyla Verrucomicrobia, Cyanobacteria, Chloroflexi, Basidiomycota, and Ascomycota remained unaffected (Figure S5B).

To gain further insight into the effect of plant genotype and treatment on root microbial diversity, we performed β- and α-diversity analyses. In the principal coordinate analysis (PCoA) of Bray-Curtis similarities (β-diversity), the microbial diversity of bulk soil clearly separates from those of the different plant genotypes (Figure 3C), indicating a significant effect of the plant on root microbiome assembly. Along the second principal coordinate, the root-associated microbial communities of iron-sufficient (+Fe) and iron-starved (-Fe) Col-0 plants differentiate (Figure 3C), suggesting that root exudates produced during iron-starvation affected microbiome assembly. The microbial communities of iron-starved Col-0 and *myb72* both displayed intermediate separation from that of iron-sufficient Col-0, while the microbial community on the scopoletin biosynthesis mutant *f6'h1* diverged most distinctly. To pinpoint genotype-mediated differences within the root-associated microbiota, the microbial diversity within each sample (α-diversity) was calculated as Shannon diversity (Figure 3D). This calculation showed that microbial communities in unplanted bulk soil are significantly more diverse and complex than the root-associated microbial communities, and that the Shannon diversity for the *f6'h1* root-associated microbiota was significantly lower than that for the other genotypes. The observation that the scopoletin-biosynthesis mutant *f6'h1* clearly separates from the other genotypes both in between- and in within-samples diversity estimations, suggesting that F6'H1 activity affects root microbiome assembly.

To dissect the plant genotype-mediated differences in root microbiome structure on lower taxonomic ranking, we performed pairwise comparisons using DESeq2. Pairwise comparison between the root-associated microbiota of iron-starved and iron-sufficient Col-0 plants revealed 21 genera with differential abundance, predominantly from the Proteobacteria and Firmicutes phyla (Figure S6A). *Psychrobacillus*, *Stenotrophomonas*, *Paeinisporosarcina* and *Dyella* were the genera with the highest differential abundance in the root microbiomes of iron-starved Col-0 plants, indicating that these genera grow better in the rhizosphere of iron-starved Col-0 plants than in that of iron-sufficient Col-0 plants. Conversely, *Adhaeribacter*, *Niastella*, and *Hymenobacter* were most-highly enriched on roots of iron-sufficient Col-0 plants, indicating that they grow better in the rhizosphere of iron-sufficient Col-0 plants than in that of iron-starved Col-0 plants. Comparison between the root microbiomes of iron-starved Col-0 and *myb72* plants yielded only 3 genera above the limit of statistical significance (Figure S6B). However, these genera were also detected in the comparison between iron-starved Col-0 and *f6'h1* plants, which revealed the largest number (35) of genera with differential abundance (Figure 4). The 22 genera significantly enriched on Col-0 over *f6'h1* roots (growth positively affected by F6'H1/scopoletin activity)

represent 7 phyla, with *Psychrobacillus* and *Paraclostridium* from the Firmicutes phylum, and *Rhizophagus*, a genus of mycorrhizal fungi from the phylum Mucoromycota, being amongst the most-strongly stimulated genera. The 13 genera significantly enriched on *f6'h1* over Col-0 roots (growth negatively affected by F6'H1/scopoletin activity) represent 4 phyla, with *Pontibacter*, *Rufibacter*, and *Adhaeribacter*, all belonging to Hymenobacteraceae family, being amongst the most-strongly affected genera. Interestingly, *Adhaeribacter* and *Hymenobacter* were both significantly less abundant on the roots of iron-starved Col-0 plants than on those of iron-starved *f6'h1* and iron-sufficient Col-0, suggesting that these genera are particularly sensitive to F6'H1-dependent root exudates that are secreted under conditions of iron starvation. Together, these results demonstrate that the F6'H1-dependent root exudation patterns, with the coumarin scopoletin as a major compound, can positively and negatively influence the abundance of specific genera in the root-associated microbiome of *Arabidopsis*, therewith impacting the assembly of the root microbiome.

Differential antimicrobial effect of scopoletin

MYB72 and BGLU42 are both important for the onset of rhizobacteria-mediated ISR and the excretion of iron-mobilizing coumarins into the rhizosphere (Zamioudis et al., 2014; Zamioudis et al., 2015). Metabolite fingerprinting using UPLC-ESI-TOF-MS confirmed that already at 48 h after colonization by *P. simiae* WCS417, Col-0 roots show increased accumulation of the coumarins scopolin, scopoletin and esculin, and the tricarboxylic acid (TCA) cycle intermediates citrate, malate and succinate (Figure 5A and S7, Dataset S6). Production of coumarins in response to colonization of *Arabidopsis* roots by ISR-inducing *P. simiae* WCS417 bacteria occurs in a F6'H1-dependent manner (Figure 5A), which raises the question how and to what extent such plant-beneficial rhizobacteria benefit from the excretion of antimicrobial compounds into the rhizosphere. To assess the effect of coumarin production on root colonization by WCS417, we monitored growth of WCS417 on roots of iron-starved and iron-sufficient Col-0 plants over a time period of 7 d after transplanting the plants into limed Reijerscamp soil (Figure 5B; same experimental setup as used for the microbiome analysis). Already within one day, the density of WCS417 bacteria increased 10-fold in the rhizosphere of Col-0 plants in comparison to that in unplanted bulk soil. This increase in WCS417 density was maintained for the 7-d period of monitoring. No difference was observed in the level of colonization on iron-starved and iron-sufficient Col-0 roots, suggesting that WCS417 is insensitive to possible antimicrobial effects of root exudates that are excreted in the rhizosphere during conditions of iron starvation.

To confirm that *P. simiae* WCS417 is insensitive to coumarins, we tested the effect of scopoletin on growth of WCS417 *in vitro*, using the antibiotic tetracyclin as a positive control (Sun et al., 2014; Figure 5C). While tetracyclin prevented growth of WCS417, scopoletin concentrations of up to 2 mM had no effect on growth of this PGPR. Additionally, we tested the effect of scopoletin on another well-characterized ISR- and *MYB72*-inducing PGPR, *Pseudomonas capeferrum* WCS358 (Berendsen et al., 2015; Zamioudis et al., 2015). WCS358 was also highly insensitive to scopoletin (Figure 5D). We then reasoned that the excretion of coumarins would aid the rhizobacteria that induce their production in selectively outcompeting other microbes in the rhizosphere that compete for the same niche. To provide proof of concept for this hypothesis, we tested the effect of scopoletin on growth of two soil-borne pathogens of *Arabidopsis*, *Fusarium oxysporum* f. sp. *raphani* and *Verticillium dahliae* JR2 (Pieterse et al., 1996; Fradin et al., 2009; Figure 5E and 5F). Scopoletin concentrations of 500 µM and higher significantly inhibited growth of both fungi *in vitro* and inhibited the growth of *V. dahliae* to the same extent as the fungicide Delvo®Cid. Since we detected scopoletin concentrations of over 3 µg ml^{-1} (~15 µM) in the

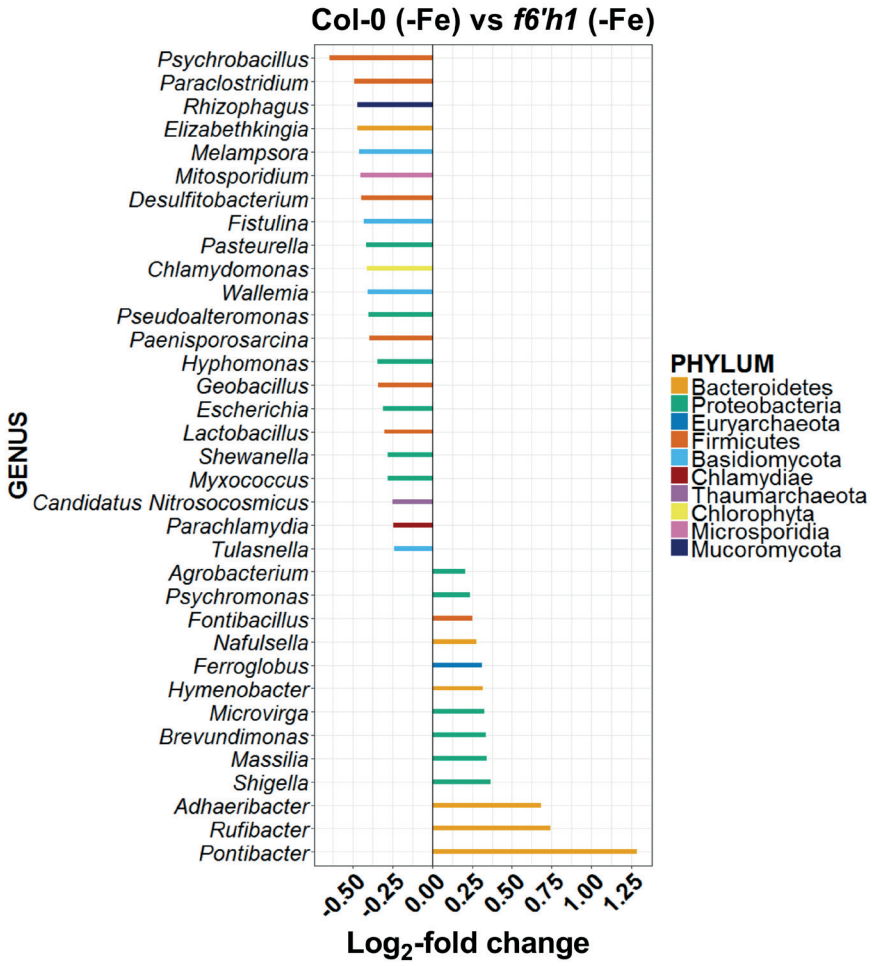

Figure 4. Differential abundance of microbial genera on *Arabidopsis* roots with different scopoletin exudation patterns. Differentially abundant bacterial and fungal genera between root samples of Col-0 (-Fe) and *f6'h1* (-Fe) as determined using DESeq2. Comparisons were performed at genus level using a false discovery rate (FDR) < 0.05 to select for significance. In all graphs, negative $\log_2$-fold change values relate to genera that are significantly enriched in iron-starved Col-0 (-Fe) root samples in comparison to the contrasting genotype/treatment combination. Different colors of the bars correspond to different Phyla.

growth medium of iron-starved Col-0 plants (Figure 2B), it is likely that in the narrow region of soil directly surrounding the roots much higher concentrations of scopoletin can occur. Together, these results indicate that scopoletin has a differential antimicrobial effect to which the tested soil-borne fungal pathogens *F. oxysporum* f. sp. *raphani* and *V. dahliae* JR2 are sensitive, while the ISR- and *MYB72*-inducing PGPR *P. simiae* WCS417 and *P. capeferrum* WCS358 are not.

To further investigate the activity of scopoletin on fungal physiology and growth, we assessed the effect of 500 µM scopoletin on *F. oxysporum* f. sp. *raphani* radial growth on PDA plates. Scopoletin reduced radial growth of the fungus and inhibited the formation of pigment in the mycelial mat (Figure S8A). Metabolites involved in fungal pigmentation can be associated with protection against abiotic stresses or competition with other microbes

(Medentsev et al., 2005; Son et al., 2008), indicating that scopoletin potentially exerts its effect on multiple determinants of fungal performance. To study the effect of scopoletin in root exudates on *F. oxysporum* f. sp. *raphani* hyphal growth, we performed a chemotropism assay as described (Turra et al., 2015). Therefore, we used root exudates of iron-starved Col-0 and scopoletin biosynthesis mutant *f6'h1* plants, increasing concentrations of scopoletin, and pectin as a positive control. Figure S8B shows that fungal hyphae from germinating conidia are chemotropically attracted towards pectin, confirming previous findings (Turra et al., 2015). Conversely, scopoletin deterred the fungal hyphae, which preferentially grew away from this antimicrobial coumarin. Root exudates of iron-starved Col-0 plants, which exude large amounts of scopoletin (Figure 1 and 2), similarly deterred the fungal hyphae, while root exudates of iron-starved *f6'h1* plants significantly attracted the fungal hyphae. Together, these results indicate that scopoletin in root exudates can have a multifaceted negative effect on the performance of scopoletin-sensitive microbes in the rhizosphere.

DISCUSSION

MYB72 and BGLU42 are required for the production and secretion of scopoletin

The rhizosphere microbiome is highly diverse and its interplay with plant roots has a marked influence on plant fitness (Berendsen et al., 2012). Specific root microbiome members can trigger ISR through the activity of the root-specific transcription factor MYB72 and the MYB72-regulated β-glucosidase BGLU42 (Van der Ent et al., 2008; Zamioudis et al., 2014). MYB72 and BGLU42 have also a role in the production and excretion of fluorescent phenolic compounds when plants grow under conditions of iron starvation (Zamioudis et al., 2014). We used this knowledge to identify the metabolites that are produced and excreted by *Arabidopsis* roots in a MYB72- and BGLU42-dependent manner and investigated their possible role in plant-microbiome interactions. Untargeted UPLC-ESI-TOF-MS metabolomics of root exudates and root extracts revealed coumarins as a major group of compounds whose production relies on MYB72 activity (Figure 2, S2 and S3). Coumarins, such as scopolin, scopoletin, esculin, esculetin, and isofraxidin, are produced via the phenylpropanoid pathway (Liu et al., 2015) and accumulate abundantly in roots and exudates of iron-starved plants (Rodríguez-Celma et al., 2013; Fourcroy et al., 2014; Schmid et al., 2014) where they play a role in the mobilization and uptake of iron (Schmid et al., 2014; Fourcroy et al., 2016). Mutant *bglu42* produced wild-type levels of coumarins, but was specifically impaired in the excretion of scopoletin, the most abundant coumarin in the root exudates (Figure 2, S2 and S3). Yet, the glycosylated form of scopoletin, scopolin accumulated to high levels in iron-starved *bglu42* roots, which suggests that BGLU42 functions in the hydrolysis of scopolin, and that this activity is required for the excretion of scopoletin into the rhizosphere. This is in line with previous findings in which the *Arabidopsis* β-glucosidases BGLU21, 22 and 23 were shown to specifically hydrolyze scopolin into scopoletin *in vitro* (Ahn et al., 2010). β-glucosidases can hydrolyze glycosidic bonds either between 2 carbohydrates or between a carbohydrate and a non-carbohydrate (Morant et al., 2008), often resulting in the release of bioactive derivatives (Jones and Vogt, 2001; Morant et al., 2008). The activity of BGLU42 seems to be specific for scopolin/scopoletin, since other coumarin pairs like esculin/esculetin were not affected in *bglu42* (Figure S2 and S3). We, thus, conclude that BGLU42 activity in iron-starved *Arabidopsis* roots plays an important role in the processing of scopolin to scopoletin, resulting in the excretion of scopoletin into the rhizosphere.

Scopoletin affects root microbiome assembly

Scopoletin possesses antimicrobial activity (Gnonlonfin et al., 2012). Hence, its excretion likely influences the composition of the microbial community in the rhizosphere. In our search for scopoletin-mediated effects on root microbiome assembly, shotgun sequencing of the microbial communities in bulk soil and on roots of Col-0, *myb72* and *f6'h1* confirmed a number of concepts that have emerged in the field of root microbiome research. First, bulk soil and root-associated microbial communities were largely different (Figure 3), resembling the rhizosphere effect (Bakker et al., 2013). Second, the relative abundance of Bacteria in the rhizosphere was reduced in comparison to bulk soil, while that of Eukaryota was higher, supporting previous findings in crop species (Figure S5A; Turner et al., 2013b). Third, at the phylum level, the relative abundance of Proteobacteria, Firmicutes, and Bacteroidetes was generally increased in root-rhizosphere samples compared to bulk soil, whereas the relative abundance of Actinobacteria and Acidobacteria was decreased (Figure S5B). Such shifts in phylum level abundance were also observed in other rhizosphere microbiome studies of *Arabidopsis*, rice and barley plants that were grown for prolonged periods in the soil (Lundberg et al., 2012; Bulgarelli et al., 2015; Edwards et al., 2015; Lebeis et al., 2015). Moreover, the α-diversity estimation with Shannon's diversity (Figure 3D) showed a diversity gradient from higher to lower between soil and rhizosphere samples, suggesting that microbial selection is occurring in the rhizosphere (Lundberg et al., 2012; Bulgarelli et al., 2015; Zgadzaj et al., 2016). In this study, we analyzed the structure of the root-associated microbial communities that were formed within 3 d after transplanting into the soil. The fact that general concepts of microbiome assembly were already detectable within this short time frame highlights the speed by which root-associated microbial communities are established in response to chemical and structural cues in the rhizosphere.

In comparison to the large differences between root-associated and bulk soil microbial communities, the plant genotype-mediated differences in root microbiome composition were more subtle (Figure 3C), which is in line with previous findings (Lebeis et al., 2015; Castrillo et al., 2017; Zhang et al., 2017). In comparison to the microbiomes assembled on Col-0 roots, those assembled on *myb72* showed less differences than those assembled on *f6'h1,* possibly because in iron-starved soil MYB72 functions redundantly with MYB10 (Palmer et al., 2013). The microbiomes assembled on the roots of Col-0 and *f6'h1* displayed the largest differences, indicating that excretion of scopoletin affects the composition of the root microbiome. Genus-level analysis showed that the abundance of genera, such as *Stenotrophomonas*, *Lactobacillus*, *Psychrobacillus*, *Elizabethkingia*, *Chlamydomonas* and *Geobacillus*, was enhanced on scopoletin-producing roots (Figure 4). Interestingly, these genera were previously found to be able to hydrolyze different coumarins (Aliotta et al., 1999; Nazina et al., 2001; Kim et al., 2005; Guan et al., 2008; Krishnamurthi et al., 2010). Amongst the most strongly promoted genera on coumarin-excreting roots are genera that promote plant growth (*Psychrobacillus*, *Variovorax*), facilitate metal uptake in plants (*Psychrobacillus*), have a role in nitrogen cycling in soil (*Candidatus* Nitrosocosmicus), or possess antimicrobial potential (*Pseudoalteromonas*; De Nys and Steinberg, 2002; Han et al., 2011; Perez Rodriguez et al., 2014; Sauder et al., 2017). Also the genera *Rhizophagus* and *Tulasnella,* both of which represent mycorrhizal fungi, performed better in coumarin-containing rhizospheres, which is in line with the observation that phenolic compounds stimulate growth and root colonization of arbuscular fungi (Fries et al., 1997).

Amongst the genera that performed better on coumarin non-producing roots (Col-0/+Fe and/or *f6'h1*/-Fe), was the genus *Nafulsella,* which was previously found to be incapable of hydrolyzing the coumarin esculin (Zhang et al., 2013). Moreover, the genera *Adhaeribacter, Hymenobacter,* and *Pontibacter,* all belonging to the Hymenobacteraceae family, were

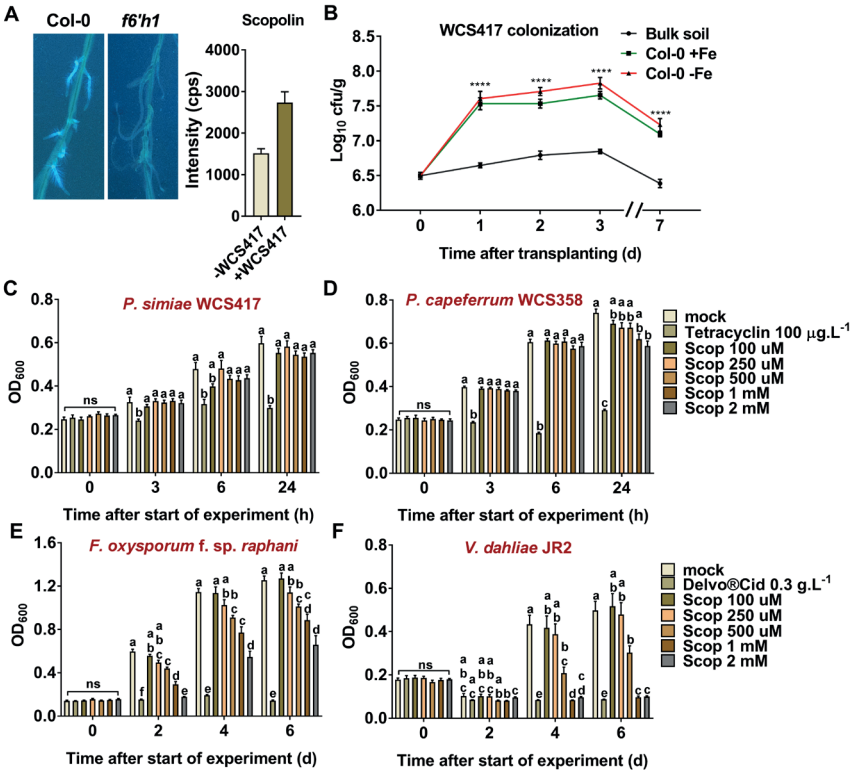

Figure 5. Effect of scopoletin on *P. simiae* WCS417 colonization and on growth of selected soil-inhabiting microbes. (A) Visualization of fluorescent phenolic compounds produced by roots of iron-sufficient Col-0 and scopoletin biosynthesis mutant *f6'h1* plants in response to colonization by *P. simiae* WCS417. Visualization of fluorescent phenolic compounds was achieved under UV light (365 nm). Photographs were taken from roots of 20-d-old *in vitro*-grown *Arabidopsis* plants, 7 d after colonization by the rhizobacteria. Bars show signal intensity in counts per second (cps) of the coumarin scopolin (detected as $[M+H]^+$) in Col-0 roots 2 d after colonization by *P. simiae* WCS417. Shown data are means (±SEM) of 3 biological replicates (see also Figure S5). **(B)** Number of *P. simiae* WCS417 bacteria recovered from rhizospheres of Col-0 grown in limed Reijerscamp soil that was amended with 10^5 cfu g^{-1} WCS417 bacteria. Root colonization was determined at indicated days after transplanting the seedlings from iron-sufficient (+Fe) or iron-starved (-Fe) Hoagland growth medium into the WCS417-amended Reijerscamp soil. Values for each time point were calculated from 5 rhizosphere or bulk soil samples. Asterisks indicate significant differences between bulk soil and colonized plants (Two-way ANOVA, Tukey's test, ****$P < 0.0001$). **(C-F)** Graphs showing growth (OD_{600}) of *P. simiae* WCS417 **(C)**, *P. capeferrum* WCS358 **(D)**, *F. oxysporum* f.sp. *raphani* **(E)**, and *V. dahliae* JR2 **(F)** in media containing the indicated concentrations of scopoletin (Scop). Tetracyclin and Delvo®Cid were used as positive controls for bacteria and fungi, respectively. Growth measurements were performed over a period of 24 h (bacteria) or 6 d (fungi). The shown data are means of 8-10 replicates. Error bars represent SEM. Different letters represent significant differences between treatments (Two-way ANOVA, Tukey's test; $P < 0.05$).

enriched in coumarin non-producing rhizospheres over coumarin-producing ones (Figure 4 and S6). Genera of this family can grow in poor substrates, can form strong biofilms, and their motility is not based on flagellar movement (gliding motility; Dastager et al., 2011; McBride et al., 2014; Srinivasan et al., 2016). However, it remains elusive to what extend these characteristics are related to the effect of coumarins on their performance.

Differential antimicrobial activity of scopoletin: selecting friends from foes?

Exudation of coumarins is a response that is shared between the iron- and the phosphate-starvation response of plants (Ziegler et al., 2016; Tsai and Schmidt, 2017b; Verbon et al., 2017). In analogy to our findings with iron uptake deficient mutants, it was shown that phosphate uptake-deficient and phosphate hyperaccumulating *Arabidopsis* genotypes assembled significantly different root-associated microbiomes than wild-type plants (Castrillo et al., 2017). Additionally, amendment of root exudates rich in phenolic compounds into the soil showed more pronounced effects on the microbial community than other classes of compounds (Badri et al., 2013). Hence, phenolic compounds in root exudates can be potent modulators of root microbiome assembly. This raises the question how ISR-inducing and plant growth-promoting microbes in the rhizosphere benefit from the induction of the MYB72- and BGLU42-dependent exudation of scopoletin in the rhizosphere. Scopoletin and other coumarins play a role in the mobilization and uptake of Fe^{3+} from the soil environment (Schmid et al., 2014; Fourcroy et al., 2016), and may therewith contribute to the mutually beneficial plant growth-promoting effect that such PGPR have on the plant. Besides its role in the iron uptake response, scopoletin possesses antimicrobial activities. In *Arabidopsis* and tobacco, scopoletin has been shown to accumulate around infection sites, where it inhibited growth of the foliar pathogens *B. cinerea, Alternaria alternata,* and *P. syringae* (El Oirdi et al., 2010; Simon et al., 2010; Sun et al., 2014). Other studies have shown that coumarins can negatively affect biofilm formation and virulence of pathogenic bacteria in different systems (Lee et al., 2014; Gutiérrez-Barranquero et al., 2015). In our experimental setup, scopoletin had no growth-inhibiting effect on the ISR-inducing PGPR *P. simiae* WCS417, neither *in vivo* on *Arabidopsis* roots nor *in vitro*, and only at high concentrations mildly reduced growth of ISR-inducer *P. capeferrum* WCS358 (Figure 5). By contrast, scopoletin strongly inhibited growth of the soil-borne fungal pathogens *F. oxysporum* and *V. dahliae* (Figure 5). Besides reducing growth of these fungi, we found that scopoletin deters germinating *F. oxysporum* spores (Figure S8B) and inhibits pigmentation of *F. oxysporum* mycelium (Figure S8A). Such mycelial pigments can have protective activities against environmental stresses (Son et al., 2008; Limón et al., 2010). Hence, inhibition of their formation by scopoletin could render this fungus less viable in the rhizosphere.

Collectively, our microbiome and targeted microbial growth analyses show that some soil-borne microbes can be sensitive to the antimicrobial activity of scopoletin, while others are tolerant. Beneficial ISR-inducing rhizobacteria, such as *P. simiae* WCS417 and *P. capeferrum* WCS358 induce *MYB72* and *BGLU42,* which leads to the onset of ISR and the excretion of scopoletin in the rhizosphere. Like *P. simiae* WCS417 (Figure 5A), ISR inducers *P. fluorescens* SS101 and *Paenibacillus polymyxa* BFKC01 (Van de Mortel et al., 2012; Zhou et al., 2016) also stimulate the production of coumarins upon colonization of *Arabidopsis* roots. It is tempting to speculate that in these mutualistic plant-microbe interactions, the rhizobacteria benefit because scopoletin outcompetes scopoletin-sensitive microbes in the same root niche, while the plant benefits because the population of plant-beneficial microbes increases while scopoletin-sensitive soil-borne pathogens are suppressed. Future research will be focused on the development of a representative microbiome-informed collection of scopoletin sensitive and insensitive microbial strains to test the hypothesis that scopoletin production favors the selection of plant-beneficial microbes in the rhizosphere.

MATERIALS AND METHODS

Plant material and growth conditions

In this study, *Arabidopsis thaliana* accession Col-0 and the mutants *myb72-2* (Van der Ent et al., 2008), *bglu42* (SALK-034026; Zamioudis et al., 2014) and *f6'h1-1* (Kai et al., 2008) were used. Mutant *f6'h1-1* was kindly provided by Prof. Jürgen Zeier. For all experiments, seeds were surface sterilized and sown on agar-solidified 1x Murashige and Skoog (MS) medium supplemented with 0.5% sucrose (Murashige and Skoog, 1962). After 2 d of stratification at 4°C, the Petri dishes were positioned vertically and transferred to a growth chamber (22°C; 10 h light, 14 h dark; light intensity 100 µmol m^{-2} s^{-1}). For growth under conditions with sufficient or limited iron, uniform 13-day-old seedlings were transferred to 12-well plates (2 seedlings per well) containing liquid Hoagland medium (5 mM KNO_3, 2 mM $MgSO_4$, 2 mM $Ca(NO_3)_2$, 2.5 mM KH_2PO_4, 70 µM H_3BO_3, 14 µM $MnCl_2$, 1 µM $ZnSO_4$, 0.5 µM $CuSO_4$, 10 µM NaCl, 0.2 µM Na_2MoO_4, 4.7 mM MES, 0.5% (w/v) sucrose; pH 5.5). For iron-sufficient growth conditions, Fe(III)EDTA was added to a final concentration of 50 µM, whereas for iron starvation conditions Fe(III)EDTA was added to a final concentration of 10 µM (medium-low iron condition) or left out of the growth medium (low iron condition).

For the metabolome analysis, roots and exudates were harvested from 20-d-old Col-0, *myb72* and *bglu42* plants that had been grown for 7 d in the media described above under low iron (no added Fe(III)EDTA) or sufficient iron (50 µM Fe(III)EDTA) conditions. For the metabolome analysis of *P. simiae* WCS417-colonized roots, 17-d-old Col-0 seedlings growing in iron sufficient conditions (as above) were inoculated at the root-shoot junction either with MgSO4 (mock) or *P. simiae* WCS417 (OD_{600}: 0.1; 10^8 colony-forming units (cfu) ml^{-1}). After 2 d, when 19-d-old, 300 to 400 roots were harvested for each biological replicate (3 biological replicates per treatment) and sent for metabolite fingerprinting.

For the root microbiome analysis, 13-day-old Col-0, *myb72* and *f6'h1* seedlings were transferred to 12-well plates containing the medium described above, with 50 µM Fe(III) EDTA (sufficient iron) or 10 µM Fe(III)EDTA (medium-low iron). Six days later, the 19-d-old plants were transferred to new 12-well plates containing either 50 µM Fe(III)EDTA (sufficient iron) or 0 µM Fe(III)EDTA (low iron). After 1 week of growth under iron-sufficient or iron-starved conditions, 26-d-old plants were transferred to 60-ml pots containing a natural soil taken from a field in nature reserve the Reijerscamp (52°01'02.55'', 5°77'99.83''), where natural *Arabidopsis* populations grow. Before use, the Reijerscamp soil was prepared as described (Berendsen et al., 2018), after which the soil was limed with CaO (0.0025 g per gram of soil) to make the soil alkaline (pH >7.5) and reduce iron availability.

Quantification and visualization of fluorescent phenolic compounds in root exudates

The production and secretion of fluorescent phenolic compounds by *Arabidopsis* roots was monitored under UV light (365 nm) as described (Zamioudis et al., 2014). In order to quantify the amount of fluorescent phenolic compounds in the root exudates, 200 µl of growth medium was transferred into a 96-well microplate. Fluorescence emitted by the root exudates (excitation at 360 nm; emission at 528 nm) was measured with a Synergy™ Multi-Mode Microplate Reader (BioTek, Winooski, VT, USA) as described (Zamioudis et al., 2014).

To visualize coumarin production in the roots in response to colonization by *P. simiae* WCS417, Col-0 and *f6'h1* seedlings were initially grown on MS medium supplemented with 0.5% sucrose. Subsequently, 7-day-old plants were transferred to plates containing Hoagland medium with sufficient iron (50 µM Fe(III)EDTA). Six days later, plants were inoculated at the root-shoot junction with 5 µl of a suspension of WCS417 bacteria (OD_{600} =

0.1). The bacteria were allowed to colonize the root system for 7 d after which production of fluorescent phenolic compounds was visualized under UV light (365 nm).

Quantitative real-time PCR analysis

Total RNA was extracted from *Arabidopsis* roots using a modified protocol of Oñate-Sánchez and Vicente-Carbajosa (Onate-Sanchez and Vicente-Carbajosa, 2008), after which it was treated with DNase according to the manufacturer's instructions (Thermo Scientific, Waltham, MA USA). Subsequently, cDNA was synthesized using SuperScript III Reverse Transcriptase (Invitrogen, Waltham, MA, USA), according to the manufacturer's instructions. PCR reactions were performed in optical 384-well plates (Applied Biosystems, Foster City, CA, USA) with an ABI PRISM® 7900 HT sequence detection system, using SYBR® Green (Applied Biosystems) to monitor the synthesis of double-stranded DNA. A standard thermal profile was used: 50°C for 2 min, 95°C for 10 min, 40 cycles of 95°C for 15 s and 60°C for 1 min. Amplicon dissociation curves were recorded after cycle 40 by heating from 60 to 95°C with a ramp speed of 1.0°C min^{-1}. Transcript levels were calculated relative to the reference gene *At1g13320* (Czechowski et al., 2005) using the $2^{-\Delta Ct}$ method described previously (Schmittgen and Livak, 2008). The expression levels of *IRT1, FRO2, MYB72, F6'H1, CYP71A12, CYP79B2, CYP79F2, PR3* and *At1g13320* were determined using the gene-specific primers that are listed in Table S4.

Metabolite fingerprinting analysis of root exudates and roots extracts

For metabolite fingerprinting of the root exudates, 200 µl exudates were extracted by two-phase-extraction with methyl-*tert*-butyl ether (MTBE) using a modified method as described (Matyash et al., 2008; Floerl et al., 2012). Polar and non-polar phases of root exudates were combined, evaporated under a nitrogen stream and, resolved in 100 µl acetonitrile/methanol/water (1:1:12, *v/v/v*). After centrifugation 80 µl of the supernatant were transferred to a micro vial and used for analysis.

For metabolite fingerprinting of the root samples, 100 mg of homogenized root material were extracted by two-phase-extraction in MTBE using a modified protocol as described (Matyash et al., 2008; Bruckhoff et al., 2016). The polar extraction phase was dried under nitrogen stream and resuspended in methanol/acetonitrile/water (15:15:100, *v/v/v*), while the non-polar extraction phase was dried and resuspended in 100 µl of chloroform/methanol/water (60:30:4.5, *v/v/v*).

The metabolite fingerprinting analysis was performed by Ultra Performance Liquid Chromatography (UPLC, ACQUITY UPLC System, Waters Corporation, Milford, USA) coupled with a photo diode array detector and an orthogonal time-of-flight mass spectrometer (TOF-MS, LCT Premier, Waters Corporation, Milford, USA) as described (König et al., 2014). Data acquisition was carried out by using the MassLynx software (MassLynx V4.1 SCN779, Waters Corporation, Milford, USA) in centroid data format. For data deconvolution (peak picking and alignment) the software MarkerLynx (Waters Corporation, Milford, USA) was used. For further data processing we used the toolbox MarVis (MarkerVisualization, http://marvis.gobics.de; Kaever et al., 2015).

This metabolite fingerprinting approach results, after peak picking and peak alignment, in large data matrixes with thousands of metabolite features (both for the positive and the negative ionization mode). A feature is defined by a specific retention time (RT), an accurate mass and the corresponding intensity values over all analysed samples. In the workflow the LC is coupled via an electrospray ionization (ESI) interface to the mass spectrometer (MS). The use of this configuration leads to the formation of numerous different adducts

of one metabolite during the ionisation in the ESI source of the MS. Therefore, LC-ESI-MS analyses can result in several mass signals for one metabolite, which then may result in several features for one metabolite. It is possible that metabolites of high abundance and a certain structure have a large number of adducts during ESI, which results in a high number of features representing one metabolite only. For data analysis and visualization, the intensity patterns of the high-quality metabolite features were clustered by means of one-dimensional self-organizing-maps (1D-SOMs). After normalization, sample aggregation was performed on mean values and marker scaling by the Euclidean norm (2-norm). Clusters with intensity pattern of interest in the respective experimental condition were selected. Features represented by these clusters were putatively identified by an automated database search within a mass deviation of 5 mDa: AraCyc (http://www.arabidopsis.org), MetaCyc (http://metacyc.org) and KEGG (http://www.genome.jp/kegg). The structure of marker metabolites was confirmed by quantitative RP-HPLC-DAD analysis (for scopoletin and scopolin), UV/VIS analysis and/or by high resolution MS^2 analysis by UHPLC ESI-QTOF-MS. Therefore, metabolites were analyzed by LC 1290 Infinity coupled with a 6540 UHD Accurate-Mass Q-TOF-MS instrument with Agilent Dual Jet Stream Technology (Agilent Technologies, Santa Clara, CA, USA) as ESI source as described (Bruckhoff et al., 2016). The compounds scopolin, esculin and isofraxidin were obtained from PhytoLab (Vestenbergsgreuth, Germany), while scopoletin and esculetin were obtained from Sigma-Aldrich (Deisenhofen, Germany).

Quantification of scopolin and scopoletin in root exudates and extracts

Root extracts of Col-0, *myb72* and *bglu42* were extracted by a protocol adapted from Zum Felde et al. (Zum Felde et al., 2007). Homogenized root material (10 mg) was extracted with 1 ml 80% methanol in the presence of zirconia beads for 30 min at room temperature. After centrifugation for 10 min at 16.000 *g* the supernatant was transferred to a fresh vial and diluted 1:1 (*v/v*) in 80% methanol. Samples of Col-0 and *bglu42* grown without iron were diluted additionally 1:50 (*v/v*) in 80% methanol. Aliquots of 5 µl were injected into an Agilent 1100 HPLC system coupled with a fluorescence detector and equipped with a Nucleosil 120-5 C-18 column (EC250/2, Machery & Nagel, Germany). Separation was achieved using a flow rate of 0.3 ml min^{-1}, a solvent system of water with 0.1% formic acid (solvent A), acetonitrile with 0.1% formic acid (solvent B) and a linear gradient from 10 to 40% B within 20 min, followed by a washing step of 100% solvent B for 5 min and re-equilibrating the column for initial flow conditions for 5 min. Scopolin and scopoletin were detected by fluorescence analysis at 336 nm (excitation) and 438 nm (emission) as described (Schmid et al., 2014). For quantification purposes, detector calibration (external calibration) was performed with a seven-point calibration curve of commercially available scopolin (Phytolab, Vestenbergsgreuth, Germany) and scopoletin (Sigma-Aldrich, Deisenhofen, Germany).

Root exudates were diluted 4:1 (*v/v*) in methanol. Exudates of Col-0 and *bglu42* grown without of iron were diluted in addition 1:20 (*v/v*) in 80 % methanol. Aliquots of 5 µl were directly used for HPLC-fluorescence analysis (see above).

Root microbiome analysis

Root samples (rhizosphere and roots) and bulk soil (3 root or soil samples per biological replicate; 3 biological replicates per treatment) were harvested 3 d after transferring 26-day-old Col-0, *myb72* and *f6'h1* plants from the *in vitro* system into pots containing limed natural Reijerscamp soil. To this end, the total pot content was carefully removed and plant roots

were gently shaken to remove loose soil particles. Roots together with adhering rhizosphere soil were transferred to 2-mL tubes, flash frozen in liquid nitrogen and stored at -80°C.

Genomic DNA isolation was performed by Vertis Biotechnologie AG (Freising, Germany). Briefly, the samples were ground with liquid nitrogen, after which genomic DNA was isolated using the RNA PowerSoil Total RNA Isolation Kit (MO BIO, Carlsbad, CA, USA) together with RNA PowerSoil® DNA Elution Accessory Kit, that allows the purification of both RNA and DNA. The genomic DNA samples (approx. 20 ng dsDNA each) were analyzed on a 0.8% agarose gel.

Library preparation was performed by Vertis Biotechnologie AG (Freising, Germany). The genomic DNA samples were treated with ultrasound (6 pulses of 30 s at 4°C). After end-repair, TruSeq sequencing adapters were ligated to the DNA fragments. Finally, the DNA was PCR-amplified to about 10-20 ng μl^{-1} using a High-fidelity DNA polymerase. The amplified DNA libraries in the size range of about 300-600 bp were then fractionated using a differential clean-up with the Agencourt AMPure kit (Beckman Coulter Brea, CA, USA). Aliquots of the size-fractionated libraries were quality checked by capillary electrophoresis. Libraries were pooled and sequenced on an Illumina NextSeq 500 platform (Utrecht University DNA sequencing facility), achieving on average 73 million paired-end reads sequencing depth per sample. The raw metagenome read data are deposited in the Short Read Archive (http://www.ncbi.nlm.nih.gov/sra/; BioProject ID: PRJNA435676). Following sequencing, raw paired-end sequencing reads generated by NextSeq 500 were demultiplexed using bcl2fastq Conversion Software (version 2.17.1) according to BaseSpace Illumina pipeline. FastQC (version v0.11.5) was used to assess length and quality of reads.

Quality-filtered Illumina reads were taxonomically classified with Kaiju (Menzel et al., 2016). Kaiju translates metagenomic sequencing reads into amino acid sequences, and then compares amino acid sequences with protein sequences in NCBI BLAST nr + euk database. The reference database consisted of non-redundant protein sequences form bacteria, archaea, viruses, fungi, microbial eukaryotes and *Arabidopsis*, which were extracted from National Center for Biotechnology Information. Running mode of Kaiju was set at the fastest MEM mode, with a default minimum match length of 11.

Statistical analyses were performed in R-studio (version 1.0.136) using R environment (version 3.3.3). Relative abundance (RA) data were normalized by the number of reads per sample replicate (total sum normalization). α-diversity (Shannon index) and β-diversity (PCoA using Bray–Curtis dissimilarities) were calculated in the "phyloseq" package (version 1.19.1; McMurdie and Holmes, 2013). Shannon diversity was calculated by applying the exponential function to the Shannon index. DESeq function of package DESeq2 (version 1.14.1) was used to perform two-class testing for differential RA of genera between different genotypes or iron treatments (Love et al., 2014). Genera were considered significantly differentially abundant between genotypes if their adjusted *P*-value was below 0.05 (corresponding to FDR < 5% under the Benjamini-Hochberg correction). Package ggplot2 (version 2.2.1) was used to create plots and graphs of the microbiome analysis (Wickham, 2016).

Cultivation of microbes and root colonization by *P. simiae* WCS417

V. dahliae isolate JR2 (kindly provided by Prof. Bart Thomma) was grown on potato dextrose agar (PDA) at 21°C (Fradin et al., 2009). *F. oxysporum* f. sp. *raphani* was grown on PDA at 28°C (Pieterse et al., 1996).

For assessing the effect of scopoletin on fungal growth in 96-well plates, *F. oxysporum* and *V. dahliae* spores were prepared by growing the fungi in 100 ml liquid SSN medium (Sinha and Wood, 1968) in 250-ml Erlenmeyer flasks at 28°C (*F. oxysporum*) or 23°C (*V.*

dahliae) under continuous shaking at 120 rpm for one week. The fungal suspension was filtered through glass wool. The filtrate was centrifuged for 10 min at 900 *g*. The pellet was suspended with ddH_2O to a final spore density of 10^5 conidia per ml.

For the chemotropism assay, *F. oxysporum* spores were prepared by growing the fungus in 100 ml liquid SSN medium in a 250-ml Erlenmeyer flask at 28°C under continuous shaking at 120 rpm for one week. The fungal suspension was filtered through glass wool. The filtrate was centrifuged for 10 min at 900 *g*. The pellet was suspended with ddH_2O to a final spore density of $2.5x10^9$ conidia per ml.

P. simiae WCS417 and *P. capeferrum* WCS358 (Berendsen et al., 2015) were cultured on King's medium B (KB) agar plates (King et al., 1954) supplemented with 50 µg ml^{-1} rifampicin at 28°C. After 24 h of growth, cells were collected in 10 mM $MgSO_4$, washed twice by centrifugation for 5 min at 5000 *g* and finally resuspended in 10 mM $MgSO_4$ to a final density of OD_{600}=0.2 ($2*10^8$ cfu ml^{-1}).

To assess root colonization by rifampicin-resistant *P. simiae* WCS417, 23-d-old Col-0 plants were transferred from the *in vitro* growth system to limed Reijerscamp soil to which WCS417 bacteria were added to a final density of 10^5 cfu g^{-1}. Rhizosphere samples (roots with adhering soil) were harvested at 1, 2, 3 and 7 d after transplanting after which bacterial densities in the rhizosphere were determined. To this end, 0.1 g of rhizosphere sample or bulk soil (soil from unplanted pots) of five replicate pots per treatment were transferred into 2-ml Eppendorf tubes containing 1 ml of 10 mM $MgSO_4$ and shaken vigorously for 1 min. Aliquots of 100 µl of serial dilutions were plated on KB agar plates containing 150 µg ml^{-1} rifampicin and 0.2 g l^{-1} Delvo®Cid. Plates were incubated overnight at 28°C after which WCS417 colonies were counted and densities in the rhizosphere and bulk soil samples were calculated.

In vitro assay for antimicrobial effect of scopoletin

To quantify the effect of scopoletin on *in vitro* growth of the fungal soil-borne pathogens *F. oxysporum* f.sp. *raphani* and *V. dahliae* JR2, and on the PGPR *P. simiae* WCS417 and *P. capeferrum* WCS358, we designed a microplate assay based on a described protocol (Pryor et al., 2007). In brief, 96-well plates (flat bottom; Greiner Bio-One, Kremsmünster, Austria) were filled with 100 µl liquid potato dextrose broth (PDB) for the fungi or 100 µl liquid KB for the bacteria. The growth media were supplemented with different concentrations of scopoletin (Sigma-Aldrich, St. Louis, MO, USA) from a 50-mM stock in 80% methanol. The blank controls contained equal amounts of methanol (3.2%) without scopoletin. The antibiotics Delvo®Cid (0.3 g l^{-1}; DSM, Heerlen, The Netherlands) and tetracyclin (100 µg ml^{-1}, Sigma-Aldrich) were used as positive controls for the inhibition of fungal and bacterial growth, respectively. At the start of the microbial growth curves, 100 µl of fungal spore or bacterial cell suspension was added to each well (final density $5x10^4$ spores per ml or 10^8cfu ml^{-1}, respectively). The 96-well plates were covered with sterile seals (Excel Scientific SealPlate film; Sigma-Aldrich) and wrapped in aluminum foil. Plates with *F. oxysporum* and the bacteria were incubated at 28°C, whereas plates with *V. dahliae* were kept at room temperature.

The inhibition of *F. oxysporum* mycelial growth by scopoletin *in vitro* was tested in Petri dishes by subculturing a mycelium plug of 5 mm diameter on PDA containing 500 µM scopoletin for 6 d in the dark at 28°C. PDA supplemented with 1% methanol served as a negative control and PDA with 0.2 g l^{-1} Delvo®Cid and 1% methanol as a positive control. The area of mycelium growth was recorded every 2 d.

Scopoletin chemotropism assay

To quantify the level of chemotropism in *F. oxysporum* in response to scopoletin, a chemotropism assay was used based on the previously described method (Turra et al., 2015). Conidia of *F. oxysporum* f.sp. *raphani* were obtained from an SSN liquid culture at a density of 2.5×10^9 conidia per ml ddH_2O. The conidia suspension was further diluted in 0.5% (w/v) water agar (Oxoid, Badhoevedorp, The Netherlands) to a final density of 2.5×10^7 spores per ml. A total volume of 4 ml of the water agar with conidia was poured into Petri dishes (Ø 94 mm with vents; Greiner Bio-One, Kremsmünster, Austria). The Petri dishes were marked on the bottom with three parallel lines crossing the width of the plate at a distance of 0.5 mm from each other. Two square wells were cut into the agar along the two outer marked lines, after which 50 µl of a test compound solution or its solvent were added to either well. Pectin (1%, *w/v*; Fluka Analytical, Buchs, Switzerland) dissolved in distilled water was used as a positive control (Turra et al., 2015). Scopoletin (Sigma-Aldrich, Steinheim, Germany) was applied in concentrations of 250 µM and 1 mM. Root exudates of Col-0 and *f6'h1* plants, pre-grown under the iron-deficient conditions described above, collected 3 d after transferring the plants in MQ were tested as well. Plates were sealed with parafilm and wrapped in aluminium foil for overnight incubation at 28°C. After 12 h, the plates were moved to 4°C after which pictures were taken of germinating conidia using a Zeiss Axioskop 2 (100x magnification) with a Lumenera Inifinity 1 camera and the software Image-Pro Insight 9.1. Using Adobe Photoshop CS6 (Adobe Systems, San Jose, CA, USA), germinating conidia in each picture were assigned a direction of germination towards the solvent, towards the test compound or towards neither ("neutral"). Chemotropism was calculated as the percentage of germinating tubes growing towards the solvent or the test compound. Between 800 and 1100 hyphae from germinating conidia growing towards either the test compound or the solvent were assessed per treatment.

ACKNOWLEDGMENTS

This work was supported by ERC Advanced Grant no. 269072 of the European Research Council (to CMJP), a fellowship of the China Scholarship Council (to KY), postdoctoral fellowship no. 12B8116N of the Research Foundation Flanders (RJ), and grant no. ZUK 45/2010 of the Deutsche Forschungsgemeinschaft (to IF). The authors would like to thank David Turrá for his suggestions on chemotropism assay, Bart Thomma for providing *Verticillium dahliae* JR2, Jürgen Zeier for *f6'h1* seeds, Richard Hickman for the discussion on the statistical analysis of microbiome data and Sabine Freitag and Hans Van Pelt for technical assistance.

Author contributions

I.A.S., K.Y., K.F., M.C.V.V., R.L.B., P.A.H.M.B., I.F., and C.M.J.P. designed experiments; I.A.S., K.Y., K.F., and S.V.B. performed experiments; I.A.S., K.Y., K.F., and R.D.J. analyzed data; and I.A.S. and C.M.J.P. wrote the paper.

SUPPLEMENTAL DATA

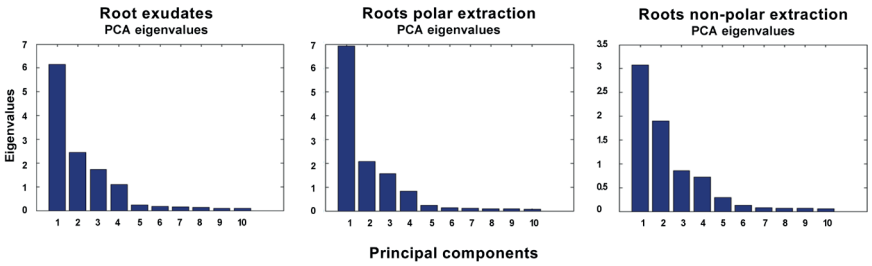

Figure S1. Bar plots with eigenvalues of the PCA plots of root exudates (Figure 1C), root extract polar extraction phase (Figure S3A) and root extract non-polar extraction phase (Figure S3B). The eigenvalues of the first 10 principle components (PCs) as calculated by the MarVis software toolbox are presented as bar plots. The largest eigenvalue defines the eigenvector 1, which is taken as principle component 1 (PC1). In case of the PCA shown in Figure 1C, the corresponding graphs of the eigenvalues indicates that PC1 explains the largest proportion of the variation of the covariance matrix, while the contribution of PC2 is much lower. Estimations based on the eigenvalues indicate that PC1 explains ~49% and PC2 ~19% of the variation in the PCA shown in Figure 1C (together ~68%). For the PCAs shown in Figures S3A and S3B estimations based on the eigenvalues indicate that PC1 and PC2 together explain ~65% of the variation in the polar extraction phase data and ~70 % of the variation in the non-polar extraction phase data.

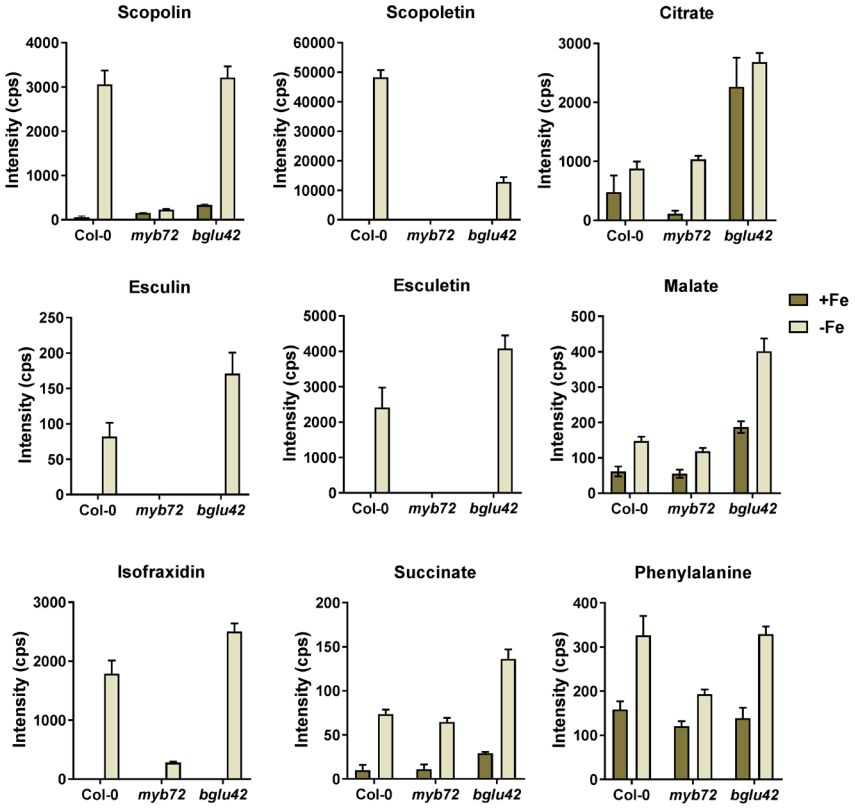

Figure S2. Root exudation patterns of metabolite features corresponding to iron-starvation associated coumarins, TCA cycle intermediates, and phenylalanine. Graphs represent the signal intensity in counts per second (cps) of the coumarins scopolin, scopoletin, esculin, esculetin and isofraxidin (detected as $[M+H]^+$), the primary metabolites citrate and phenylalanine (detected as $[M+H]^+$) and malate and succinate (detected as $[M-H]^-$) in root exudates of Col-0, *myb72,* and *bgu42* grown under iron sufficient (+Fe) or iron deficient (-Fe) conditions. The shown data are means of 3 replicates. Error bars represent SEM.

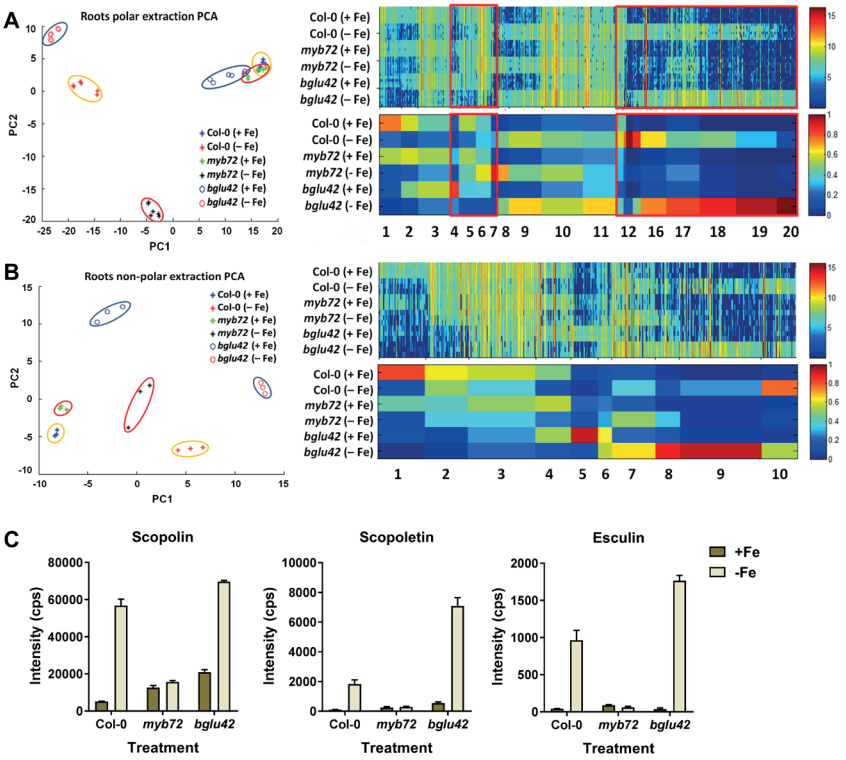

Figure S3. Metabolite fingerprinting of features detected in the root extracts of Col-0, *myb72* and *bglu42* grown under iron sufficient and iron starvation conditions. (A) PCA plot of UPLC-ESI-TOF-MS metabolite profiles of polar compounds identified in the root extracts of 20-d-old Col-0 (encircled in yellow), *myb72* (encircled in red) and *bglu42* (encircled in blue) plants grown in Hoagland medium with (+Fe) or without (-Fe). On the right, 1D-SOM clustering and prototype assignment of 1354 high-quality metabolite features (FDR < 10^{-8}). Individual features (top panel) and prototypes (bottom panel) mostly affected by iron deficiency are highlighted in the red box. Heatmaps correspond to the intensity of each individual feature (top panel) and the average intensity of each cluster/prototype (bottom panel). **(B)** PCA plot of UPLC-ESI-TOF-MS metabolite profiles of non-polar compounds identified in the root extracts of 20-d-old Col-0 (encircled in yellow), *myb72* (encircled in red) and *bglu42* (encircled in blue) plants grown in Hoagland medium with (+Fe) or without (-Fe). On the right, 1D-SOM clustering and prototype assignment of 554 high-quality metabolite features (FDR < 0.001). Heatmaps correspond to the intensity of each individual feature (top panel) and the average intensity of each cluster/prototype (bottom panel). **(C)** Signal intensity in counts per second (cps) of scopolin, scopoletin and esculin (all detected as $[M+H]^+$) in the root extracts of Col-0, *myb72* and *bgu42* plants grown under iron-sufficient (+Fe) or iron-deficient (-Fe) conditions. The shown data are means of 3 replicates. Error bars represent SEM.

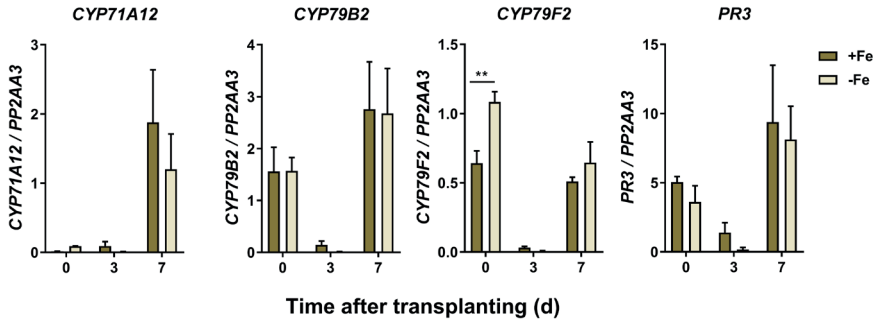

Figure S4. Levels of root defense marker gene expression are similar in roots of seedlings pre-grown under sufficient iron (+Fe) or low iron (-Fe) conditions. Gene expression profiles of root immunity marker gene *CYP71A12,* glucosinolate biosynthesis genes *CYP79B2* and *CYP79F2,* and pathogenesis-related protein gene *PR3* in roots of Col-0 plants pre-grown for 14 days in liquid Hoagland medium under iron-sufficient (+Fe) or low iron (-Fe) conditions before they were transplanted on day 0 to limed Reijerscamp soil. Gene expression was quantified by qRT-PCR just prior to (d 0) and 3 and 7 d after transplanting. Transcript levels were normalized to that of reference gene *PP2AA3* (At1g13320). Data are means of 3 biological replicates. Error bars represent SEM. Asterisks indicate significant differences between treatments (Two-way ANOVA, Sidak's test, $^{**}P$ <0.01).

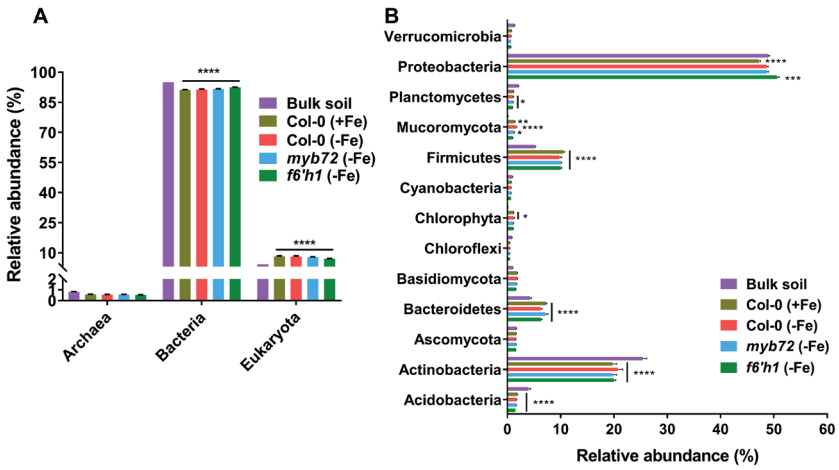

Figure S5. Microbial community shifts between bulk soil and the rhizosphere. (A) Average relative abundance of Archaea, Bacteria and Eukaryota domains in bulk soil and root-associated microbial communities. Bars correspond to the average of 3 replicates and error bars represent SEM. Asterisks indicate significant differences of root samples compared to bulk soil (Two-way ANOVA, Tukey's test; $^{****}P$ < 0.0001). **(B)** Average relative abundance (RA) of most-abundant phyla (RA > 0.5%) in bulk soil and root-associated microbial communities. Bars correspond to the average of 3 replicates and error bars represent SEM. Asterisks indicate significant differences of root samples compared to bulk soil (Two-way ANOVA, Tukey's test; $^{****}P$ < 0.0001; $^{***}P$ < 0.001; $^{**}P$ < 0.01; $^{*}P$ < 0.05).

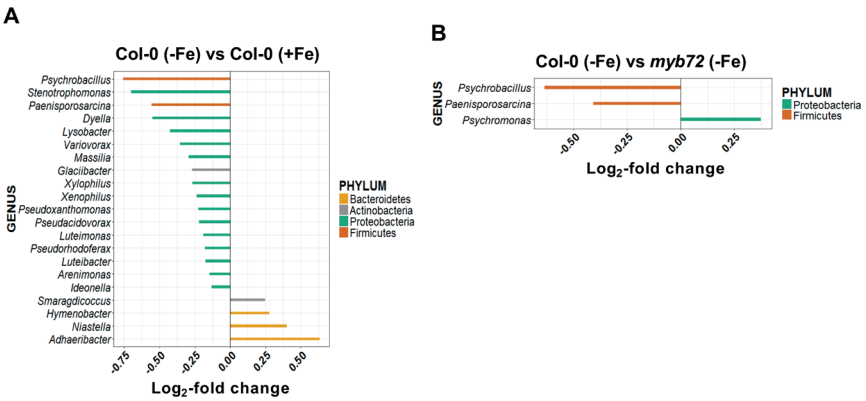

Figure S6. Differential abundance of microbial genera on Arabidopsis roots with different scopoletin exudation patterns. Differentially abundant bacterial and fungal genera between root samples of Col-0 (-Fe) and **(A)** Col-0 (+Fe) and **(B)** *myb72* (-Fe), as determined using DESeq2. Comparisons were performed at genus level using a false discovery rate (FDR) < 0.05 to select for significance. In all graphs, negative $\log_2$-fold change values relate to genera that are significantly enriched in iron-starved Col-0 (-Fe) root samples in comparison to the contrasting genotype/ treatment combination. Different colors of the bars correspond to different Phyla.

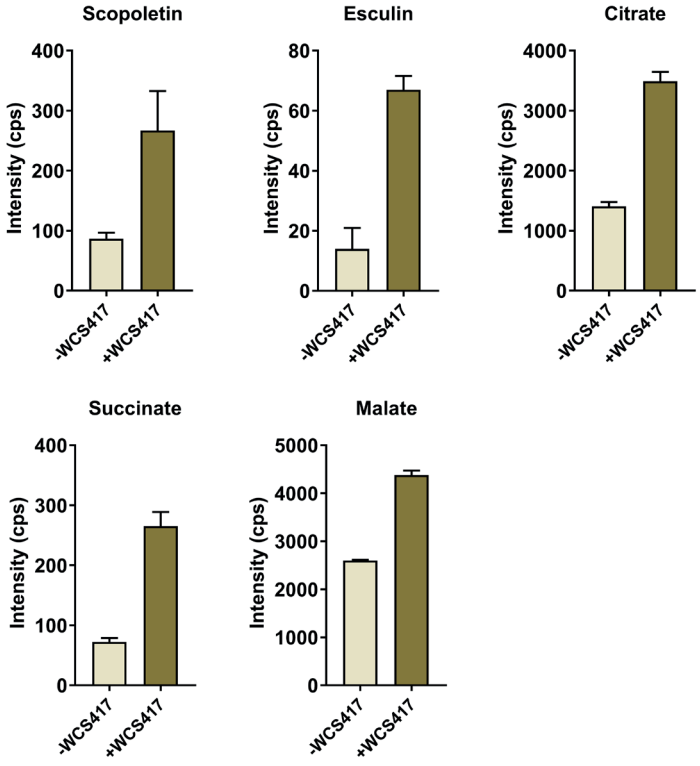

Figure S7. Increased accumulation of coumarins following root colonization by *Pseudomonas simiae* WCS417. Graphs represent the signal intensity in counts per second (cps) of the coumarins scopoletin and esculin (detected as $[M+H]^+$) and the TCA cycle intermediates citrate, succinate (detected as $[M+H]^+$) and malate (detected as $[M-H]^-$) in the root extracts of Col-0 plants 2 d after mock (-WCS417) or *P. simiae* WCS417 (+WCS417) inoculation of the roots. The shown data are means of 3 replicates. Error bars represent SEM.

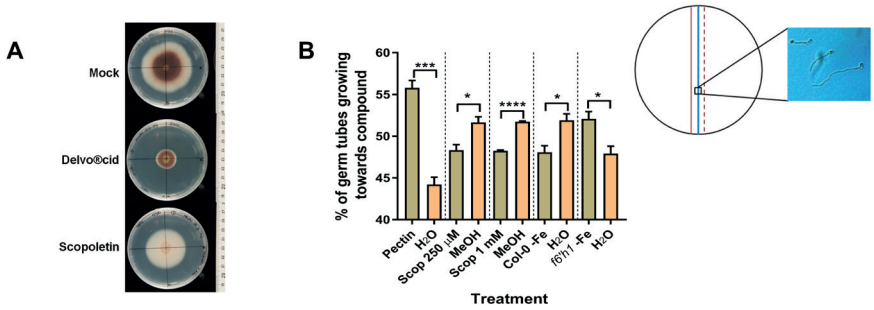

Figure S8. Effect of scopoletin on *F. oxysporum* physiology. (A) Growth of *F. oxysporum* f.sp. *raphani* mycelium on PDA plates supplemented with 0.2 g l^{-1} of the fungicide Delvo®cid or 500 µM of scopoletin. Pictures of representative plates were taken after 7 d of fungal growth at 28˚C. **(B)** Chemotropism of *F. oxysporum* f. sp. *raphani* spores towards pectin (1 %, *w/v*), scopoletin (250 µM and 1 mM) and root exudates of iron-starved Col-0 and *f6'h1* plants. Chemotropism was evaluated as percentage of the germinating spores growing towards the tested compound or its solvent. Pectin was used as a positive control. Dashed lines separate the different compound-solvent combinations tested. In each combination, percentages of spores attracted either by the solvent or the tested compound add up to 100%. Shown are the mean percentages of three replicates per treatment, each based on hyphal orientation counts of ca. 900 conidia. Error bars represent SEM. Asterisks indicate significant differences within each treatment combination (Student's *t*-test, ****$P < 0.0001$; ***$P < 0.001$; *$P < 0.05$). The inset provides a representation of the chemotropism test (Turra et al., 2015), in which the orientation of hyphal growth was tested on the blue line in the middle, with the solvent on the red line and the test compound on the dashed line. The photo is a representative image of germinating *Fusarium* spores at the moment of scoring.

Table S1: Confirmation of the identity of metabolite features corresponding to the selected coumarins, TCA cycle intermediates, and phenylalanine shown in Figure S2, by HPLC-ESI-QTOF-MS2 analysis or coelution.

Metabolite marker	RT (min)	m/z	Detected ion	Calculated mass (Da)	Sum formula	Error (mDa)
Coumarin derivatives:						
Scopoletin/7-Hydroxy-6-methoxy-coumarin	3.96	193.0482	[M+H+]+	192.0423	$C_{10}H_8O_4$	-1.4
Scopolin	3.06	355.1005	[M+H+]+	354.0951	$C_{16}H_{18}O_9$	-1.9
Esculetin/6,7-Dihydroxy-coumarin	3.15	179.0319	[M+H+]+	178.0266	$C_9H_6O_4$	-2
Esculin	2.78	341.0853	[M+H+]+	340.0794	$C_{15}H_{16}O_9$	-1.4
Isofraxidin (8-Hydroxy-6,8-dimethoxy-coumarin)	4.06	223.059	[M+H+]+	222.0528	$C_{11}H_{10}O_5$	-1.1
Amino acids and TCA cycle intermediates:						
Phenylalanine	1.99	166.0845	[M+H+]+	165.079	$C_9H_{11}NO_2$	-1.8
Citrate	0.78	191.0202	[M-H+]-	192.027	$C_6H_8O_7$	0.5
Succinate	0.97	119.0328	[M+H+]+	118.0266	$C_4H_6O_4$	-1.1
Malate	0.59	133.0161	[M-H+]-	134.0215	$C_4H_6O_5$	1.9

A) MS/MS fragment information from literature, METLIN data base (http://metlin.scripps.edu/) or MassBank data base (http://www.massbank.jp/)
B) MS/MS fragment information from authentic standard or corresponding compounds (in brackets)
C) Coelution with authentical standard
D) Qualitative RP-HPLC-DAD analysis

Cluster nr.	Compound identified by	MS^2 fragmentation	CE (eV)	λ max (nm)
4	A (METLIN: MID6956), B, C, D	193.0482 [M+H]+ , 178.0255, 150.0303, 133.0278, 137.0593, 122.0357, 94.0412, 77.0386	15	207, 290, 340
5	A (METLIN for scopoletin: MID6956), D	355.1005 [M+H]+, 193.049 [M-Glc+H]+, 178.0251, 133.0274,	20	
9	A (MassBank: ML003901, BML01641)	179.0319 [M+H]+, 151.039, 133.0273, 123.0433	10	
9	A (MassBank: ML003901, BML01641) for esculetin	341.085 [M+H]+, 179.0333 [M-Glc+H]+, 153.0906, 123.0409, 87.0441	20	
9	B, C	223.0589 [M+H]+, 208.0360, 207.0274, 190.0248, 179.0326, 162.0301, 134.0352 , 107.0486	15	214, 282, 330
8	A (METLIN: MID28)	166.0863 [M+H]+, 149.0676, 131.0482, 120.0808, 103.0546, 93.0698, 77.0386, 65.0387	10	
8	A (METLIN: MID124)	193.0303 [M+H]+, 157.0125, 139.0016, 111.0073, 87.0076, 68.997	8	
8	A (METLIN: MID114)	117.0181 [M-H]-, 99.0074, 73.0287	8	
8	A (METLIN: MID118)	133.0121 [M-H]-, 115.0023, 71.0131	8	

Table S2: Confirmation of the identity of metabolite features corresponding to the selected coumarins shown in Figure S3C, by retention time (RT) comparison with the root exudate data in Table S1.

Metabolite marker	RT (min)	m/z	Detected ion	Calculated mass (Da)	Sum formula	Error (mDa)	Cluster nr.
Coumarin derivatives							
Scopoletin/7-Hydroxy-6-methoxycoumarin	3.98	193.0482	$[M+H^+]^+$	192.0423	$C_{10}H_8O_4$	-1.4	19
Scopolin	3.09	355.1011	$[M+H^+]^+$	354.0951	$C_{16}H_{18}O_9$	-1.3	13
Esculin	2.80	341.0850	$[M+H^+]^+$	340.0794	$C_{15}H_{16}O_9$	-1.7	18

Table S3. Data related to shotgun metagenomic sequencing and classification of obtained reads by Kaiju. Samples from the compartments "bulk soil" and "root-rhizosphere" were subjected to shotgun metagenome sequencing. The root-rhizosphere samples were sampled from 3 different *Arabidopsis* genotypes (Col-0, *myb72*, and *f6'h1*) pre-grown under iron-sufficient (+Fe) or iron-deficient (-Fe) conditions. Paired-end sequencing reads (in millions, M) were classified with Kaiju (Menzel et al., 2016) using a database containing protein sequences of Bacteria, Archaea, Viruses, Fungi, microbial eukaryotes (collectively called "Microbiome") and *Arabidopsis*. Reads that could not be classified to *Arabidopsis* or a microbial genus were excluded from downstream statistical processing (Not classified).

Sample characteristics				Reads			
				Sequencing output	Kaiju		
					Classified		Not classified (%)
Sample name	Sample type	Genotype	Iron	Paired-end reads (M)	Microbiome (%)	Arabidopsis (%)	
B 1	bulk soil	n/a	n/a	66.8	37.43	0.03	62.54
B 2	bulk soil	n/a	n/a	65.8	37.89	0.01	62.10
B 3	bulk soil	n/a	n/a	52.4	37.70	0.01	62.29
Col +Fe 1	root-rhizosphere	Col-0	yes	83.6	21.62	29.81	48.57
Col +Fe 2	root-rhizosphere	Col-0	yes	64.5	21.74	30.54	47.72
Col +Fe 3	root-rhizosphere	Col-0	yes	55.6	23.11	28.27	48.62
Col -Fe 1	root-rhizosphere	Col-0	no	63.4	24.16	26.59	49.25
Col -Fe 2	root-rhizosphere	Col-0	no	77.2	22.11	29.86	48.03
Col - Fe 3	root-rhizosphere	Col-0	no	67.6	21.91	32.12	45.97
myb72 - Fe 1	root-rhizosphere	myb72	no	76.0	22.45	30.03	47.52
myb72 - Fe 2	root-rhizosphere	myb72	no	75.7	20.90	30.12	48.98
myb72 - Fe 3	root-rhizosphere	myb72	no	108.7	23.04	28.88	48.08
f6'h1 - Fe 1	root-rhizosphere	f6'h1	no	79.0	22.12	29.95	47.93
f6'h1 - Fe 2	root-rhizosphere	f6'h1	no	80.3	22.93	30.40	46.67
f6'h1 - Fe 3	root-rhizosphere	f6'h1	no	82.0	21.58	31.61	46.81
Total				1098.6			

Table S4: List of primers used in this study.

Primer name	Gene	Primer sequence
*PP2AA3*_Fw	At1g13320	5'-TAACGTGGCCAAAATGATGC-3'
*PP2AA3*_Rev	At1g13320	5'-GTTCTCCACAACCGCTTGGT-3'
*MYB72*_Fw	At1g56160	5'-ACGAGATCAAAAACGTGTGGAAC-3'
*MYB72*_Rev	At1g56160	5'-TCATGATCTGCTTTTGTGCTTTG-3'
*IRT1*_Fw	At4g19690	5'-ACCCGTGCGTCAACAAAGCTAAAG-3'
*IRT1*_Rev	At4g19690	5'-TCCCGGAGGCGAAACACTTAATGA-3'
*FRO2*_Fw	At1g01580	5'-TGTGGCTCTTCTTCTCTGGTGCTT-3'
*FRO2*_Rev	At1g01580	5'-TGCCACAAAGATTCGTCATGTGCG-3'
*F6'H1*_Fw	At3g13610	5'-TGATATCTGCAGGAATGAAACG-3'
*F6'H1*_Rev	At3g13610	5'-GGGTAGTAGTTAAGGTTGACTC-3'
*CYP71A12*_Fw	At2g30750	5'-GATTATCACCTCGGTTCCT-3'
*CYP71A12*_Rev	At2g30750	5'-CCACTAATACTTCCCAGATTA-3'
*CYP79B2*_Fw	At4g39950	5'-AACAAAAAGAAACCGTATCTGCCAC-3'
*CYP79B2*_Rev	At4g39950	5'-TCCTAACTTCACGCATGCTATCTC-3'
*CYP79F2*_Fw	At1g16400	5'-GGAGAGAGCGAAAGTGAATGT-3'
*CYP79F2*_Rev	At1g16400	5'-ACCTTTTTCCCTCCAAATTTC-3'
*PR3*_Fw	At3g12500	5'-CAATGCAACTGTCGTGGAAC-3'
*PR3*_Rev	At3g12500	5'-TGAGCAGTCATCCAGAACCA-3'

The following data sets are available at: https://doi.org/10.1073/pnas.1722335115

Dataset S1. The marker candidate ID, retention time (RT), mass (in dalton), relative intensities and putative identity of features identified in root exudates of Col-0, *myb72,* and *bglu42* plants growing under iron-sufficient and iron-starved conditions (Figure 1D).

Dataset S2. The marker candidate ID, retention time (RT), mass (in dalton), relative intensities and putative identity of features identified in root exudates of Col-0, *myb72,* and *bglu42* plants growing under iron-starved conditions (Figure 2A).

Dataset S3. The marker candidate ID, retention time (RT), mass (in dalton), relative intensities and putative identity of features identified in root extracts of Col-0, *myb72,* and *bglu42* plants growing under iron-sufficient and iron-starved conditions (polar extraction phase; Figure S3A).

Dataset S4. The marker candidate ID, retention time (RT), mass (in dalton), relative intensities and putative identity of features identified in root extracts of Col-0, *myb72,* and *bglu42* plants growing under iron-sufficient and iron-starved conditions (non-polar extraction phase; Figure S3B).

Dataset S5. Number of reads assigned to microbes classified at Genus level with Kaiju and their taxonomy.

Dataset S6. Relative abundance of selected coumarins and TCA cycle intermediates in roots of mock-treated and *P. simiae* WCS417-inoculated Col-0 plants (corresponds to graphs shown in Figure 5A and Figure S7).

CHAPTER 4

Root metabolic changes induced by plant-beneficial *Pseudomonas simiae* WCS417

Ke Yu[1,4], Ioannis A. Stringlis[1,4], Kirstin Feussner[2], Ivo Feussner[2,3], Corné M. J. Pieterse[1], Peter A. H. M. Bakker[1] and Roeland L. Berendsen[1]

[1]Plant-Microbe Interactions, Institute of Environmental Biology, Utrecht University, Padualaan 8, 3584 CH Utrecht, The Netherlands
[2]Department of Plant Biochemistry, Albrecht-von-Haller-Institute for Plant Sciences, University of Goettingen, 37077 Goettingen, Germany
[3]Department of Plant Biochemistry, Goettingen Center for Molecular Biosciences (GZMB), University of Goettingen, 37077 Goettingen, Germany
[4]These authors contributed equally to this work

ABSTRACT

Induced systemic resistance (ISR) elicited upon root colonization by specific rhizobacteria is an effective defense mechanism of plants against pathogen and insect attack. The root-specific transcription factor MYB72 is a key regulator in the onset of rhizobacteria-mediated ISR in *Arabidopsis thaliana* (hereafter *Arabidopsis*). MYB72 also regulates the biosynthesis and excretion of coumarins, which is induced when plants grow under iron deficient conditions. Coumarins, such as scopoletin, are fluorescent phenolic compounds that mobilize iron in the root environment. Moreover, they possess an antimicrobial activity that can significantly affect the composition of the root microbiome. The ISR-eliciting and plant growth-promoting rhizobacterium *Pseudomonas simiae* WCS417 (hereafter WCS417) is a strong inducer of *MYB72* in *Arabidopsis* roots, but is insensitive to the antimicrobial activity of scopoletin. This suggests that the mutualist WCS417 induces the production of antimicrobial coumarins by plant roots to improve its own niche establishment and in return provides growth and immunity benefits for the host plant. To characterize the metabolites that are produced in response to colonization by WCS417, we fingerprinted the *Arabidopsis* root metabolome of both wild-type Col-0 and mutant *myb72* plants. Our data show that WCS417 stimulates the biosynthesis of the coumarins scopolin, scopoletin and esculin in *Arabidopsis* roots. WCS417 also significantly affected the biosynthesis of glucosinolates and fatty acid metabolites with predicted functions in plant immunity. Col-0 and *myb72* displayed relatively minor differences in the totality of the WCS417-induced metabolome changes, suggesting that MYB72 regulates only a subset of the WCS417-induced metabolites or partly acts redundantly. These results provide novel insight into the metabolites that play a role in the mutualistic interaction between plant roots and ISR-inducing rhizobacteria.

INTRODUCTION

Plant roots deposit carbon into the directly surrounding soil, making the rhizosphere an important niche for microbial proliferation and activity in the otherwise carbon-starved soil environment (Badri and Vivanco, 2009; Badri et al., 2009; Sasse et al., 2018; Yuan et al., 2018; Zhalnina et al., 2018). Root exudates consist of a complex mixture of organic compounds that can support but also inhibit specific microbes. Thus, these root exudates affect the complex microbial community associated with plant roots, the so-called root microbiome (Hu et al., 2018; Sasse et al., 2018; Stringlis et al., 2018b; Yuan et al., 2018; Zhalnina et al., 2018; Chapter 3). Specific members of the root microbiome promote plant growth or are beneficial for plant health. Such mutualistic microbiota members provide important services to the plant, such as acquiring scarce nutrients or fixing nitrogen (Bulgarelli et al., 2013; Tkacz and Poole, 2015; Bakker et al., 2018). Others provide protection by inhibiting soil-borne pathogens or by priming the plant immune system via induced systemic resistance (ISR), a defense mechanism that is effective against a broad spectrum of microbial pathogens and insect herbivores (Berendsen et al., 2012; Pieterse et al., 2014; Raaijmakers and Mazzola, 2016; Hacquard et al., 2017). The molecular basis of such a beneficial ISR-inducing root-microbe association has been extensively studied in the interaction between *Arabidopsis thaliana* (hereafter *Arabidopsis*) and the plant growth-promoting rhizobacterium *Pseudomonas simiae* WCS417 (hereafter WCS417; Pieterse et al., 1996; Van der Ent et al., 2008; Pieterse et al., 2014; Zamioudis et al., 2014; Zamioudis et al., 2015; Cole et al., 2017; Stringlis et al., 2018a). Plant hormones emerged as essential regulators of rhizobacteria-conferred beneficial traits. WCS417-mediated growth promotion and the associated modulation of the root architecture requires auxin, while WCS417-ISR relies on jasmonic acid (JA) and ethylene signaling (Pieterse et al., 1998; Zamioudis et al., 2013). Although ISR is observed in

numerous plant-microbe associations, little is known about the metabolites and signals that play a role in the communication between the plant roots and the ISR-inducing microbes in the rhizosphere.

Colonization of *Arabidopsis* roots by WCS417 results in the development of ISR in aboveground plant tissues. This enhanced protection against pathogen and insect attack is typically not associated with substantial changes in gene expression in the tissues distant of *Arabidopsis* roots colonized by WCS417 (Van Wees et al., 1999; Pieterse et al., 2000). In these systemic foliar tissues, ISR relies on potentiated expression of defense-related genes that become activated only upon pathogen or insect attack (Verhagen et al., 2004; Pozo et al., 2008). This phenomenon is called defense priming and provides the plant with a cost-efficient protection mechanism (Martinez-Medina et al., 2016). In contrast, *Arabidopsis* roots show substantial transcriptional changes upon WCS417 colonization (Verhagen et al., 2004; Zamioudis et al., 2014; Zamioudis et al., 2015; Stringlis et al., 2018a). The root-specific transcription factor MYB72 and the MYB72-dependent β-glucosidase BGLU42 were identified as essential components of ISR signaling, as mutants *myb72* and *bglu42* are unable to mount WCS417-ISR (Van der Ent et al., 2008; Segarra et al., 2009; Zamioudis et al., 2014). Overexpression of BGLU42 led to constitutive disease resistance in *Arabidopsis* (Zamioudis et al., 2014), highlighting the important role of the MYB72-BGLU42 module in the onset of ISR. However, in contrast to BGLU42, overexpression of its regulator MYB72 did not confer constitutive disease resistance (Van der Ent et al., 2008), suggesting that co-expression of MYB72 with one or more additional factors is required for the onset of ISR.

Interestingly, *MYB72* is also activated in iron-starved *Arabidopsis* roots (Colangelo and Guerinot, 2004; Buckhout et al., 2009; Palmer et al., 2013). In fact, WCS417-induced genes in *Arabidopsis* roots largely overlaps with the genes set that are in responses to iron deficiency, suggesting that the onset of rhizobacteria-ISR shares components of the iron deficiency response (Zamioudis et al., 2015; Verbon et al., 2017). MYB72 was shown to act redundantly with its closest paralog MYB10 to maintain the survival of plants growing in alkaline soil with limited iron availability (Palmer et al., 2013). Under iron deficiency, MYB72 regulates the biosynthesis of coumarins and the subsequent excretion to root exterior (Zamioudis et al., 2014; Stringlis et al., 2018b; Chapter 3). These coumarins are synthesized via the key enzyme FERULOYL-COA 6'-HYDROXYLASE1 (F6'H1) in the phenylpropanoid pathway (Figure S1) and secreted via the ABC transporter PDR9 into the rhizosphere, where they aid in iron mobilization or uptake (Rodríguez-Celma et al., 2013; Fourcroy et al., 2014; Schmid et al., 2014; Schmidt et al., 2014; Tsai and Schmidt, 2017b; Rajniak et al., 2018; Tsai et al., 2018). Iron acquisition facilitated by coumarins likely include three steps: 1) chelation and mobilization of Fe(III) from the soil environment by coumarins, which makes Fe(III)-coumarin complex available for the FERRIC REDUCTASE OXIDASE 2 (FRO2); 2) reduction of Fe(III) to Fe(II) by FRO2 reductase; 3) transport of Fe(II) by IRON REGULATED TRANSPORTER 1 (IRT1) across the plasma membrane into the root interior (Fourcroy et al., 2016; Tsai and Schmidt, 2017b). Alternatively, coumarins may partly contribute to the accumulation of Fe(II) in the root environment via their reduction activity (Tsai and Schmidt, 2017b). Whereas the coumarin scopolin is the most dominant MYB72-dependent metabolite inside the roots, its aglycone scopoletin is prevalent in root exudates (Stringlis et al., 2018b; Chapter 3). BGLU42 was shown to catalyze the deglycosylation of scopolin after which the product scopoletin is excreted into the rhizosphere (Zamioudis et al., 2014; Stringlis et al., 2018b; Chapter 3).

Both scopolin and scopoletin have selective antimicrobial activity *in vivo* (Kai et al., 2006; Grosskinsky et al., 2011; Sun et al., 2014; Chezem et al., 2017; Stringlis et al., 2018b; Chapter 3). In the rhizosphere of *Arabidopsis*, these coumarins play a role in root microbiome assembly where several bacterial and fungal genera were differentially affected in

abundance on coumarin-excreting and non-excreting root systems (Stringlis et al., 2018b; Chapter 3). WCS417 and the ISR-inducing *Pseudomonas capeferrum* strain WCS358 were both shown to be insensitive to the antimicrobial activity of scopoletin (Stringlis et al., 2018b; Chapter 3). This led to the hypothesis that WCS417 and other ISR-inducing microbes induce the production of coumarins to outcompete neighboring microbes and enhance root niche establishment, therewith benefitting both partners in this beneficial plant-microbe interaction (Stringlis et al., 2018b; Chapter 3).

Although colonization of *Arabidopsis* roots by WCS417 results in the activation of *MYB72* and *BGLU42* gene expression (Zamioudis et al., 2014; Zamioudis et al., 2015) and the visually detectable production of F6'H1-dependent fluorescent compounds by the colonized roots (Stringlis et al., 2018b; Chapter 3), the exact nature of the metabolites that are produced in *Arabidopsis* roots in response to colonization by WCS417 are to date unknown. Therefore, in this study we set out to investigate the WCS417-induced metabolic changes in *Arabidopsis* roots. To this end we analyzed extracts of WCS417-colonized and non-colonized *Arabidopsis* roots by metabolite fingerprinting using ultra-performance liquid chromatography - electrospray ionization - time-of-flight - mass spectrometry (UPLC-ESI-TOF/MS). We found that WCS417 induced the production of the coumarins scopolin, scopoletin and esculin. Moreover, we found that colonized roots produce a range of other metabolites, including glucosinolates and fatty acids with predicted roles in plant immune responses. Collectively, the results give novel insight into the chemical signals that play a role in the interaction between plants and the model ISR-inducing rhizobacterium WCS417.

RESULTS

Metabolite fingerprinting of the roots

To identify the metabolites that are synthesized in *Arabidopsis* roots in response to colonization by the ISR-eliciting rhizobacterium WCS417, we compared the metabolomes of WCS417-colonized and control roots of both wild-type Col-0 and mutant *myb72* plants. In the wild-type plants, *MYB72* was significantly induced by WCS417 at 2 d after inoculation (Figure 1A), indicating the molecular initiation of ISR and the coumarin metabolic pathway (Zamioudis et al., 2014; Zamioudis et al., 2015). We then used UPLC-ESI-TOF/MS to analyze the profiles of the root metabolites. In total, we detected 8484 metabolite features from the polar phase and 5166 features from the nonpolar phase of *Arabidopsis* root extracts. We selected those metabolite features that differed significantly (false discovery rate (FDR) corrected $P < 0.01$) in any comparison of the four treatments, resulting in 605 features from the polar phase and 893 features from the nonpolar phase, and used them for further analysis. A principal component analysis (PCA) of the selected features shows that roots colonized by WCS417 are metabolically distinct from control roots. Their metabolite features were separated by the first principal component (PC), which explained most of the variation in both the polar (80.5%) and the nonpolar phase extraction (82.3%; Figure 1B and 1C). The second PC, explaining 9.4% of the total variation in the polar phase extraction (Figure 1B) and 6.5% in the nonpolar phase extraction (Figure 1C), separated Col-0 and *myb72* roots from each other, suggesting a clear genotype effect on the root metabolome. Moreover, the genotype differences are spatially more distant in WCS417-colonized than in control roots (Figure 1B and 1C), suggesting that colonization of the roots by WCS417 increases the metabolic dissimilarity between Col-0 and *myb72* roots.

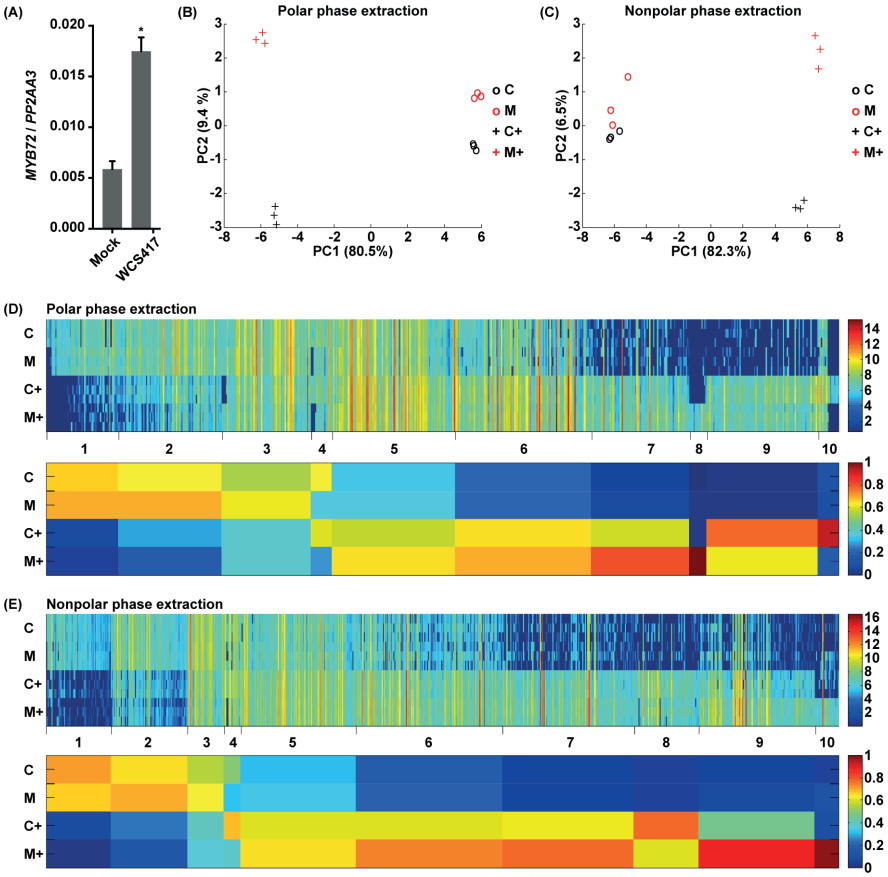

Figure 1. Effect of colonization by WCS417 on metabolite profiles in the roots of Col-0 and *myb72*. **(A)** *MYB72* expression in *Arabidopsis* roots in response to WCS417 colonization. Transcript levels were normalized to that of reference gene *PP2AA3* (At1g13320). The data shown are means of 3 biological replicates. Error bars represent SEM. The asterisk indicates significant difference (Two-tailed *t* test; $P < 0.05$). **(B)** Principal component analysis (PCA) of root metabolites of the polar phase extraction and **(C)** nonpolar phase extraction from WCS417-colonized and control roots of Col-0 and *myb72*. Root material was analyzed by metabolite fingerprinting. PCA plots represent the filtered dataset of metabolite features with a $P < 0.01$ corrected by false discovery rate (FDR). **(D)** One-dimensional self-organizing maps (1D-SOMs) of the dataset presented in **(B)**. **(E)** 1D-SOMs of the dataset presented in **(C)**. The top panel in **(D)** and **(E)** shows the intensity of individual features and the bottom panel shows the clusters representing the average intensity of all features in each cluster. Color key indicates the range of signal intensities. The data shown are obtained from 3 biological replicates. C: Col-0; M: *myb72*; C+: Col-0 colonized by WCS417; M+: *myb72* colonized by WCS417.

We then utilized one-dimensional self-organizing maps (1D-SOMs) to cluster the intensity patterns and to visualize signal intensities of each metabolite feature. The metabolite features from both polar phase and nonpolar phase extractions were organized into 10 distinct clusters (Figure 1D and 1E). For most metabolite feature clusters, the average intensity clearly responded to WCS417 colonization, reflecting either a decrease (clusters 1-3 in both the polar and nonpolar phases) or an increase (clusters 5-10 in both the polar and nonpolar phases) in abundance (Figure 1D and 1E). Like in the PCA (Figure 1B and 1C), in the 1D-SOMs analysis the effect of WCS417 colonization on the metabolite profiles was more pronounced than the effect of plant genotype (Figure 1D and 1E). Nonetheless, cluster

4 in both the polar and nonpolar phase represent a group of metabolite features with higher intensity in wild-type compared to the *myb72* mutant irrespective of colonization (Figure 1D and 1E). The production of these metabolites apparently depends on MYB72, but their production does not respond to WCS417-mediated *MYB72* activation. Moreover, there are clusters that respond to rhizobacteria colonization in a MYB72-dependent manner. The intensities of the metabolite features that are represented by cluster 8 (polar phase) and cluster 10 (nonpolar phase) are higher upon colonization by WCS417, but only in the *myb72* mutant (Figure 1D and 1E). Apparently, *MYB72* activation suppresses the production of these metabolites in wild-type plants in response to WCS417. In contrast, the intensities of the metabolite features represented by polar-phase cluster 10 are higher upon colonization only in wild-type Col-0 plants (Figure 1D), suggesting that the production of these metabolites is induced in response to WCS417-mediated *MYB72* activation. Taken together, these results show that WCS417 colonization induces significant changes in the *Arabidopsis* root metabolome, and that MYB72 affects part of these changes.

WCS417 affects diverse metabolic pathways in *Arabidopsis* roots

To investigate the changes of the root metabolome upon WCS417 colonization, we compared the root metabolome in colonized and control roots of Col-0 in more detail. In this comparison, filtering the data with an FDR corrected $P < 0.05$ resulted in a metabolite profile that consisted of 453 features from polar phase and 855 features from nonpolar phase extractions. The metabolite features from both polar and nonpolar phase extractions were organized into 15 clusters by means of 1D-SOMs (Figure 2A). In the WCS417-colonized roots, metabolite features of clusters 1-6 in both the polar and nonpolar phase extractions showed lower intensities than in the control roots (Figure 2A), indicating that the metabolites represented by these clusters are produced in lower quantities in response to the colonization by WCS417. Metabolite features of clusters 7-15 in both the polar and nonpolar phase extractions showed higher intensities in the colonized roots (Figure 2A), indicating that the metabolites represented by these features are produced in higher quantities in response to WCS417 colonization.

We then used the exact mass information of the metabolite features with decreased and increased intensities in colonized roots to annotate them by using the *A. thaliana* reference database in the Kyoto Encyclopedia of Genes and Genomes (KEGG). A set enrichment analysis (SEA) was performed to identify KEGG pathways that are significantly enriched or repressed. Of the metabolite features that were significantly depleted in colonized roots, only 14 polar-phase and 11 nonpolar-phase features could be mapped into KEGG pathways, which proved insufficient for SEA. Nonetheless, of the metabolite features that were enriched in WCS417-colonized roots, 75 polar-phase features could be mapped to 63 KEGG pathways. Of these, 21 pathways were significantly enriched upon root colonization by WCS417 (Figure 2B; polar phase extraction). Of the nonpolar-phase features that were enriched in WCS417-colonized roots, 100 features could be mapped to 75 KEGG pathways, among which 3 pathways were significantly enriched upon root colonization (Figure 2B; nonpolar phase extraction).

WCS417-stimulated metabolome shows signatures of immune-related metabolic pathways

Although all identified metabolite features need validation by MS^2 analysis, metabolic responses of *Arabidopsis* roots to colonization by WCS417 were tentatively identified. Among the enriched WCS417-induced metabolic pathways, glucosinolate biosynthesis (KEGG entry:

(A)

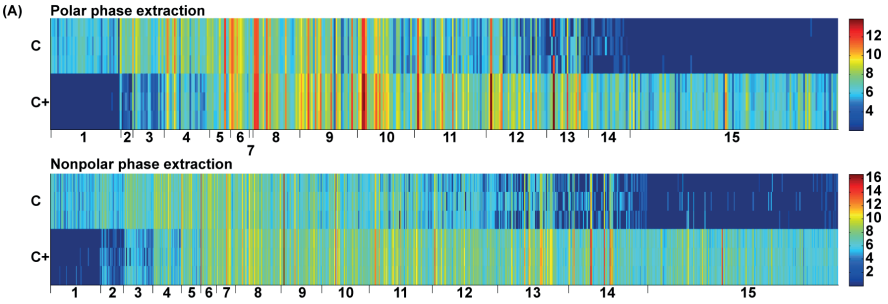

(B)

Extraction phase	Index	Entry ID	Pathway name	Adjusted *P* value
Polar	1	map01210	2-Oxocarboxylic acid metabolism	4.11E-08
	2	map00250	Alanine; aspartate and glutamate metabolism	1.12E-06
	3	map01230	Biosynthesis of amino acids	7.45E-06
	4	map00970	Aminoacyl-tRNA biosynthesis	1.03E-05
	5	map00966	Glucosinolate biosynthesis	2.56E-05
	6	map00460	Cyanoamino acid metabolism	0.0007621
	7	map00330	Arginine and proline metabolism	0.001004
	8	map00020	Citrate cycle (TCA cycle)	0.001941
	9	map00630	Glyoxylate and dicarboxylate metabolism	0.002491
	10	map00340	Histidine metabolism	0.01044
	11	map00750	Vitamin B6 metabolism	0.01578
	12	map00350	Tyrosine metabolism	0.01578
	13	map01110	Biosynthesis of secondary metabolites	0.01733
	14	map00650	Butanoate metabolism	0.02493
	15	map00053	Ascorbate and aldarate metabolism	0.02895
	16	map00380	Tryptophan metabolism	0.03799
	17	map00300	Lysine biosynthesis	0.03799
	18	map00270	Cysteine and methionine metabolism	0.03799
	19	map02010	ABC transporters	0.04098
	20	map00710	Carbon fixation in photosynthetic organisms	0.04098
	21	map01200	Carbon metabolism	0.04098
Nonpolar	22	map00591	Linoleic acid metabolism	4.63E-09
	23	map00073	Cutin; suberine and wax biosynthesis	4.83E-06
	24	map00592	alpha-Linolenic acid metabolism	0.0003386

Figure 2. Effect of colonization by WCS417 on metabolite profiles in roots of Col-0. (A) One-dimensional self-organizing maps (1D-SOMs) of root metabolites extracted from WCS417-colonized and control roots of Col-0. Root material was analyzed by metabolite fingerprinting. 1D-SOMs represent the filtered dataset of metabolite features with a $P < 0.05$ corrected by false discovery rate (FDR). The panel shows the intensities of individual features in each cluster. Color key indicates the range of signal intensities. The data shown are obtained from 3 biological replicates. (C: Col-0; C+: Col-0 colonized by WCS417) **(B)** Set enrichment analysis (SEA) of mapped KEGG pathways in *Arabidopsis* roots after WCS417 colonization. The table represents the KEGG pathways with $P < 0.05$ for multiple testing based on the Benjamini-Hochberg method.

map00966) and fatty acid metabolism (KEGG entry: map00591, linoleic acid metabolism; KEGG entry: map00073, cutin, suberin and wax biosynthesis; KEGG entry: map00592, alpha-linolenic acid metabolism) have been implicated in plant innate immune responses (Burow and Halkier, 2017; Lim et al., 2017). Fatty acids actively participate in multiple layers of the plant immune system, contributing to basal immunity and the regulation of induced immune responses (Kachroo and Kachroo, 2009). Two unsaturated fatty acids, linoleic acid (18:2) and alpha-linolenic acid (18:3), which are associated with enhanced resistance against fungal and bacterial pathogens (Lim et al., 2017), are also significantly enriched upon root colonization

by WCS417 (Figure 3). Linoleic acid and alpha-linolenic acid are substrates of lipoxygenases that can be modified to other oxylipins involved in plant defense, such as JA (Mosblech et al., 2009; Wasternack and Feussner, 2018). However, we did not detect any significant

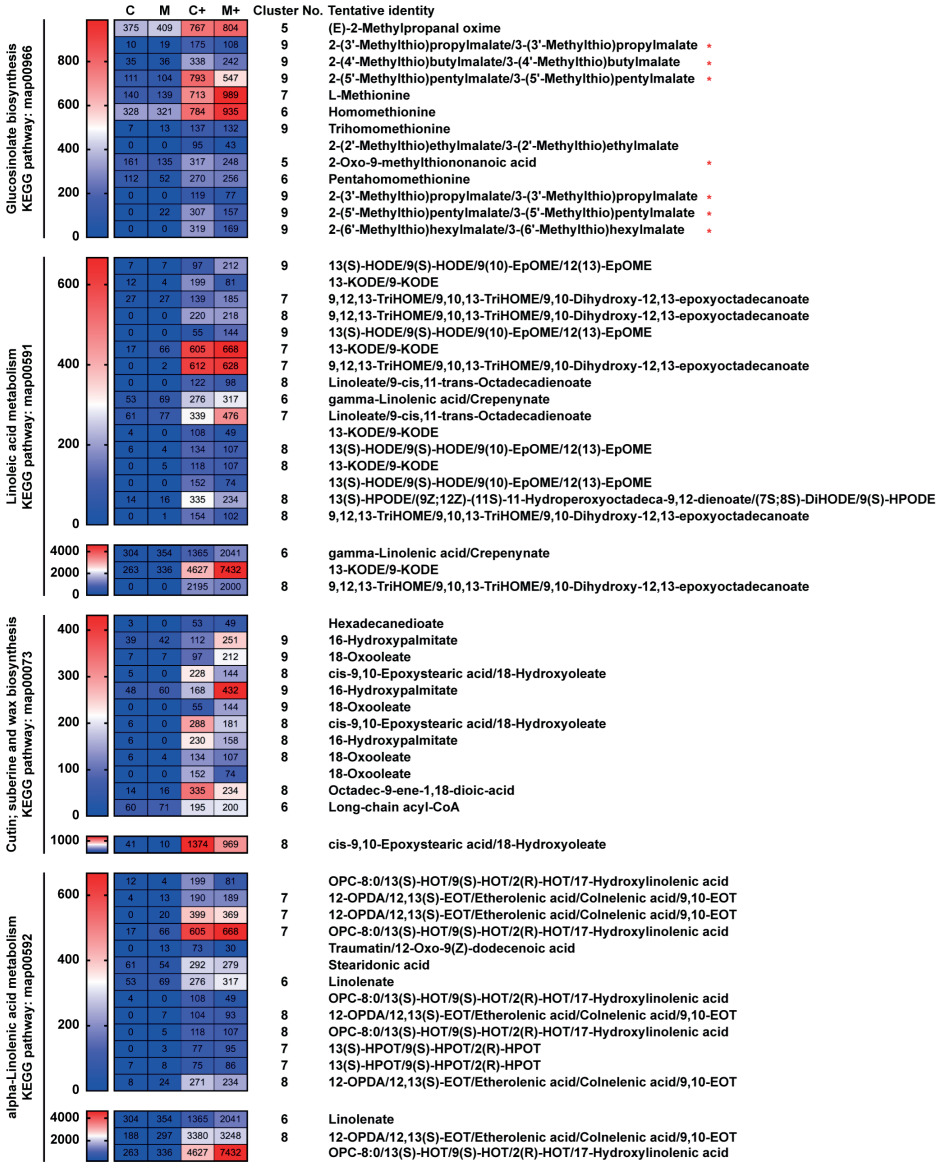

Figure 3. Metabolite profile of features in immune-related metabolic pathways induced by WCS417 colonization. The heatmap shows the intensity of the enriched features in each immune-related KEGG pathway. The values in the cells show the means of the metabolite feature intensities of 3 biological replicates. Color key indicates the range of signal intensities. The cluster No. represents the number of the corresponding cluster of each metabolite feature in Figure 1D and 1E. For a better graphical representation, metabolite features were grouped based on the maximal signal intensity of each feature (above or below 1000) in each metabolic pathway. The red asterisk indicates metabolite features matching with intermediates in aliphatic glucosinolate biosynthesis. The identifies of all shown compounds are tentative and need validation by MS^2. (C: Col-0; M: *myb72*; C+: Col-0 colonized by WCS417; M+: *myb72* colonized by WCS417)

changes in JA or JA-derivatives in the analysis. Another class of fatty-acid derivatives induced upon WCS417 colonization includes cutin, suberin and wax (Figure 3), which participate in resistance against multiple biotic and abiotic stresses (Fich et al., 2016; Barberon, 2017). Although the overlapping tentative identities of those metabolite features mentioned above

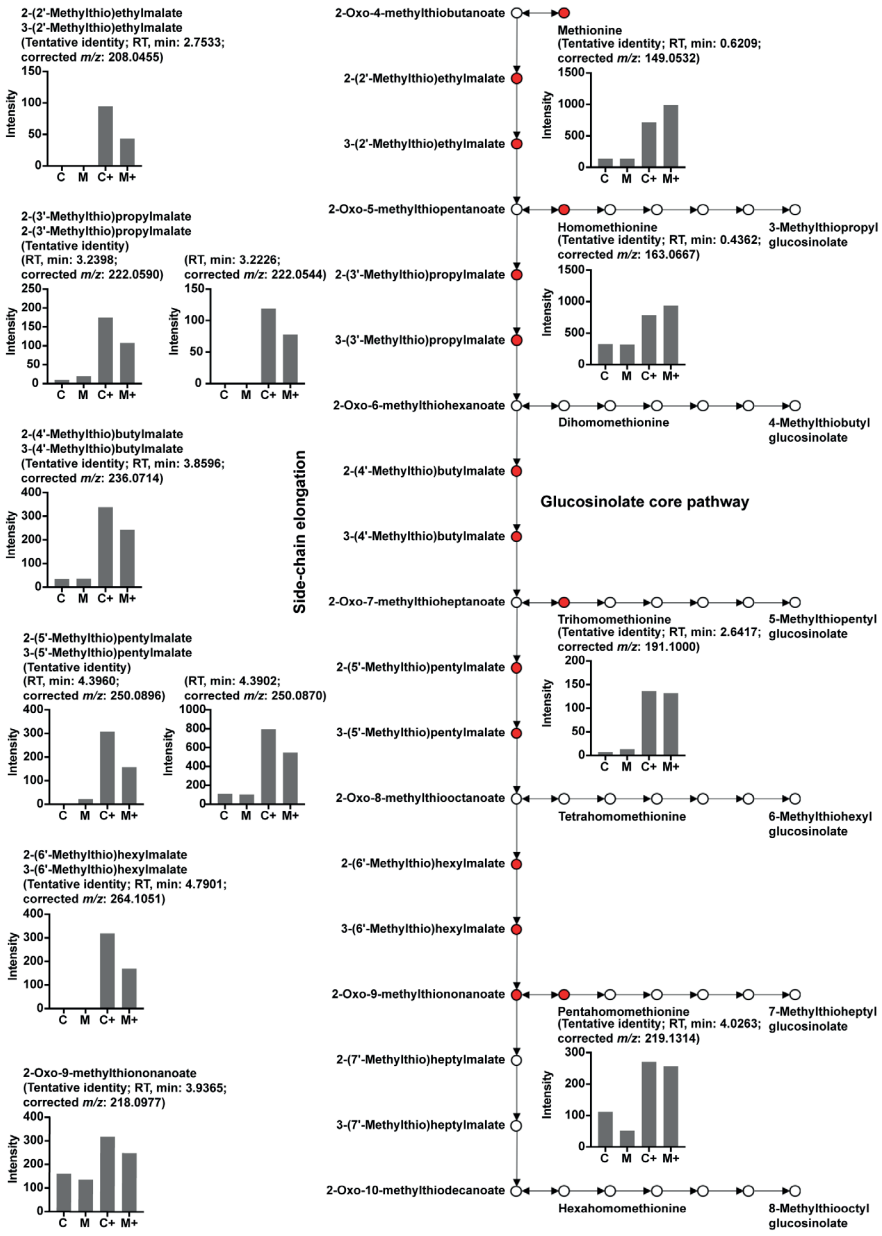

Figure 4. Relative intensities of features in the aliphatic glucosinolate pathway induced by WCS417 colonization. The bar graphs represent the intensities of metabolite features. The data shown are means of 3 biological replicates. The red dots indicate identified metabolite features. The identities of all shown compounds are tentative and need validation by MS^2. (C: Col-0; M: *myb72*; C+: Col-0 colonized by WCS417; M+: *myb72* colonized by WCS417; RT: retention time)

require further confirmation (Figure 3), these results suggest that defense-related metabolic pathways are induced in *Arabidopsis* roots upon colonization by WCS417.

Glucosinolates synthesized by *Arabidopsis* mainly consist of two classes: methionine-derived aliphatic glucosinolates and tryptophan-derived indole glucosinolates (Sonderby et al., 2010; Jørgensen et al., 2015). Here, we found that in WCS417-colonized roots, intermediates of aliphatic glucosinolate biosynthesis were significantly more abundant, whereas indole glucosinolate biosynthesis intermediates were not found to be affected by WCS417 colonization (Figure 3). Our data resembles previous findings where root colonization by WCS417 enhances the biosynthesis of aliphatic glucosinolates in the foliar tissues of *Arabidopsis,* but not the biosynthesis of indolic glucosinolates (Pangesti et al., 2016). Among the WCS417-induced metabolic features matching with the intermediates of aliphatic glucosinolate biosynthesis were several features that showed reduced accumulation in WCS417-colonized *myb72* roots (Figure 4). These intermediates are part of the side chain elongation and core structure formation steps for the biosynthesis of short/long chained glucosinolates (Jørgensen et al., 2015), suggesting that MYB72 may play a role in regulating the biosynthesis of aliphatic glucosinolates. The effect of MYB72 on WCS417-mediated changes in the root metabolite profile is analyzed in more detail below.

Metabolite features affected by MYB72 upon colonization by WCS417

To identify MYB72-dependent changes in the *Arabidopsis* root metabolome upon WCS417 colonization, we analyzed the root metabolome in colonized roots of Col-0 and *myb72* in more detail. In this comparison, we detected 20 features from the polar phase extraction and 23 features from the nonpolar phase extraction that differed between the treatments with an FDR-corrected $P < 0.05$ (Figure 5). Functional annotation of the metabolite features resulted in 19 features that matched with markers in the KEGG databases. However, SEA on these metabolite features did not yield any significantly enriched KEGG pathways. We then scanned through all 19 features for metabolite candidates of particular interest. One feature (retention time: 2.6673; corrected *m/z*: 477.2857) was tentatively identified as 18-deoxycytochalasin H, with a markedly higher intensity in colonized roots of *myb72* than Col-0 (Figure 5). This compound is also produced by the plant-beneficial fungus *Trichoderma harzianum* (Montero-Barrientos et al., 2010; Chen et al., 2015). To what extent the detected plant metabolite is similar to fungal 18-deoxycytochalasin H is currently unknown and further validation of the compound is required. Another feature (retention time: 4.7963; corrected *m/z*: 330.2772), tentatively identified as α-monopalmitin, also has markedly higher intensity in WCS417-colonized roots of *myb72* than Col-0 (Figure 5). Monopalmitin was recently proven to be an essential fatty acid supplied to arbuscular mycorrhizal fungi in arbusculated cells through ABCG transporters (Luginbuehl et al., 2017). The observation that the metabolite features pointing to 18-deoxycytochalasin H and monopalmitin are both produced at higher levels in WCS417-colonized *myb72* roots, suggests that their production in WCS417-colonized Col-0 roots is suppressed in a MYB72-dependent manner. Again, the identities of these two compounds still need to be validated.

Coumarins are induced by WCS417 in *Arabidopsis* roots

MYB72 is an important regulatory protein in both rhizobacteria-elicited ISR and in responses to iron deficiency (Colangelo and Guerinot, 2004; Van der Ent et al., 2008; Palmer et al., 2013; Zamioudis et al., 2014; Zamioudis et al., 2015). Thus, we investigated if changes that were reported for the *Arabidopsis* root metabolome incited by iron starvation were also observed in response to colonization by WCS417. Coumarin biosynthesis is one of the

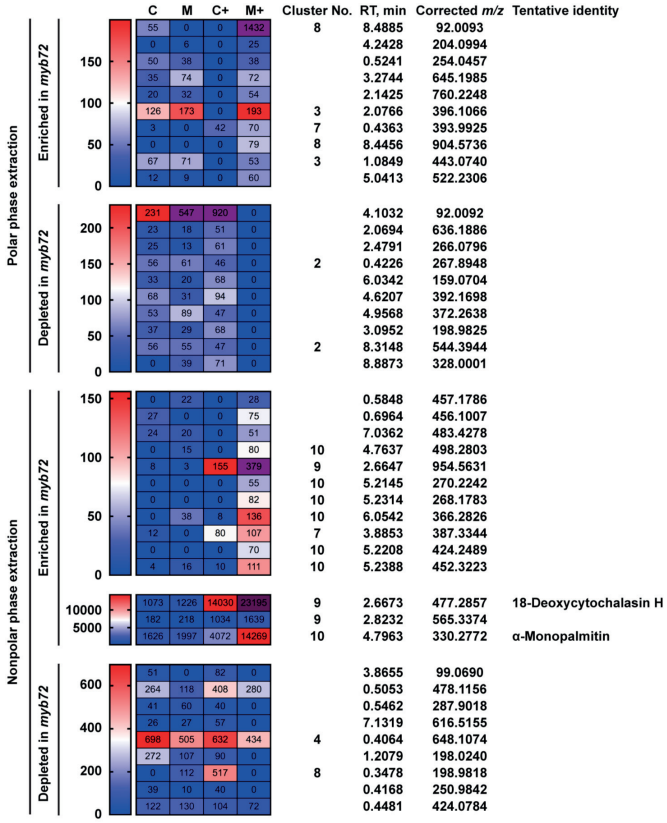

Figure 5. Metabolite profile of features with significantly different intensities in WCS417 colonized of Col-0 and *myb72*. The heatmap shows the intensity of all features in polar and nonpolar phase extractions. The values in the cells show the means of 3 biological replicates. Color key indicates the range of signal intensities. For a better graphical representation, metabolite features were grouped based on the maximal signal intensity of each feature (above or below 1500) in nonpolar phase extraction. The purple color indicates that the value is outside the defined range. The cluster No. represents the number of corresponding cluster of each metabolite feature in Figure 1D and 1E. The identities of all shown compounds are tentative and need validation by MS^2. (C: Col-0; M: *myb72*; C+: Col-0 colonized by WCS417; M+: *myb72* colonized by WCS417; RT: retention time)

most notable metabolic changes in plant roots when experiencing iron deficiency (Tsai and Schmidt, 2017b; Stringlis et al., 2018b; Chapter 3). The biosynthetic route of coumarins in *Arabidopsis* roots is depicted in Figure S1. We indeed detected and validated increased production of the dominant iron-deficiency-induced coumarins scopolin, scopoletin, and esculin in WCS417-colonized roots (Figure 6A). However, while the biosynthesis of these metabolites is severely impaired in roots of *myb72* mutants when exposed to conditions of iron deficiency (Stringlis et al., 2018b; Chapter 3), we found no effect of MYB72 on scopolin, scopoletin and esculin production in response to colonization of the roots by WCS417 (Figure 6A). These results suggest that in response to WCS417 colonization, coumarins are either produced via a MYB72-independent biosynthetic route, or that MYB72 acts in concerted action with other regulators, such as its paralog MYB10 (Palmer et al., 2013).

Apart from increased coumarin production, the tricarboxylic acid (TCA) cycle is also strongly induced under conditions of iron deficiency, leading to enhanced production of TCA cycle intermediates such as citrate, malate and succinate (Thimm et al., 2001; Schmidt

et al., 2014; Stringlis et al., 2018b, Chapter 3). We found that colonization by WCS417 also increased the levels of citrate, malate and succinate in the roots of Col-0 (Figure 6B). The increased levels of the TCA cycle intermediates were also observed in the roots of *myb72* after colonization by WCS417, suggesting that these metabolites are not regulated by MYB72 (Figure 6B). Yet another metabolite frequently found associated with the root response to iron deficiency is the plant hormone auxin (Chen et al., 2010). Under iron deficiency, the auxin level in *Arabidopsis* roots increases and positively regulates downstream iron deficiency responses through the bHLH transcription factor FIT, which in turn regulates *MYB72* activity (Chen et al., 2010; Sivitz et al., 2012; Brumbarova et al., 2015). We identified two metabolite features matching with indole-3-acetaldehyde (IAAld) and 2-oxoindole-3-acetic acid (oxIAA; Figure 6C). Both IAAld and axIAA are important components in Trp-dependent indole-3-acetic acid (IAA) metabolism (Ljung, 2013). IAAld acts as a precursor of IAA, while oxIAA is the major degradation product of IAA (Won et al., 2011; Novak et

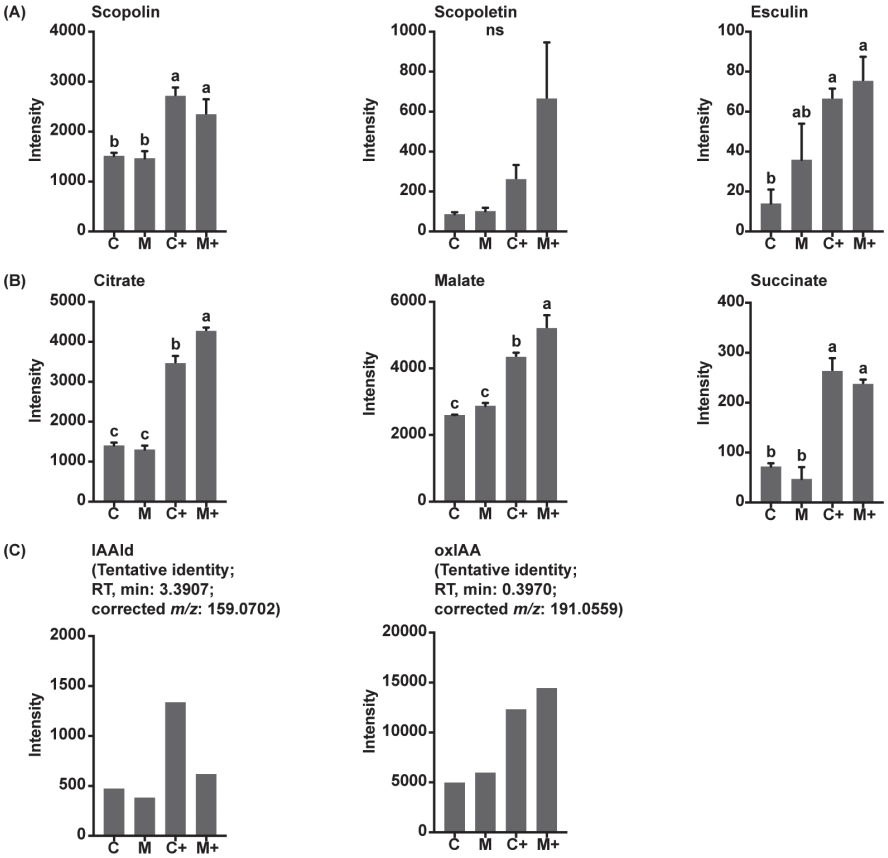

Figure 6. Effect of colonization by WCS417 on iron deficiency-related metabolites in roots of Col-0 and *myb72*. (A) Signal intensities of scopolin, scopoletin and esculin, **(B)** Tricarboxylic acid (TCA) cycle intermediates citrate, malate and succinate and **(C)** metabolite features matching with indole-3-acetaldehyde (IAAld) and 2-oxoindole-3-acetic acid (oxIAA). The identities of all shown compounds in **(A)** and **(B)** were confirmed by retention time comparison with internal databases. The identifies of all shown compounds in **(C)** are tentative and need validation by MS^2 and consequently their intensities were not analyzed statistically. The data shown are obtained from 3 biological replicates. Error bars represent SEM. The letters indicate significant difference (One-way ANOVA followed by Tukey's test; $P < 0.05$). (C: Col-0; M: *myb72*; C+: Col-0 colonized by WCS417; M+: *myb72* colonized by WCS417; RT: retention time)

al., 2012). Increased intensities of IAAld and oxIAA in WCS417-colonized roots of wild-type *Arabidopsis* suggest enhanced auxin metabolism in response to rhizobacterial colonization (Figure 6C). This is consistent with previous findings that *Arabidopsis* roots display enhanced auxin-dependent growth responses after colonization by WCS417 (Zamioudis et al., 2013; Stringlis et al., 2018a). Interestingly, the increased intensity of IAAld was not observed in the *myb72* mutant (Figure 6C), suggesting a possible involvement of MYB72 in this auxin response. However, the identities of IAAld and oxIAA still need to be confirmed. Collectively, these results indicate that root metabolites induced by WCS417 colonization partly resemble those observed in roots under conditions of iron deficiency, including coumarins, intermediates from the TCA cycle and auxin metabolism.

DISCUSSION

WCS417 stimulates production of coumarins in *Arabidopsis* roots

In this study, we investigated *Arabidopsis* root metabolic changes in response to colonization by the ISR-eliciting rhizobacterium WCS417, and the involvement of the root-specific transcription factor MYB72 in these changes. Previously, we demonstrated that the transcriptional response of *Arabidopsis* roots to colonization by WCS417 shows a significant overlap with that of roots of iron-starved seedlings (Zamioudis et al., 2015). This transcriptional overlap contained many genes with roles in the biosynthesis and excretion of iron-mobilizing coumarins , including *F6'H1* (Rodríguez-Celma et al., 2013; Schmid et al., 2014)*, MYB72* and *MYB10* (Palmer et al., 2013; Stringlis et al., 2018b; Chapter 3), *S8H* (Rajniak et al., 2018; Tsai et al., 2018), *CYP82C4* (Rajniak et al., 2018), *BGLU42* (Zamioudis et al., 2014)*,* and *PDR9* (Fourcroy et al., 2014; Zamioudis et al., 2014). Hence, we anticipated to identify coumarins in the metabolite profile of WCS417-colonized roots. Indeed, the levels of the coumarins scopolin, scopoletin and esculin were significantly increased in roots colonized by WCS417. However, while their production in roots of *in vitro*-grown, iron-starved *myb72* plants is almost fully blocked (Stringlis et al., 2018b; Chapter 3), we here found that *myb72* and Col-0 roots accumulated similar levels of scopolin, scopoletin and esculin in response to colonization by WCS417 (Figure 6A). This suggests that in response to WCS417, coumarin biosynthesis in roots functions independently of MYB72. However, under specific conditions, the closest paralogue of MYB72, MYB10, can act redundantly with MYB72, therewith masking the regulatory role of MYB72 in coumarin biosynthesis. This is exemplified by the fact that the *myb72myb10* double mutant is unable to survive in alkaline soils, where iron availability is very low, while the single mutants *myb72* and *myb10* show wild-type phenotypes (Palmer et al., 2013). In line with this, we previously found only minor compositional differences between the *Arabidopsis* root microbiomes of Col-0 and *myb72* plants grown under low-iron conditions in a natural soil (Stringlis et al., 2018b; Chapter 3). By contrast, mutant *f6'h1*, which is completely impaired in coumarin biosynthesis and does not display the WCS417-induced fluorescent phenolic compound accumulation that is visible in colonized Col-0 roots, assembled a significantly distinct root microbiome in the low-iron natural soil (Stringlis et al., 2018b; Chapter 3). Collectively, these results indicate that colonization of the roots by WCS417 stimulates the biosynthesis of the coumarins scopolin, scopoletin and esculin. However, due to redundancy with MYB10, our data are not conclusive about the role of MYB72 in this process. For this, the metabolite profiles of the roots of the single and double mutants *myb72, myb10,* and *myb72myb10* should be analyzed in response to colonization by WCS417, preferably alongside those of mutant *f6'h1.*

WCS417 stimulates TCA cycle intermediates in *Arabidopsis* roots

Iron deficiency induces the production of TCA cycle intermediates in many plant species, including *Arabidopsis* (Zocchi, 2006; Li et al., 2008; López-Millán et al., 2009; Rellan-Alvarez et al., 2010; Vigani, 2012; Stringlis et al., 2018b; Chapter 3). Here we found that colonization by WCS417 significantly increases the levels of three TCA cycle intermediates, citrate, malate and succinate in *Arabidopsis* roots (Figure 6B), again confirming that root responses to WCS417 colonization largely overlap with responses to iron starvation (Zamioudis et al., 2015). Increased TCA cycle intermediates under iron deficiency are proposed to function in modifying the root environment due to their strong acidity, thus increasing the iron availability in the soil environment to facilitate iron uptake (Vigani, 2012). Recently, citrate was shown to be an effective priming agent in *Arabidopsis*, conferring enhanced resistance against the bacterial pathogen *Pseudomonas syringae* pv. *tomato* DC3000 (*Pst*; Balmer et al., 2018). Besides boosting plant immunity, TCA cycle intermediates are also implicated in the chemical communication between roots and rhizobacteria. In response to foliar infection by *Pst*, malate is secreted by *Arabidopsis* roots into the rhizosphere. The ISR-inducing rhizobacterium *Bacillus subtilis* FB17 was shown to be recruited by malate, resulting in enhanced protection against *Pst* (Rudrappa et al., 2008b; Lakshmanan et al., 2012). Malate can specifically chemoattract this beneficial strain and promote its biofilm formation on *Arabidopsis* roots (Rudrappa et al., 2008b). The abovementioned examples suggest that TCA cycle intermediates in WCS417-colonized *Arabidopsis* roots may function either as signaling molecules involved in adaptive plant responses to abiotic or biotic stresses, or as chemical cues that can promote the establishment of beneficial plant-microbe associations.

WCS417 stimulates defense-related glucosinolates in *Arabidopsis* roots

In addition to the coumarins and TCA cycle intermediates, we found that WCS417 stimulates many other metabolic features in the roots of wild-type plants. Systematic analysis of these metabolite changes through SEA showed that defense-related metabolite intermediates of the glucosinolate biosynthesis pathway and fatty acid metabolism are enriched in WCS417-colonized *Arabidopsis* roots (Figure 2 and 3). Glucosinolates are essential plant defense compounds that act against pathogens or insect herbivores (Bednarek et al., 2009; Clay et al., 2009; Muller et al., 2010). In *Arabidopsis* roots, indole glucosinolates are essential for bacterial MAMP-induced deposition of callose (Millet et al., 2010), a cell wall-strengthening defense mechanism that helps to prevent pathogen ingress (Luna et al., 2010). We detected many metabolite features matching precursors of aliphatic glucosinolates, whereas intermediates of indole glucosinolates biosynthesis were not detected (Figure 3 and 4). WCS417 was previously found to suppress the expression of the genes that are involved in indole glucosinolates biosynthesis (Millet et al., 2010; Zamioudis, 2012; Stringlis et al., 2018a). In line with our findings, root colonization by WCS417 strongly induces the production of anti-insect aliphatic glucosinolates in foliar tissue, while biosynthesis of indole glucosinolates was repressed (Pangesti et al., 2016). Although the role of WCS417-induced aliphatic glucosinolate production in roots is unknown and a direct effect of glucosinolates on bacteria has never been reported, a transgenic *Arabidopsis* line producing an exogenous glucosinolate assembled a significantly altered root microbial community (Bressan et al., 2009), suggesting a role of this class of glucosinolates in shaping root microbiome composition. In analogy to the selective antimicrobial activity of coumarins (Stringlis et al., 2018b; Chapter 3), it is tempting to speculate that aliphatic glucosinolates have a similar role in root microbiome assembly. Moreover, glucosinolate transporters may relocate root-produced glucosinolates to foliar tissues where they can be effective against microbial

pathogens and insect herbivores (Nour-Eldin et al., 2012; Jørgensen et al., 2015; Pangesti et al., 2016).

WCS417 stimulates defense-related fatty acid metabolites in *Arabidopsis* roots

Our metabolite profiling also pointed to a number of fatty acid metabolites in WCS417-colonized roots (Figure 2 and 3). Unsaturated fatty acids are associated with disease resistance in multiple plant species. Colonization of bean roots by the ISR-inducing rhizobacterium *Pseudomonas putida* BTP1 significantly reduced *Botrytis cinerea* disease symptoms, which correlated with the stimulation of lipoxygenase activity and with increased levels of linoleic acid and linolenic acid (Ongena et al., 2004). In *Arabidopsis*, linoleic acid and linolenic acid are involved in the defense response that is induced by avirulent strains of the bacterial leaf pathogen *P. syringae*, in which they play a role in regulating NADPH oxidase activity required for the generation of reactive oxygen intermediates (Yaeno et al., 2004). Unsaturated fatty acids also contribute to plant defense as they are the main substrates for the biosynthesis of JA (Mosblech et al., 2009; Wasternack and Feussner, 2018). JA is a major plant defense hormone involved in both WCS417-mediated ISR and the regulation of iron deficiency responses (Pieterse et al., 1998; Van der Ent et al., 2009; Maurer et al., 2011). However, we did not find any JA or JA-derivatives in WCS417-colonized roots, which is consistent with the fact that WCS417-elicited ISR does not rely on enhanced biosynthesis of JA in the absence of invaders (Pieterse et al., 2000; Verhagen et al., 2004). In view of the fact that WCS417-ISR is associated with priming for enhanced JA-dependent defenses (Verhagen et al., 2004; Pozo et al., 2008), it is tempting to speculate that the increased levels of linoleic acid and linolenic acid in WCS417-colonized roots may constitute a metabolic pool of JA precursors for the enhanced pathogen-induced JA biosynthesis and the subsequent potentiated expression of defense-related genes upon attack.

Besides metabolites that are involved in defense responses, we also found higher levels of metabolites implicated in the biosynthesis of cutin, suberin and wax in WCS417-colonized roots. Cutin and wax are important physical barriers against pathogens as well as many other environmental stresses, but are mostly functional in aboveground plant parts (Fich et al., 2016). Suberin lamellae in the root endodermis are thought to play a major role in the acquisition of nutrients, including iron (Barberon, 2017). Together with the Casparian strip, suberin lamellae on the endodermal cells form a dynamic layer that seals the endodermis and regulates the transport of water and nutrients going in and out of the root interior. However, whether WCS417-mediated changes in suberin metabolism are functional in this plant-beneficial microbe interaction is currently unknown.

Role of MYB72 in WCS417-induced metabolic changes

MYB72 is essential for ISR, as *myb72* mutants are incapable of mounting ISR in response to colonization of the roots by WCS417 (Van der Ent et al., 2008). Some of the MYB72-regulated metabolites produced in response to WCS417 may therefore either be functional in systemic signaling within the plant or important for the communication between the plant roots and the beneficial bacteria prior to the onset of ISR. Despite the possible redundancy with MYB10 in our experimental setup (see above), we did find a number of MYB72-dependent changes in root metabolite features in response to WCS417 colonization (Figure 5 and 6). Unfortunately, many of these metabolite features could not be precisely identified, as they did not match with markers in any of the databases. A notable MYB72-regulated metabolite feature that we could identify was monopalmitin. Monopalmitin was more abundant in WCS417-colonized roots of *myb72* plants, suggesting that its production was suppressed via MYB72 in WCS417-colonized roots of Col-0 (Figure 5). Recently, monopalmitin was found to be a dominant carbon source provided by legume plants to sustain arbuscular mycorrhizal

fungi (Luginbuehl et al., 2017). When supported by a host plant, *Arabidopsis* can be infected by mycorrhizal fungi, albeit that this interaction is not a functional symbiosis and even results in growth repression of the plant (Veiga et al., 2013; Cosme et al., 2018). Because monopalmitin might also function in providing other members of the plant-associated microbiome with a carbon source, the down-regulation of monopalmitin biosynthesis by MYB72 might limit this nourishment to prevent that specific members of the microbiome become problematically abundant. Another feature was tentatively identified as 18-deoxycytochalasin H, a natural product derived from an ISR-eliciting fungus *T. harzianum* (Montero-Barrientos et al., 2010; Chen et al., 2015). Cytochalasin has been widely used in the study of actin dynamics, due to its inhibitory effect on actin polymerization (Cooper, 1987). However, the relationship between MYB72 and deoxycytochalasin is not known yet and the genuine identities of the features require validation.

In summary, this study shows that root colonization by WCS417 considerably affects the root metabolome of *Arabidopsis*. Besides the production of coumarins and TCA cycle intermediates, we also identified defense-related aliphatic glucosinolates and fatty acid metabolites as being stimulated upon colonization of the roots by WCS417. However, our experimental setup was inconclusive about the role of MYB72 in the regulation of the WCS417-stimulated metabolites. Future research will be focused on unraveling the role of the different components of the coumarin biosynthesis pathway, including MYB72, MYB10, and BGLU42 in the regulation of WCS417-induced coumarin biosynthesis and their putative function in the onset of ISR. In addition, we will further validate the identities of the selected metabolite features and test hypotheses on their putative role in the chemical communication between plant roots and beneficial rhizobacteria.

MATERIALS AND METHODS

Plant growth conditions

Wild-type *Arabidopsis thaliana* accession Col-0 and mutant *myb72-2* (Van der Ent et al., 2008) were used in this study. *Arabidopsis* seeds were surface sterilized for 4 h in a bell jar containing a beaker filled with 100 ml bleach and 3.2 ml 37% HCl. Surface-sterilized seeds were left in the flow cabinet for an additional 2 h to clear the chlorine gas. For all experiments, *Arabidopsis* seeds were transferred to 4°C for a 2-d stratification period before being moved to climate-conditioned plant growth chamber.

Arabidopsis seeds were sown on square Petri dishes (20 x 20 cm) containing 50 ml agar-solidified Murashige and Skoog (MS) medium (Murashige and Skoog, 1962) supplemented with 0.5 g l^{-1} of MES monohydrate and 5 g l^{-1} of sucrose. The pH of the MS medium was adjusted to 5.7 by adding droplets of 1 M KOH. The plates were placed in a plant growth chamber simulating short-day conditions (21°C, 10 h light/14 h dark, light intensity 100 µmol m^{-2} s^{-1}). After 5 d, *Arabidopsis* seedlings were transferred to new square Petri dishes containing 50 ml agar-solidified modified Hoagland medium (5 mM KNO_3, 2 mM $MgSO_4$, 2 mM $Ca(NO_3)_2$, 2.5 mM KH_2PO_4, 70 µM H_3BO_3, 14 µM $MnCl_2$, 1 µM $ZnSO_4$, 0.5 µM $CuSO_4$, 10 µM NaCl, 0.2 µM Na_2MoO_4, 4.7 mM MES, 50 µM Fe(III)EDTA) supplemented with 14.7 g l^{-1} of sucrose, as described (Stringlis et al., 2018b; Chapter 3). The pH of Hoagland medium was adjusted to 5.5 with KOH.

Bacteria cultivation and inoculation

The rhizobacterial strain *P. simiae* WCS417 (Berendsen et al., 2015) was grown on King's B agar medium (King et al., 1954) supplemented with 150 µg ml^{-1} of rifampicin at 28°C for

16 h. Then the bacterial cells were scraped off the plates and suspended in 10 mM $MgSO_4$. Bacterial suspensions were pelleted by centrifugation (3500 *g* for 5 min), gently washed and resuspended in 10 mM $MgSO_4$. This pellet-wash-resuspend step was repeated 3 times and then the bacteria suspension was adjusted to a final OD_{660} of 0.1. For bacterial inoculation on *Arabidopsis* roots, 10 µl of the suspension was inoculated directly below the hypocotyls of 17-d old *Arabidopsis* seedlings (Zamioudis et al., 2015).

Root sample collection

Root material for quantitative real-time PCR and metabolites fingerprinting analysis was collected as described (Stringlis et al., 2018b; Chapter 3). In brief, at 2 d after bacteria inoculation, the seedlings were cut with a scalpel at the root-hypocotyl junction to separate the roots from the shoots. To remove excess of adhering microbes and wash away exudates at the exterior, *Arabidopsis* roots were washed for three times in Milli-Q water (5 sec each time), dried on tissues and then snap frozen in liquid nitrogen and stored at -80°C.

Quantitative real-time PCR

Total RNA was extracted from *Arabidopsis* roots as described (Onate-Sanchez and Vicente-Carbajosa, 2008) with slight modifications. DNase treatment was performed using DNase I (Thermo Scientific, Waltham, MA USA). Subsequently, cDNA was synthesized using SuperScript III Reverse Transcriptase (Thermo Fisher Scientific Inc., Waltham, MA). All steps were performed according to the manufacturer's instructions. PCR reactions were performed in optical 384-well plates (Applied Biosystems, Foster City, CA) with an ABI PRISM® 7900 HT sequence detection system, using SYBR® Green (Applied Biosystems, Foster City, CA) to monitor the synthesis of double stranded DNA. The thermal profile used was: 2 min at 50°C, 10 min at 95°C for initial denaturation; 40 cycles of 15 s at 95°C, 1 min at 60°C. Amplicon dissociation curves were recorded after cycle 40 by heating from 60 to 95°C with a ramp speed of 1°C per min. Transcript levels were calculated relative to the reference gene *At1g13320* (Czechowski et al., 2005) using the $2^{-\Delta Ct}$ method (Schmittgen and Livak, 2008). The expression levels of *MYB72* and *At1g13320* were determined using the gene-specific primers that are listed as follows: Forward 5'-ACGAGATCAAAAACGTGTGGAAC-3' and reverse 5'-TCATGATCTGCTTTTGTGCTTTG-3' for *MYB72*; forward 5'-TAACGTGGCCAAAATGATGC-3' and reverse 5'-GTTCTCCACAACCGCTTGGT-3' for *At1g13320*.

Metabolite fingerprinting

For metabolite fingerprinting of the root samples, 100 mg of homogenized root material were extracted by two-phase-extraction in methyl-*tert*-butyl ether using a previously described protocol (Matyash et al., 2008; Floerl et al., 2012). The polar extraction phase was dried under a nitrogen stream and resuspended in a mixture of methanol/acetonitrile/water (15:15:100, *v*/*v*/*v*), while the nonpolar extraction phase was dried and resuspended in 100 µl of chloroform/methanol/water (60:30:4.5, *v*/*v*/*v*). The metabolite fingerprinting analysis was performed using Ultra Performance Liquid Chromatography (UPLC, ACQUITY UPLC System, Waters Corporation, Milford, USA) coupled with a photo diode array detector and an orthogonal time-of-flight mass spectrometer (TOF-MS, LCT Premier, Waters Corporation, Milford, USA) as described (König et al., 2014). Data acquisition was performed by using the MassLynx software (MassLynx V4.1 SCN779, Waters Corporation, Milford, USA) in centroid data format. Data deconvolution (peak picking and alignment) was performed using the MarkerLynx software (Waters Corporation, Milford, MA).

Metabolite data analysis

Metabolite data analysis was performed using the software MarVis-Suite 2.6 (Marker Visualization, http://marvis.gobics.de) for marker visualization, filtering, clustering, and functional analysis (Kaever et al., 2015). For marker visualization, the intensity patterns of the high-quality metabolite features were clustered by means of one-dimensional self-organizing-maps (1D-SOMs). After normalization, sample aggregation was performed on mean values and marker scaling by the Euclidean norm (2-norm). Clusters with intensity pattern of interest in the respective experimental conditions were selected. Features represented by these clusters were putatively identified by an automated database search within a mass deviation of 5 mDa: AraCyc (http://www.arabidopsis.org), MetaCyc (http://metacyc.org) and KEGG (http://www.genome.jp/kegg). Principal component analysis plots were generated by using datasets of significantly enriched features in polar and nonpolar phase extraction. Metabolite set enrichment analysis was entry-based, using the cumulative hypergeometric distribution. The pathway-specific *P*-values were adjusted for multiple testing based on the Benjamini-Hochberg method (Benjamini and Hochberg, 1995). The identities of the marker metabolites scopolin, scopoletin, esculin, citrate, malate and succinate were confirmed by retention time comparison with internal databases.

Author contributions

K.Y., I.A.S., K.F., I.F., C.M.J.P., P.A.H.M.B., and R.L.B. designed experiments; K.Y., I.A.S., and K.F. performed experiments; K.Y., and I.A.S. analyzed data; and K.Y., C.M.J.P., P.A.H.M.B., and R.L.B. wrote the manuscript.

SUPPLEMENTAL DATA

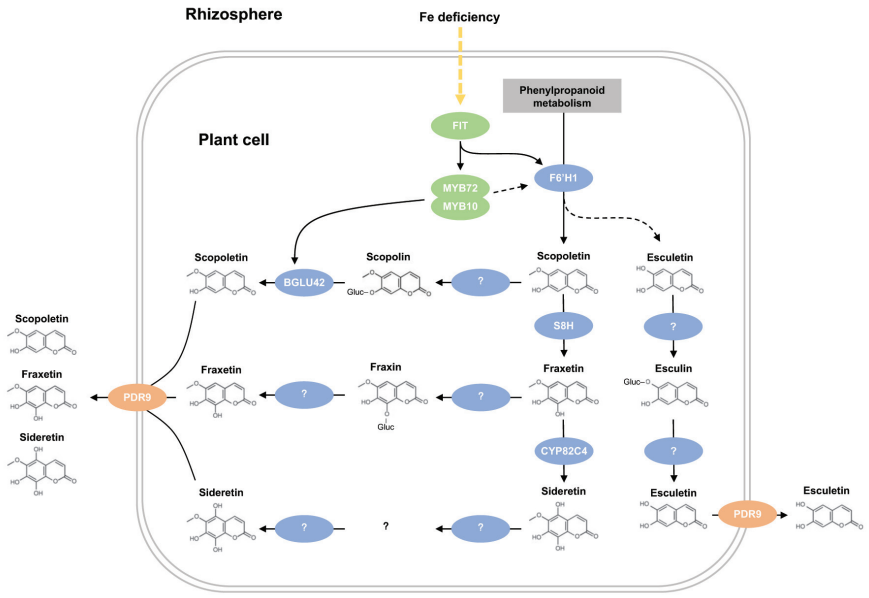

Figure S1. Biosynthetic pathway of coumarins in *Arabidopsis* roots. Under iron deficiency, the root transcription factor FIT (FER-like iron deficiency-induced transcription factor) is activated (Colangelo and Guerinot, 2004). FIT regulates the expression of *F6'H1*, which encodes Feruloyl-CoA 6'-Hydroxylase1, the key enzyme in coumarin biosynthesis (Rodríguez-Celma et al., 2013; Schmid et al., 2014). F6'H1 catalyzes the conversion of the intermediates of phenylpropanoid metabolism into scopoletin, and possibly also esculetin. Scopoletin is then hydroxylated by scopoletin 8-hydroxylase (S8H) into fraxetin (Rajniak et al., 2018; Tsai et al., 2018). Fraxetin can be further oxidized into sideretin by a cytochrome P450 enzyme encoded by *CYP82C4* (Rajniak et al., 2018). Meanwhile, the corresponding glucosides of those coumarins are synthesized via as yet unknown glucosyltransferases and stored inside plant cells (Tsai and Schmidt, 2017b). FIT also regulates the expression of other transcription factors including MYB72 and MYB10, both of which act redundantly to regulate the early iron deficiency regulatory network (Palmer et al., 2013). F6'H1 is likely regulated by MYB72/MYB10 (Stringlis et al., 2018b; Chapter 3). A MYB72-dependent β-glucosidase, BGLU42, may function specifically in the hydrolysis of scopolin and is required for the excretion of scopoletin into root exterior (Zamioudis et al., 2014; Stringlis et al., 2018b; Chapter 3). Apparently, more β-glucosidases remain to be identified for the other glycosylated coumarins. Finally, coumarins are exuded into root exterior via the ABC transporter PDR9 (Fourcroy et al., 2014; Ziegler et al., 2017). Black dashed arrows indicate predicted relationship and question marks indicate enzymes unidentified in *Arabidopsis* or coumarins.

CHAPTER 5

Pseudomonas simiae WCS417 transcriptome changes triggered by root exudates reveal a role for coumarins in plant-rhizobacteria communication

Ke Yu[1,5], Ioannis A. Stringlis[1,5], Ronnie de Jonge[1,2,3], Basten L. Snoek[4], Corné M. J. Pieterse[1], Peter A. H. M. Bakker[1] and Roeland L. Berendsen[1]

[1]Plant-Microbe Interactions, Institute of Environmental Biology, Utrecht University, Padualaan 8, 3584 CH Utrecht, The Netherlands
[2]Department of Plant Systems Biology, VIB, Technologiepark 927, 9052 Ghent, Belgium
[3]Department of Plant Biotechnology and Bioinformatics, Ghent University, Technologiepark 927, 9052 Ghent, Belgium
[4] Theoretical Biology and Bioinformatics, Utrecht University, Padualaan 8, 3584 CH Utrecht, The Netherlands
[5]These authors contributed equally to this work

ABSTRACT

Pseudomonas simiae WCS417 is a root-colonizing bacterium with well-established plant-beneficial effects on a range of plant species, including the model plant *Arabidopsis thaliana*. Upon colonization of *Arabidopsis* roots, WCS417 triggers an induced systemic resistance (ISR) that is effective against a broad spectrum of pathogens. The onset of WCS417-ISR shows similarities with the iron deficiency response, as both responses are associated with the production and exudation of Feruloyl-CoA 6'-Hydroxylase1 (F6'H1)-dependent coumarins. These coumarins mobilize iron from the soil environment and can have a selective antimicrobial activity that impacts microbiome assembly in the rhizosphere. Being highly coumarin-tolerant, WCS417 induces the excretion of these compounds likely to improve its own niche establishment and in return provide growth and immunity benefits for the host. To investigate the possible semiochemical function of F6'H1-dependent coumarins in the mutualistic interaction between WCS417 and *Arabidopsis* roots, we analyzed the transcriptome of WCS417 growing in root exudates of iron-deprived *Arabidopsis* Col-0 and *f6'h1* plants. We found that coumarins significantly affect the expression of 439 bacterial genes. WCS417 genes with functions related to transport and metabolism of carbohydrates, amino acids, and nucleotides were induced, while genes with functions related to cell motility, the bacterial mobilome, and energy production and conversion were repressed. Most strikingly, genes related to flagellar biosynthesis were down-regulated by F6'H1-dependent coumarins in the root exudates. These results suggest that coumarins function in the rhizosphere as semiochemicals in the communication between the roots and mutualists such as WCS417. It is tempting to speculate that these metabolites repress bacterial motility to stimulate the onset of biofilm formation on the root surface and at the same time reduce flagellin production to avoid the activation of root immune responses.

INTRODUCTION

Plants often form beneficial associations with diverse members of their root microbiome (Oldroyd et al., 2011; Bulgarelli et al., 2013; Pieterse et al., 2014). Plant roots actively release carbon-rich root exudates into the rhizosphere that can be either nutritious or deleterious to rhizosphere microbes, thus actively shaping the root microbiome (Sasse et al., 2018; Stringlis et al., 2018b; Yuan et al., 2018; Zhalnina et al., 2018; Chapter 3). Specific beneficial members of the root microbiome can enhance the plant immune system by eliciting an induced systemic resistance (ISR) against pathogens and herbivorous insects (Berendsen et al., 2012; Pieterse et al., 2014). Different components of the ISR signaling pathway have been revealed using the model system *Pseudomonas simiae* WCS417 (hereafter WCS417) on *Arabidopsis thaliana* (hereafter *Arabidopsis*; Pieterse et al., 1996; Van Wees et al., 1997; Pieterse et al., 1998; Pozo et al., 2008; Van der Ent et al., 2008; Zamioudis et al., 2014). The root-specific transcription factor MYB72 and the MYB72-dependent β-glucosidase BGLU42 emerged as key regulators in the onset of ISR (Van der Ent et al., 2008; Segarra et al., 2009; Zamioudis et al., 2014). Although overexpression of MYB72 failed to confer ISR, overexpression of its downstream target BGLU42 led to constitutive disease resistance, highlighting the importance of the MYB72-BGLU42 module in ISR (Van der Ent et al., 2008; Zamioudis et al., 2014). Interestingly, root transcriptome analysis in response to WCS417 revealed the up-regulation of a substantial set of genes that are also up-regulated when plants are grown under conditions of iron deficiency, even though the WCS417-colonized plants were grown under iron-sufficient conditions (Zamioudis et al., 2015). The overlapping gene set includes *MYB72* and *BGLU42,* but also genes encoding key enzymes in the biosynthesis of iron-mobilizing coumarins (Tsai and Schmidt, 2017b), suggesting that WCS417 hijacks the iron

deficiency during the onset of ISR (Zamioudis et al., 2014; Zamioudis et al., 2015; Verbon et al., 2017). MYB72 acts together with its paralog MYB10 for the survival of plants growing in iron-limited alkaline soil (Palmer et al., 2013). Under such iron deficient conditions, MYB72 regulates the production of coumarins and their subsequent release into the rhizosphere (Zamioudis et al., 2014; Stringlis et al., 2018b; Chapter 3). These iron-mobilizing fluorescent phenolic compounds are synthesized via FERULOYL-COA 6'-HYDROXYLASE1 (F6'H1) in the phenylpropanoid pathway and secreted by the iron deficiency-regulated ABC transporter PDR9 to facilitate root iron acquisition (Rodríguez-Celma et al., 2013; Fourcroy et al., 2014; Schmid et al., 2014; Schmidt et al., 2014; Tsai and Schmidt, 2017b; Rajniak et al., 2018). The most abundant MYB72-dependent metabolites inside and outside the roots are coumarin scopolin and its aglycone scopoletin, respectively (Stringlis et al., 2018b; Chapter 3). β-glucosidase BGLU42 was shown to catalyze the deglycosylation of scopolin to scopoletin, which is subsequently excreted to the root exterior (Zamioudis et al., 2014; Stringlis et al., 2018b; Chapter 3).

Besides their iron-mobilizing capacity, scopolin and scopoletin also possess antimicrobial activity. They are also produced upon pathogen attack, and aid in the inhibition of pathogen growth (Kai et al., 2006; Grosskinsky et al., 2011; Sun et al., 2014; Chezem et al., 2017). In the rhizosphere, coumarins can have a selective effect on the composition of the microbial community. Mutant *Arabidopsis f6'h1* plants assembled a distinct root microbiome compared to wild-type plants, suggesting a role for F6'H1-dependent coumarins in shaping the root microbiome (Stringlis et al., 2018b; Chapter 3). We found that two ISR-eliciting rhizobacteria, WCS417 and *Pseudomonas capeferrum* WCS358, are highly tolerant to the antimicrobial effect of scopoletin (Stringlis et al., 2018b; Chapter 3). Moreover, we found that colonization by WCS417 induces the production of these coumarins in *Arabidopsis* roots (Chapter 4). Hence, we postulated that WCS417 induces the production and excretion of antimicrobial coumarins to improve its own niche establishment and in return provide growth and immunity benefits for the host. The constant chemical dialogue between roots and microbes is essential for the establishment and maintenance of mutually beneficial associations, such as those formed by rhizobia and mycorrhizal fungi with their hosts (Oldroyd, 2013). Here, we hypothesized that coumarins can act as semiochemicals that are excreted by the plant roots to communicate with free-living mutualists, such as WCS417. In order to test this hypothesis, we employed RNA sequencing to decipher bacterial transcriptional responses to F6'H1-dependent coumarins in *Arabidopsis* root exudates. We found a large set of WCS417 genes to be regulated by F6'H1-dependent root exudates. The functions of the up-regulated genes pointed to roles in transport and metabolism of carbohydrates, amino acids, and nucleotides, while the down-regulated genes were associated with functions such as flagellar biosynthesis that affects not only motility but also recognition by the host immune system. Our results provide novel insight into the role of coumarins as semiochemicals in plant-beneficial microbe interactions.

RESULTS

F6'H1-dependent coumarins induce transcriptional changes in WCS417

Previously, we found that coumarins are produced by *Arabidopsis* roots in response to root colonization by WCS417 and under iron deficiency (Stringlis et al., 2018b; Chapters 3 and 4). Here we utilized root exudates of iron-starved *Arabidopsis* seedlings to identify the bacterial transcriptional responses to coumarins. Seedlings of wild-type Col-0 and mutants *myb72* and *f6'h1* that are impaired in coumarin biosynthesis, were pre-grown for 7 days in

liquid Hoagland medium with or without supplemented iron and subsequently incubated for three days in Milli-Q water to collect root exudates. In line with previous findings, only iron-deprived Col-0 seedlings exuded fluorescent compounds (indicative for the presence of the fluorescent coumarins, including scopoletin), while *myb72* and *f6'h1* did not (Figure 1A). To test the effect of MYB72/F6'H1-dependent coumarins on WCS417 growth, we inoculated the root exudates of iron-starved Col-0, *myb72* and *f6'h1* with WCS417. After a 16-h growth period, we observed a ~2500-fold increase in bacterial population densities in all exudates tested (Figure 1B). This suggests that MYB72/F6'H1-dependent coumarins do not significantly affect growth of this rhizobacterium, which is in line with the previously described tolerance of WCS417 to the coumarin scopoletin (Stringlis et al., 2018b; Chapter 3).

To investigate the effect of MYB72/F6'H1-dependent coumarins on WCS417 gene transcription, we exposed WCS417 for 1 h to the root exudates of iron-starved Col-0, *myb72* and *f6'h1* seedlings, after which the bacteria were collected for RNA sequencing (RNA-seq) analysis. The genome of WCS417 contains 5545 coding genes (Berendsen et al., 2015), of which 5414 expressed genes were detected in our data set with an expression of at least 1 read count in all samples (Dataset S1). We then normalized the read counts for each gene to "transcripts per million" (TPM; Dataset S2), which is a normalized expression unit that also takes gene length into account (Li et al., 2010). The TPM data was then used in a principal component analysis (PCA) to obtain an overview of the effect of MYB72/F6'H1-dependent coumarins on gene transcription in WCS417 (Figure 1C). The first principal component (PC), explaining 33.93% of the total variation, clearly separates one divergent *myb72* sample from the other samples. The second PC, explaining 27.12% of the total variation, separates

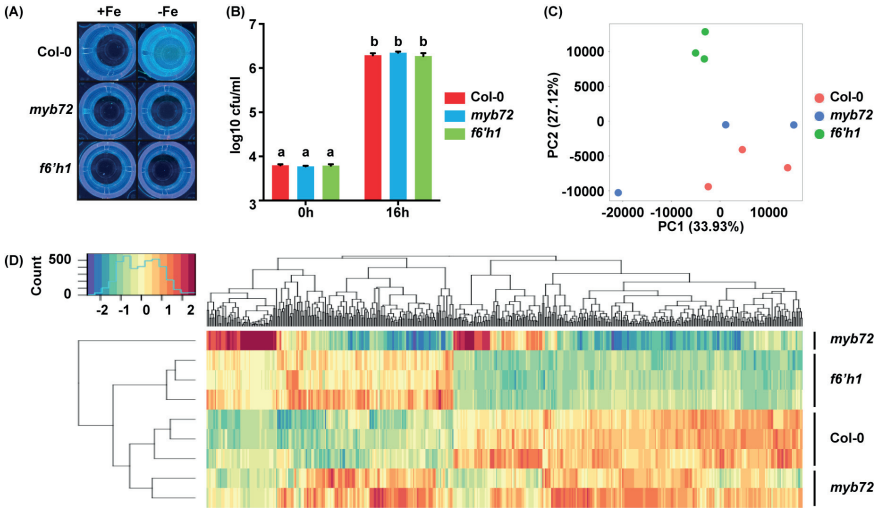

Figure 1. WCS417 transcriptome responds to F6'H1-dependent coumarins in root exudates. (A) Accumulation of fluorescent phenolic compounds in root exudates collected from Col-0, *myb72,* and *f6'h1* seedlings that were pre-grown in Hoagland medium with (+Fe) or without (-Fe) iron. Photos of fluorescence were taken under UV light (365 nm). **(B)** Growth of WCS417 in root exudates collected from Col-0, *myb72,* and *f6'h1* seedlings that were pre-grown in Hoagland medium without iron. The data shown are means of 5 biological replicates. Error bars represent SEM. Letters indicate statistically significant differences (Two-way ANOVA followed by Tukey's test, $P < 0.05$). **(C)** Principal component analysis (PCA) of transcripts per million (TPM) counts of all 5545 WCS417 genes obtained from RNA sequencing results of the WCS417 transcriptome in responses to root exudates from iron-starved Col-0, *myb72,* and *f6'h1* seedlings. **(D)** Heatmap and hierarchical clustering of TPM retrieved from 439 differentially expressed genes (DEGs) that are affected by F6'H1-dependent root exudates. TPM were centered and scaled. DEGs and *Arabidopsis* genotypes were organized according to hierarchical clustering using complete linkage method.

bacterial samples grown in root exudates from different plant genotypes. The close distance between bacterial samples grown in root exudates from Col-0 and *myb72* suggests that the genotype-dependent effect in PC2 is largely attributed to F6'H1 activity (Figure 1C).

We then compared the transcriptomes of bacteria grown in root exudates of Col-0 and *f6'h1* and identified 439 differentially expressed genes (DEGs) with false discovery rate (FDR) below 0.05 (Dataset S3). From these 439 DEGs, 285 genes were up-regulated and 181 genes were down-regulated by F6'H1-dependent root exudates. Figure 1D shows a heatmap and the hierarchical clustering of the 3 replicate expression profiles of the 439 F6'H1-dependent DEGs of WCS417 in response to root exudates from Col-0, *myb72* and *f6'h1*. The Col-0 exudate-induced profiles clearly differ from those induced by the *f6'h1* exudates. The comparison between transcriptomes of bacteria growing in the root exudates of Col-0 and *myb72* resulted in only 2 MYB72-dependent DEGs, which were both up-regulated in response to Col-0 root exudates. These two DEGs, encoding an alcohol dehydrogenase (Locus tag: PS417_RS27420) and a GMC family oxidoreductase (Locus tag: PS417_RS27425), were also F6'H1-dependent. Hierarchical clustering of the TPM counts retrieved from all 439 F6'H1-dependent DEGs indicates that WCS417 also responds differently to root exudates derived from iron-starved Col-0 and *myb72* plants (Figure 1D). However, one of the *myb72* samples differs markedly from all other samples and likely interferes with the identification of MYB72-dependent DEGs. Nonetheless, our results clearly indicate that F6'H1-dependent coumarins in root exudates have a significant impact on the transcriptional profile of WCS417.

Biological functions represented by WCS417 DEGs affected by F6'H1-dependent coumarins

To gain insight into the biological functions affected by coumarins, we analyzed which biological functions are overrepresented among the 439 DEGs of WCS417 affected by F6'H1-dependent root exudates. We analyzed the overrepresentation of functions using two methods. First, we functionally annotated the genome of WCS417 and performed a gene ontology (GO) term enrichment analysis. GO terms are generally defined by one of three categories: biological process, cellular component and molecular function (Table 1). Among the 258 up-regulated genes in response to F6'H1-dependent coumarins in the root exudates, 8 biological processes, 2 cellular components and 14 molecular functions were found to be overrepresented with a *P*-value < 0.05 (Table 1). Among the 181 down-regulated genes by F6'H1-dependent coumarins, 6 biological processes, 1 cellular component and 8 molecular functions were found to be overrepresented (Table 1). Most of the enriched GO terms were unique for either up- or down-regulated genes, with the exception of GO:0003333 (amino acid transmembrane transport), that was enriched in both the up-regulated and down-regulated genes (Table 1).

Secondly, we analyzed the expression of the F6'H1-dependent DEGs that could be assigned to clusters of orthologous groups (COG). COG and GO term enrichment analysis are similar but not mutually exclusive. By combining these two approaches we aimed for a more comprehensive and reliable profile of functions affected by F6'H1-dependent root exudates. COG assignment is based on phylogenetic classification of proteins and each COG category represents a broad functional category containing a cluster of proteins that are functionally related (Tatusov et al., 2001; Galperin et al., 2015). The COG annotation of WCS417 DEGs was retrieved from published data (Cole et al., 2017). We examined the expression of those DEGs that could be assigned to COG categories. Of the 439 DEGS regulated by F6'H1-dependent root exudates, 383 DEGs were found with a valid COG annotation, which covered most of the COG categories present in the COG annotation of the WCS417

Table 1. Gene ontology (GO) terms enrichment analysis of differentially expressed genes (DEGs) of WCS417 in response to root exudates from iron-starved Col-0 and *f6'h1* plants[1].

GO term	Up-regulated by F6'H1-dependent coumarins				Down-regulated by F6'H1-dependent coumarins			
	Accession	Description	Identified genes /All genes	*P*-value	Accession	Description	Identified genes /All genes	*P*-value
Biological Process	GO:0019310	inositol catabolic process	3/3	0	GO:0071973	bacterial-type flagellum-dependent cell motility	9/20	1.49E-10
	GO:0046653	tetrahydrofolate metabolic process	3/3	0	GO:0006412	translation	5/57	1.02E-02
	GO:0006810	transport	32/330	1.92E-05	GO:0008152	metabolic process	15/275	1.71E-02
	GO:0009401	phosphoenolpyruvate-dependent sugar phosphotransferase system	4/10	4.36E-05	GO:0007165	signal transduction	8/123	1.86E-02
	GO:0006807	nitrogen compound metabolic process	6/26	1.34E-04	GO:0003333	amino acid transmembrane transport	3/33	2.15E-02
	GO:0055114	oxidation-reduction process	31/412	2.53E-03	GO:0006935	chemotaxis	3/40	4.02E-02
	GO:0005975	carbohydrate metabolic process	7/53	2.82E-03				
	GO:0003333	amino acid transmembrane transport	5/33	3.67E-03				
Cellular Component	GO:0016020	membrane	40/514	3.50E-04	GO:0005840	ribosome	5/49	4.85E-03
	GO:0009279	cell outer membrane	3/20	1.23E-02				
Molecular Function	GO:0008115	sarcosine oxidase activity	3/3	0	GO:0005198	structural molecule activity	4/7	6.99E-07
	GO:0016151	nickel cation binding	6/7	4.37E-10	GO:0003774	motor activity	3/7	3.56E-05
	GO:0005215	transporter activity	30/216	1.21E-08	GO:0015171	amino acid transmembrane transporter activity	3/15	1.13E-03
	GO:0016887	ATPase activity	17/127	1.94E-05	GO:0015288	porin activity	3/15	1.13E-03
	GO:0016773	phosphotransferase activity, alcohol group as acceptor	5/19	1.56E-04	GO:0003735	structural constituent of ribosome	5/54	7.83E-03
	GO:0016810	hydrolase activity, acting on carbon-nitrogen (but not peptide) bonds	5/27	1.24E-03	GO:0030170	pyridoxal phosphate binding	5/56	9.33E-03
	GO:0016491	oxidoreductase activity	22/262	2.27E-03	GO:0003824	catalytic activity	22/441	1.60E-02
	GO:0016614	oxidoreductase activity, acting on CH-OH group of donors	4/21	2.31E-03	GO:0004871	signal transducer activity	6/91	2.84E-02
	GO:0015424	amino acid-transporting ATPase activity	3/15	4.16E-03				
	GO:0050661	NADP binding	3/18	8.36E-03				
	GO:0005524	ATP binding	23/322	1.41E-02				
	GO:0050660	flavin adenine dinucleotide binding	6/60	2.04E-02				
	GO:0009055	electron carrier activity	6/65	3.03E-02				
	GO:0016787	hydrolase activity	7/81	3.37E-02				

[1] Overrepresented GO terms were identified in both up- and down-regulated DEGs that were responsive to F6'H1-dependent coumarins in the root exudates. Table represents GO terms with a *P*-value < 0.05. Listed are the number of identified genes in the set of DEGs relative to all genes in the WCS417 genome that are assigned to each GO term. Up-/down-regulated DEGs are WCS417 genes with a significantly higher/lower level of expression (FDR < 0.05) in response to root exudates from Col-0, in comparison to the response to root exudates from *f6'h1*.

genome (Figure 2A; Dataset S4). Both up- and down-regulated DEGs were identified in most COG categories, except for three COG categories. DEGs associated with the cell cycle control, cell division, chromosome partitioning, and with the extracellular structures were exclusively up-regulated, whereas those associated with the mobilome such as prophages and transposons were down-regulated (Figure 2A). We then performed an enrichment analysis to identify bacterial functions that are significantly induced or repressed (Figure 2B). In the 235 up-regulated DEGs, we found 3 overrepresented COG categories: 1) Carbohydrate transport and metabolism; 2) Amino acid transport and metabolism, and 3) Nucleotide transport and metabolism, suggesting that F6'H1-dependent coumarins in

(A)

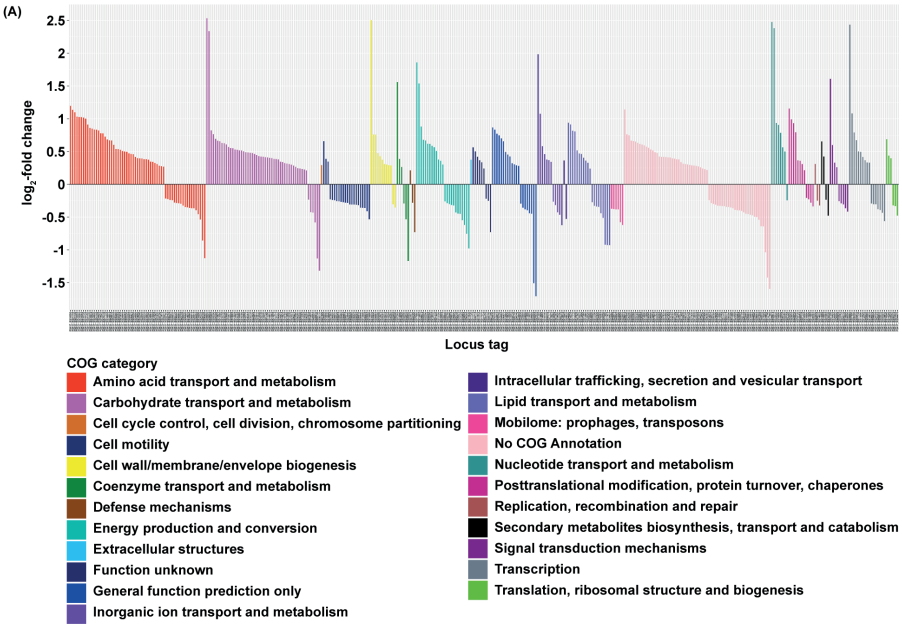

(B)

COG enrichment	COG category	Identified genes/All genes	*P*-value
Up-regulated by F6'H1-dependent coumarins	Carbohydrate transport and metabolism	47/247	1.09E-16
	Amino acid transport and metabolism	44/477	2.75E-05
	Nucleotide transport and metabolism	7/63	1.44E-02
Down-regulated by F6'H1-dependent coumarins	Cell motility	19/139	1.17E-08
	Mobilome: prophages, transposons	6/22	3.65E-06
	Energy production and conversion	12/191	8.32E-03

Figure 2. COG category analysis of differentially expressed genes (DEGs) of WCS417 in response to root exudates from iron-starved Col-0 and *f6'h1* plants. (A) Expression levels of selected differentially expressed genes (DEGs) in responses to root exudates derived from Col-0 and *f6'h1* under iron deficiency. Up/down-regulated DEGs are WCS417 genes with a significantly higher/lower level of expression (FDR < 0.05) in response to root exudates from Col-0, in comparison to the response to root exudates from *f6'h1*. DEGs with a valid annotation of clusters of orthologous groups (COG) were selected. In $\log_2$-fold change, positive values mean that the genes are up-regulated and negative values mean that the genes are down-regulated by F6'H1-dependent coumarins in the root exudates. Different colors of the bars correspond to different COG categories. **(B)** COG enrichment analysis of selected DEGs in responses to root exudates derived from Col-0 and *f6'h1* under iron deficiency. Overrepresented COG categories (*P*-value < 0.05) were identified in both up- and down-regulated DEGs by F6'H1-dependent coumarins. Listed are the number of identified genes in the set of DEGs relative to all genes in the WCS417 genome that are assigned to each COG category.

the root exudates induce these functions in WCS417. In the 148 down-regulated DEGs, we also found 3 overrepresented COG categories: 1) Cell motility; 2) Mobilome: prophages, transposons and 3) Energy production and conversion, suggesting that F6'H1-dependent coumarins repress these functions in WCS417.

F6'H1-dependent coumarins repress bacterial cell motility required for root colonization

Cole and co-workers completed a genome-wide identification of plant root colonization-related genes in WCS417 using randomly barcoded transposon mutagenesis sequencing and identified a total of 358 genes that are colonization-related (Cole et al., 2017). Of these, 115 genes positively affect the root colonization capability of WCS417, whereas 243 genes negatively affect root colonization capability (Cole et al., 2017). We compared the genes that were differentially expressed in response to F6'H1-dependent root exudates with these colonization-related genes (Figure 3A). Amongst the 115 genes that positively affect root colonization of WCS417, 10 genes were up-regulated and 17 genes were down-regulated by F6'H1-dependent coumarins in the root exudates (Figure 3A and 3B). The 10 DEGs that were induced are associated with 5 COG categories, among which only the categories "Carbohydrate transport and metabolism" and "Amino acid transport and metabolism" were found to be overrepresented (Figure 3B and 3D). The 17 significantly repressed DEGs are associated with 5 COG categories, among which only 'Cell motility' was overrepresented (Figure 3B and 3D). Of the genes that negatively affect the root colonizing capability of WCS417, 14 genes were up-regulated and 9 genes were down-regulated by F6'H1-dependent coumarins (Figure 3A and 3C). The 14 induced DEGs are associated with 6 COG categories, among which the categories "Cell wall/membrane/envelope biogenesis" and, again, "Carbohydrate transport and metabolism" were found overrepresented (Figure 3C and 3D). The 9 repressed DEGs were associated with 5 COG categories, but none of these COG categories were overrepresented (Figure 3C and 3D). The genome-wide identification of root colonization-related genes revealed that "Carbohydrate transport and metabolism" and "Cell motility" are two common functional categories that are associated with colonization capability of WCS417 (Cole et al., 2017). Our data indicates that F6'H1-dependent coumarins in the root exudates affect bacterial carbohydrate transport and metabolism both positively as well as negatively. Moreover, 13 genes that are involved in cell motility and required for colonization were exclusively repressed (Figure 3B), indicating that F6'H1-dependent coumarins may have a negative effect on bacterial cell motility.

The clear negative effect of F6'H1-dependent coumarins on cell motility-related gene expression in WCS417, prompted us to take a closer look at the expression and annotation data of all the 22 DEGs in response to F6'H1-dependent root exudates that were assigned to the cell motility COG category (Table 2). In the genome of WCS417, there are 139 genes that are associated with cell motility, among which 31 genes have positive and 6 genes have negative effects on root colonization (Cole et al., 2017). The 19 genes that were down-regulated by F6'H1-dependent coumarins, include 1 gene involved in cellulose biosynthesis (*bcsQ*, encoding a cobyric acid synthase), 13 genes involved in flagellar biosynthesis (*flgB*, *flgD*, *flgE*, *flgF*, *flgG*, *flgH*, *flgL*, *fliS*, *fliF*, *fliG*, *fliH*, *flhA* and *flhF*) and 5 genes involved in chemotaxis (Table 2). Interestingly, most of the down-regulated DEGs (except *flgF*) involved in flagellar biosynthesis were shown to have a positive effect on the root colonization capability of WCS417 (Cole et al., 2017; Table 2). The remaining 3 genes that were up-regulated by F6'H1-dependent root exudates, encode chemotaxis-related proteins (Table 2). However, those 3 genes are not essential for the root colonization capability of WCS417 (Cole et al., 2017). These results indicate that F6'H1-dependent coumarins negatively affect cell motility of WCS417 by repressing flagellar biosynthesis.

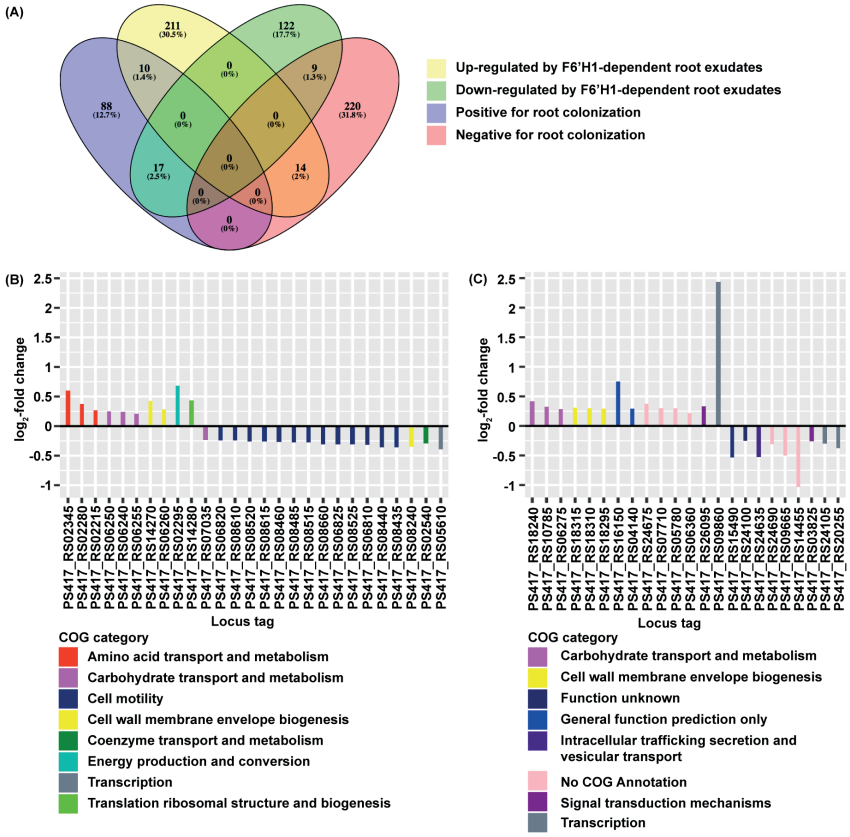

(D)

Colonization	F6'H1-dependent coumarins	COG category	Identified genes/All genes	*P*-value
Positive	Up-regulated	Carbohydrate transport and metabolism	3/248	1.36E-03
		Amino acid transport and metabolism	3/477	1.47E-02
	Down-regulated	Cell motility	13/139	1.86E-19
Negative	Up-regulated	Cell wall/membrane/envelope biogenesis	3/177	1.60E-03
		Carbohydrate transport and metabolism	3/248	5.47E-03

Figure 3. Comparison of genes affected by F6'H1-dependent root exudates and colonization-related genes of WCS417. (A) Venn-diagram of overlapping members between F6'H1-affected and colonization-related genes. All selected genes have valid annotation of clusters of orthologous groups (COG). F6'H1-affected genes are WCS417 genes with a significantly higher/lower level of expression (FDR < 0.05) in response to root exudates from Col-0, in comparison to the response to root exudates from *f6'h1*. **(B)** Expression profile of overlapping genes between F6'H1-affected and colonization-positive genes. **(C)** Expression profile of overlapping genes between F6'H1-affected and colonization-negative genes. In $\log_2$-fold change of **(B)** and **(C)**, positive values mean that the genes are up-regulated and negative values mean that the genes are down-regulated by F6'H1-dependent coumarins in the root exudates. Different colors of the bars correspond to different COG categories. **(D)** COG enrichment analysis of selected differentially expressed genes (DEGs) in responses to root exudates derived from Col-0 and *f6'h1* under iron deficiency. Overrepresented COG categories (*P*-value < 0.05) were identified in both up- and down-regulated DEGs by F6'H1-dependent coumarins. Listed are the number of identified genes in the set of DEGs relative to all genes in the WCS417 genome that are assigned to each COG category.

Table 2. Expression and annotation data of 22 DEGs in the Cell Motility COG category.

	Locus tag	COG Description	Product Description	Colonization	log_2-fold change
Cellulose biosynthesis	PS417_RS08660	Cellulose biosynthesis protein BcsQ	cobyric acid synthase	+	-0.31
Flagellar biosynthesis	PS417_RS06810	Flagellar basal body rod protein FlgB	flagellar basal body rod protein FlgB	+	-0.32
	PS417_RS06820	Flagellar hook assembly protein FlgD	flagellar basal body rod modification protein FlgD	+	-0.24
	PS417_RS06825	Flagellar hook protein FlgE	flagellar hook protein FlgE	+	-0.31
	PS417_RS08430	Flagellar basal body rod protein FlgF	flagellar basal body rod protein FlgF		-0.31
	PS417_RS08435	Flagellar basal body rod protein FlgG	flagellar basal body rod protein FlgG	+	-0.36
	PS417_RS08440	Flagellar basal body L-ring protein FlgH	flagellar basal body L-ring protein	+	-0.36
	PS417_RS08460	Flagellin and related hook-associated protein FlgL	flagellar hook-associated protein FlgL	+	-0.27
	PS417_RS08485	Flagellin-specific chaperone FliS	flagellar biosynthesis protein FliS	+	-0.27
	PS417_RS08515	Flagellar biosynthesis/type III secretory pathway M-ring protein FliF/YscJ	flagellar M-ring protein FliF	+	-0.28
	PS417_RS08520	Flagellar motor switch protein FliG	flagellar motor switch protein FliG	+	-0.26
	PS417_RS08525	Flagellar biosynthesis/type III secretory pathway protein FliH	flagellar assembly protein FliH	+	-0.31
	PS417_RS08610	Flagellar biosynthesis pathway, component FlhA	flagellar biosynthesis protein FlhA	+	-0.24
	PS417_RS08615	Flagellar biosynthesis GTPase FlhF	flagellar biosynthesis regulator FlhF	+	-0.26
Chemotaxis	PS417_RS00895	Methyl-accepting chemotaxis protein	chemotaxis protein		0.66
	PS417_RS05665	Methyl-accepting chemotaxis protein	methyl-accepting chemotaxis protein		-0.41
	PS417_RS07665	Methyl-accepting chemotaxis protein	chemotaxis protein		-0.23
	PS417_RS13440	Methyl-accepting chemotaxis protein	chemotaxis protein		-0.36
	PS417_RS15490	Methyl-accepting chemotaxis protein	methyl-accepting chemotaxis protein		-0.53
	PS417_RS18840	Methyl-accepting chemotaxis protein	chemotaxis protein		0.35
	PS417_RS18940	Methyl-accepting chemotaxis protein	methyl-accepting chemotaxis protein		0.39
	PS417_RS23840	Methyl-accepting chemotaxis protein	methyl-accepting chemotaxis protein		-0.28

[1] Up/down-regulated DEGs are WCS417 genes with a significantly higher/lower level of expression (FDR < 0.05) in response to root exudates from Col-0, in comparison to the response to root exudates from *f6'h1*. "+" means that the gene positively affects the root colonization capability of WCS417 (Cole et al., 2017). In log_2-fold change, positive values mean that the genes are up-regulated while negative values mean that the genes are down-regulated by F6'H1-dependent coumarins in the root exudates.

DISCUSSION

Free living rhizobacteria actively respond to specific components in root exudates that either stimulate or restrain bacterial proliferation on the roots (Badri et al., 2009; Chagas et al., 2018). *Arabidopsis* roots synthesize and exude fluorescent coumarins when growing under iron deficiency (Schmid et al., 2014; Zamioudis et al., 2014; Stringlis et al., 2018b; Chapter 3), but also in response to colonization by the plant-beneficial rhizobacterium WCS417 (Chapter 4). It is likely that WCS417 can perceive those root-derived metabolites and rearrange its transcriptional profile to adapt to the new environment. Here, we investigated the transcriptomes of WCS417 growing in root exudates of iron-starved Col-0, *myb72* and *f6'h1* plants. Whereas MYB72 plays a role in regulating coumarin biosynthesis in *Arabidopsis* growing under iron deficiency (Stringlis et al., 2018b; Chapter 3), F6'H1 is absolutely required for their production (Schmid et al., 2014). Although F6'H1-dependent root exudates strongly affected the bacterial transcriptome, our RNA sequencing results suggest that the effect of MYB72-dependent coumarins on bacterial responses is much less profound (Figure 1C and 1D). This can be explained by the fact that either the deviant *myb72* sample negated the effect of MYB72-dependent coumarins in the statistical analysis, or MYB72 can act redundantly with its paralog MYB10 (Palmer et al., 2013), resulting in less

profound effects on coumarin biosynthesis in *myb72* than in *f6'h1* (Stringlis et al., 2018b; Chapter 3). The only two MYB72-dependent DEGs were also F6'H1-dependent. However, the function of these two DEGs in WCS417 biology cannot be easily distilled from their annotation as an alcohol dehydrogenase and a GMC family oxidoreductase, respectively.

To increase our understanding of the bacterial coumarin-responding genes, we performed GO term enrichment analysis and, in parallel, identified overrepresented COGs. Both strategies used to identify bacterial functions that are activated in response to F6'H1-dependent root exudates, brought forward that especially genes involved in the transport and metabolism of carbohydrates and amino acids, and genes involved in bacterial motility were overrepresented among the DEGs. A recent genome-wide study demonstrated that most genes that are required for WCS417 colonization of *Arabidopsis* roots, are involved in carbohydrate metabolism or cell motility (Cole et al., 2017). Here, we found that F6'H1-dependent root exudates had a negative effect on the expression of 19 genes involved in cell motility (Table 2), 13 of which were found to be required for root colonization (Cole et al., 2017). Most of these 13 genes function in flagellar biosynthesis (Table 2). The flagellum is an important bacterial organelle required for multiple bacterial functions, such as movement, chemotaxis, adherence and host immune modulation (Rossez et al., 2015). The flagella of the rhizobacterial strain *Pseudomonas defensor* WCS374 were also demonstrated to be required for efficient colonization of potato roots (De Weger et al., 1987). Among the 13 flagellar biosynthesis genes, *flhA* and *flhF* are considered as the flagellar master regulators in multiple bacterial species including *Pseudomonas putida* MK1 (Pandza et al., 2000; Kusumoto et al., 2006; Salvetti et al., 2007; Schuhmacher et al., 2015), suggesting that the negative effect of coumarins on bacterial cell motility likely results from transcriptional regulation of *flhA* and *flhF*.

Although the 13 cell-motility-related genes that are repressed in response to F6'H1-dependent root exudates are required for colonization by WCS417, this does not necessarily imply that F6'H1-dependent root exudates negatively affect the root colonization capability. Likely motility is important in initial stages of the colonization process, when motility is required to move towards the root, whereas the impact of F6'H1-dependent root exudates occurs only when WCS417 have reached a quorum and induce coumarin production by *Arabidopsis* roots (Stringlis et al., 2018b; Chapter 3 and 4). Intriguingly, the flagellin of WCS417 is a potent elicitor of root immune responses in *Arabidopsis* (Stringlis et al., 2018a; Chapter 2). Thus, down-regulation of flagellin production by F6'H1-dependent root exudates may be a strategy of WCS417 to avoid triggering root immune responses. This is supported by the fact that live WCS417 cells are potent suppressors of flg22-induced immune responses (Millet et al., 2010; Stringlis et al., 2018a; Chapter 2).

In addition to cell motility, biofilm formation is also crucial for long-term root colonization (Danhorn and Fuqua, 2007). Plant-associated rhizobacteria, including pathogenic and beneficial pseudomonads, can form dense biofilms on the root surface (Danhorn and Fuqua, 2007; Rudrappa et al., 2008a). Components in root exudates have been shown to regulate the bacterial biofilm formation process. For example, maize root exudates can promote the biofilm formation of plant-beneficial *Bacillus amyloliquefaciens* SQR9 (Zhang et al., 2015). When under pathogen attack, malic acid secretion by roots can promote biofilm formation of *B. subtilis* FB17 strain on *Arabidopsis* roots (Rudrappa et al., 2008b). Cell motility is conditionally required for the initiation of biofilm formation, since biofilm formation always starts with bacterial cell attachment to a surface (Danhorn and Fuqua, 2007; Belas, 2014). In *Pseudomonas fluorescens* WCS365, mutants that are defective in flagellar biosynthesis were also found defective in biofilm formation (O'Toole and Kolter, 1998). Nonetheless, it is generally accepted that the inhibition of motility can promote the formation of biofilm

at some point and there are several examples of how this switch in lifestyle is molecularly enforced through negative feedback loops (Guttenplan and Kearns, 2013). For example, EpsE, an operon that is essential for biofilm formation, also functions in the inhibition of cell motility of *B. subtilis* (Blair et al., 2008). Thus, the repression of bacterial cell motility by F6'H1-dependent root exudates might be part of a bacterial motility-to-biofilm transition, that is required for successful root colonization.

Carbohydrate metabolism was also found to be involved in biofilm formation of many bacterial species under different environmental conditions (O'Toole et al., 2000; Wen and Burne, 2002; Jefferson, 2004; Wu et al., 2014). In *Pseudomonas aeruginosa*, the mutation in the global carbon metabolism regulator Crc caused a defect in type IV pilus biosynthesis, which eventually led to the inability of biofilm formation (O'Toole et al., 2000). In the human pathogen *Haemophilus influenzae*, it was found that antibiotic treatment stimulated biofilm-formation by activating carbohydrate metabolism (Wu et al., 2014). We indeed found that F6'H1-dependent root exudates strongly induced bacterial carbohydrate transport and metabolism (Figure 2), supporting the hypothesis that F6'h1-dependent coumarins stimulate biofilm formation.

Alternatively, the function of coumarins in the establishment and maintenance of beneficial association between WCS417 and *Arabidopsis* roots may not rely on enhanced expression of colonization features, but rather on relatively high tolerance of WCS417 to coumarins (Stringlis et al., 2018b; Chapter 3), therewith providing WCS417 with a selective advantage over coumarin-sensitive root microbiota resulting in enhanced niche establishment. However, the root colonization capability of WCS417 on the roots of *Arabidopsis* mutants that are defective in coumarin biosynthesis, such as *f6'h1*, are not assessed yet. Considering the antimicrobial activities of coumarins (Kai et al., 2006; Grosskinsky et al., 2011; Sun et al., 2014; Chezem et al., 2017), enhanced coumarin production in responses to WCS417 might be a strategy of plants supporting the population of this mutualist.

Collectively, this study showed that coumarins in root exudates function as semiochemicals that induce transcriptional changes in the plant-beneficial rhizobacterium WCS417. The nature of the coumarin-induced transcriptional changes surfaced several putative mechanisms, including effects on flagellar biosynthesis that could aid in the mobility-to-biofilm transition and evasion of host immunity. Future research will be focused on experimental validation of the theories that emerged from this study to shed new light on the role of the identified bacterial features in the establishment of beneficial plant-microbe associations.

MATERIALS AND METHODS

Plant growth conditions

Wild-type *Arabidopsis thaliana* accession Col-0 and mutants *myb72-2* (Van der Ent et al., 2008) and *f6'h1-1* (Schmid et al., 2014) were used in this study. Mutant *f6'h1-1* was kindly provided by Dr. Jürgen Zeier (Heinrich Heine University, Düsseldorf, Germany). For experiments performed *in vitro*, seeds were surface sterilized for 4 h in a bell jar containing a beaker filled with 100 ml bleach and 3.2 ml 37% HCl. Surface sterilized seeds were left in the flow cabinet for an additional 2 h to clear the chlorine gas. *Arabidopsis* seeds were sown on square Petri dishes filled with 50 ml agar-solidified Murashige and Skoog (MS) medium (Murashige and Skoog, 1962) supplemented with 0.5 g l^{-1} of MES monohydrate and 5 g l^{-1} of sucrose. The pH of MS medium was adjusted to 5.7 by adding droplets of 1 M KOH. The plates were transferred to 4°C for a 2-d stratification after which they were moved to a

climate chamber simulating short-day condition (21°C, 10 h light/14 h dark, light intensity 100 µmol m^{-2} s^{-1}). After 5 d, *Arabidopsis* seedlings were transferred to square Petri dishes filled with 50 ml agar-solidified modified Hoagland medium (5 mM KNO_3, 2 mM $MgSO_4$, 2 mM $Ca(NO_3)_2$, 2.5 mM KH_2PO_4, 70 µM H_3BO_3, 14 µM $MnCl_2$, 1 µM $ZnSO_4$, 0.5 µM $CuSO_4$, 10 µM NaCl, 0.2 µM Na_2MoO_4, 4.7 mM MES, 50 µM Fe(III)EDTA) supplemented with 14.7 g l^{-1} of sucrose, as described (Stringlis et al., 2018b; Chapter 3). The pH of Hoagland medium was adjusted to 5.5 with KOH.

Root exudates collection

To collect root exudates, 14-d-old *Arabidopsis* seedlings were transferred to Petri dishes with a diameter of 14.5 cm. Each Petri dish contained 70 ml modified liquid Hoagland medium without Fe(III)EDTA and 280 seedlings. Plates were moved back to the climate chamber. After 7 d, 21-d-old *Arabidopsis* seedlings were rinsed 5 times in Milli-Q water, transferred to new Petri dishes containing 70 ml Milli-Q water, and placed back in the climate chamber. After 3 d, root exudates were collected by filtering the solution in which the seedlings had been incubated through 0.2 µM Millipore filters (Merck KGaA, Darmstadt, Germany). The production of fluorescent phenolic compounds was visualized under UV light (365 nm).

Bacteria cultivation and inoculation

The bacterial strain *P. simiae* WCS417 (Berendsen et al., 2015) was inoculated on agar-solidified King's B medium (King et al., 1954) supplemented with 150 µg ml^{-1} of rifampicin. Bacteria were incubated at 28°C for 16 h. Then the bacteria were scraped off the plates and suspended in 10 mM $MgSO_4$. The bacterial suspension was pelleted by centrifugation at a speed of 3500 *g* for 5 min, gently washed and resuspended in 10 ml 10 mM $MgSO_4$. This pellet-wash-resuspend step was repeated 3 times and the bacterial suspension was then concentrated to a final OD_{660} of 1.

For experiments to determine bacterial growth, live bacteria were inoculated in 96-well microtiter plates. Each well contained 200 µl of root exudates with an initial bacteria density at OD_{660} of 10^{-5}. Plates with bacteria were then moved to the climate chamber. Bacterial densities were assessed at 0 and 16 h after inoculation by diluting and plating the dilution series of bacterial cultures on agar-solidified KB plates supplemented with 150 µg ml^{-1} of rifampicin. The plates were incubated at 28°C for 24 h after which the number of colony-forming units (cfu) were counted. For experiments to collect bacterial samples for RNA sequencing, live bacteria were inoculated in 50-ml Falcon tubes. Each tube contained 10 ml root exudates with an initial bacterial density at OD_{660} of 0.15. Tubes with bacteria were incubated in a shaker with a speed of 100 rpm min^{-1} at 21°C.

Bacteria sample collection

After 1 h of cultivation in root exudates, 1 ml of the bacterial culture was taken and mixed with 2 ml RNAprotect® Bacteria Reagent (QIAGEN, Venlo, The Netherlands). Bacterial samples were mixed immediately by vortex for 5 s and incubated for 5 min at room temperature according to instructions described in RNAprotect® Bacteria Reagent Handbook (QIAGEN, Venlo, The Netherlands). Bacterial suspensions were pelleted by centrifuging at a speed of 5000 *g* for 10 min and the pellet was stored at -80°C before usage.

cDNA Library preparation

Total bacterial RNA was isolated using RNeasy Mini Kit (QIAGEN, Venlo, The Netherlands). Lysozyme (Sigma-Aldrich, Inc., St. Louis, MO) was used in the enzymatic lysis step and QIAGEN RNase-Free DNase Set (QIAGEN, Venlo, The Netherlands) was used in the on-column DNase digestion step. All abovementioned steps were performed according to instructions described in RNAprotect® Bacteria Reagent Handbook (QIAGEN, Venlo, The Netherlands). The quality of total RNA was analyzed using Agilent RNA6000 Nano Kit (Agilent Technologies, Waldbronn, Germany). Ribosomal RNA in 5 µg of total RNA was depleted using Ribo-Zero kit for bacteria (Illumina, San Diego, CA). RNA purification was performed using RNeasy MinElute Column (QIAGEN, Venlo, The Netherlands) according to instructions described in Ribo-Zero Magnetic Kits User Guide (Illumina, San Diego, CA). The quality and quantity of rRNA-depleted total RNA was analyzed using the Agilent RNA6000 Pico Kit (Agilent Technologies, Waldbronn, Germany). Library preparation was performed using TruSeq Stranded mRNA LT Sample Prep Kit (Illumina, San Diego, CA), with 12 ng of rRNA-depleted total RNA, according to manufacturer's instructions. The standard adapters provided by Illumina (Illumina, San Diego, CA) were used in the adapter ligation step. Agencourt AMPure kit (Beckman Coulter Brea, CA, USA) was used in the PCR clean-up step. The quality of cDNA library was analyzed using Agilent High Sensitivity DNA Kit (Agilent Technologies, Waldbronn, Germany). The quantity of cDNA library was measured with Qubit™ 3 Fluorometer with Qubit™ dsDNA BR Assay Kit (Thermo Fisher Scientific Inc., Waltham, MA).

RNA sequencing

Sequencing of the cDNA libraries was performed using a NextSeq500 platform in a single-end run with a read length of 75 bp (Utrecht Sequencing Facility, Utrecht, The Netherlands). FastQC (version 0.11.5, https://www.bioinformatics.babraham.ac.uk/projects/fastqc/) software was used to check the quality and Trimmomatic (version 0.32) software was used to trim the reads (Bolger et al., 2014). Kallisto (version 0.43.1) software was used to quantify the abundance of transcripts (Bray et al., 2016) based on the coding sequences of WCS417 retrieved from National Center for Biotechnology Information (https://www.ncbi.nlm.nih.gov). From the Kallisto output, the transcripts per million (TPM) counts were used in a principal component analysis (PCA) and estimated counts were used in a differential analysis. The differential analysis was performed using the DESeq2 (version 1.18.1) package in RStudio (version 1.1.383, R version 3.4.4) software and genes with a false discovery rate (FDR) < 0.05 were selected as differentially expressed genes (DEGs) for further analysis (Love et al., 2014). Functional annotation of the genome of WCS417 was performed using Annie (version 1.0, http://genomeannotation.github.io/annie) software. Enrichment analysis of DEGs was performed using the phyper function in R. Clusters of orthologous group of DEGs were retrieved from previously published data (Cole et al., 2017).

Statistics

Analysis of variance in all experiments was performed using GraphPad Prism 7 (GraphPad Software, La Jolla, CA).

Author contributions

K.Y., I.A.S., C.M.J.P., P.A.H.M.B., and R.L.B. designed experiments; K.Y., and I.A.S. performed experiments; K.Y., R.D.J., and B.L.S. analyzed data; and K.Y., C.M.J.P., P.A.H.M.B., and R.L.B. wrote the manuscript.

SUPPLEMENTAL DATA

The following data sets are available upon request.

Dataset S1. Estimated counts of 5545 coding genes of *P. simiae* WCS417 in responses to root exudates derived from Col-0, *myb72* and *f6'h1* plants growing under iron deficiency.

Dataset S2. Transcripts per million of 5545 coding genes of *P. simiae* WCS417 in responses to root exudates derived from Col-0, *myb72* and *f6'h1* plants growing under iron deficiency.

Dataset S3. 439 differentially expressed genes (DEGs) of *P. simiae* WCS417 in responses to root exudates derived from Col-0 and *f6'h1* plants growing under iron deficiency. Dataset is organized according to the $\log_2$-fold change.

Dataset S4. 383 differentially expressed genes (DEGs) that are associated with clusters of orthologous groups (COG) of *P. simiae* WCS417 in responses to root exudates derived from Col-0 and *f6'h1* plants growing under iron deficiency. Dataset is organized according to the COG category and then to the $\log_2$-fold change. Data was retrieved from published data (Cole et al., 2017).

CHAPTER 6

Summarizing discussion

There is an urgent need for novel strategies to increase crop productivity and to feed the ever-growing population on Earth using the limited amount of arable land available to us. Root-associated microbiomes are increasingly considered a vital determinant of plant health and crop yields (Berendsen et al., 2012; Bulgarelli et al., 2013; Philippot et al., 2013; Turner et al., 2013a; Tkacz and Poole, 2015; Raaijmakers and Mazzola, 2016). The fundamental basis of root-microbiome interactions has consequently received more and more attention in recent years, as a better understanding of microbiome functioning is thought to drive future innovations in agriculture. Plant roots form diverse associations with members of the root microbiome, of which many are proven beneficial for plant health (Berendsen et al., 2012; Bulgarelli et al., 2013). Interestingly, selected plant growth-promoting rhizobacteria (PGPR) were found to not only enhance plant growth but also boost the immune responses in the entire plant body against potential attacks by pathogens and insects (Pieterse et al., 2014). This phenomenon, known as induced systemic resistance (ISR), has been extensively investigated and different components of ISR signaling have been revealed using the model system *Pseudomonas simiae* WCS417 (hereafter WCS417) on *Arabidopsis thaliana* (hereafter *Arabidopsis*; Pieterse et al., 1996; Van Wees et al., 1997; Pieterse et al., 1998; Pozo et al., 2008; Van der Ent et al., 2008; Zamioudis et al., 2014). However, many molecular events in the early stages of this beneficial association, such as the communication between plant roots and free-living rhizobacteria, remain in the dark. In this thesis, we have presented our multi-omics approach to decipher the chemical communications during the establishment of beneficial associations between roots and members of root microbiome.

Root immune suppression by non-invasive beneficial rhizobacteria

Beneficial microbes need to colonize plant roots or the rhizosphere to confer their beneficial traits on host plants (Lugtenberg and Kamilova, 2009; Pieterse et al., 2014). Like all microorganisms, beneficial microbes are confronted with the sophisticated plant immune system. Pattern recognition receptors (PRRs) can perceive conserved microbe-associated molecular patterns (MAMPs) and initiate immune signaling (Jones and Dangl, 2006). Many beneficial microbes, including the ISR-eliciting WCS417, do elicit immune responses in host plant roots, but these often become swiftly repressed, likely to facilitate a long-term relationship with the host (Liu et al., 2003; Libault et al., 2010; Millet et al., 2010; Jacobs et al., 2011; Stringlis et al., 2018a). Significant progress has been achieved in understanding the molecular mechanism of root immune suppression by beneficial microbes that are invading host roots, such as rhizobia and mycorrhizal fungi that are living in symbiosis with their hosts (Zamioudis and Pieterse, 2012; Chapter 1). However, much less is known about the immune modulation strategies of non-invasive beneficial microbes. In chapter 2, we investigated the strategy deployed by non-invasive beneficial rhizobacteria to subvert root immune responses. We screened a Tn5 transposon mutant library of the PGPR strain *Pseudomonas capeferrum* WCS358 (hereafter WCS358) using an *Arabidopsis* transgenic line carrying a *CYP71A12*$_{pro}$*:GUS* reporter (Millet et al., 2010). Like WCS417, WCS358 is able to elicit ISR in many plant species including *Arabidopsis* (Berendsen et al., 2015). *CYP71A12* is highly expressed in *Arabidopsis* roots upon PRR-mediated MAMP recognition (Denoux et al., 2008; Millet et al., 2010). Flg22, the 22-amino acid peptide epitope of bacterial flagellin, is a widely used synthetic MAMP that can be recognized by the cognate PRR FLS2 in *Arabidopsis* (Felix et al., 1999; Gomez-Gomez and Boller, 2000). We first demonstrated that WCS358 can actively suppress root immune responses, as pre-inoculation of WCS358 blocks flg22-induced *CYP71A12*$_{pro}$*:GUS* expression. This immune suppressive phenotype is mediated by diffusible heat-resistant bacterial signals produced by WCS358. Then we demonstrated that the WCS358 genome encodes immunogenic MAMPs that can be

recognized by *Arabidopsis*, as our data shows that *Arabidopsis* can recognize the synthetic flg22 peptide of WCS358 in a FLS2-dependent manner (Figure 1). In the following mutant screening assay, we identified 2 mutants, *pqqF*::Tn5 and *cyoB*::Tn5, that lost their ability to block the flg22-induced *CYP71A12*$_{pro}$*:GUS* expression. Both PqqF and CyoB function in the oxidation of glucose, resulting in the production of gluconic acid (GA) and 2-keto gluconic acid (2-KGA), and significant acidification of the bacterial growth environment (Figure 1). We found that simply lowering the environmental pH is sufficient to block the flg22-induced *CYP71A12*$_{pro}$*:GUS* expression, indicating that WCS358 suppresses root immune responses by acidifying the root environment via excretion of GA and 2-KGA (Figure 1).

Modulation of environmental pH is often found associated with fungal pathogenicity (Masachis et al., 2016; Vylkova, 2017), but it was not clear how environmental acidification contributes to the establishment of beneficial associations between rhizobacteria and plant roots. Our data indicate that it is a strategy of beneficial rhizobacteria to suppress local root immune responses. Although the pH dependency of immune responses has been reported previously, the molecular mechanism remains elusive. Following the FLS2-mediated recognition of flg22, a rapid extracellular alkalization process is typically observed (Navarro et al., 2004) and acidification of the root exterior may interfere with this process, thus preventing downstream immune signaling initiation. Interestingly, apoplastic acidification was found to up-regulate many genes that clearly overlap with flagellin-induced genes in *Arabidopsis* roots, including defense-related *WRKY40* and *ERF6* (Lager et al., 2010). In another study, however, it was shown that the expression of immune-responsive marker genes such as *FRK1* and *WRKY30* in response to flagellin declined along with the increased environmental acidity (Lee et al., 2012). Our current data supports a suppressive effect of apoplastic acidification on the expression of an immune-responsive marker gene, indicating a complicated role of pH in regulating immune responses. The constant activation of root immunity has a detrimental effect on the establishment of beneficial associations. Therefore, active immune interference might be important for successful bacterial colonization. It is known that induction of root immune responses adversely affects the rhizobial associations with legumes and colonization by the beneficial fungus *Piriformospora indica* in *Arabidopsis* roots (Jacobs et al., 2011; Lopez-Gomez et al., 2012). In line with this, rhizosphere population densities of the *pqqF*::Tn5 mutant were significantly reduced compared to wild-type WCS358, suggesting that effects of the plant immune system can extend into the rhizosphere and that modulation of the root immune responses affects bacterial rhizosphere colonization. In a recent study, Liu and colleagues also identified two genes, *morA* and *spuC*, that are required for the beneficial *Pseudomonas* sp. WCS365 to evade plant immune responses in the rhizosphere (Liu et al., 2018). Both *morA* and *spuC* function in balancing biofilm formation and deletion of either gene resulted in impaired rhizosphere fitness (Liu et al., 2018). Besides, we also found that a selection of rhizobacteria isolated from the *Arabidopsis* rhizosphere have distinct effects on flg22-induced root immune responses. Many soil-borne rhizobacteria seem to share the ability to suppress root immune responses, while others act as potent elicitors of root immune responses. This raises the question of how plants are able to coordinate their responses to the beneficial, commensal and pathogenic microbes that simultaneously occupy the rhizosphere. Although there is no doubt that the plant immune system can shape the composition and proliferation of certain microbiome members in both root endophytic compartments and rhizosphere (Carvalhais et al., 2013; Carvalhais et al., 2015; Lebeis et al., 2015; Castrillo et al., 2017; Liu et al., 2017), the temporal and spatial dimensions in microbiome compositional shifts, the effect of root immune responses on bacterial

functions at the strain and community level, and the role of plant immunity in controlling microbiome homeostasis require further investigation.

Overlapping root responses to rhizobacterial colonization and iron deficiency

Upon successful rhizosphere colonization, ISR-eliciting PGPRs such as WCS417 and WCS358 can initiate transcriptional changes in plant roots which ultimately lead to growth promotion and ISR (Pieterse et al., 2014; Verbon and Liberman, 2016). The root-specific transcription

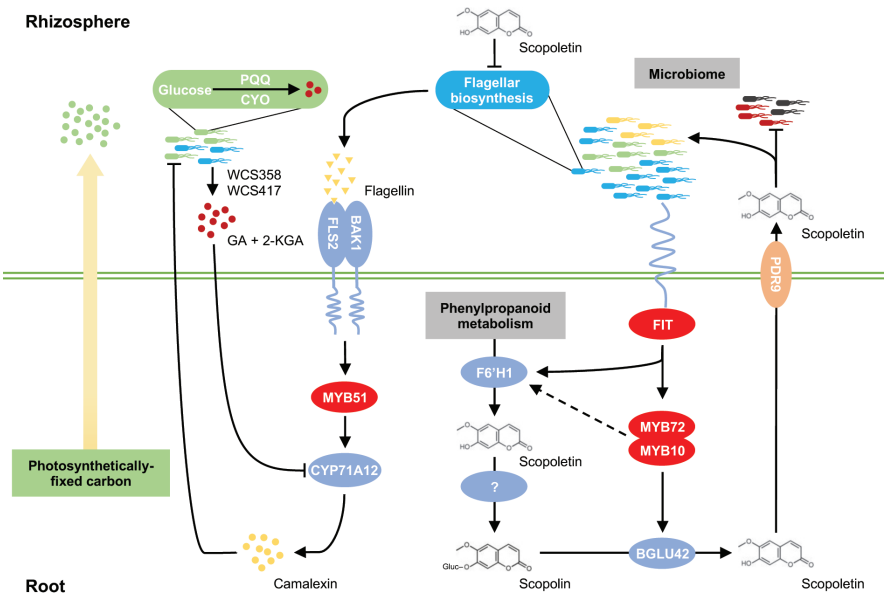

Figure 1. Chemical communication in root-microbiome interactions. FLS2, a cell surface-localized pattern recognition receptor in *Arabidopsis*, can recognize bacterial flagellin molecules. Together with a co-receptor BAK1, FLS2-mediated flagellin recognition initiates immune signaling and lead to the biosynthesis of antimicrobial camalexin. Both MYB51 (a transcription factor) and CYP71A12 (an enzyme) are key regulators in camalexin biosynthesis. *Pseudomonas capeferrum* WCS358 (hereafter WCS358) and *Pseudomonas simiae* WCS417 (hereafter WCS417) are plant-beneficial rhizobacteria that are able to utilize photosynthetically-fixed carbon exuded by *Arabidopsis* roots. WCS358, and possibly WCS417, produce gluconic acid (GA) and 2-keto gluconic acid (2-KGA) via glucose metabolism, in which both pyrroloquinoline quinone (PQQ) and cytochrome bo_3 oxidase (CYO) participate. The production of GA and 2-KGA significantly increases environmental acidity. Environmental acidification suppresses FLS2-dependent defenses in *Arabidopsis* roots, thereby facilitating root colonization by WCS358. WCS417 is also able to hijack the iron deficiency responses, which leads to coumarin biosynthesis in *Arabidopsis* roots. Under iron deficiency, the root transcription factor FIT is activated. FIT regulates the expression of *F6'H1*, which encodes Feruloyl-CoA 6'-Hydroxylase1, the key enzyme in coumarin biosynthesis. F6'H1 catalyzes the conversion of the intermediates of phenylpropanoid metabolism into scopoletin. The corresponding glucoside, scopolin, is synthesized via as yet unknown glucosyltransferase and stored inside plant cells. FIT also regulates the expression of other transcription factors including MYB72 and MYB10, both of which act redundantly in the regulation of iron deficiency responses. F6'H1 is likely regulated by MYB72/MYB10. A MYB72-dependent β-glucosidase, BGLU42, may function specifically in the hydrolysis of scopolin to scopoletin and is required for the excretion of scopoletin into root exterior. Scopoletin is secreted by the root via the ABC transporter PDR9, and this secretion significantly affects the composition of the root microbiome. Moreover, scopoletin negatively regulates the expression of genes involved in flagellar biosynthesis in WCS417, which may benefit bacterial motility-to-biofilm transition. Black dashed arrows indicate predicted relationship and question marks indicate enzymes unidentified in *Arabidopsis*.

factor MYB72 and the MYB72-dependent β-glucosidase BGLU42 act as key components of WCS417-elicited ISR signaling in *Arabidopsis*, as both *myb72* and *bglu42* mutants failed to mount ISR (Van der Ent et al., 2008; Zamioudis et al., 2014). The fact that overexpression of MYB72's downstream target BGLU42 led to constitutive disease resistance, stresses the indispensable role of MYB72-BGLU42 module in ISR (Van der Ent et al., 2008; Zamioudis et al., 2014). Intriguingly, a large overlap in transcriptomes was observed between roots colonized by WCS417 and roots growing under iron deficiency (Zamioudis et al., 2015). The overlapping gene set includes *MYB72* and *BGLU42,* but also genes encoding key enzymes in the biosynthesis of phenolic compounds including coumarins (Zamioudis et al., 2014), suggesting that WCS417 can hijack iron deficiency responses (Zamioudis et al., 2015; Verbon et al., 2017). In alkaline soil where iron availability is extremely low, MYB72 acts together with its paralog MYB10 to maintain plant survival (Palmer et al., 2013). MYB72 and BGLU42 were also found to regulate the production and excretion of fluorescent phenolics in iron-starved *Arabidopsis* roots (Zamioudis et al., 2014). Considering that MYB72 plays a dual role in the onset of rhizobacteria-elicited ISR and production of phenolics in iron-starved *Arabidopsis* roots, we sought to unravel the identities of these compounds and their roles in root-microbiome interactions.

In chapter 3, we utilized metabolite fingerprinting to investigate the metabolic changes in *Arabidopsis* roots growing under iron deficiency. Our data show that *Arabidopsis* roots synthesize and secrete coumarins into the rhizosphere under iron deficiency, consistent with other studies (Fourcroy et al., 2014; Schmid et al., 2014; Schmidt et al., 2014; Strehmel et al., 2014; Ziegler et al., 2017; Rajniak et al., 2018; Tsai et al., 2018). Root-borne coumarins are able to facilitate root iron uptake via reduction and chelation of Fe(III) from the soil environment (Tsai and Schmidt, 2017b). We found that scopoletin and its glycosylated form scopolin are among the most dominant coumarins in roots and root exudates of *Arabidopsis* plants grown under iron deficiency (Figure 1). Moreover, coumarins, including scopolin and scopoletin, are synthesized in a MYB72-dependent manner in *Arabidopsis* roots, as their production was depleted in *myb72* mutant, confirming that MYB72 regulates the production and accumulation of coumarins under iron deficiency (Figure 1). Interestingly, scopolin accumulated to similar levels in the roots of *bglu42* mutant and those of Col-0, whereas scopoletin was almost depleted in the root exudates of the *bglu42* mutant. This shows that BGLU42 functions in the deglycosylation of scopolin to scopoletin, which is required for the excretion of scopoletin into rhizosphere (Figure 1). As we know that the ISR-eliciting rhizobacteria hijack iron deficiency responses and induce the transcription of genes involved in coumarin biosynthesis during the onset of ISR (Zamioudis et al., 2015), it was unknown whether *Arabidopsis* roots actually synthesize coumarins in response to the colonization of ISR-eliciting rhizobacteria. In chapter 4, we therefore utilized metabolite fingerprinting to analyze the metabolic changes in WCS417-colonized *Arabidopsis* roots. We found that colonization by WCS417 indeed strongly induced the production and accumulation of scopoletin, scopolin and esculin in *Arabidopsis* roots (Figure 1). This confirmed that the transcriptionally overlapping responses of *Arabidopsis* roots in response to iron deficiency and to rhizobacteria colonization are indeed reflected by the metabolic changes. Additionally, we found accumulation of certain TCA cycle intermediates, mainly citrate, malate and succinate, in response to both iron deficiency (Chapter 3) and to colonization by WCS417 in *Arabidopsis* roots (Chapter 4). Interestingly, it was recently demonstrated TCA intermediates, including citrate, can induce defense priming in *Arabidopsis* against foliar pathogen infection (Balmer et al., 2018). Moreover, disease-induced malate secretions by roots of *Arabidopsis* plants were involved in the recruitment of the ISR-eliciting rhizobacterium *Bacillus subtilis* FB17 (Rudrappa et al.,

2008b; Lakshmanan et al., 2012). Therefore, the production of TCA cycle intermediates in response to colonization by WCS417 may boost plant immune responses by priming of defense responses, but may also reinforce the colonization by WCS417 and thus strengthen the mutualistic relationship with this beneficial rhizobacterium.

Coumarins function as assembly cues for the root microbiome

We have shown in Chapter 3 and 4 that metabolic reprograming of *Arabidopsis* roots in response to iron deficiency, and to WCS417 colonization, results in substantial accumulation of coumarins. WCS417 and many other *Arabidopsis* natural microbiome members have been shown to activate MYB72 (Zamioudis et al., 2015). MYB72 is a key component of ISR and coumarin biosynthesis (Van der Ent et al., 2008; Stringlis et al., 2018b; Chapter 3), and because WCS417 can hijack the root iron deficiency response (Zamioudis et al., 2015), we wondered what the impact of these metabolic changes on the root-associated microbiome and, more specifically, on WCS417 would be. Since coumarins are among the most dominant metabolites synthesized by *Arabidopsis* roots under iron deficiency (Stringlis et al., 2018b; Chapter 3), we investigated the effect of coumarins on root microbiome assembly using metagenomic sequencing. Therefore, we assessed the root microbiome composition of *Arabidopsis* wild-type Col-0 and mutant *f6'h1*, which is defective in coumarin biosynthesis (Schmid et al., 2014). Due to the antimicrobial activity of coumarins (Kai et al., 2006; Grosskinsky et al., 2011; Sun et al., 2014), we expected these compounds to cause a compositional shift in the root microbiome. Indeed, *f6'h1* assembled a distinct microbiome compared to that of wild-type, in which 22 microbial genera were depleted and 13 genera enriched. This indicates that root-produced coumarins can actively shape root microbiome assembly by stimulating or inhibiting specific microbial genera (Figure 1). Interestingly, we found that the ISR-eliciting rhizobacteria WCS417 and WCS358 are highly tolerant to scopoletin (Figure 1), while two fungal plant pathogens are sensitive. It is likely that, by stimulating the MYB72-mediated excretion of scopoletin, these ISR-eliciting rhizobacteria deter at least part of the microbes with which they compete for space and nutrients on the root, thereby improving their niche establishment and enabling them to enhance plant growth and protection.

It is known that the initiation of certain symbiotic signaling relies on the constant chemical communication between roots and microbes (Oldroyd, 2013). For example, in rhizobia-legume symbiosis, flavonoids are released into the rhizosphere by legume roots, which are perceived by free-living rhizobia. Transcriptional reprogramming in rhizobia upon perception of these flavonoids results in the rhizobial production and secretion of nodulation factors, which in-turn activate symbiosis signaling in the plant roots (Oldroyd, 2013; Zipfel and Oldroyd, 2017). Considering the fact that coumarins are produced and secreted in response to WCS417 but have limited effect on the growth of WCS417 *in vitro* (Chapter 3), we hypothesized that coumarins may also act as semiochemicals involved in the communication between roots and WCS417. Thus, in chapter 5, we investigated the effect of coumarins on activity of WCS417 using RNA-sequencing. Indeed, we found that WCS417 drastically alters its transcriptional profile in responses to F6'H1-dependent root exudates. Interestingly, enrichment analysis of the functional categories of all differentially expressed genes suggested that F6'H1-dependent coumarins also affects bacterial functions that are required for colonization of *Arabidopsis* roots, such as cell motility and carbohydrate metabolism. We then compared our data to a set of colonization-related genes previously identified in WCS417 (Cole et al., 2017), and found that the expression of 13 cell motility-related genes was exclusively repressed by F6'H1-dependent coumarins, while those 13 genes are required for full colonization capability of WCS417. It has been demonstrated

that inhibition of cell motility often coincides with a switch to increased biofilm formation (Guttenplan and Kearns, 2013), which is necessary for the long-term root colonization of many rhizobacteria (Danhorn and Fuqua, 2007; Rudrappa et al., 2008a). It is possible that WCS417 can benefit from the inhibition of motility as F6'H1-dependent coumarins would be produced only after WCS417 has reached the root in sufficient number to induce the expression of *F6'H1*. However, this hypothesis needs further confirmation. Besides, the down-regulated cell motility-related genes are mostly associated with flagellar biosynthesis (Figure 1), suggesting that WCS417 actively avoids excessive production of flagella in order to evade recognition by the plant and subsequent initiation of root immune responses. Our data provides evidence that coumarins are semiochemicals in the communication between roots and members of the root microbiome. The picture that emerges from our work is that WCS417 is attracted by nutrients in root exudates, thus moving towards the active sites of root exudation. The initial gathering of WCS417 cells may induce iron deficiency responses in *Arabidopsis* roots, resulting in enhanced coumarin biosynthesis and secretion of scopoletin in the rhizosphere. Altered root exudates potentially repress scopoletin-sensitive microbes in the same niche, while WCS417 can benefit from the niche occupation and start forming biofilm on the root surface as a response to coumarins.

Local immune modulation: roots for ISR?

Besides coumarins and TCA cycle intermediates, we also discovered that intermediates of glucosinolate biosynthesis and fatty acid metabolism, two immune-related groups of metabolites, are significantly more abundant upon colonization by WCS417 (Chapter 4). Glucosinolates in *Arabidopsis* mainly consist of methionine-derived aliphatic glucosinolates and tryptophan-derived indole glucosinolates, both of which are considered plant defense compounds (Bednarek et al., 2009; Clay et al., 2009; Muller et al., 2010; Sonderby et al., 2010; Jørgensen et al., 2015). Interestingly, we detected many metabolites matching precursors of aliphatic glucosinolates, but not of indolic glucosinolates. Moreover, it is known that WCS417 is able to induce alphatic glucosinolate biosynthesis in systemic foliar tissues (Pangesti et al., 2016), and suppress the expression of the genes involved in the biosynthesis of indole glucosinolates in *Arabidopsis* roots, such as *MYB51* and *MYB122* (Millet et al., 2010; Zamioudis, 2012; Frerigmann and Gigolashvili, 2014; Stringlis et al., 2018a; Chapter 2). However, the roles of WCS417-induced aliphatic and WCS417-repressed indole glucosinolate biosynthesis are not clear yet. We speculate that the enhanced biosynthesis of aliphatic glucosinolates, which have antimicrobial activity, may have a role in root microbiome assembly or are prepared as defense compounds in the *Arabidopsis* roots that can be effectively relocated to protect plants against pathogens and insects. Effective glucosinolate transporters required for such relocation have been described (Nour-Eldin et al., 2012; Jørgensen et al., 2015). The apparently enhanced fatty acids metabolism in WCS417-colonized *Arabidopsis* roots is likely associated with activation of defense responses. Two unsaturated fatty acids, linoleic acid and linolenic acid, which are more abundantly produced in WCS417-colonized *Arabidopsis* roots, are also enriched in plant defense responses against *Botrytis cinerea* and *P. syringae* (Ongena et al., 2004; Yaeno et al., 2004). Interestingly, they are also the main substrates for the biosynthesis of JA (Mosblech et al., 2009; Wasternack and Feussner, 2018), a major plant defense hormone involved in regulating not only plant immune signaling (Pieterse et al., 2012), but also in WCS417-elicited ISR in *Arabidopsis* (Pieterse et al., 1998; Van der Ent et al., 2009). However, we failed to detect any JA or JA-derivatives in our analysis, which is consistent with the fact that WCS417-elicited ISR does not enhance JA biosynthesis in *Arabidopsis* without invaders (Pieterse et al., 2000; Verhagen et al., 2004). Possibly, the enhanced fatty acids metabolism

in WCS417-colonized roots may contribute to the accumulation of JA precursors, creating a reservoir for the subsequent enhanced JA biosynthesis and potentiated defense responses upon attack.

Redundant functioning of MYB72 and MYB10

MYB72 and its close paralog MYB10 emerged as important components in regulating iron deficiency responses. They function redundantly to maintain plant survival under iron deficient conditions, as only the double *myb72myb10* mutant failed to survive in alkaline soils, while growth of *myb72* and *myb10* single mutant plants was similar to that of wild-type plants (Palmer et al., 2013). During the onset of WCS417-elicited ISR, however, knocking out *MYB72* suffices to eliminate expression of ISR (Van der Ent et al., 2008). Moreover, we found that coumarin biosynthesis was dependent on MYB72 in *Arabidopsis* roots under iron deficiency (Stringlis et al., 2018b; Chapter 3), whereas in roots colonized by WCS417, the production of coumarins was not affected by the mutation of *MYB72* (Chapter 4), indicating that MYB72 is conditionally required for coumarin production. Correspondingly, after induction of the iron deficiency response, we only observed a rather small shift in the relative abundance of three genera in the root microbiome of the *myb72* mutant, while the coumarin biosynthesis mutant *f6'h1* showed a more distinct root microbiome composition (Stringlis et al., 2018b; Chapter 3), suggesting that in this condition the presence of *MYB10* may compensate the mutation of *MYB72* in the single *myb72* mutant. It appears that under specific circumstances, a redundant genetic factor in *Arabidopsis*, likely to be *MYB10*, can compensate the functioning of *MYB72* in response to colonization by WCS417 as well as to iron deficiency. In this thesis, we did not elucidate those specific conditions but suggest using the double mutant *myb72myb10* in future studies when either an ISR- or iron-deficiency-response negative mutant is required. Nonetheless, it would be interesting to decipher the genetic regulatory network of MYB72 and MYB10 to understand their exact roles in both ISR signaling and the iron deficiency response.

Coumarins, TCA cycle intermediates, glucosinolates and fatty acids were found in increased concentrations in the *Arabidopsis* roots colonized by WCS417 (Chapter 4). The production of these compounds did not depend on MYB72 in our study, however, due to possible redundancy with MYB10, our data are not conclusive about the role of MYB72 in this process. A notable MYB72-affected metabolite produced in response to WCS417 that we could identify was monopalmitin. Monopalmitin was more abundant in roots colonized by WCS417 and even more so in *myb72* roots. Although we can only speculate about the role of monopalmitin in the *Arabidopsis*-WCS417 interaction, it is a fatty acid that was recently identified as a dominant carbon source produced by plants to accommodate arbuscular mycorrhizal fungi (Luginbuehl et al., 2017). Mycorrhizal fungi cannot form a functional symbiosis with *Arabidopsis* roots (Veiga et al., 2013; Cosme et al., 2018), but monopalmitin might also function in providing other members of the plant-associated microbiome with a carbon source. The down-regulation of monopalmitin biosynthesis by MYB72 might limit this nourishment to prevent that specific members of the microbiome become problematically abundant.

Concluding remarks

In this study the interplay between the plant root and its microbiome was shown to involve both active suppression of root immune responses by beneficial bacteria and secretion of coumarins by the root that differentially affect growth and activity of specific members of the microbiota. Moreover, these coumarins are involved in shaping the composition of the

microbial community in the rhizosphere. In response to these coumarins, expression of root colonization-related genes in a beneficial bacterium is affected. Our results point to a model in which beneficial microbes can interfere with the root immune response to establish significant populations in the rhizosphere. Upon perception of specific semiochemicals in the root exudates, that are actually induced in the plant upon colonization by the beneficial bacterium, the bacteria seem to avoid recognition by the plant by down-regulation of MAMPs. Both the plant and the bacteria benefit from this intriguing and complex interaction. A thorough understanding of such interactions at the molecular and genetic level for both the plant and the microbiome can ultimately lead to the development of stable beneficial microbiomes that sustain efficient and durable crop production. Future breeding programs can employ this knowledge to develop elite crops that are better able to sustain plant-favorable and disease-suppressive microbiomes. Moreover, it should be possible to improve the field performance of plant-growth-promoting microbes by using those beneficial microbes that are specifically supported by crop plants. Unleashing the power of the plant microbiome will prove an important step in improving crop yields whilst reducing the environmental damage of chemical fertilizers and pesticides and thus providing future food for mankind's expanding population.

REFERENCES

Ahn, Y.O., Shimizu, B., Sakata, K., Gantulga, D., Zhou, C., Bevan, D.R., and Esen, A. 2010. Scopolin-hydrolyzing beta-glucosidases in roots of *Arabidopsis*. Plant Cell Physiol 51:132-143.

Akum, F.N., Steinbrenner, J., Biedenkopf, D., Imani, J., and Kogel, K.H. 2015. The *Piriformospora indica* effector PIIN_08944 promotes the mutualistic Sebacinalean symbiosis. Front Plant Sci 6:906.

Aliotta, G., De Feo, V., Pinto, G., and Pollio, A. 1999. *In vitro* inhibition of algal growth by *rut a graveolens* L. extracts: biological and chemical aspects. Plant Biosyst 133:185-191.

An, R., and Moe, L.A. 2016. Regulation of pyrroloquinoline quinone-dependent glucose dehydrogenase activity in the model rhizosphere-dwelling bacterium *Pseudomonas putida* KT2440. Appl Environ Microb 82:4955-4964.

Aslam, S.N., Newman, M.A., Erbs, G., Morrissey, K.L., Chinchilla, D., Boller, T., Jensen, T.T., De Castro, C., Ierano, T., Molinaro, A., Jackson, R.W., Knight, M.R., and Cooper, R.M. 2008. Bacterial polysaccharides suppress induced innate immunity by calcium chelation. Curr Biol 18:1078-1083.

Badri, D.V., and Vivanco, J.M. 2009. Regulation and function of root exudates. Plant Cell Environ 32:666-681.

Badri, D.V., Weir, T.L., Van der Lelie, D., and Vivanco, J.M. 2009. Rhizosphere chemical dialogues: plant–microbe interactions. Curr Opin Biotech 20:642-650.

Badri, D.V., Chaparro, J.M., Zhang, R., Shen, Q., and Vivanco, J.M. 2013. Application of natural blends of phytochemicals derived from the root exudates of *Arabidopsis* to the soil reveal that phenolic-related compounds predominantly modulate the soil microbiome. J Biol Chem 288:4502-4512.

Bais, H.P., Weir, T.L., Perry, L.G., Gilroy, S., and Vivanco, J.M. 2006. The role of root exudates in rhizosphere interactions with plants and other organisms. Annu Rev Plant Biol 57:233-266.

Bakker, P.A.H.M., Pieterse, C.M.J., and Van Loon, L.C. 2007. Induced systemic resistance by fluorescent *Pseudomonas* spp. Phytopathology 97:239-243.

Bakker, P.A.H.M., Pieterse, C.M.J., De Jonge, R., and Berendsen, R.L. 2018. The soil-borne legacy. Cell 172:1178-1180.

Bakker, P.A.H.M., Berendsen, R.L., Doornbos, R.F., Wintermans, P.C., and Pieterse, C.M.J. 2013. The rhizosphere revisited: root microbiomics. Front Plant Sci 4:165.

Balmer, A., Pastor, V., Glauser, G., and Mauch-Mani, B. 2018. Tricarboxylates induce defense priming against bacteria in *Arabidopsis thaliana*. Front Plant Sci 9:1221.

Barad, S., Sela, N., Kumar, D., Kumar-Dubey, A., Glam-Matana, N., Sherman, A., and Prusky, D. 2016. Fungal and host transcriptome analysis of pH-regulated genes during colonization of apple fruits by *Penicillium expansum*. BMC Genomics 17:330.

Barberon, M. 2017. The endodermis as a checkpoint for nutrients. New Phytol 213:1604-1610.

Bardoel, B.W., Van der Ent, S., Pel, M.J.C., Tommassen, J., Pieterse, C.M.J., Van Kessel, K.P.M., and Van Strijp, J.A.G. 2011. *Pseudomonas* evades immune recognition of flagellin in both mammals and plants. PLoS Pathog 7:e1002206.

Bartsev, A.V., Deakin, W.J., Boukli, N.M., McAlvin, C.B., Stacey, G., Malnoe, P., Broughton, W.J., and Staehelin, C. 2004. NopL, an effector protein of *Rhizobium* sp. NGR234, thwarts activation of plant defense reactions. Plant Physiol 134:871-879.

Beck, M., Wyrsch, I., Strutt, J., Wimalasekera, R., Webb, A., Boller, T., and Robatzek, S. 2014. Expression patterns of *FLAGELLIN SENSING 2* map to bacterial entry sites in plant shoots and roots. J Exp Bot 65:6487-6498.

Bednarek, P., Pislewska-Bednarek, M., Svatos, A., Schneider, B., Doubsky, J., Mansurova, M., Humphry, M., Consonni, C., Panstruga, R., Sanchez-Vallet, A., Molina, A., and Schulze-Lefert, P. 2009. A glucosinolate metabolism pathway in living plant cells mediates broad-spectrum antifungal defense. Science 323:101-106.

Belas, R. 2014. Biofilms, flagella, and mechanosensing of surfaces by bacteria. Trends Microbiol 22:517-527.

Benjamini, Y., and Hochberg, Y. 1995. Controlling the false discovery rate: a practical and powerful approach to multiple testing. J Roy Stat Soc B Met:289-300.

Berendsen, R.L., Pieterse, C.M.J., and Bakker, P.A.H.M. 2012. The rhizosphere microbiome and plant health. Trends Plant Sci 17:478-486.

Berendsen, R.L., Van Verk, M.C., Stringlis, I.A., Zamioudis, C., Tommassen, J., Pieterse, C.M.J., and Bakker, P.A.H.M. 2015. Unearthing the genomes of plant-beneficial *Pseudomonas* model strains WCS358, WCS374 and WCS417. BMC Genomics 16:539.

Berendsen, R.L., Vismans, G., Yu, K., Song, Y., De Jonge, R., Burgman, W.P., Burmølle, M., Herschend, J., Bakker, P.A.H.M., and Pieterse, C.M.J. 2018. Disease-induced assemblage of a plant-beneficial bacterial consortium. ISME J 12:1496-1507.

Blair, K.M., Turner, L., Winkelman, J.T., Berg, H.C., and Kearns, D.B. 2008. A molecular clutch disables flagella in the *Bacillus subtilis* biofilm. Science 320:1636-1638.

Bolger, A.M., Lohse, M., and Usadel, B. 2014. Trimmomatic: a flexible trimmer for Illumina sequence data. Bioinformatics 30:2114-2120.

Boller, T., and Felix, G. 2009. A renaissance of elicitors: perception of microbe-associated molecular patterns and danger signals by pattern-recognition receptors. Annu Rev Plant Biol 60:379-406.

Bolton, M.D., Van Esse, H.P., Vossen, J.H., De Jonge, R., Stergiopoulos, I., Stulemeijer, I.J.E., Van den Berg, G.C.M., Borras-Hidalgo, O., Dekker, H.L., De Koster, C.G., De Wit, P.J.G.M., Joosten, M.H.A.J., and Thomma, B.P.H.J. 2008. The novel *Cladosporium fulvum* lysin motif effector Ecp6 is a virulence factor with orthologues in other fungal species. Mol Microbiol 69:119-136.

Boutrot, F., and Zipfel, C. 2017. Function, discovery, and exploitation of plant pattern recognition receptors for broad-spectrum disease resistance. Annu Rev Phytopathol 55:257-286.

Bozsoki, Z., Cheng, J., Feng, F., Gysel, K., Vinther, M., Andersen, K.R., Oldroyd, G., Blaise, M., Radutoiu, S., and Stougaard, J. 2017. Receptor-mediated chitin perception in legume roots is functionally separable from Nod factor perception. Proc Natl Acad Sci U S A 114:E8118-E8127.

Bray, N.L., Pimentel, H., Melsted, P., and Pachter, L. 2016. Near-optimal probabilistic RNA-seq quantification. Nat Biotechnol 34:525-527.

Bressan, M., Roncato, M.A., Bellvert, F., Comte, G., Haichar, F.Z., Achouak, W., and Berge, O. 2009. Exogenous glucosinolate produced by *Arabidopsis thaliana* has an impact on microbes in the rhizosphere and plant roots. ISME J 3:1243-1257.

Bruckhoff, V., Haroth, S., Feussner, K., König, S., Brodhun, F., and Feussner, I. 2016. Functional characterization of CYP94-genes and identification of a novel jasmonate catabolite in flowers. PLoS One 11:e0159875.

Brumbarova, T., Bauer, P., and Ivanov, R. 2015. Molecular mechanisms governing *Arabidopsis* iron uptake. Trends Plant Sci 20:124-133.

Buckhout, T.J., Yang, T.J., and Schmidt, W. 2009. Early iron-deficiency-induced transcriptional changes in *Arabidopsis* roots as revealed by microarray analyses. BMC Genomics 10:147.

Bulgarelli, D., Schlaeppi, K., Spaepen, S., Ver Loren van Themaat, E., and Schulze-Lefert, P. 2013. Structure and functions of the bacterial microbiota of plants. Annu Rev Plant Biol 64:807-838.

Bulgarelli, D., Garrido-Oter, R., Munch, P.C., Weiman, A., Droge, J., Pan, Y., McHardy, A.C., and Schulze-Lefert, P. 2015. Structure and function of the bacterial root microbiota in wild and domesticated barley. Cell Host Microbe 17:392-403.

Bulgarelli, D., Rott, M., Schlaeppi, K., Ver Loren van Themaat, E., Ahmadinejad, N., Assenza, F., Rauf, P., Huettel, B., Reinhardt, R., Schmelzer, E., Peplies, J., Gloeckner, F.O., Amann, R., Eickhorst, T., and Schulze-Lefert, P. 2012. Revealing structure and assembly cues for *Arabidopsis* root-inhabiting bacterial microbiota. Nature 488:91-95.

Burow, M., and Halkier, B.A. 2017. How does a plant orchestrate defense in time and space? Using glucosinolates in *Arabidopsis* as case study. Curr Opin Plant Biol 38:142-147.

Cao, Y., Liang, Y., Tanaka, K., Nguyen, C.T., Jedrzejczak, R.P., Joachimiak, A., and Stacey, G. 2014. The kinase LYK5 is a major chitin receptor in *Arabidopsis* and forms a chitin-induced complex with related kinase CERK1. Elife 3:e03766.

Carvalhais, L.C., Dennis, P.G., Badri, D.V., Tyson, G.W., Vivanco, J.M., and Schenk, P.M. 2013. Activation of the jasmonic acid plant defence pathway alters the composition of rhizosphere bacterial communities. PLoS One 8:e56457.

Carvalhais, L.C., Dennis, P.G., Badri, D.V., Kidd, B.N., Vivanco, J.M., and Schenk, P.M. 2015. Linking jasmonic acid signaling, root exudates, and rhizosphere microbiomes. Mol Plant Microbe In 28:1049-1058.

Castrillo, G., Teixeira, P.J., Paredes, S.H., Law, T.F., De Lorenzo, L., Feltcher, M.E., Finkel, O.M., Breakfield, N.W., Mieczkowski, P., Jones, C.D., Paz-Ares, J., and Dangl, J.L. 2017. Root microbiota drive direct integration of phosphate stress and immunity. Nature 543:513-518.

Chagas, F.O., Pessotti, R.C., Caraballo-Rodriguez, A.M., and Pupo, M.T. 2018. Chemical signaling involved in plant-microbe interactions. Chem Soc Rev 47:1652-1704.

Chen, H., Daletos, G., Okoye, F., Lai, D., Dai, H., and Proksch, P. 2015. A new cytotoxic cytochalasin from the endophytic fungus *Trichoderma harzianum*. Nat Prod Commun 10:585-587.

Chen, W.W., Yang, J.L., Qin, C., Jin, C.W., Mo, J.H., Ye, T., and Zheng, S.J. 2010. Nitric oxide acts downstream of auxin to trigger root ferric-chelate reductase activity in response to iron deficiency in *Arabidopsis*. Plant Physiol 154:810-819.

Cheng, X., Van der Voort, M., and Raaijmakers, J.M. 2015. Gac-mediated changes in pyrroloquinoline quinone biosynthesis enhance the antimicrobial activity of *Pseudomonas fluorescens* SBW25. Environ Microbiol Rep 7:139-147.

Chezem, W.R., Memon, A., Li, F.S., Weng, J.K., and Clay, N.K. 2017. SG2-Type R2R3-MYB transcription factor MYB15 controls defense-induced lignification and basal immunity in *Arabidopsis*. Plant Cell 29:1907-1926.

Clay, N.K., Adio, A.M., Denoux, C., Jander, G., and Ausubel, F.M. 2009. Glucosinolate metabolites required for an *Arabidopsis* innate immune response. Science 323:95-101.
Colangelo, E.P., and Guerinot, M.L. 2004. The essential basic helix-loop-helix protein FIT1 is required for the iron deficiency response. Plant Cell 16:3400-3412.
Cole, B.J., Feltcher, M.E., Waters, R.J., Wetmore, K.M., Mucyn, T.S., Ryan, E.M., Wang, G., Ul-Hasan, S., McDonald, M., Yoshikuni, Y., Malmstrom, R.R., Deutschbauer, A.M., Dangl, J.L., and Visel, A. 2017. Genome-wide identification of bacterial plant colonization genes. PLoS Biol 15:e2002860.
Cooper, J.A. 1987. Effects of cytochalasin and phalloidin on actin. J Cell Biol 105:1473-1478.
Cosme, M., Fernandez, I., Van der Heijden, M.G.A., and Pieterse, C.M.J. 2018. Non-mycorrhizal plants: the exceptions that prove the rule. Trends Plant Sci 23:577-587.
Couto, D., and Zipfel, C. 2016. Regulation of pattern recognition receptor signalling in plants. Nat Rev Immunol 16:537-552.
Czechowski, T., Stitt, M., Altmann, T., Udvardi, M.K., and Scheible, W.R. 2005. Genome-wide identification and testing of superior reference genes for transcript normalization in *Arabidopsis*. Plant Physiol 139:5-17.
Dakora, F.D., and Phillips, D.A. 2002. Root exudates as mediators of mineral acquisition in low-nutrient environments. Pages 201-213 in: Food Security in Nutrient-Stressed Environments: Exploiting Plants' Genetic Capabilities, J.J. Adu-Gyamfi, ed. Springer Netherlands, Dordrecht.
Danhorn, T., and Fuqua, C. 2007. Biofilm formation by plant-associated bacteria. Annu Rev Microbiol 61:401-422.
Dastager, S.G., Deepa, C.K., and Pandey, A. 2011. Plant growth promoting potential of *Pontibacter niistensis* in cowpea (*Vigna unguiculata* (L.) Walp.). Appl Soil Ecol 49:250-255.
De Jonge, R., Van Esse, H.P., Kombrink, A., Shinya, T., Desaki, Y., Bours, R., Van der Krol, S., Shibuya, N., Joosten, M.H.A.J., and Thomma, B.P.H.J. 2010. Conserved fungal LysM effector Ecp6 prevents chitin-triggered immunity in plants. Science 329:953-955.
De Nys, R., and Steinberg, P.D. 2002. Linking marine biology and biotechnology. Curr Opin Biotech 13:244-248.
De Weger, L.A., Van der Vlugt, C., Wijfjes, A.H.M., Bakker, P.A.H.M., Schippers, B., and Lugtenberg, B.J.J. 1987. Flagella of a plant-growth-stimulating *Pseudomonas fluorescens* strain are required for colonization of potato roots. J Bacteriol 169:2769-2773.
Deakin, W.J., and Broughton, W.J. 2009. Symbiotic use of pathogenic strategies: rhizobial protein secretion systems. Nat Rev Microbiol 7:312-321.
Denoux, C., Galletti, R., Mammarella, N., Gopalan, S., Werck, D., De Lorenzo, G., Ferrari, S., Ausubel, F.M., and Dewdney, J. 2008. Activation of defense response pathways by OGs and Flg22 elicitors in *Arabidopsis* seedlings. Mol Plant 1:423-445.
Desbrosses, G.J., and Stougaard, J. 2011. Root nodulation: a paradigm for how plant-microbe symbiosis influences host developmental pathways. Cell Host Microbe 10:348-358.
Dodds, P.N., and Rathjen, J.P. 2010. Plant immunity: towards an integrated view of plant-pathogen interactions. Nat Rev Genet 11:539-548.
Dudenhöffer, J., Scheu, S., Jousset, A., and Cahill, J. 2016. Systemic enrichment of antifungal traits in the rhizosphere microbiome after pathogen attack. J Ecol 104:1566-1575.
Edwards, J., Johnson, C., Santos-Medellin, C., Lurie, E., Podishetty, N.K., Bhatnagar, S., Eisen, J.A., and Sundaresan, V. 2015. Structure, variation, and assembly of the root-associated microbiomes of rice. Proc Natl Acad Sci U S A 112:E911-920.
Eide, D., Broderius, M., Fett, J., and Guerinot, M.L. 1996. A novel iron-regulated metal transporter from plants identified by functional expression in yeast. Proc Natl Acad Sci U S A 93:5624-5628.
El Oirdi, M., Trapani, A., and Bouarab, K. 2010. The nature of tobacco resistance against *Botrytis cinerea* depends on the infection structures of the pathogen. Environ Microbiol 12:239-253.
Federhen, S. 2012. The NCBI Taxonomy database. Nucleic Acids Res 40:D136-143.
Felix, G., Duran, J.D., Volko, S., and Boller, T. 1999. Plants have a sensitive perception system for the most conserved domain of bacterial flagellin. Plant J 18:265-276.
Fender, J.E., Bender, C.M., Stella, N.A., Lahr, R.M., Kalivoda, E.J., and Shanks, R.M. 2012. *Serratia marcescens* quinoprotein glucose dehydrogenase activity mediates medium acidification and inhibition of prodigiosin production by glucose. Appl Environ Microb 78:6225-6235.
Fich, E.A., Segerson, N.A., and Rose, J.K.C. 2016. The plant polyester cutin: biosynthesis, structure, and biological roles. Annu Rev Plant Biol 67:207-233.
Floerl, S., Majcherczyk, A., Possienke, M., Feussner, K., Tappe, H., Gatz, C., Feussner, I., Kues, U., and Polle, A. 2012. *Verticillium longisporum* infection affects the leaf apoplastic proteome, metabolome, and cell wall properties in *Arabidopsis thaliana*. PLoS One 7:e31435.
Fourcroy, P., Tissot, N., Gaymard, F., Briat, J.F., and Dubos, C. 2016. Facilitated Fe nutrition by phenolic compounds excreted by the *Arabidopsis* ABCG37/PDR9 transporter requires the IRT1/FRO2 high-affinity root Fe(2+) transport system. Mol Plant 9:485-488.

Fourcroy, P., Siso-Terraza, P., Sudre, D., Saviron, M., Reyt, G., Gaymard, F., Abadia, A., Abadia, J., Alvarez-Fernandez, A., and Briat, J.F. 2014. Involvement of the ABCG37 transporter in secretion of scopoletin and derivatives by *Arabidopsis* roots in response to iron deficiency. New Phytol 201:155-167.

Fradin, E.F., Zhang, Z., Juarez Ayala, J.C., Castroverde, C.D., Nazar, R.N., Robb, J., Liu, C.M., and Thomma, B.P.H.J. 2009. Genetic dissection of *Verticillium* wilt resistance mediated by tomato Ve1. Plant Physiol 150:320-332.

Frerigmann, H., and Gigolashvili, T. 2014. MYB34, MYB51, and MYB122 distinctly regulate indolic glucosinolate biosynthesis in *Arabidopsis thaliana*. Mol Plant 7:814-828.

Fries, L.L.M., Pacovsky, R.S., Safir, G.R., and Siqueira, J.O. 1997. Plant growth and arbuscular mycorrhizal fungal colonization affected by exogenously applied phenolic compounds. J Chem Ecol 23:1755-1767.

Galperin, M.Y., Makarova, K.S., Wolf, Y.I., and Koonin, E.V. 2015. Expanded microbial genome coverage and improved protein family annotation in the COG database. Nucleic Acids Res 43:D261-269.

Garcia, K., Delaux, P.M., Cope, K.R., and Ane, J.M. 2015. Molecular signals required for the establishment and maintenance of ectomycorrhizal symbioses. New Phytol 208:79-87.

Ge, Y.Y., Xiang, Q.W., Wagner, C., Zhang, D., Xie, Z.P., and Staehelin, C. 2016. The type 3 effector NopL of *Sinorhizobium* sp. strain NGR234 is a mitogen-activated protein kinase substrate. J Exp Bot 67:2483-2494.

Gibson, K.E., Kobayashi, H., and Walker, G.C. 2008. Molecular determinants of a symbiotic chronic infection. Annu Rev Genet 42:413-441.

Gnonlonfin, G.J.B., Sanni, A., and Brimer, L. 2012. Review scopoletin – a coumarin phytoalexin with medicinal properties. Crit Rev Plant Sci 31:47-56.

Gomez-Gomez, L., and Boller, T. 2000. FLS2: an LRR receptor-like kinase involved in the perception of the bacterial elicitor flagellin in *Arabidopsis*. Mol Cell 5:1003-1011.

Grosskinsky, D.K., Naseem, M., Abdelmohsen, U.R., Plickert, N., Engelke, T., Griebel, T., Zeier, J., Novak, O., Strnad, M., Pfeifhofer, H., Van der Graaff, E., Simon, U., and Roitsch, T. 2011. Cytokinins mediate resistance against *Pseudomonas syringae* in tobacco through increased antimicrobial phytoalexin synthesis independent of salicylic acid signaling. Plant Physiol 157:815-830.

Guan, S., Ji, C., Zhou, T., Li, J., Ma, Q., and Niu, T. 2008. Aflatoxin B1 degradation by *Stenotrophomonas Maltophilia* and other microbes selected using coumarin medium. Int J Mol Sci 9:1489.

Gutiérrez-Barranquero, J.A., Reen, F.J., McCarthy, R.R., and O'Gara, F. 2015. Deciphering the role of coumarin as a novel quorum sensing inhibitor suppressing virulence phenotypes in bacterial pathogens. Appl Microbiol Biot 99:3303-3316.

Guttenplan, S.B., and Kearns, D.B. 2013. Regulation of flagellar motility during biofilm formation. FEMS Microbiol Rev 37:849-871.

Hacquard, S., Spaepen, S., Garrido-Oter, R., and Schulze-Lefert, P. 2017. Interplay between innate immunity and the plant microbiota. Annu Rev Phytopathol 55:565-589.

Hacquard, S., Kracher, B., Hiruma, K., Munch, P.C., Garrido-Oter, R., Thon, M.R., Weimann, A., Damm, U., Dallery, J.F., Hainaut, M., Henrissat, B., Lespinet, O., Sacristan, S., Ver Loren van Themaat, E., Kemen, E., McHardy, A.C., Schulze-Lefert, P., and O'Connell, R.J. 2016. Survival trade-offs in plant roots during colonization by closely related beneficial and pathogenic fungi. Nat Commun 7:11362.

Han, J.I., Choi, H.K., Lee, S.W., Orwin, P.M., Kim, J., Laroe, S.L., Kim, T.G., O'Neil, J., Leadbetter, J.R., Lee, S.Y., Hur, C.G., Spain, J.C., Ovchinnikova, G., Goodwin, L., and Han, C. 2011. Complete genome sequence of the metabolically versatile plant growth-promoting endophyte *Variovorax paradoxus* S110. J Bacteriol 193:1183-1190.

Hiruma, K., Gerlach, N., Sacristan, S., Nakano, R.T., Hacquard, S., Kracher, B., Neumann, U., Ramirez, D., Bucher, M., O'Connell, R.J., and Schulze-Lefert, P. 2016. Root endophyte *Colletotrichum tofieldiae* confers plant fitness benefits that are phosphate status dependent. Cell 165:464-474.

Hu, L., Robert, C.A.M., Cadot, S., Zhang, X., Ye, M., Li, B., Manzo, D., Chervet, N., Steinger, T., Van der Heijden, M.G.A., Schlaeppi, K., and Erb, M. 2018. Root exudate metabolites drive plant-soil feedbacks on growth and defense by shaping the rhizosphere microbiota. Nat Commun 9:2738.

Huot, B., Yao, J., Montgomery, B.L., and He, S.Y. 2014. Growth-defense tradeoffs in plants: a balancing act to optimize fitness. Mol Plant 7:1267-1287.

Jacobs, S., Zechmann, B., Molitor, A., Trujillo, M., Petutschnig, E., Lipka, V., Kogel, K.H., and Schafer, P. 2011. Broad-spectrum suppression of innate immunity is required for colonization of *Arabidopsis* roots by the fungus *Piriformospora indica*. Plant Physiol 156:726-740.

Jefferson, K. 2004. What drives bacteria to produce a biofilm? FEMS Microbiol Lett 236:163-173.

Jimenez-Guerrero, I., Perez-Montano, F., Monreal, J.A., Preston, G.M., Fones, H., Vioque, B., Ollero, F.J., and Lopez-Baena, F.J. 2015. The *Sinorhizobium* (*Ensifer*) *fredii* HH103 type 3 secretion system suppresses early defense responses to effectively nodulate soybean. Mol Plant Microbe In 28:790-799.

Jones, J.D.G., and Dangl, J.L. 2006. The plant immune system. Nature 444:323-329.

Jones, P., and Vogt, T. 2001. Glycosyltransferases in secondary plant metabolism: tranquilizers and stimulant controllers. Planta 213:164-174.

Jørgensen, M.E., Nour-Eldin, H.H., and Halkier, B.A. 2015. Transport of defense compounds from source to sink: lessons learned from glucosinolates. Trends Plant Sci 20:508-514.

Kachroo, A., and Kachroo, P. 2009. Fatty Acid-derived signals in plant defense. Annu Rev Phytopathol 47:153-176.

Kaever, A., Landesfeind, M., Feussner, K., Mosblech, A., Heilmann, I., Morgenstern, B., Feussner, I., and Meinicke, P. 2015. MarVis-Pathway: integrative and exploratory pathway analysis of non-targeted metabolomics data. Metabolomics 11:764-777.

Kai, K., Shimizu, B., Mizutani, M., Watanabe, K., and Sakata, K. 2006. Accumulation of coumarins in *Arabidopsis thaliana*. Phytochemistry 67:379-386.

Kai, K., Mizutani, M., Kawamura, N., Yamamoto, R., Tamai, M., Yamaguchi, H., Sakata, K., and Shimizu, B. 2008. Scopoletin is biosynthesized via *ortho*-hydroxylation of feruloyl CoA by a 2-oxoglutarate-dependent dioxygenase in *Arabidopsis thaliana*. Plant J 55:989-999.

Kawaharada, Y., Kelly, S., Nielsen, M.W., Hjuler, C.T., Gysel, K., Muszynski, A., Carlson, R.W., Thygesen, M.B., Sandal, N., Asmussen, M.H., Vinther, M., Andersen, S.U., Krusell, L., Thirup, S., Jensen, K.J., Ronson, C.W., Blaise, M., Radutoiu, S., and Stougaard, J. 2015. Receptor-mediated exopolysaccharide perception controls bacterial infection. Nature 523:308-312.

Kazan, K., and Manners, J.M. 2013. MYC2: the master in action. Mol Plant 6:686-703.

Kazan, K., and Lyons, R. 2014. Intervention of phytohormone pathways by pathogen effectors. Plant Cell 26:2285-2309.

Kim, K.K., Kim, M.K., Lim, J.H., Park, H.Y., and Lee, S.T. 2005. Transfer of *Chryseobacterium meningosepticum* and *Chryseobacterium miricola* to *Elizabethkingia* gen. nov. as *Elizabethkingia meningoseptica* comb. nov. and *Elizabethkingia miricola* comb. nov. Int J Syst Evol Microbiol 55:1287-1293.

Kim, Y.H., Choi, D.I., Yeo, W.H., Kim, Y.S., Chae, S.Y., Park, E.Y., and Kim, S.S. 2000. Scopoletin production related to induced resistance of tobacco plants against Tobacco mosaic virus. Plant Pathol J 16:264-268.

Kimura, S., Waszczak, C., Hunter, K., and Wrzaczek, M. 2017. Bound by fate: the role of reactive oxygen species in receptor-like kinase signaling. Plant Cell 29:638-654.

King, E.O., Ward, M.K., and Raney, D.E. 1954. Two simple media for the demonstration of pyocyanin and fluorescin. J Lab Clin Med 44:301-307.

Kloppholz, S., Kuhn, H., and Requena, N. 2011. A secreted fungal effector of *Glomus intraradices* promotes symbiotic biotrophy. Curr Biol 21:1204-1209.

Kobayashi, T., and Nishizawa, N.K. 2012. Iron uptake, translocation, and regulation in higher plants. Annu Rev Plant Biol 63:131-152.

Kong, H.G., Kim, B.K., Song, G.C., Lee, S., and Ryu, C.M. 2016. Aboveground whitefly infestation-mediated reshaping of the root microbiota. Front Microbiol 7:1314.

König, S., Feussner, K., Kaever, A., Landesfeind, M., Thurow, C., Karlovsky, P., Gatz, C., Polle, A., and Feussner, I. 2014. Soluble phenylpropanoids are involved in the defense response of *Arabidopsis* against *Verticillium longisporum*. New Phytol 202:823-837.

Krishnamurthi, S., Ruckmani, A., Pukall, R., and Chakrabarti, T. 2010. *Psychrobacillus* gen. nov. and proposal for reclassification of *Bacillus insolitus* Larkin & Stokes, 1967, *B. psychrotolerans* Abd-El Rahman et al., 2002 and *B. psychrodurans* Abd-El Rahman et al., 2002 as *Psychrobacillus insolitus* comb. nov., *Psychrobacillus psychrotolerans* comb. nov. and *Psychrobacillus psychrodurans* comb. nov. Syst Appl Microbiol 33:367-373.

Kumar, A.S., Lakshmanan, V., Caplan, J.L., Powell, D., Czymmek, K.J., Levia, D.F., and Bais, H.P. 2012. Rhizobacteria *Bacillus subtilis* restricts foliar pathogen entry through stomata. Plant J 72:694-706.

Kusumoto, A., Kamisaka, K., Yakushi, T., Terashima, H., Shinohara, A., and Homma, M. 2006. Regulation of polar flagellar number by the *flhF* and *flhG* genes in *Vibrio alginolyticus*. J Biochem 139:113-121.

Lager, I., Andreasson, O., Dunbar, T.L., Andreasson, E., Escobar, M.A., and Rasmusson, A.G. 2010. Changes in external pH rapidly alter plant gene expression and modulate auxin and elicitor responses. Plant Cell Environ 33:1513-1528.

Lakshmanan, V., Kitto, S.L., Caplan, J.L., Hsueh, Y.H., Kearns, D.B., Wu, Y.S., and Bais, H.P. 2012. Microbe-associated molecular patterns-triggered root responses mediate beneficial rhizobacterial recruitment in *Arabidopsis*. Plant Physiol 160:1642-1661.

Lamers, J.G., Schippers, B., and Geels, F.P. 1988. Soil-borne diseases of wheat in the Netherlands and results of seed bacterization with *Pseudomonas* against *Gaeumannomyces graminis* var. *tritici*. Pages 134-139 in: Cereal breeding related to integrated cereal production, J. M.L. and S. L.A.J., eds. PUDOC, Wageningen, the Netherlands.

Le Roy, J., Huss, B., Creach, A., Hawkins, S., and Neutelings, G. 2016. Glycosylation is a major regulator of phenylpropanoid availability and biological activity in plants. Front Plant Sci 7:735.

Lebeis, S.L., Paredes, S.H., Lundberg, D.S., Breakfield, N., Gehring, J., McDonald, M., Malfatti, S., Glavina del Rio, T., Jones, C.D., Tringe, S.G., and Dangl, J.L. 2015. Salicylic acid modulates colonization of the root microbiome by specific bacterial taxa. Science 349:860-864.

Lee, H., Khatri, A., Plotnikov, J.M., Zhang, X.C., and Sheen, J. 2012. Complexity in differential peptide-receptor signaling: response to Segonzac et al. and Mueller et al. commentaries. Plant Cell 24:3177-3185.

Lee, J.H., Kim, Y.G., Cho, H.S., Ryu, S.Y., Cho, M.H., and Lee, J. 2014. Coumarins reduce biofilm formation and the virulence of *Escherichia coli* O157:H7. Phytomedicine 21:1037-1042.

Leeman, M., Den Ouden, F.M., Van Pelt, J.A., Dirkx, F.P.M., Steijl, H., Bakker, P.A.H.M., and Schippers, B. 1996. Iron availability affects induction of systemic resistance to *Fusarium* wilt of radish by *Pseudomonas fluorescens*. Phytopathology 86:149-155.

Li, B., Ruotti, V., Stewart, R.M., Thomson, J.A., and Dewey, C.N. 2010. RNA-Seq gene expression estimation with read mapping uncertainty. Bioinformatics 26:493-500.

Li, J., Wu, X.D., Hao, S.T., Wang, X.J., and Ling, H.Q. 2008. Proteomic response to iron deficiency in tomato root. Proteomics 8:2299-2311.

Liang, Y., Toth, K., Cao, Y., Tanaka, K., Espinoza, C., and Stacey, G. 2014. Lipochitooligosaccharide recognition: an ancient story. New Phytol 204:289-296.

Liang, Y., Cao, Y., Tanaka, K., Thibivilliers, S., Wan, J., Choi, J., Kang, C., Qiu, J., and Stacey, G. 2013. Nonlegumes respond to rhizobial Nod factors by suppressing the innate immune response. Science 341:1384-1387.

Libault, M., Farmer, A., Brechenmacher, L., Drnevich, J., Langley, R.J., Bilgin, D.D., Radwan, O., Neece, D.J., Clough, S.J., May, G.D., and Stacey, G. 2010. Complete transcriptome of the soybean root hair cell, a single-cell model, and its alteration in response to *Bradyrhizobium japonicum* infection. Plant Physiol 152:541-552.

Lim, G.H., Singhal, R., Kachroo, A., and Kachroo, P. 2017. Fatty acid- and lipid-mediated signaling in plant defense. Annu Rev Phytopathol 55:505-536.

Limón, M.C., Rodríguez-Ortiz, R., and Avalos, J. 2010. Bikaverin production and applications. Appl Microbiol Biot 87:21-29.

Liu, H., Carvalhais, L.C., Schenk, P.M., and Dennis, P.G. 2017. Effects of jasmonic acid signalling on the wheat microbiome differ between body sites. Sci Rep 7:41766.

Liu, J., Osbourn, A., and Ma, P. 2015. MYB transcription factors as regulators of phenylpropanoid metabolism in plants. Mol Plant 8:689-708.

Liu, J., Blaylock, L.A., Endre, G., Cho, J., Town, C.D., VandenBosch, K.A., and Harrison, M.J. 2003. Transcript profiling coupled with spatial expression analyses reveals genes involved in distinct developmental stages of an arbuscular mycorrhizal symbiosis. Plant Cell 15:2106-2123.

Liu, J.Z., Horstman, H.D., Braun, E., Graham, M.A., Zhang, C., Navarre, D., Qiu, W.L., Lee, Y., Nettleton, D., Hill, J.H., and Whitham, S.A. 2011. Soybean homologs of MPK4 negatively regulate defense responses and positively regulate growth and development. Plant Physiol 157:1363-1378.

Liu, Z., Beskrovnaya, P., Melnyk, R.A., Hossain, S.S., Khorasani, S., O'Sullivan, L.R., Wiesmann, C.L., Bush, J., Richard, J.D., and Haney, C.H. 2018. A genome-wide screen identifies genes in rhizosphere-associated *Pseudomonas* required to evade plant defenses. mBio *In press*.

Ljung, K. 2013. Auxin metabolism and homeostasis during plant development. Development 140:943-950.

Lo Presti, L., Lanver, D., Schweizer, G., Tanaka, S., Liang, L., Tollot, M., Zuccaro, A., Reissmann, S., and Kahmann, R. 2015. Fungal effectors and plant susceptibility. Annu Rev Plant Biol 66:513-545.

Loper, J.E., Hassan, K.A., Mavrodi, D.V., Davis, E.W., 2nd, Lim, C.K., Shaffer, B.T., Elbourne, L.D., Stockwell, V.O., Hartney, S.L., Breakwell, K., Henkels, M.D., Tetu, S.G., Rangel, L.I., Kidarsa, T.A., Wilson, N.L., Van de Mortel, J.E., Song, C., Blumhagen, R., Radune, D., Hostetler, J.B., Brinkac, L.M., Durkin, A.S., Kluepfel, D.A., Wechter, W.P., Anderson, A.J., Kim, Y.C., Pierson, L.S., 3rd, Pierson, E.A., Lindow, S.E., Kobayashi, D.Y., Raaijmakers, J.M., Weller, D.M., Thomashow, L.S., Allen, A.E., and Paulsen, I.T. 2012. Comparative genomics of plant-associated *Pseudomonas* spp.: insights into diversity and inheritance of traits involved in multitrophic interactions. PLoS Genet 8:e1002784.

Lopez-Gomez, M., Sandal, N., Stougaard, J., and Boller, T. 2012. Interplay of flg22-induced defence responses and nodulation in *Lotus japonicus*. J Exp Bot 63:393-401.

López-Millán, A., Morales, F., Gogorcena, Y., Abadía, A., and Abadía, J. 2009. Metabolic responses in iron deficient tomato plants. J Plant Physiol 166:375-384.

Love, M.I., Huber, W., and Anders, S. 2014. Moderated estimation of fold change and dispersion for RNA-seq data with DESeq2. Genome Biol 15:550.

Luginbuehl, L.H., Menard, G.N., Kurup, S., Van Erp, H., Radhakrishnan, G.V., Breakspear, A., Oldroyd, G.E.D., and Eastmond, P.J. 2017. Fatty acids in arbuscular mycorrhizal fungi are synthesized by the host plant. Science 356:1175-1178.

Lugtenberg, B., and Kamilova, F. 2009. Plant-growth-promoting rhizobacteria. Annu Rev Microbiol 63:541-556.

Luna, E., Pastor, V., Robert, J., Flors, V., Mauch-Mani, B., and Ton, J. 2010. Callose deposition: a multifaceted plant defense response. Mol Plant Microbe In 24:183-193.

Lundberg, D.S., Lebeis, S.L., Paredes, S.H., Yourstone, S., Gehring, J., Malfatti, S., Tremblay, J., Engelbrektson, A., Kunin, V., Del Rio, T.G., Edgar, R.C., Eickhorst, T., Ley, R.E., Hugenholtz, P., Tringe, S.G., and Dangl, J.L. 2012. Defining the core *Arabidopsis thaliana* root microbiome. Nature 488:86-90.

Macho, A.P., and Zipfel, C. 2014. Plant PRRs and the activation of innate immune signaling. Mol Cell 54:263-272.

Macho, A.P., and Zipfel, C. 2015. Targeting of plant pattern recognition receptor-triggered immunity by bacterial type-III secretion system effectors. Curr Opin Microbiol 23:14-22.

Martin, F., Aerts, A., Ahren, D., Brun, A., Danchin, E.G., Duchaussoy, F., Gibon, J., Kohler, A., Lindquist, E., Pereda, V., Salamov, A., Shapiro, H.J., Wuyts, J., Blaudez, D., Buee, M., Brokstein, P., Canback, B., Cohen, D., Courty, P.E., Coutinho, P.M., Delaruelle, C., Detter, J.C., Deveau, A., DiFazio, S., Duplessis, S., Fraissinet-Tachet, L., Lucic, E., Frey-Klett, P., Fourrey, C., Feussner, I., Gay, G., Grimwood, J., Hoegger, P.J., Jain, P., Kilaru, S., Labbe, J., Lin, Y.C., Legue, V., Le Tacon, F., Marmeisse, R., Melayah, D., Montanini, B., Muratet, M., Nehls, U., Niculita-Hirzel, H., Oudot-Le Secq, M.P., Peter, M., Quesneville, H., Rajashekar, B., Reich, M., Rouhier, N., Schmutz, J., Yin, T., Chalot, M., Henrissat, B., Kues, U., Lucas, S., Van de Peer, Y., Podila, G.K., Polle, A., Pukkila, P.J., Richardson, P.M., Rouze, P., Sanders, I.R., Stajich, J.E., Tunlid, A., Tuskan, G., and Grigoriev, I.V. 2008. The genome of *Laccaria bicolor* provides insights into mycorrhizal symbiosis. Nature 452:88-92.

Martinez-Garcia, E., Calles, B., Arevalo-Rodriguez, M., and De Lorenzo, V. 2011. pBAM1: an all-synthetic genetic tool for analysis and construction of complex bacterial phenotypes. BMC Microbiol 11:38.

Martinez-Medina, A., Van Wees, S.C.M., and Pieterse, C.M.J. 2017. Airborne signals from *Trichoderma* fungi stimulate iron uptake responses in roots resulting in priming of jasmonic acid-dependent defences in shoots of *Arabidopsis thaliana* and *Solanum lycopersicum*. Plant Cell Environ 40:2691-2705.

Martinez-Medina, A., Flors, V., Heil, M., Mauch-Mani, B., Pieterse, C.M.J., Pozo, M.J., Ton, J., Van Dam, N.M., and Conrath, U. 2016. Recognizing plant defense priming. Trends Plant Sci 21:818-822.

Masachis, S., Segorbe, D., Turra, D., Leon-Ruiz, M., Furst, U., El Ghalid, M., Leonard, G., Lopez-Berges, M.S., Richards, T.A., Felix, G., and Di Pietro, A. 2016. A fungal pathogen secretes plant alkalinizing peptides to increase infection. Nat Microbiol 1:16043.

Matyash, V., Liebisch, G., Kurzchalia, T.V., Shevchenko, A., and Schwudke, D. 2008. Lipid extraction by methyl-*tert*-butyl ether for high-throughput lipidomics. J Lipid Res 49:1137-1146.

Mauchline, T.H., and Malone, J.G. 2017. Life in earth - the root microbiome to the rescue? Curr Opin Microbiol 37:23-28.

Maurer, F., Muller, S., and Bauer, P. 2011. Suppression of Fe deficiency gene expression by jasmonate. Plant Physiol Bioch 49:530-536.

Mavrodi, D.V., Joe, A., Mavrodi, O.V., Hassan, K.A., Weller, D.M., Paulsen, I.T., Loper, J.E., Alfano, J.R., and Thomashow, L.S. 2011. Structural and functional analysis of the type III secretion system from *Pseudomonas fluorescens* Q8r1-96. J Bacteriol 193:177-189.

McBride, M.J., Liu, W., Lu, X., Zhu, Y., and Zhang, W. 2014. The family *Cytophagaceae*. Pages 577-593 in: The Prokaryotes, E. Rosenberg, E.F. DeLong, S. Lory, E. Stackebrandt, and F. Thompson, eds. Springer Berlin Heidelberg, Berlin, Heidelberg.

McMurdie, P.J., and Holmes, S. 2013. phyloseq: an R package for reproducible interactive analysis and graphics of microbiome census data. PLoS One 8:e61217.

Medentsev, A.G., Arinbasarova, A., and Akimenko, V.K. 2005. Biosynthesis of naphthoquinone pigments by fungi of the genus *Fusarium*. Appl Biochem Micro+ 41:573-577.

Mendes, R., Kruijt, M., De Bruijn, I., Dekkers, E., Van der Voort, M., Schneider, J.H.M., Piceno, Y.M., DeSantis, T.Z., Andersen, G.L., Bakker, P.A.H.M., and Raaijmakers, J.M. 2011. Deciphering the rhizosphere microbiome for disease-suppressive bacteria. Science 332:1097-1100.

Meng, X., and Zhang, S. 2013. MAPK cascades in plant disease resistance signaling. Annu Rev Phytopathol 51:245-266.

Menzel, P., Ng, K.L., and Krogh, A. 2016. Fast and sensitive taxonomic classification for metagenomics with Kaiju. Nat Commun 7:11257.

Meziane, H., Van Der Sluis, I., Van Loon, L.C., Höfte, M., and Bakker, P.A.H.M. 2005. Determinants of *Pseudomonas putida* WCS358 involved in inducing systemic resistance in plants. Mol Plant Pathol 6:177-185.

Millet, Y.A., Danna, C.H., Clay, N.K., Songnuan, W., Simon, M.D., Werck-Reichhart, D., and Ausubel, F.M. 2010. Innate immune responses activated in *Arabidopsis* roots by microbe-associated molecular patterns. Plant Cell 22:973-990.

Mimmo, T., Del Buono, D., Terzano, R., Tomasi, N., Vigani, G., Crecchio, C., Pinton, R., Zocchi, G., and Cesco, S. 2014. Rhizospheric organic compounds in the soil-microorganism-plant system: their role in iron availability. Eur J Soil Sci 65:629-642.

Miwa, H., and Okazaki, S. 2017. How effectors promote beneficial interactions. Curr Opin Plant Biol 38:148-154.

Montero-Barrientos, M., Hermosa, R., Cardoza, R.E., Gutierrez, S., Nicolas, C., and Monte, E. 2010. Transgenic expression of the *Trichoderma harzianum* hsp70 gene increases *Arabidopsis* resistance to heat and other abiotic stresses. J Plant Physiol 167:659-665.

Morales, G., Ugidos, A., and Rojo, F. 2006. Inactivation of the *Pseudomonas putida* cytochrome *o* ubiquinol oxidase leads to a significant change in the transcriptome and to increased expression of the CIO and *cbb3*-1 terminal oxidases. Environ Microbiol 8:1764-1774.

Morant, A.V., Jorgensen, K., Jorgensen, C., Paquette, S.M., Sanchez-Perez, R., Moller, B.L., and Bak, S. 2008. beta-Glucosidases as detonators of plant chemical defense. Phytochemistry 69:1795-1813.

Mosblech, A., Feussner, I., and Heilmann, I. 2009. Oxylipins: structurally diverse metabolites from fatty acid oxidation. Plant Physiol Bioch 47:511-517.

Muller, R., De Vos, M., Sun, J.Y., Sønderby, I.E., Halkier, B.A., Wittstock, U., and Jander, G. 2010. Differential effects of indole and aliphatic glucosinolates on lepidopteran herbivores. J Chem Ecol 36:905-913.

Murashige, T., and Skoog, F. 1962. A revised medium for rapid growth and bioassays with tobacco tissue cultures. Physiol Plantarum 15:473-497.

Navarro, L., Zipfel, C., Rowland, O., Keller, I., Robatzek, S., Boller, T., and Jones, J.D.G. 2004. The transcriptional innate immune response to flg22. Interplay and overlap with Avr gene-dependent defense responses and bacterial pathogenesis. Plant Physiol 135:1113-1128.

Navarro, L., Bari, R., Achard, P., Lison, P., Nemri, A., Harberd, N.P., and Jones, J.D. 2008. DELLAs control plant immune responses by modulating the balance of jasmonic acid and salicylic acid signaling. Curr Biol 18:650-655.

Nazina, T.N., Tourova, T.P., Poltaraus, A.B., Novikova, E.V., Grigoryan, A.A., Ivanova, A.E., Lysenko, A.M., Petrunyaka, V.V., Osipov, G.A., Belyaev, S.S., and Ivanov, M.V. 2001. Taxonomic study of aerobic thermophilic bacilli: descriptions of *Geobacillus subterraneus* gen. nov., sp. nov. and *Geobacillus uzenensis* sp. nov. from petroleum reservoirs and transfer of *Bacillus stearothermophilus*, *Bacillus thermocatenulatus*, *Bacillus thermoleovorans*, *Bacillus kaustophilus*, *Bacillus thermodenitrificans* to *Geobacillus* as the new combinations *G. stearothermophilus*, *G. th*. Int J Syst Evol Microbiol 51:433-446.

Nour-Eldin, H.H., Andersen, T.G., Burow, M., Madsen, S.R., Jorgensen, M.E., Olsen, C.E., Dreyer, I., Hedrich, R., Geiger, D., and Halkier, B.A. 2012. NRT/PTR transporters are essential for translocation of glucosinolate defence compounds to seeds. Nature 488:531-534.

Novak, O., Henykova, E., Sairanen, I., Kowalczyk, M., Pospisil, T., and Ljung, K. 2012. Tissue-specific profiling of the *Arabidopsis thaliana* auxin metabolome. Plant J 72:523-536.

O'Toole, G.A., and Kolter, R. 1998. Initiation of biofilm formation in *Pseudomonas fluorescens* WCS365 proceeds via multiple, convergent signalling pathways: a genetic analysis. Mol Microbiol 28:449-461.

O'Toole, G.A., Gibbs, K.A., Hager, P.W., Phibbs, P.V., and Kolter, R. 2000. The global carbon metabolism regulator Crc is a component of a signal transduction pathway required for biofilm development by *Pseudomonas aeruginosa*. J Bacteriol 182:425-431.

Ofek-Lalzar, M., Sela, N., Goldman-Voronov, M., Green, S.J., Hadar, Y., and Minz, D. 2014. Niche and host-associated functional signatures of the root surface microbiome. Nat Commun 5:4950.

Oldroyd, G.E. 2013. Speak, friend, and enter: signalling systems that promote beneficial symbiotic associations in plants. Nat Rev Microbiol 11:252-263.

Oldroyd, G.E., Murray, J.D., Poole, P.S., and Downie, J.A. 2011. The rules of engagement in the legume-rhizobial symbiosis. Annu Rev Genet 45:119-144.

Onate-Sanchez, L., and Vicente-Carbajosa, J. 2008. DNA-free RNA isolation protocols for *Arabidopsis thaliana*, including seeds and siliques. BMC Res Notes 1:93.

Ongena, M., Duby, F., Rossignol, F., Fauconnier, M.L., Dommes, J., and Thonart, P. 2004. Stimulation of the lipoxygenase pathway is associated with systemic resistance induced in bean by a nonpathogenic *Pseudomonas* strain. Mol Plant Microbe In 17:1009-1018.

Palmer, C.M., Hindt, M.N., Schmidt, H., Clemens, S., and Guerinot, M.L. 2013. MYB10 and MYB72 are required for growth under iron-limiting conditions. PLoS Genet 9:e1003953.

Pandza, S., Baetens, M., Park, C.H., Au, T., Keyhan, M., and Matin, A. 2000. The G-protein FlhF has a role in polar flagellar placement and general stress response induction in *Pseudomonas putida*. Mol Microbiol 36:414-423.

Pangesti, N., Reichelt, M., Van de Mortel, J.E., Kapsomenou, E., Gershenzon, J., Van Loon, J.J.A., Dicke, M., and Pineda, A. 2016. Jasmonic acid and ethylene signaling pathways regulate glucosinolate levels in plants during rhizobacteria-induced systemic resistance against a leaf-chewing herbivore. J Chem Ecol 42:1212-1225.

Panke-Buisse, K., Poole, A.C., Goodrich, J.K., Ley, R.E., and Kao-Kniffin, J. 2015. Selection on soil microbiomes reveals reproducible impacts on plant function. ISME J 9:980-989.

Pel, M.J.C. (2013). Evasion and suppression of plant immunity. In Department of Biology (Utrecht, The Netherlands: Utrecht University).

Pel, M.J.C., and Pieterse, C.M.J. 2013. Microbial recognition and evasion of host immunity. J Exp Bot 64:1237-1248.
Pel, M.J.C., Van Dijken, A.J.H., Bardoel, B.W., Seidl, M.F., Van der Ent, S., Van Strijp, J.A.G., and Pieterse, C.M.J. 2014. *Pseudomonas syringae* evades host immunity by degrading flagellin monomers with alkaline protease AprA. Mol Plant Microbe In 27:603-610.
Perez Rodriguez, N., Langella, F., Rodushkin, I., Engstrom, E., Kothe, E., Alakangas, L., and Ohlander, B. 2014. The role of bacterial consortium and organic amendment in Cu and Fe isotope fractionation in plants on a polluted mine site. Environ Sci Pollut Res Int 21:6836-6844.
Philippot, L., Raaijmakers, J.M., Lemanceau, P., and van der Putten, W.H. 2013. Going back to the roots: the microbial ecology of the rhizosphere. Nat Rev Microbiol 11:789-799.
Pieterse, C.M.J., Leon-Reyes, A., Van der Ent, S., and Van Wees, S.C.M. 2009. Networking by small-molecule hormones in plant immunity. Nat Chem Biol 5:308-316.
Pieterse, C.M.J., Van Wees, S.C.M., Hoffland, E., Van Pelt, J.A., and Van Loon, L.C. 1996. Systemic resistance in *Arabidopsis* induced by biocontrol bacteria is independent of salicylic acid accumulation and pathogenesis-related gene expression. Plant Cell 8:1225-1237.
Pieterse, C.M.J., Van der Does, D., Zamioudis, C., Leon-Reyes, A., and Van Wees, S.C.M. 2012. Hormonal modulation of plant immunity. Annu Rev Cell Dev Bi 28:489-521.
Pieterse, C.M.J., Zamioudis, C., Berendsen, R.L., Weller, D.M., Van Wees, S.C.M., and Bakker, P.A.H.M. 2014. Induced systemic resistance by beneficial microbes. Annu Rev Phytopathol 52:347-375.
Pieterse, C.M.J., Van Wees, S.C.M., Van Pelt, J.A., Knoester, M., Laan, R., Gerrits, H., Weisbeek, P.J., and Van Loon, L.C. 1998. A novel signaling pathway controlling induced systemic resistance in *Arabidopsis*. Plant Cell 10:1571-1580.
Pieterse, C.M.J., Van Pelt, J.A., Ton, J., Parchmann, S., Mueller, M.J., Buchala, A.J., Métraux, J., and Van Loon, L.C. 2000. Rhizobacteria-mediated induced systemic resistance (ISR) in *Arabidopsis* requires sensitivity to jasmonate and ethylene but is not accompanied by an increase in their production. Physiol Mol Plant P 57:123-134.
Plett, J.M., Daguerre, Y., Wittulsky, S., Vayssieres, A., Deveau, A., Melton, S.J., Kohler, A., Morrell-Falvey, J.L., Brun, A., Veneault-Fourrey, C., and Martin, F. 2014. Effector MiSSP7 of the mutualistic fungus *Laccaria bicolor* stabilizes the *Populus* JAZ6 protein and represses jasmonic acid (JA) responsive genes. Proc Natl Acad Sci U S A 111:8299-8304.
Poitout, A., Martiniere, A., Kucharczyk, B., Queruel, N., Silva-Andia, J., Mashkoor, S., Gamet, L., Varoquaux, F., Paris, N., Sentenac, H., Touraine, B., and Desbrosses, G. 2017. Local signalling pathways regulate the *Arabidopsis* root developmental response to *Mesorhizobium loti* inoculation. J Exp Bot 68:1199-1211.
Pozo, M.J., Van Der Ent, S., Van Loon, L.C., and Pieterse, C.M.J. 2008. Transcription factor MYC2 is involved in priming for enhanced defense during rhizobacteria-induced systemic resistance in *Arabidopsis thaliana*. New Phytol 180:511-523.
Pryor, S.W., Gibson, D.M., Bergstrom, G.C., and Walker, L.P. 2007. Minimization of between-well sample variance of antifungal activity using a high-throughput screening microplate bioassay. Biotechniques 42:168, 170, 172.
Raaijmakers, J.M., and Mazzola, M. 2016. Soil immune responses. Science 352:1392-1393.
Rajniak, J., Giehl, R.F.H., Chang, E., Murgia, I., Von Wiren, N., and Sattely, E.S. 2018. Biosynthesis of redox-active metabolites in response to iron deficiency in plants. Nat Chem Biol 14:442-450.
Ranf, S., Gisch, N., Schaffer, M., Illig, T., Westphal, L., Knirel, Y.A., Sanchez-Carballo, P.M., Zahringer, U., Huckelhoven, R., Lee, J., and Scheel, D. 2015. A lectin S-domain receptor kinase mediates lipopolysaccharide sensing in *Arabidopsis thaliana*. Nat Immunol 16:426-433.
Rellan-Alvarez, R., Andaluz, S., Rodriguez-Celma, J., Wohlgemuth, G., Zocchi, G., Alvarez-Fernandez, A., Fiehn, O., Lopez-Millan, A.F., and Abadia, J. 2010. Changes in the proteomic and metabolic profiles of *Beta vulgaris* root tips in response to iron deficiency and resupply. BMC Plant Biol 10:120.
Robinson, N.J., Procter, C.M., Connolly, E.L., and Guerinot, M.L. 1999. A ferric-chelate reductase for iron uptake from soils. Nature 397:694-697.
Rodríguez-Celma, J., Lin, W.D., Fu, G.M., Abadia, J., Lopez-Millan, A.F., and Schmidt, W. 2013. Mutually exclusive alterations in secondary metabolism are critical for the uptake of insoluble iron compounds by *Arabidopsis* and *Medicago truncatula*. Plant Physiol 162:1473-1485.
Rossez, Y., Wolfson, E.B., Holmes, A., Gally, D.L., and Holden, N.J. 2015. Bacterial flagella: twist and stick, or dodge across the kingdoms. PLoS Pathog 11:e1004483.
Rudrappa, T., Biedrzycki, M.L., and Bais, H.P. 2008a. Causes and consequences of plant-associated biofilms. FEMS Microbiol Ecol 64:153-166.
Rudrappa, T., Czymmek, K.J., Pare, P.W., and Bais, H.P. 2008b. Root-secreted malic acid recruits beneficial soil bacteria. Plant Physiol 148:1547-1556.

Salvetti, S., Ghelardi, E., Celandroni, F., Ceragioli, M., Giannessi, F., and Senesi, S. 2007. FlhF, a signal recognition particle-like GTPase, is involved in the regulation of flagellar arrangement, motility behaviour and protein secretion in *Bacillus cereus*. Microbiology 153:2541-2552.

Santi, S., and Schmidt, W. 2009. Dissecting iron deficiency-induced proton extrusion in *Arabidopsis* roots. New Phytol 183:1072-1084.

Sasse, J., Martinoia, E., and Northen, T. 2018. Feed your friends: do plant exudates shape the root microbiome? Trends Plant Sci 23:25-41.

Sauder, L.A., Albertsen, M., Engel, K., Schwarz, J., Nielsen, P.H., Wagner, M., and Neufeld, J.D. 2017. Cultivation and characterization of *Candidatus* Nitrosocosmicus exaquare, an ammonia-oxidizing archaeon from a municipal wastewater treatment system. ISME J 11:1142.

Scheidle, H., Groß, A., and Niehaus, K. 2005. The Lipid A substructure of the *Sinorhizobium meliloti* lipopolysaccharides is sufficient to suppress the oxidative burst in host plants. New Phytol 165:559-565.

Schlaeppi, K., and Bulgarelli, D. 2015. The plant microbiome at work. Mol Plant Microbe In 28:212-217.

Schmid, N.B., Giehl, R.F., Doll, S., Mock, H.P., Strehmel, N., Scheel, D., Kong, X., Hider, R.C., and Von Wiren, N. 2014. Feruloyl-CoA 6'-Hydroxylase1-dependent coumarins mediate iron acquisition from alkaline substrates in *Arabidopsis*. Plant Physiol 164:160-172.

Schmidt, H., Gunther, C., Weber, M., Sporlein, C., Loscher, S., Bottcher, C., Schobert, R., and Clemens, S. 2014. Metabolome analysis of *Arabidopsis thaliana* roots identifies a key metabolic pathway for iron acquisition. PLoS One 9:e102444.

Schmittgen, T.D., and Livak, K.J. 2008. Analyzing real-time PCR data by the comparative *C*T method. Nat Protoc 3:1101-1108.

Schmitz, A.M., and Harrison, M.J. 2014. Signaling events during initiation of arbuscular mycorrhizal symbiosis. J Integr Plant Biol 56:250-261.

Schuhmacher, J.S., Thormann, K.M., Bange, G., and Albers, S. 2015. How bacteria maintain location and number of flagella? FEMS Microbiol Rev 39:812-822.

Segarra, G., Van der Ent, S., Trillas, I., and Pieterse, C.M.J. 2009. MYB72, a node of convergence in induced systemic resistance triggered by a fungal and a bacterial beneficial microbe. Plant Biol 11:90-96.

Shen, Y.Q., Bonnot, F., Imsand, E.M., RoseFigura, J.M., Sjolander, K., and Klinman, J.P. 2012. Distribution and properties of the genes encoding the biosynthesis of the bacterial cofactor, pyrroloquinoline quinone. Biochemistry 51:2265-2275.

Shimizu, T., Nakano, T., Takamizawa, D., Desaki, Y., Ishii-Minami, N., Nishizawa, Y., Minami, E., Okada, K., Yamane, H., Kaku, H., and Shibuya, N. 2010. Two LysM receptor molecules, CEBiP and OsCERK1, cooperatively regulate chitin elicitor signaling in rice. Plant J 64:204-214.

Simon, C., Langlois-Meurinne, M., Bellvert, F., Garmier, M., Didierlaurent, L., Massoud, K., Chaouch, S., Marie, A., Bodo, B., Kauffmann, S., Noctor, G., and Saindrenan, P. 2010. The differential spatial distribution of secondary metabolites in *Arabidopsis* leaves reacting hypersensitively to *Pseudomonas syringae* pv. *tomato* is dependent on the oxidative burst. J Exp Bot 61:3355-3370.

Sinha, A.K., and Wood, R.K.S. 1968. Studies on the nature of resistance in tomato plants to *Verticillium albo-atrum*. Ann Appl Biol 62:319-327.

Sivitz, A.B., Hermand, V., Curie, C., and Vert, G. 2012. *Arabidopsis* bHLH100 and bHLH101 control iron homeostasis via a FIT-independent pathway. PLoS One 7:e44843.

Son, S.W., Kim, H.Y., Choi, G.J., Lim, H.K., Jang, K.S., Lee, S.O., Lee, S., Sung, N.D., and Kim, J.C. 2008. Bikaverin and fusaric acid from *Fusarium oxysporum* show antioomycete activity against *Phytophthora infestans*. J Appl Microbiol 104:692-698.

Sonderby, I.E., Geu-Flores, F., and Halkier, B.A. 2010. Biosynthesis of glucosinolates - gene discovery and beyond. Trends Plant Sci 15:283-290.

Srinivasan, N., Gordon, O., Ahrens, S., Franz, A., Deddouche, S., Chakravarty, P., Phillips, D., Yunus, A.A., Rosen, M.K., Valente, R.S., Teixeira, L., Thompson, B., Dionne, M.S., Wood, W., and Reis e Sousa, C. 2016. Actin is an evolutionarily-conserved damage-associated molecular pattern that signals tissue injury in *Drosophila melanogaster*. Elife 5:e19662.

Stenberg, F., Von Heijne, G., and Daley, D.O. 2007. Assembly of the cytochrome *bo3* complex. J Mol Biol 371:765-773.

Strehmel, N., Bottcher, C., Schmidt, S., and Scheel, D. 2014. Profiling of secondary metabolites in root exudates of *Arabidopsis thaliana*. Phytochemistry 108:35-46.

Stringlis, I.A., Proietti, S., Hickman, R., Van Verk, M.C., Zamioudis, C., and Pieterse, C.M.J. 2018a. Root transcriptional dynamics induced by beneficial rhizobacteria and microbial immune elicitors reveal signatures of adaptation to mutualists. Plant J 93:166-180.

Stringlis, I.A., Yu, K., Feussner, K., De Jonge, R., Van Bentum, S., Van Verk, M.C., Berendsen, R.L., Bakker, P.A.H.M., Feussner, I., and Pieterse, C.M.J. 2018b. MYB72-dependent coumarin exudation shapes root microbiome assembly to promote plant health. Proc Natl Acad Sci U S A 115:E5213-E5222.

Sun, H., Wang, L., Zhang, B., Ma, J., Hettenhausen, C., Cao, G., Sun, G., Wu, J., and Wu, J. 2014. Scopoletin is a phytoalexin against *Alternaria alternata* in wild tobacco dependent on jasmonate signalling. J Exp Bot 65:4305-4315.

Sun, Y., Li, L., Macho, A.P., Han, Z., Hu, Z., Zipfel, C., Zhou, J.M., and Chai, J. 2013. Structural basis for flg22-induced activation of the *Arabidopsis* FLS2-BAK1 immune complex. Science 342:624-628.

Tatusov, R.L., Natale, D.A., Garkavtsev, I.V., Tatusova, T.A., Shankavaram, U.T., Rao, B.S., Kiryutin, B., Galperin, M.Y., Fedorova, N.D., and Koonin, E.V. 2001. The COG database: new developments in phylogenetic classification of proteins from complete genomes. Nucleic Acids Res 29:22-28.

Tellstrom, V., Usadel, B., Thimm, O., Stitt, M., Kuster, H., and Niehaus, K. 2007. The lipopolysaccharide of *Sinorhizobium meliloti* suppresses defense-associated gene expression in cell cultures of the host plant *Medicago truncatula*. Plant Physiol 143:825-837.

Thimm, O., Essigmann, B., Kloska, S., Altmann, T., and Buckhout, T.J. 2001. Response of *Arabidopsis* to iron deficiency stress as revealed by microarray analysis. Plant Physiol 127:1030-1043.

Tkacz, A., and Poole, P. 2015. Role of root microbiota in plant productivity. J Exp Bot 66:2167-2175.

Torres, M.A., Jones, J.D.G., and Dangl, J.L. 2006. Reactive oxygen species signaling in response to pathogens. Plant Physiol 141:373-378.

Trda, L., Fernandez, O., Boutrot, F., Heloir, M.C., Kelloniemi, J., Daire, X., Adrian, M., Clement, C., Zipfel, C., Dorey, S., and Poinssot, B. 2014. The grapevine flagellin receptor VvFLS2 differentially recognizes flagellin-derived epitopes from the endophytic growth-promoting bacterium *Burkholderia phytofirmans* and plant pathogenic bacteria. New Phytol 201:1371-1384.

Tsai, H.H., and Schmidt, W. 2017a. One way. Or another? Iron uptake in plants. New Phytol 214:500-505.

Tsai, H.H., and Schmidt, W. 2017b. Mobilization of iron by plant-borne coumarins. Trends Plant Sci 22:538-548.

Tsai, H.H., Rodriguez-Celma, J., Lan, P., Wu, Y.C., Velez-Bermudez, I.C., and Schmidt, W. 2018. Scopoletin 8-hydroxylase-mediated fraxetin production is crucial for iron mobilization. Plant Physiol 177:194-207.

Turner, T.R., James, E.K., and Poole, P.S. 2013a. The plant microbiome. Genome Biol 14:209.

Turner, T.R., Ramakrishnan, K., Walshaw, J., Heavens, D., Alston, M., Swarbreck, D., Osbourn, A., Grant, A., and Poole, P.S. 2013b. Comparative metatranscriptomics reveals kingdom level changes in the rhizosphere microbiome of plants. ISME J 7:2248-2258.

Turra, D., El Ghalid, M., Rossi, F., and Di Pietro, A. 2015. Fungal pathogen uses sex pheromone receptor for chemotropic sensing of host plant signals. Nature 527:521-524.

Van de Mortel, J.E., De Vos, R.C., Dekkers, E., Pineda, A., Guillod, L., Bouwmeester, K., Van Loon, J.J., Dicke, M., and Raaijmakers, J.M. 2012. Metabolic and transcriptomic changes induced in *Arabidopsis* by the rhizobacterium *Pseudomonas fluorescens* SS101. Plant Physiol 160:2173-2188.

Van den Burg, H.A., Harrison, S.J., Joosten, M.H.A.J., Vervoort, J., and De Wit, P.J.G.M. 2006. *Cladosporium fulvum* Avr4 protects fungal cell walls against hydrolysis by plant chitinases accumulating during infection. Mol Plant Microbe In 19:1420-1430.

Van der Ent, S., Van Wees, S.C.M., and Pieterse, C.M.J. 2009. Jasmonate signaling in plant interactions with resistance-inducing beneficial microbes. Phytochemistry 70:1581-1588.

Van der Ent, S., Verhagen, B.W.M., Van Doorn, R., Bakker, D., Verlaan, M.G., Pel, M.J.C., Joosten, R.G., Proveniers, M.C.G., Van Loon, L.C., Ton, J., and Pieterse, C.M.J. 2008. MYB72 Is required in early signaling steps of rhizobacteria-induced systemic resistance in *Arabidopsis*. Plant Physiol 146:1293-1304.

Van Loon, L.C., Bakker, P.A.H.M., Van der Heijdt, W.H.W., Wendehenne, D., and Pugin, A. 2008. Early responses of tobacco suspension cells to rhizobacterial elicitors of induced systemic resistance. Mol Plant Microbe In 21:1609-1621.

Van Peer, R., Niemann, G.J., and Schippers, B. 1991. Induced resistance and phytoalexin accumulation in biological control of *Fusarium* wilt of carnation by *Pseudomonas* sp. strain WCS417r. Phytopathology 81:728-734.

Van Wees, S.C.M., Van Pelt, J.A., Bakker, P.A.H.M., and Pieterse, C.M.J. 2013. Bioassays for assessing jasmonate-dependent defenses triggered by pathogens, herbivorous insects, or beneficial rhizobacteria. Pages 35-49 in: Jasmonate Signaling: Methods in Molecular Biology (Methods and Protocols), A. Goossens and L. Pauwels, eds. Humana Press, Totowa, NJ.

Van Wees, S.C.M., Luijendijk, M., Smoorenburg, I., Van Loon, L.C., and Pieterse, C.M.J. 1999. Rhizobacteria-mediated induced systemic resistance (ISR) in *Arabidopsis* is not associated with a direct effect on expression of known defense-related genes but stimulates the expression of the jasmonate-inducible gene *Atvsp* upon challenge. Plant Mol Biol 41:537-549.

Van Wees, S.C.M., Pieterse, C.M.J., Trijssenaar, A., Van 't Westende, Y.A., Hartog, F., and Van Loon, L.C. 1997. Differential induction of systemic resistance in *Arabidopsis* by biocontrol bacteria. Mol Plant Microbe In 10:716-724.

Veiga, R.S., Faccio, A., Genre, A., Pieterse, C.M.J., Bonfante, P., and Van der Heijden, M.G.A. 2013. Arbuscular mycorrhizal fungi reduce growth and infect roots of the non-host plant *Arabidopsis thaliana*. Plant Cell Environ 36:1926-1937.

Verbon, E.H., and Liberman, L.M. 2016. Beneficial microbes affect endogenous mechanisms controlling root development. Trends Plant Sci 21:218-229.

Verbon, E.H., Trapet, P.L., Stringlis, I.A., Kruijs, S., Bakker, P.A.H.M., and Pieterse, C.M.J. 2017. Iron and immunity. Annu Rev Phytopathol 55:355-375.

Verhagen, B.W.M., Glazebrook, J., Zhu, T., Chang, H.S., Van Loon, L.C., and Pieterse, C.M.J. 2004. The transcriptome of rhizobacteria-induced systemic resistance in *Arabidopsis*. Mol Plant Microbe In 17:895-908.

Vigani, G. 2012. Discovering the role of mitochondria in the iron deficiency-induced metabolic responses of plants. J Plant Physiol 169:1-11.

Vos, I.A., Pieterse, C.M.J., and Van Wees, S.C.M. 2013. Costs and benefits of hormone‐regulated plant defences. Plant Pathol 62:43-55.

Vylkova, S. 2017. Environmental pH modulation by pathogenic fungi as a strategy to conquer the host. PLoS Pathog 13:e1006149.

Wang, L., Albert, M., Einig, E., Furst, U., Krust, D., and Felix, G. 2016. The pattern-recognition receptor CORE of Solanaceae detects bacterial cold-shock protein. Nat Plants 2:16185.

Wang, L., Tsuda, K., Truman, W., Sato, M., Nguyen le, V., Katagiri, F., and Glazebrook, J. 2011. CBP60g and SARD1 play partially redundant critical roles in salicylic acid signaling. Plant J 67:1029-1041.

Wasternack, C., and Feussner, I. 2018. The oxylipin pathways: biochemistry and function. Annu Rev Plant Biol 69:363-386.

Wawra, S., Fesel, P., Widmer, H., Timm, M., Seibel, J., Leson, L., Kesseler, L., Nostadt, R., Hilbert, M., Langen, G., and Zuccaro, A. 2016. The fungal-specific β-glucan-binding lectin FGB1 alters cell-wall composition and suppresses glucan-triggered immunity in plants. Nat Commun 7:13188.

Wei, Q., Ran, T., Ma, C., He, J., Xu, D., and Wang, W. 2016. Crystal structure and function of PqqF protein in the pyrroloquinoline quinone biosynthetic pathway. J Biol Chem 291:15575-15587.

Wen, Z.T., and Burne, R.A. 2002. Functional genomics approach to identifying genes required for biofilm development by *Streptococcus* mutans. Appl Environ Microb 68:1196-1203.

Wickham, H. 2016. ggplot2: elegant graphics for data analysis. Springer-Verlag New York, New York, USA.

Win, J., Chaparro-Garcia, A., Belhaj, K., Saunders, D.G., Yoshida, K., Dong, S., Schornack, S., Zipfel, C., Robatzek, S., Hogenhout, S.A., and Kamoun, S. 2012. Effector biology of plant-associated organisms: concepts and perspectives. Cold Spring Harb Symp Quant Biol 77:235-247.

Won, C., Shen, X., Mashiguchi, K., Zheng, Z., Dai, X., Cheng, Y., Kasahara, H., Kamiya, Y., Chory, J., and Zhao, Y. 2011. Conversion of tryptophan to indole-3-acetic acid by TRYPTOPHAN AMINOTRANSFERASES OF *ARABIDOPSIS* and YUCCAs in *Arabidopsis*. Proc Natl Acad Sci U S A 108:18518-18523.

Wu, S., Li, X., Gunawardana, M., Maguire, K., Guerrero-Given, D., Schaudinn, C., Wang, C., Baum, M.M., and Webster, P. 2014. Beta-lactam antibiotics stimulate biofilm formation in non-typeable *Haemophilus influenzae* by up-regulating carbohydrate metabolism. PLoS One 9:e99204.

Wyrsch, I., Dominguez-Ferreras, A., Geldner, N., and Boller, T. 2015. Tissue-specific FLAGELLIN-SENSING 2 (FLS2) expression in roots restores immune responses in *Arabidopsis fls2* mutants. New Phytol 206:774-784.

Xin, D.W., Liao, S., Xie, Z.P., Hann, D.R., Steinle, L., Boller, T., and Staehelin, C. 2012. Functional analysis of NopM, a novel E3 ubiquitin ligase (NEL) domain effector of *Rhizobium* sp. strain NGR234. PLoS Pathog 8:e1002707.

Xin, X.F., and He, S.Y. 2013. *Pseudomonas syringae* pv. *tomato* DC3000: a model pathogen for probing disease susceptibility and hormone signaling in plants. Annu Rev Phytopathol 51:473-498.

Yaeno, T., Matsuda, O., and Iba, K. 2004. Role of chloroplast trienoic fatty acids in plant disease defense responses. Plant J 40:931-941.

Yu, X., Feng, B., He, P., and Shan, L. 2017. From chaos to harmony: responses and signaling upon microbial pattern recognition. Annu Rev Phytopathol 55:109-137.

Yuan, J., Zhao, J., Wen, T., Zhao, M., Li, R., Goossens, P., Huang, Q., Bai, Y., Vivanco, J.M., Kowalchuk, G.A., Berendsen, R.L., and Shen, Q. 2018. Root exudates drive the soil-borne legacy of aboveground pathogen infection. Microbiome 6:156.

Zamioudis, C. (2012). Signaling in *Arabidopsis* roots in response to beneficial rhizobacteria. In Department of Biology (Utrecht, The Netherlands: Utrecht University).

Zamioudis, C., and Pieterse, C.M.J. 2012. Modulation of host immunity by beneficial microbes. Mol Plant Microbe In 25:139-150.

Zamioudis, C., Hanson, J., and Pieterse, C.M.J. 2014. β-Glucosidase BGLU42 is a MYB72-dependent key regulator of rhizobacteria-induced systemic resistance and modulates iron deficiency responses in *Arabidopsis* roots. New Phytol 204:368-379.

Zamioudis, C., Mastranesti, P., Dhonukshe, P., Blilou, I., and Pieterse, C.M.J. 2013. Unraveling root developmental programs initiated by beneficial *Pseudomonas* spp. bacteria. Plant Physiol 162:304-318.

Zamioudis, C., Korteland, J., Van Pelt, J.A., Van Hamersveld, M., Dombrowski, N., Bai, Y., Hanson, J., Van Verk, M.C., Ling, H., Schulze-Lefert, P., and Pieterse, C.M.J. 2015. Rhizobacterial volatiles and photosynthesis-related signals coordinate *MYB72* expression in *Arabidopsis* roots during onset of induced systemic resistance and iron-deficiency responses. Plant J 84:309-322.

Zgadzaj, R., Garrido-Oter, R., Jensen, D.B., Koprivova, A., Schulze-Lefert, P., and Radutoiu, S. 2016. Root nodule symbiosis in *Lotus japonicus* drives the establishment of distinctive rhizosphere, root, and nodule bacterial communities. Proc Natl Acad Sci U S A 113:E7996-E8005.

Zhalnina, K., Louie, K.B., Hao, Z., Mansoori, N., da Rocha, U.N., Shi, S., Cho, H., Karaoz, U., Loque, D., Bowen, B.P., Firestone, M.K., Northen, T.R., and Brodie, E.L. 2018. Dynamic root exudate chemistry and microbial substrate preferences drive patterns in rhizosphere microbial community assembly. Nat Microbiol 3:470-480.

Zhang, L., Shen, X., Liu, Y., and Li, S. 2013. *Nafulsella turpanensis* gen. nov., sp. nov., a member of the phylum *Bacteroidetes* isolated from soil. Int J Syst Evol Microbiol 63:1639-1645.

Zhang, L., Chen, X.J., Lu, H.B., Xie, Z.P., and Staehelin, C. 2011. Functional analysis of the type 3 effector nodulation outer protein L (NopL) from *Rhizobium* sp. NGR234: symbiotic effects, phosphorylation, and interference with mitogen-activated protein kinase signaling. J Biol Chem 286:32178-32187.

Zhang, N., Yang, D., Wang, D., Miao, Y., Shao, J., Zhou, X., Xu, Z., Li, Q., Feng, H., Li, S., Shen, Q., and Zhang, R. 2015. Whole transcriptomic analysis of the plant-beneficial rhizobacterium *Bacillus amyloliquefaciens* SQR9 during enhanced biofilm formation regulated by maize root exudates. BMC Genomics 16:685.

Zhang, Y., Xu, J., Riera, N., Jin, T., Li, J., and Wang, N. 2017. Huanglongbing impairs the rhizosphere-to-rhizoplane enrichment process of the citrus root-associated microbiome. Microbiome 5:97.

Zhang, Y., Xu, S., Ding, P., Wang, D., Cheng, Y.T., He, J., Gao, M., Xu, F., Li, Y., Zhu, Z., Li, X., and Zhang, Y. 2010. Control of salicylic acid synthesis and systemic acquired resistance by two members of a plant-specific family of transcription factors. Proc Natl Acad Sci U S A 107:18220-18225.

Zhou, C., Guo, J., Zhu, L., Xiao, X., Xie, Y., Zhu, J., Ma, Z., and Wang, J. 2016. *Paenibacillus polymyxa* BFKC01 enhances plant iron absorption via improved root systems and activated iron acquisition mechanisms. Plant Physiol Bioch 105:162-173.

Ziegler, J., Schmidt, S., Strehmel, N., Scheel, D., and Abel, S. 2017. *Arabidopsis* transporter ABCG37/PDR9 contributes primarily highly oxygenated coumarins to root exudation. Sci Rep 7:3704.

Ziegler, J., Schmidt, S., Chutia, R., Müller, J., Böttcher, C., Strehmel, N., Scheel, D., and Abel, S. 2016. Non-targeted profiling of semi-polar metabolites in *Arabidopsis* root exudates uncovers a role for coumarin secretion and lignification during the local response to phosphate limitation. J Exp Bot 67:1421-1432.

Zipfel, C., and Oldroyd, G.E. 2017. Plant signalling in symbiosis and immunity. Nature 543:328-336.

Zipfel, C., Kunze, G., Chinchilla, D., Caniard, A., Jones, J.D.G., Boller, T., and Felix, G. 2006. Perception of the bacterial PAMP EF-Tu by the receptor EFR restricts *Agrobacterium*-mediated transformation. Cell 125:749-760.

Zocchi, G. 2006. Metabolic changes in iron-stressed dicotyledonous plants. Pages 359-370 in: Iron Nutrition in Plants and Rhizospheric Microorganisms, L.L. Barton and J. Abadia, eds. Springer Netherlands, Dordrecht.

Zuccaro, A., Lahrmann, U., Guldener, U., Langen, G., Pfiffi, S., Biedenkopf, D., Wong, P., Samans, B., Grimm, C., Basiewicz, M., Murat, C., Martin, F., and Kogel, K.H. 2011. Endophytic life strategies decoded by genome and transcriptome analyses of the mutualistic root symbiont *Piriformospora indica*. PLoS Pathog 7:e1002290.

Zum Felde, T., Baumert, A., Strack, D., Becker, H.C., and Möllers, C. 2007. Genetic variation for sinapate ester content in winter rapeseed (*Brassica napus* L.) and development of NIRS calibration equations. Plant Breeding 126:291-296.

SAMENVATTING

De gezondheid van een plant wordt in hoge mate bepaald door de microbiële gemeenschap die is geassocieerd met de plantenwortel. Naast interacties met micro-organismen die de plant kunnen schaden, interacteren planten ook met specifieke groeibevorderende micro-organismen op hun wortels. Het tot stand komen van dergelijke allianties vereist een constante moleculaire dialoog tussen de groeibevorderende microben en hun gastheer. Wortelexudaten spelen een belangrijke rol bij het vormen van het wortelmicrobioom, de microbiële gemeenschap op de plantenwortel. In dit proefschrift is de interactie tussen wortels van de modelplant *Arabidopsis thaliana* met plantvriendelijke micro-organismen onderzocht om een beter zicht te krijgen op de chemische communicatie tussen plantenwortels en het wortelmicrobioom.

Het immuunsysteem van de plant kan microbe-geassocieerde moleculaire patronen (MAMPs) detecteren en de daarop geïnitieerde afweerreacties kunnen de groei van micro-organismen beïnvloeden. In hoofdstuk 1 wordt aan de hand van literatuur onderzocht of actieve demping van deze afweerreactie door plantvriendelijke microben noodzakelijk is om effectief de wortel te kunnen koloniseren. Voor sommige plantvriendelijke rhizobacteriën is aangetoond dat ze de door MAMPs geactiveerde afweerrespons in wortels van *Arabidopsis* kunnen onderdrukken (Millet et al., 2010; Lakshmanan et al., 2012; Stringlis et al., 2018a). In hoofdstuk 2, wordt een dergelijke onderdrukking van de immuunrespons door de bacterie stam *Pseudomonas capeferrum* WCS358 (WCS358) bestudeerd. WCS358 kan het afweersysteem van de plant versterken en er na kolonisatie van de wortels voor zorgen dat alle delen van de plant minder vatbaar worden voor ziekteverwekkers, een fenomeen dat bekend is onder de term geïnduceerde systemische resistentie (*induced systemic resistance;* ISR). Tegelijkertijd onderdrukt WCS358 in de wortels de afweerrespons die volgt op toediening van flg22, een MAMP dat ook door WCS358 wordt geproduceerd. In dit hoofdstuk werd ontdekt dat de bacteriële genen *pqqF* en *cyoB* nodig zijn voor de onderdrukking van flg22-geïnduceerde afweerreactie. De eiwitten PqqF en CyoB zijn beide betrokken bij de oxidatie van glucose tot gluconzuur. Door de productie van gluconzuur verlaagt de bacterie de pH van het omringende milieu. De verlaging van pH bleek ook voldoende om de afweerrespons van de wortel te onderdrukken. Bovendien was een mutant van WCS358 zonder functioneel *pqqF* verminderd in staat de plantenwortel te koloniseren. Deze resultaten tonen aan dat WCS358 afweerreacties in de wortel kan onderdrukken door de pH van het wortelmilieu te verlagen en suggereren dat onderdrukking van de afweerrespons door plantvriendelijke micro-organismen bijdraagt aan kolonisatie van de plantenwortel door deze micro-organismen.

MYB72 is een transcriptiefactor met een voor ISR essentiële functie in de plantenwortel. *Arabidopsis* planten die dit eiwit missen of waarin het eiwit niet functioneel is, vertonen geen verminderde vatbaarheid voor ziekteverwekkers na kolonisatie door ISR-veroorzakende micro-organismen. In de wortels van *Arabidopsis* is MYB72 ook betrokken is bij de synthese van fluorescerende coumarines in reactie op een ijzertekort. Coumarines zijn fenolische verbindingen die bij ijzer deficiëntie accumuleren in het wortelexudaat en die de beschikbaarheid van ijzer voor de plant verhogen. In hoofdstuk 3 worden deze MYB72-afhankelijke metabolieten geanalyseerd en hun betrokkenheid bij de assemblage van het wortelmicrobioom bestudeerd. Zowel MYB72 als de, ook voor ISR noodzakelijke, beta-glucosidase BGLU42 zijn betrokken bij de biosynthese van coumarines. In de wortel van *Arabidopsis* is scopoline dominant aanwezig, terwijl scopoletine het dominant coumarine

in het wortelexudaat is. In *myb72* mutanten zijn deze coumarines nauwelijks aanwezig, wat aangeeft dat MYB72 de synthese van deze coumarines reguleert. In *bglu42* planten is scopoletine afwezig in het exudaat, terwijl scopoline nog wel aanwezig is in de plantenwortel. Scopoline is de geglycolyseerde vorm van scopoletine, waarmee het glucosidase BGLU42 waarschijnlijk verantwoordelijk is voor deze omzetting en dat alleen scopoletine wordt gesecreteerd. Hoewel scopoletine sterke antimicrobiële activiteit heeft, zijn de ISR-veroorzakende rhizobacteriën *Pseudomonas simiae* WCS417 (WCS417) en WCS358 zeer ongevoelig voor deze verbinding. Bovendien rekruteert de coumarine-deficiënte *f6'h1*-mutant een significant ander wortelmicrobioom dan wild type planten, wat erop wijst dat coumarines de assemblage van het wortelmicrobioom vormgeven.

Door WCS417 veroorzaakte veranderingen in het transcriptoom van *Arabidopsis* overlappen met de veranderingen veroorzaakt door ijzerdeficiëntie (Zamioudis et al., 2015). Echter was nog niet duidelijk of veranderingen in metabolietsamenstelling van de wortel in reactie op WCS417 en op ijzertekort ook overeenkomsten vertonen. Daarom werd in hoofdstuk 4 onderzocht of er na kolonisatie door WCS417 metabole veranderingen in wortels van *Arabidopsis* optreden. Inderdaad bleek WCS417 het wortelmetaboloom sterk te beïnvloeden met een verhoogde productie van de coumarines scopoline, scopoletine en esculine. Daarnaast werd ook de biosynthese van alifatische glucosinolaten en het vetzuurmetabolisme, beide geassocieerd met wortelimmuunreacties, gestimuleerd door WCS417.

Coumarinen worden geproduceerd in reactie op zowel ijzer tekort (hoofdstuk 3) als door kolonisatie van de wortel door WCS417 (hoofdstuk 4). De verhoogde productie van de antimicrobiële coumarines zou indirect kolonisatie door WCS417 kunnen bevorderen, aangezien WCS417 relatief ongevoelig is voor de groeiremmende effecten van coumarines. De reactie van WCS417 op coumarines was echter nog niet onderzocht. Daarom werd in hoofdstuk 5 de transcriptionele respons van WCS417 op coumarines in wortelexudaten van *Arabidopsis* onderzocht. In deze experimenten werd gevonden dat coumarine bevattende wortelexudaten het transport en metabolisme van koolhydraten, aminozuren en nucleotiden induceren, terwijl celmotiliteit, het bacteriële mobiloom en energieproductie en -conversie word onderdrukt. Mogelijk draagt deze respons bij aan de capaciteit van WCS417 om wortels te koloniseren.

In hoofdstuk 6 worden de verkregen resultaten besproken in context van bestaande literatuur en met het oog op mogelijk vervolgonderzoek.

ACKNOWLEDGEMENTS

This is it.

I would like to thank to my dear promoter: Prof. Corné Pieterse. Thanks for your reply to my application 5 years ago, which eventually brought me to Plant-Microbe Interactions group. Your great mind inspired me so much not only in the scientific research during the PhD period but also my career path in the future. Moreover, great thanks for your full support to PhD students from abroad. That means a lot for me as a new student in a distant foreign country. I wish you the best!

I would like to thank to my daily supervisors: Dr. Roeland Berendsen and Dr. Peter Bakker. Roeland, thanks for your daily supervision with great patience and professionality. We had rough time, but we also learnt so much from each other, which I believe will be a fortune for both of us. I wish you great success in career! Peter, thanks for your daily supervision with great ideas that I could never come up with. Interesting thoughts indeed emerge from a new angle. I wish you healthy and happy!

I would like to thank to the other staff members who keep PMI running: Ronnie, Saskia, Guido, Hans and Anja. Ronnie, thanks for helping in the work and enthusiastic discussion in your office. I wish you great success in science! And watch out the labels! Saskia and Guido, thanks for stimulating discussion and nice advices in the past 4 years. I wish you more papers in this field! Hans and Anja, you are the magicians for photograph and molecular biology. Thanks a lot for making the lab a better place!

I would like to thank to my dear roommates: Silvia Proietti, Giannis Stringlis and Marciel Pereira Mendes. We had so much fun in W301/W305 and places around the world. Silvia, you are the star always shining upon me! It was my luck that I met you the first day when I entered the office. I appreciate everything that you did for me. It was sad when you left the office but there is always a place reserved for you in my heart. I wish you young and passionate about things you love all the time! Giannis, you are my best collaborator! I miss the time that we discussed science and food in the office and restaurants till 9 in the night. Some ideas have become published work and some are on the way! I wish you happier and smooth in the Postdoc! Marciel, you are my brother! Your positivity perfectly neutralizes my negativity, which keeps the Yin-yang balance around us. I will miss your philosophy and the mysterious jungle juice anytime I start my meditation! You have found a girl and I wish you can settle down someday! I also would like to thank to Chrysa, Sara and Elaine. Chrysa, do not abandon Giannis and I wish you a magnificent wedding! Sara, take it easy and do not lose too much weight! Elanie, good luck in your next job and see you someday in LA!

I would like to thank to Corné's people: Christos, Pauline and Eline. Christos, thanks for helping me with *Arabidopsis*! Pauline, thanks for your passion in both life and work! Eline, thanks for nice planning when we work together! Saskia's people: Yeling, Richard, Lotte, Merel, Ainohoa, Ivan and Marcel. Yeling, thanks for great advices for surviving! Richard, thanks for helping in statistics and being a royal model! Lotte and Merel, thanks for being nice to me all the time! Ainohoa and Ivan, thanks for bringing fun to everyone! Marcel, thanks for great advices in my projects! Peter's people: Paul and Gilles, thanks for being good company to people from the east! Also thanks to Colette, Marco, Gonzalo, Francisco, Juan!

And Guido's people: Miek, Joyce, Kim, Dongping, Claudia, Nora, Alexandra, Joël, Manon, Tom and Tijmen. Thanks for your help in the lab and some occasional fun outside the lab!

I would like to thank to Erqin, Hao, Yang, Zeguang, Tianjie, Cunliang, Mei, Jinling, Yin and Minggang. Erqin, thanks for caring about me so much! You will be a great scientist. Hao, be active and be strong! Yang, enjoy the Netherlands! Zeguang, thanks for great dinner and keep cooking! Tianjie, good luck with everything! Cunliang, tell me more about AI! Mei, take care and enjoy painting! Jinling, enjoy the U.S! Yin, enjoy Yangling! Minggang, enjoy Sweden! We keep in touch.

I would like to thank to the students who I have worked with: Wilco, Pablo, Nina, Ramon, Pim, Sanne, Renda and Floris. You have done marvelous job during the internship! I wish you all the best in the following study! Special thanks to Dieter for sharing thoughts and experiences in and after the PAA course! Good luck!

I would like to thank to the following people: Ria from Molecular Microbiology group for helping me with electroporation; Balu from Tamil Nadu Agricultural University for helping me with tri-parental mating; Ellen from Koppert for helping me with UPLC-MS; Basten from Theoretical Biology and Bioinformatics group for helping me with analyzing RNA sequencing data. Special thanks to Kirstin and Ivo Feussner from Goettingen University for contributions in two of my shared projects!

I would like to thank to my dear old friends Xiaowei and Jian. Xiaowei, thanks for introducing Corné and ISR to me. You are the person who I am chasing all the time! Jian, thanks for being my best man during my wedding. You are the person I get to know a lot of different things! I wish both of you well in everything! We keep in touch!

I would like to thank to my wife and my parents for their understanding of this long journey and full support for my decisions without doubt. I will do my best.

I would like to thank to the China Scholar Council for financially supporting my PhD!

That is it.

CURRICULUM VITAE

Ke Yu was born on 2 December 1987 in Zhengzhou, Henan, China. He started the bachelor study in September 2006 in the College of Plant Protection, Northwest A&F University, Yangling, Shannxi, China. In the last year of his bachelor study, he did an internship in the lab of Prof. Qing Ma, to investigate the role of actin cytoskeleton in nonhost resistance of crop plants against fungal pathogens. After his graduation in June 2010, he continued this research as a master student in the same lab and graduated in June 2013. In May 2013, he obtained a scholarship from China Scholarship Council, which allowed him to continue as a PhD student from November 2013 to October 2017 in Plant-Microbe Interactions group, Institute of Environmental biology, Utrecht University, the Netherlands. Under the supervision of Prof. Corné Pieterse, Dr. Peter Bakker and Dr. Roeland Berendsen, he investigated the chemical communications in the root-microbiome interactions. After his PhD thesis defense in February 2019, he will be continuing as a postdoctoral research fellow in the Institute of Synthetic Biology, Shenzhen, China.

LIST OF PUBLICATIONS

Berendsen, R.L.*, Vismans, G.*, **Yu, K.**, Song, Y., De Jonge, R., Burgman, W.P., Burmølle, M., Herschend, J., Bakker, P.A.H.M., and Pieterse, C.M.J. 2018. Disease-induced assemblage of a plant-beneficial bacterial consortium. ISME J 12:1496-1507.

Stringlis, I.A.*, **Yu, K.***, Feussner, K.*, De Jonge, R., Van Bentum, S., Van Verk, M.C., Berendsen, R.L., Bakker, P.A.H.M., Feussner, I., and Pieterse, C.M.J. 2018b. MYB72-dependent coumarin exudation shapes root microbiome assembly to promote plant health. Proc Natl Acad Sci U S A 115:E5213-E5222.

* These authors contributed equally to the work